The Human Adenosine A$_{2B}$ Receptor:

Homology Modeling, Virtual Screening, and

Computer-aided Drug Design

vorgelegt von

Farag Farouk Sherbiny Selim

aus

Giza, Ägypten

Bonn, 2011

Angefertigt mit der Genehmigung der Mathematisch-Naturwissenschaftlichen Fakultät

der Rheinischen Friedrich-Wilhelms-Universität Bonn

<u>Promotionskommission</u>

1. Gutachter:	Prof. Dr. Christa E. Müller
2. Gutachter:	Prof. Dr. Michael Gütschow
3. Fachnahes Mitglied:	Prof. Dr. Harald G. Schweim
4. Fachangrenzendes Mitglied:	Prof. Dr. Ivar von Kügelgen

Tag der Promotion: 31. Januar 2011

Erscheinungsjahr: 2011

ACKNOWLEDGEMENTS

DEDICATION

To the memory of my father

To my beloved mother, my wife and my children's

CONTENTS

LIST OF ABBREVIATIONS

3D	Three-dimensional structure
7TM	Seven transmembrane receptors
Å	Angstrom
A_{2B}-I	A_{2B} model based on bovine rhodopsin
A_{2B}-II	A_{2B} model based on the β_2-adrenergic receptor
A_{2B}-III	A_{2B} model based on the adenosine A_{2A} receptor
AC	Adenylyl cyclise
AFM	Atomic force microscopy
Ag	Agonist
Ant	Antagonist
ARs	Adenosine receptors
ATP	Adenosine triphosphate
B-factor	Temperature factor, Debye-Waller factor given in X-ray sructures
cAMP	Cyclic adenosine monophosphate
cGMP	Guanosine 3'-5'-cyclic monophosphate
CADO	2-Chloroadenosine
CPA	N^6-Cyclopentyladenosine
DAG	Diacylglycerol
EL	Extracellular loop
EC_{50}	Agonist concentration of a ligand that is required for a 50% of the maximum effect
FTrees	Feature trees program
G-protein	Guanine nucleotide binding protein

GPCRs	G protein-coupled receptors
GPCRDB	G protein-coupled receptor database
HTS	High throughput screening
IFS	Interaction fingerprint based similarity
IC_{50}	Antagonist concentration which suppresses 50% of an agonist induced effect
IL	Intracellular loop
IL-6	Interleukin-6
IPs	Inositol phosphates
K_i	Dissociation constant (competition binding assay)
MD	Molecular dynamic simulations
MM	Molecular mechanics
MM-GBSA	Molecular Mechanics Generalized Born Surface Area
NC	No change
NECA	5'-N-ethylcarboxamidoadenosine
NMR	Nuclear magnetic resonance
ns	Nanosecond
PDB	Protein Data Base
POPC	1-Palmitoyl-2-oleoyl-*sn*-glycero-3-phosphatidylcholine
ps	Picosecond
QSAR	Quantitative structure-activity relationships
RMSD	Root mean square deviation
SAR	Structure activity relationships

LIST OF FIGURES

LIST OF TABLES

1 Introduction

1.1 G Protein-Coupled Receptors

An important class of transmembrane proteins is the superfamily of G protein-coupled receptors (GPCRs) which are known as seven transmembrane (7TM) or heptahelical receptors. They constitute a prominent superfamily targeted by many drugs [1]. Up to 50% of all modern-day medicines act on GPCRs [2]. This makes GPCRs of great interest to both pharmaceutical and academic research, which is focused on drug discovery and the function and malfunction of various human systems. GPCRs play a vital role in signal transduction and may be activated by a wide variety of ligands, including photons, amines, hormones, neurotransmitters and proteins. GPCRs are single polypeptide chains having seven hydrophobic transmembrane-spanning segments that couple in the presence of an activator to an intracellular effector molecule through a trimeric G protein complex [3]. The latter protein name originates from its interaction with guanine nucleotides. The class of guanine nucleotide binding proteins (G proteins) initiate some of the important signalling pathways in the cell.

The members of the GPCR superfamily share two major structural and functional similarities. The first principal feature are the setup by seven membrane-spanning α-helices (TM1-7) connected by alternating intracellular (IL1, IL2, and IL3) and extracellular loop domains (EL1, EL2, and EL3). The orientation of the N and C terminus is also conserved across all GPCRs. The N-terminal tail is exposed to the extracellular environment and the C-terminal tail is located in the cytosol of the cell and thought to maintain an interaction with cytosolic G proteins. Moreover, two cysteine residues, one in the TM3/EL1 interface and one in EL2, which are conserved in almost all GPCRs, form an essential disulfide linkage responsible for the packing and stabilization of a restricted number of conformations of these seven TM domains (Figure **1.1**). Besides sequence variations, the various GPCRs differ mainly in the length and function of their N-terminal extracellular domain, their C-terminal intracellular domain and their intracellular loops. Each of these domains provides specific properties to the various receptor proteins. However, significant sequence homology is found within several subfamilies. Secondly, the binding of agonistic ligands to the receptors elicits conformational

changes of the receptor and activates the G protein. In this manner the receptors transfer extracellular signals to intracellular targets [4].
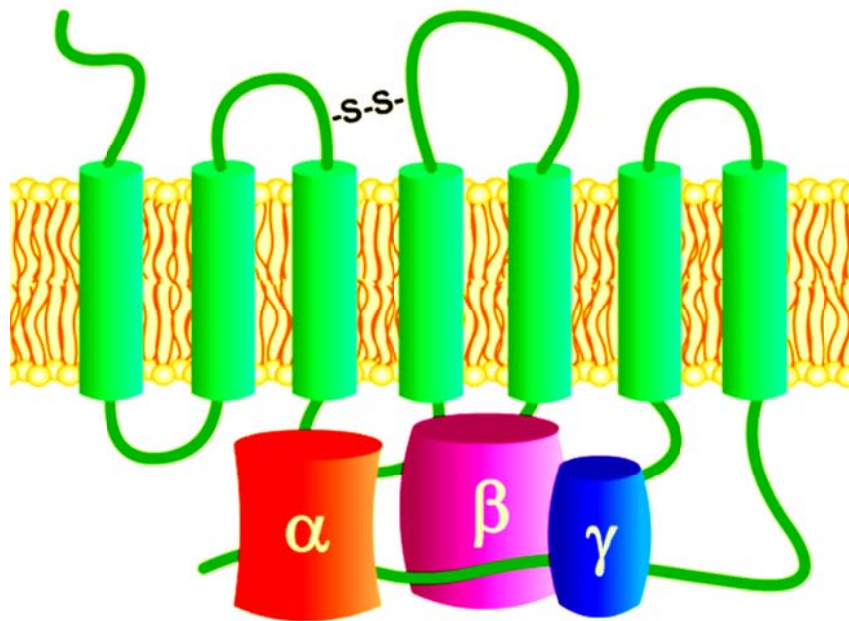
Figure 1.1 Schematic view of GPCR structure, associated with the trimeric guanine-nucleotide binding protein at the cytosolic side of the membrane

The GPCRs' very simple, but elegant mechanism of linking the presence of an extracellular signalling molecule to an intracellular response has proven to be extremely successful during evolution. Thus, by the means of repeated gene duplication, recombination and point mutations over time, nowadays GPCRs are abundant in most animal organisms. Consequently, all known amino acid sequences of GPCRs can be divided into different subfamilies. Based upon the degree of sequence homology and functional similarity, all known GPCRs are divided into different subfamilies: Family A receptors are related to the "light receptor" rhodopsin and the β_2-adrenergic receptor, family B receptors are related to glucagon receptors, family C receptors are related to the metabotropic glutamate receptors, family D receptors (STE2 receptors) are related to yeast pheromone receptors, family E receptors (STE3 receptors) are also related to yeast pheromone receptors and family F comprises four different cyclic adenosine monophosphate (cAMP) receptors in Dictyostelium discoideum [5]. Some families in this A-F classification do not exist in humans. For example, class D and E are fungal pheromone and cAMP receptors, and class F contains archaebacterial opsins. In general the mammalian GPCRs have been grouped into three

classes A, B and C excluding the subfamily IV in class A comprising invertebrate opsin receptors [6].

The family A of receptors, which comprises the experimentally well characterized rhodopsin/β_2-adrenergic receptors, contains 90% of all GPCRs and is by far the largest and the most studied. The overall homology among all type A receptors is low and restricted to a number of highly conserved key residues. The high degree of conservation among these key residues suggests that they have an essential role for either the structural or functional integrity of the receptors. In addition, class A GPCRs often contain two conserved cysteine residues, which link the extracellular end of TM3 and the extracellular domain by a disulfide bridge, as well as two conserved motifs, i.e. the Arg in the Asp-Arg-Tyr E(D)RY motif at the cytoplasmic side of transmembrane segment (TM3) and the NPxxY(x)5,6F motif in TM7, that might have a prerequisite role in the physiological function [1]. Only for class A, crystal structures of four GPCRs are known providing detailed molecular information on these receptors. A sequence alignment of GPCRs with known tertiary structure reveals the E(D)RY and NPxxY(x)5,6F motifs, as well as a conserved CWxP motif in TM6 involved in GPCR activation ("toggle switch residues"). Common to class A GPCRs are also glycosylation sites at the N-terminus, palmitoylation sites after TM7 and phosphorylation sites in the C-terminus.

G proteins transmit extracellular signals from GPCRs to downstream effector proteins, which then cause further rapid changes in intracellular responses through signalling molecules such as cAMP, cGMP, inositol phosphates (IPs), diacylglycerol (DAG), arachidonic acid and cytosolic ions. According to the classification of the heterotrimeric G proteins, GPCRs are classified into four families: G_s-, G_i-, G_q- and G_{12}-linked receptors. In most cases, ligand-bound GPCRs activate downstream effectors such as adenylyl cyclase (AC) and phospholipase Cβ (PLCβ) through the Gα and G$\beta\gamma$ subunits [7]. These family-wide characteristics allow to predict structures and functions of other GPCRs based on information gathered from known GPCRs.

1.2   Adenosine Receptors

Adenosine is formed from ATP, the universal energy molecule in the animal and plant kingdoms. In addition to its role in cellular energy metabolism, adenosine acts in mammalian tissues as a signal molecule to produce a broad spectrum of physiological effects through cell signalling. Most of these responses are mediated by the activation of cell surface adenosine

receptors which are members of the guanine nucleotide protein (G protein) coupled receptor family. The adenosine receptors (ARs) are members of the superfamily of GPCRs belonging to the subfamily of rhodopsin-like receptors and thus, show the typical heptahelical structure. The adenosine receptor subtypes in a tissue or isolated cells are characterized by their G protein coupling preference.

Biological functions of extracellular adenosine are mediated by four different membrane-spanning adenosine receptor subtypes; these include the A_1 and A_3 receptor subtypes, which couple to a G protein (G_i) inhibiting the intracellular adenylate cyclase (AC) and thus leading to a decrease of cAMP, and the A_{2A} and A_{2B} adenosine receptors, which couple to a G protein (G_s) that stimulates AC activity and elevates the intracellular cAMP concentration [8]. The four adenosine receptors have been cloned from several mammalian species, including human. There is extensive sequence similarity between species for the A_1, A_{2A} and A_{2B} receptors, whereas A_3 receptors are more variable [9]. Each adenosine receptor has different but overlapping functions. Each of them is unique in pharmacological profile, tissue distribution and binding partners. Coupling to other second messenger systems, e.g. activation of K^+ channels (A_1), or phospholipase C (all subtypes) has been described [10]. Generally, the A_{2B} receptor requires higher concentration of adenosine than other subtypes to be significantly activated. In particular, all of the adenosine receptor subtypes can also be characterized according to the potency of the natural agonist adenosine: in most native systems the rank order of potency for adenosine is as follows: $A_1 \geq A_{2A} \gg A_3 \approx A_{2B}$ [11], i.e. the A_1 and A_{2A} subtypes are high-affinity receptors activated by adenosine in nanomolar concentrations, while the A_{2B} and A_3 receptors are low-affinity subtypes that require high micromolar concentrations for activation. However, in artificial systems with high receptor expression at least the A_3 receptor can also be activated by low adenosine concentrations [12].

Based on the extensive roles of adenosine receptor subtypes in both physiologic and pathophysiologic events, these receptors are becoming important drug targets in the treatment of a variety of diseases because of their key roles in controlling physiological processes. By exploiting the distinguishable pharmacological profiles of the particular receptors there is hope to be able to target a given disease specifically by a selective compound.

Such therapeutic agents under development include drugs for the treatment of central nervous system disorders (e.g. Parkinson's disease), inflammatory diseases, asthma, kidney failure, and ischemic injuries and many other physiopathological states that are believed to be associated with changes in adenosine levels [13] (Figure **1.2**). Similar to other GPCRs, adenosine receptors consist of seven transmembrane helices which accommodate the binding site for ligands. Each helix is constituted of approximately 21 to 28 amino acid residues. The transmembrane helices are connected by three extracellular and three cytoplasmic loops of unequal size of amino acid residues. The N-terminal of the protein is on the extracellular side and the C-terminal on the cytoplasmic side of the membrane.
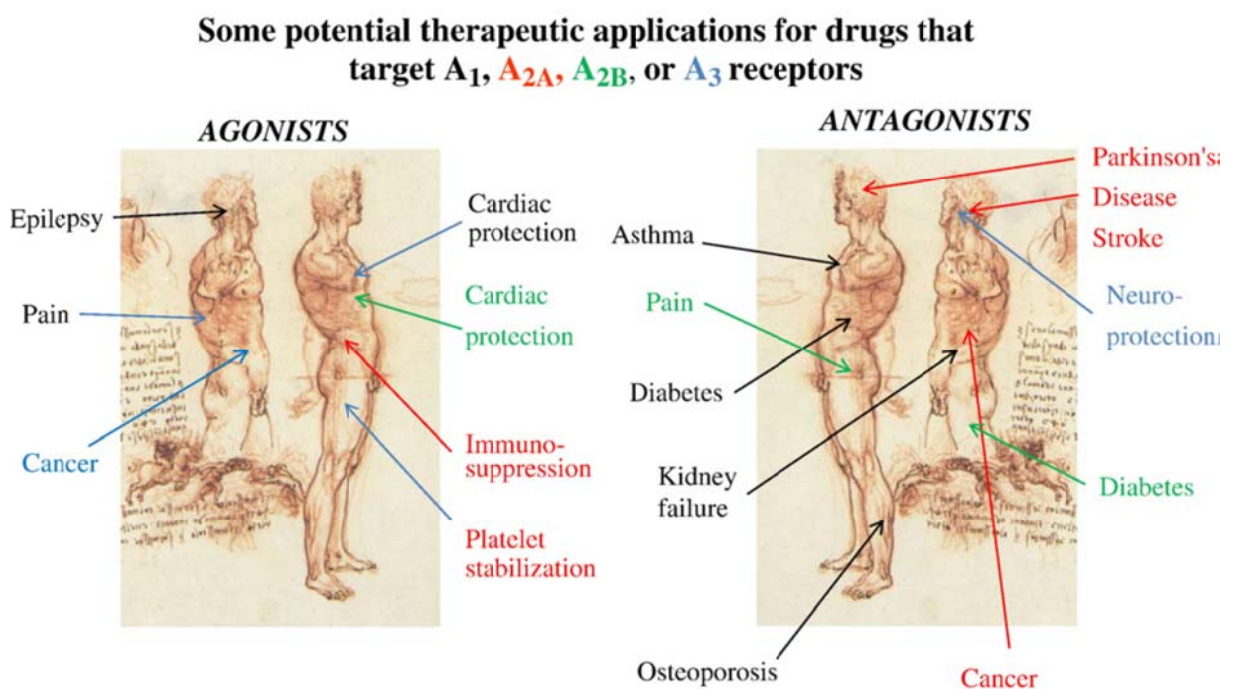
Figure 1.2 Some of the potential uses of drugs that act as agonists (left) and antagonists (right) at the four different adenosine receptors are indicated [14]

1.3   Adenosine A$_{2B}$ Receptor

The adenosine A$_{2B}$ receptor has been generally defined as the "low-affinity adenosine receptor," due to its considerably lower affinity for the endogenous ligand, adenosine, and for some typical agonists, such as 5'-N-ethylcarboxamidoadenosine (NECA), compared to the other adenosine receptor subtypes [15]. Recently, significant advancement has been made in the understanding of the molecular pharmacology and physiological relevance of the adenosine receptors in general; however the knowledge of the A$_{2B}$ adenosine receptor falls

behind that of other receptor subtypes mainly because of the lack of specific agonists for the A_{2B} receptor subtype. As a result, the quantitative tissue distribution of the A_{2B} adenosine receptor is so far unknown. Activation of AC in membranes and accumulation of cAMP in cells is used to characterize the A_{2B} adenosine receptor.

The A_{2B} receptor encodes a protein of 328 to 332 amino acid residues depending on the species. Like with the other adenosine receptor subtypes, there are differences in the amino acid sequences of the A_{2B} receptor among species; for example there is approximately 86% amino acid sequence homology between the rat and human A_{2B} receptors [16] and 45% amino acid sequence homology with human A_1 and A_{2A} receptors. For closely related species, e.g. rat and mouse, the A_{2B} receptors share 96% amino acid sequence homology. The highest degree of identity in amino acid sequences between A_{2B} receptors of different species is found in the transmembrane domains.

The proposed 3D-protein structure of A_{2B} receptors is the typical one of GPCRs, i.e. seven transmembrane domains connected by three extracellular and three intracellular loops, and flanked by an extracellular N-terminus and an intracellular C-terminus [17]. Since the A_{2B} adenosine receptor shares a high similarity with the A_{2A} adenosine receptor in the primary sequences (Figure **1.3**), the extensive knowledge of A_{2A} adenosine receptors would provide a useful guide for the research on A_{2B} adenosine receptor. For example, many binding partners of A_{2A} adenosine receptor have been discovered, and they might also interact with A_{2B} adenosine receptor.
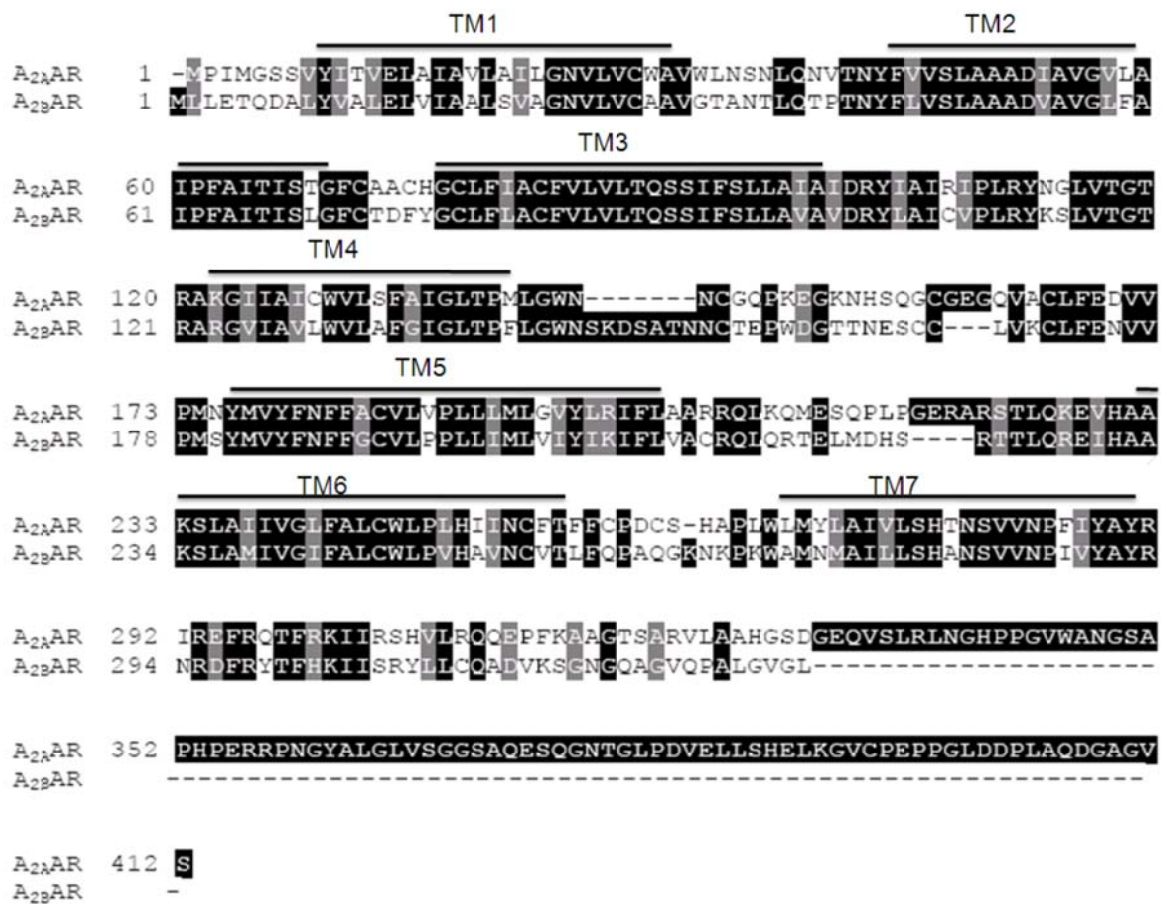
Figure 1.3 Alignment of the primary amino acid sequences of the human A_{2A} and A_{2B} adenosine receptor subtypes in one-letter-code. Domains presumably spanning the membrane are indicated by bars and labelled accordingly. Black-background indicates identity among amino acid residues, while closely similar amino acid residues are highlighted grey. Dashed lines represent gaps which were introduced to optimize the degree of alignment

The second extracellular loop of the human A_{2B} adenosine receptor contains two potential N-glycosylation sites (Figure **1.4**). However the functional role of glycosylation in adenosine receptors is still unknown. So far, the crystal structure of the A_{2B} adenosine receptor has not yet been experimentally elucidated. Due to the fact that selective agonists for the A_{2B} adenosine receptor were lacking in the past decades, the functional significance of this receptor is not fully understood despite intensive experimental efforts. Therefore this work contributes to a deeper understanding of the adenosine A_{2B} receptor by using theoretical methods to link experimental evidence from various sources to yield a more detailed, consistent picture of the adenosine A_{2B} receptor.
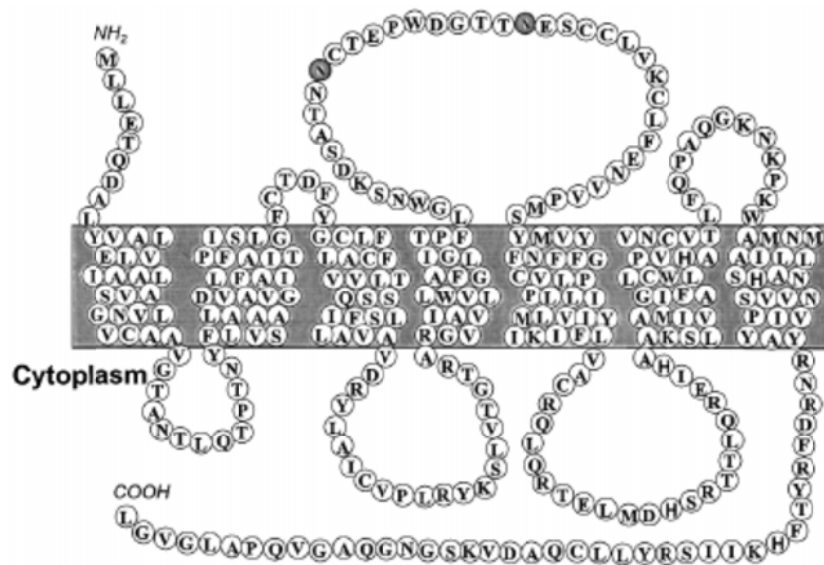
Figure 1.4 Proposed scheme of the human A_{2B} receptor. The receptor is drawn according to the seven-membrane spanning motif common to the G protein-coupled receptor superfamily. Possible sites of N-linked glycosylation on the second extracellular loop are highlighted [18]

1.4   Therapeutic Applications of the A_{2B} Receptor Ligands

Due to the widespread occurrence of the adenosine A_{2B} receptor in diverse tissues, it is a target for a large number of therapeutic applications. In particular, since adenosine plays an important role in the pathophysiology of asthma, the adenosine A_{2B} subtype may serve as a novel drug target for the treatment of this disease [19] [20]. In addition, an A_{2B} selective antagonist was found to prevent the development of pulmonary inflammation and airway fibrosis in the lungs. All this evidence points to an important role for adenosine A_{2B} receptors in the pathophysiology of lung diseases and suggests that this receptor might become a key player in the therapy of lung diseases [21]. Thus treatment of asthma with selective A_{2B} adenosine receptor *antagonists* is proposed to be a therapeutic approach for asthma due to their bronchodilatory and anti-inflammatory effects. Besides, the therapeutic benefit of A_{2B} antagonists includes the treatment of type-II diabetes, Alzheimer's disease and many other diseases [22].

In particular, Interleukin-6 (IL-6) is involved in many different physiological and pathophysiological processes including inflammation. Inteleukin-6 is another cytokine whose production may be regulated via A_{2B} adenosine receptors. Fiebich et al. [23] have shown that NECA induces an increase of both IL-6 mRNA and synthesis of the respective protein product in human astroglioma cells. Increasing evidence suggest that elevated IL-6 levels

plays a role in the pathogenesis of Alzheimer's disease [24]. Thus, the selective antagonists at A_{2B} adenosine receptors, may help to control IL-6 levels and thereby of Alzheimer's disease.

On the other hand, several remarkable therapeutic applications have been proposed for the employment of adenosine A_{2B} receptor **agonists**. A critical function of adenosine signalling is angiogenesis which is the multi-step process of sprouting new capillaries from pre-existing blood vessels. Angiogenesis is involved in both physiological and pathological events. It plays an important role in physiological conditions such as embryonic vascular development and differentiation, female reproductive tract renewal, and organ regeneration [25].

It has been shown that the adenosine A_{2B} receptor is known to induce angiogenesis, to reduce vascular permeabilisation and to increase anti-inflammatory cytokine levels. Thus adenosine A_{2B} receptor selective agonists are proposed for the treatment of septic shock, cystic fibrosis, and cardiac, kidney and pulmonary diseases associated with hyperplasia [26]. Furthermore, adenosine, through A_{2B} adenosine receptor, can exert long-term control over glycogen levels in primary cultures of mouse cortical astrocytes and might therefore play a significant role in pathophysiological processes involving long-term modulation of brain-energy metabolism [27]. In addition, there is evidence of a probable involvement of adenosine A_{2B} receptor in the growth and development of some tumours thus adenosine A_{2B} receptors have been proposed as targets to control cell growth and proliferation in a human breast cancer cell line [28]. Consequently, selective and potent agonists or antagonists at the adenosine A_{2B} receptor subtype are needed for therapeutic intervention and could be useful for the treatment of several diseases.

1.5 Adenosine A_{2B} Receptor Agonists

Because of the widespread distribution of A_{2B} adenosine receptors and the involvement of this receptor subtype in important (patho)-physiological processes both in peripheral tissues and in the central nervous system, many efforts have been carried out in order to identify potent and selective A_{2B} ligands yielded with noteworthy therapeutic potential. However, the lack of highly selective agents has hampered efforts to better characterize the adenosine A_{2B} receptor subtype and consequently to fully define its therapeutic potential. NECA (**1**), a non-selective agonist, is currently considered to be one of the most potent agonists at the adenosine A_{2B} receptor, with an EC_{50} of 140 nM [29] expressed in CHO cells and is the most frequently used ligand to activate this subtype. In order to identify selective and high affinity

agonists for the adenosine A_{2B} receptor many efforts have been devoted to modify the purine ring and ribose moiety of the adenosine. Nucleoside-based agonists are the result of modifying the endogenous ligand, adenosine, by substitution at the N^6-, and C_2-positions of the purine heterocycle and/or at the 5′-position of the ribose moiety. The various substitutions at these positions are designed to increase metabolic stability in biological systems, binding specificity and/or affinity at different adenosine receptor subtypes. In consequence, equally and more selective NECA derivatives (**2**), for the adenosine A_{2B} receptor were obtained. These compounds have EC_{50} values ranging from 82 to 450 nM for the adenosine A_{2B} receptor and showed selectivity towards the other adenosine receptor subtypes [30].

A major invention resulting in an improved affinity and selectivity for the A_{2B} receptor was achieved with the discovery of a new series of non-adenosine derivatives. Substituted 2-thio-4-aryl-3,5-dicyano-6-aminopyrimidine derivatives were claimed to behave as potent non-nucleosidic agonists for adenosine receptors [31]. Recently, a new adenosine A_{2B} receptor agonist 2-[6-amino-3,5-dicyano-4-(4-hydroxyphenyl)pyridin-2-ylsulfanyl]acetamide BAY-606583 [32] (**3**), was patented by Bayer HealthCare and was used to study the cardioprotective function of A_{2B} receptors [33]. This compound is very selective for the adenosine A_{2B} receptor with an EC_{50} value of 3–10 nM for the human A_{2B} receptor and EC_{50} values > 10 μM for the A_1, A_{2A} and A_3 receptor subtypes (Figure **1.5**), characterized by CHO cells in a gene-reporter assay expressing recombinant human receptors in high density [34].

1

NECA [29]
hA_1 = 6.8 nM
hA_{2A} = 2.2 nM
hA_{2B} = 140 nM
hA_3 = 16.0 nM

2

NECA derivative [30]
hA_1 = 1050 nM
hA_{2A} = 1550 nM
hA_{2B} = 82 nM
hA_3 > 5000 nM

3

BAY-606583 [32]
hA_1 > 1000 nM
hA_{2A} > 1000 nM
hA_{2B} = 3-10 nM
hA_3 > 1000 nM
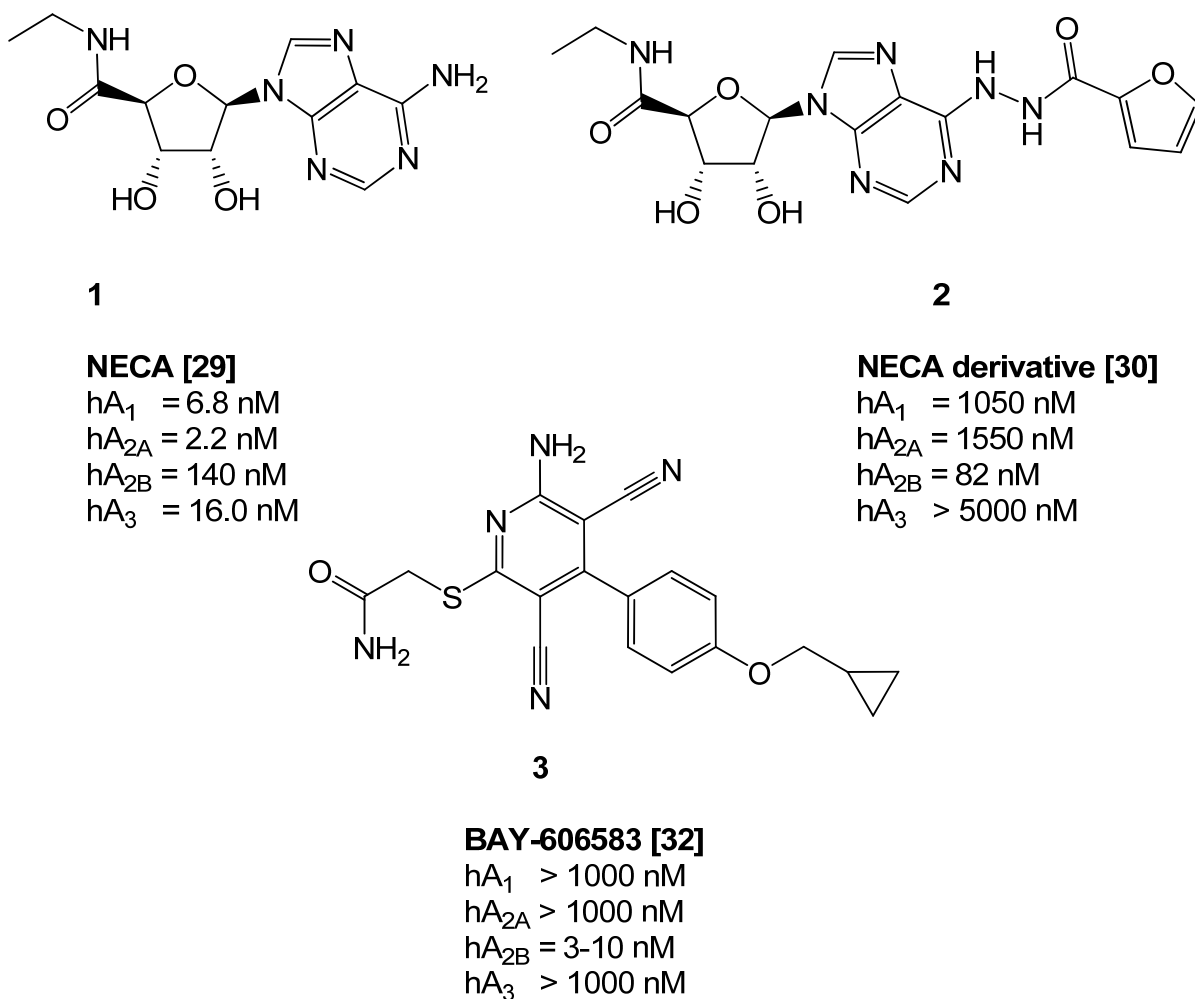
Figure 1.5 The chemical structures of nonselective agonist (NECA) and selective agonists (a substituted NECA derivative, and BAY-606583) for the adenosine A_{2B} receptor

1.6 Adenosine A_{2B} Receptor Antagonists

In contrast to agonists, which are mostly the derivatives of the physiological agonist, adenosine A_{2B} receptor antagonists are diverse in structure. A_{2B} antagonists can be divided into two classes of compounds, xanthine and non-xanthine derivatives. Between these types of compounds, the best results were initially achieved with the xanthine and the pyrrolopyrimidine scaffolds.

1.6.1 Xanthine Antagonists

Extensive research on the adenosine receptor subtypes (A_1, A_{2A} and A_3) showed that xanthines contain a promising core structure, modification of which led to the identification of selective antagonists for these receptor subtypes. Therefore, initial efforts to develop

selective antagonists for the adenosine A_{2B} receptor is focused on this class of compounds. The first adenosine receptor antagonists identified were the naturally occurring xanthines caffeine [35] (**5**), and theophylline [36] (**4**), which is used therapeutically for the treatment of asthma. These compounds are of weak affinity and thus, are non-selective at the adenosine receptor subtypes and theophylline has a narrow therapeutic window. Thus identification of selective antagonists for the adenosine A_{2B} receptor is desirable. Therefore, similar to agonists, structure-activity relationships (SAR) of the xanthines have been extensively studied in an attempt to improve their potency and selectivity at adenosine receptors [37].

Alkylxanthines are the classical antagonists for adenosine receptors and have considerable potency at the adenosine A_{2B} receptor subtype. Following further structural exploration of the xanthine moiety by several groups, the discovery of 8-phenylxanthines as selective A_{2B} adenosine receptor antagonists was made. Among these 8-phenylxanthine derivatives, p-cyanonilide MRS-1754 (**6**), of Jacobson et al. [38] displayed high affinity for the human adenosine A_{2B} receptor (K_i =1.97 nM) and 210-, 260-, and 290-fold selectivity versus A_1, A_{2A} and A_3 adenosine receptor subtypes. However, this compound is not metabolically stable. Consequently, Zablocki et al. [39] used MRS-1754 as a lead compound to synthesize a series of metabolically more stable analogs. Within this series, CVT-5440 (**7**) was identified by high selectivity and an affinity of 50 nM for the human adenosine A_{2B} receptor. Furthermore, a negatively charged compound PSB-1115 (**8**) of Müller et al. [40] was found to display one of the most selective compounds of this family, exhibiting a K_i value of 53.4 nM at the human A_{2B} adenosine receptor and selectivity versus rat A_1 adenosine receptors (41-fold) and versus the other human adenosine receptor subtypes (A_{2A} > 400-fold and A_3 > 180-fold). This compound is highly water soluble due to its sulfonate functional group.

Several heterocycles, such as pyrazole, isoxazole, pyridine and pyridazine linked by different spacers (substituted acetamido, oxyacetamido and urea moieties) at the 8-position of the xanthine nucleus were investigated, e.g. Baraldi's group evaluated a series of 8-heterocyclic substituted xanthines as antagonists for the adenosine A_{2B} receptor subtype. The 5-pyrazolyl class resulted in a lead compound MRE-2029F20 (**9**), that has high affinity and selectivity for the adenosine A_{2B} receptor [37]. In addition, PSB-603 (**10**), of Müller et al. with high potency and specificity across species, including rodents and humans, was demonstrated to possess excellent A_{2B} affinity and promising selectivity which displayed a K_i value of 0.553 nM for binding to human A_{2B} adenosine receptors. A selective and high affinity radioligand, [^{3}H]

PSB-603 was prepared that can be a useful tool in further characterization of the adenosine A_{2B} receptor subtype [41] (Figure **1.6**).

4

Theophylline [36]
hA_1 = 6920 nM
hA_{2A} = 6700 nM
hA_{2B} = 9070 nM
hA_3 = 22,300 nM

5

Caffeine [35]
hA_1 = 10,700 nM
hA_{2A} = 9,560 nM
hA_{2B} = 10,400 nM

6

MRS-1754 [38]
hA_1 = 403 nM
hA_{2A} = 503 nM
hA_{2B} = 1.97 nM
hA_3 = 570 nM

7

CVT-5440 [39]
hA_1 > 10,000 nM
hA_{2A} > 10,000 nM
hA_{2B} = 50 nM
hA_3 > 8,000 nM

8

PSB-1115 [40]
hA_1 > 10,000 nM
hA_{2A} > 10,000 nM
hA_{2B} = 53.4 nM
hA_3 > 10,000 nM

9

MRE-2029F20 [37]
hA_1 = 200 nM
hA_{2A} > 1000 nM
hA_{2B} = 5.5 nM
hA_3 > 1000 nM

10

PSB-603 [41]
hA_1 > 10,000 nM
hA_{2A} > 10,000 nM
hA_{2B} = 0.553 nM
hA_3 > 10,000 nM

Figure 1.6 The chemical structures of some nonselective antagonists (theophylline and caffeine) and selective antagonists (MRS-1754, CVT-5440, PSB-1115, MRE-2029F20 and PSB-603) for the adenosine A_{2B} receptor

1.6.2 9-Deazaxanthines

In the xanthine family, 9-deazaxanthines (pyrrolo[2,3-d]pyrimidinones) were initially investigated by Grahner et al. and Hayallah et al. as antagonists for the A_1 and A_2 adenosine receptors [42] [40]. The authors observed that the structure-activity relationships of 9-deazaxanthines are similar to those of xanthine derivatives and also noticed an increased selectivity over A_1 adenosine receptor. In addition, they concluded that the xanthines and 9-deazaxanthines bind in the same mode to the adenosine receptors, and thus, they have similar structure-activity relationships. Furthermore, the 9-deazaxanthine derivative [43] (**11**), with a meta-fluoro substitution on the pyrazole ring has the same affinity as the direct xanthine analog. However, the meta-CF_3-substituted derivative displayed a lower affinity for the A_{2B} adenosine receptor but good selectivity. Vidal et al. have identified a series of 8-phenyl-9-deazaxanthines that have a sulfonamide linker at the para-position of the phenyl group, and many compounds exhibited good A_{2B} adenosine receptor affinity [44]. For instance, compound (**12**) of the above series showed 6 nM affinity for the A_{2B} adenosine receptor and displayed good selectivity versus A_1 and A_3 receptor subtypes. Recently, Carotti et al. have presented and evaluated several 9-deazaxanthines that have a piperidine substituent [45]. Among the compounds tested, compounds (**13**) (5.5 nM) and (**14**) (11 nM), respectively, displayed both high affinity and selectivity for the A_{2B} adenosine receptor. Overall the 9-deazaxanthines afforded similar SAR to the parent xanthines with respect to A_{2B} adenosine receptor affinity (Figure **1.7**).

11 [43]

hA$_1$ = 170 nM
hA$_{2A}$ = 75 nM
hA$_{2B}$ = 13 nM
hA$_3$ = 50 nM

12 [44]

hA$_1$ = 370 nM
hA$_{2B}$ = 6 nM
hA$_3$ = 950 nM

13 [45]

hA$_1$ = 660 nM
hA$_{2A}$ = 3465 nM
hA$_{2B}$ = 5.5 nM
hA$_3$ = 990 nM

14 [45]

hA$_1$ > 1000 nM
hA$_{2A}$ > 10,000 nM
hA$_{2B}$ = 11 nM
hA$_3$ > 1000 nM
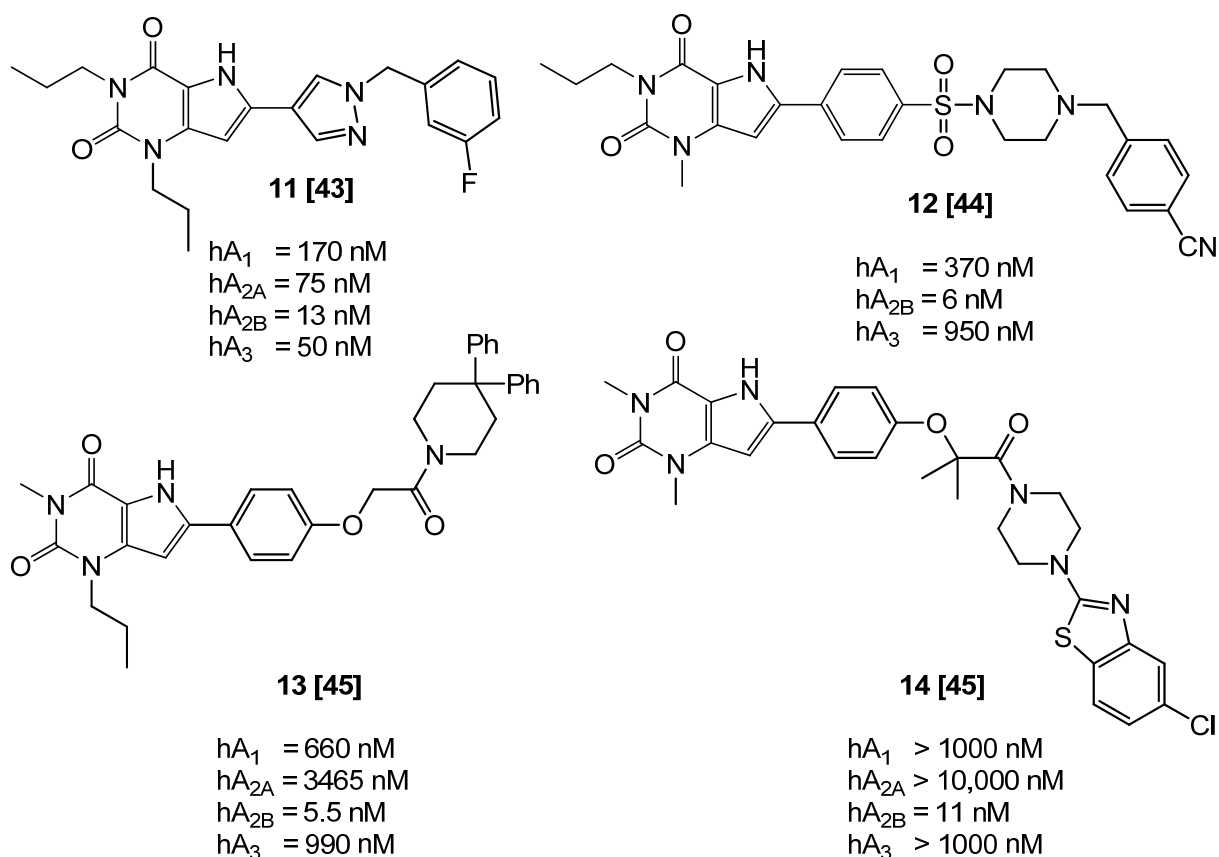
Figure 1.7 The chemical structures of selected deazaxanthines as antagonists for the adenosine A$_{2B}$ receptor

1.6.3   Non-xanthine Antagonists

In order to identify highly potent and selective A$_{2B}$ ligands, a large number of non-xanthine structures have been screened to search for adenosine receptor antagonists. Therefore, numerous classes of heterocycles were identified as antagonists at the adenosine A$_{2B}$ receptor and other receptor subtypes as well. SAR of those non-xanthine heterocycles has been extensively studied and a number of highly potent and selective antagonists have been obtained.

Two series of compounds, 2-aminopyridines and 2-aminopyrimidines, were published as A$_{2B}$ adenosine receptor antagonists. From these series of compounds, Vidal et al. recently published, a novel series of N-heteroaryl-4'-(2-furyl)-4,5'-bipyrimidin-2'-amines, as A$_{2B}$ adenosine receptor antagonists. In particular, the 2'-amino-(3-pyridyl) derivative LAS38096 (**16**) has an A$_{2B}$ affinity of 17 nM and has very good selectivity. In addition, LAS38096, which represents the lead for this series, was capable of inhibiting A$_{2B}$ adenosine receptor-

mediated NECA-dependent increases in intracellular cAMP, with IC_{50} values of 321 nM and 349 nM in cells expressing human and mouse adenosine receptors, respectively [46].

Adenine derivatives have been explored as adenosine receptor antagonists by several research groups [11] [47]. Modifying pyrrolopyrimidines resulted in an even more potent antagonist with a decent selectivity: Scientists at OSI Pharmaceuticals have shown that 2-phenyl-7-deazaadenines (pyrrolopyrimidines) display good A_{2B} adenosine receptor affinity, such as OSIP-339391 (**15**) which had an affinity of 0.5 nM toward the human adenosine A_{2B} receptor and had a selectivity of greater than 70-fold selective with respect to the human A_1, A_{2A}, and A_3 receptors [48] (Figure **1.8**).

15

OSIP339391 [48]
hA_1 = 37 nM
hA_{2A} = 328 nM
hA_{2B} = 0.5 nM
hA_3 = 450 nM

16

LAS38096 [46]
hA_1 > 1000 nM
hA_{2A} > 2500 nM
hA_{2B} = 17 nM
hA_3 > 1000 nM

17

ZM241385 [49]
rA_1 = 255 nM
rA_{2A} = 1.78 nM
hA_{2B} = 16.5 nM
hA_3 = 3090 nM

18

LUF5452 [49]
rA_1 = 7.1 nM
rA_{2A} = 5.4 nM
hA_{2B} = 9.9 nM
hA_3 = 1450 nM
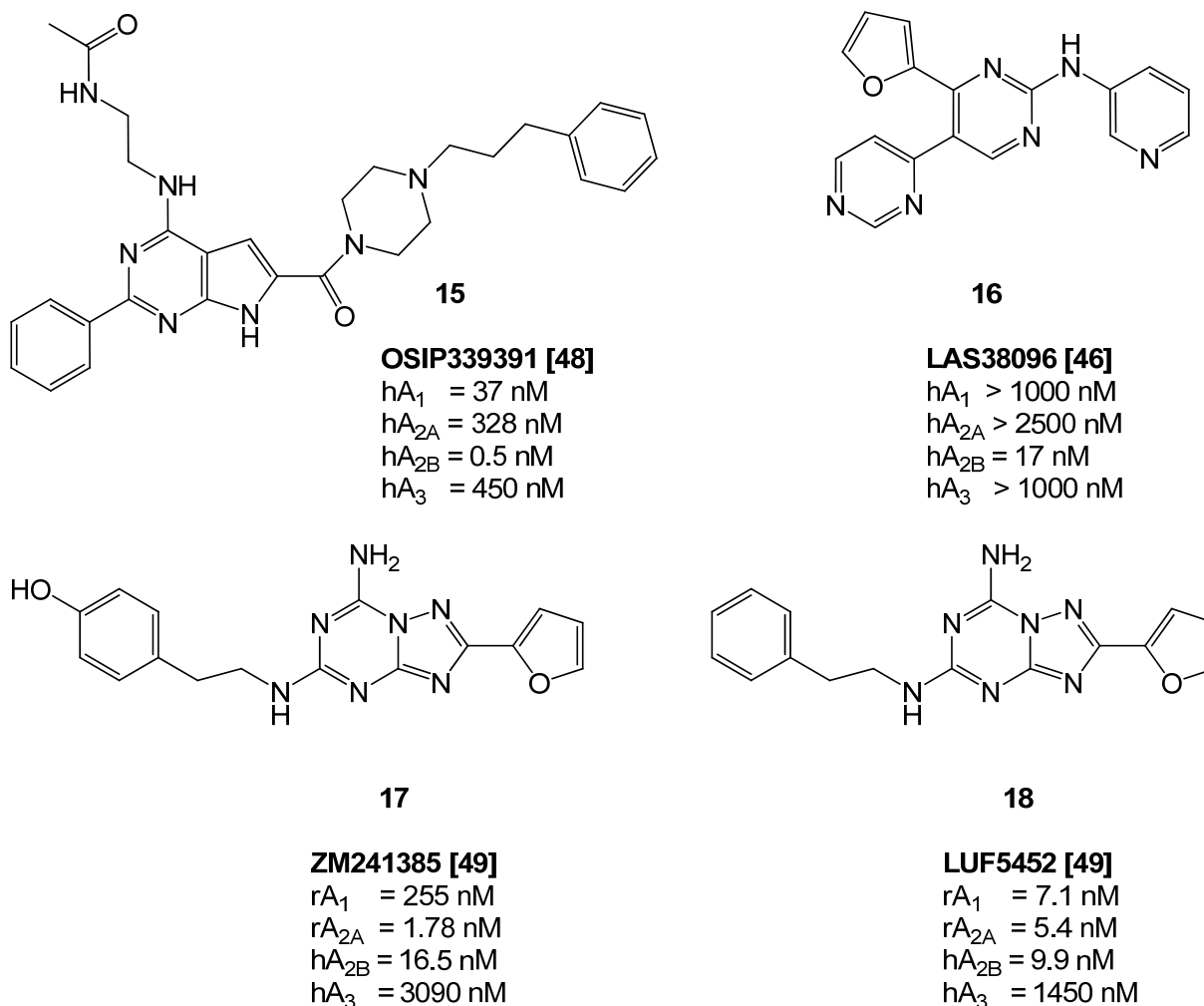
Figure 1.8 Chemical structures of some nonxanthine antagonists for the adenosine A_{2B} receptor

1.6.4   Triazolotriazine Antagonists

One of the most attractive bicyclic cores is represented by the triazolotriazine nucleus, which led to the discovery of ZM241385 (**17**). ZM241385, an excellent radioligand for A_{2A} receptors, is slightly (10-fold) selective for the adenosine A_{2A} versus the A_{2B} receptor subtype [49], it had a K_i value of 16.5 nM at A_{2B} receptors in radioligand binding studies on Chinese hamster ovary cells expressing human A_{2B} receptors. Elimination of the 4-hydroxyl group on the phenyl ring of ZM241385, yielding LUF5452 (**18**), resulted in a slightly improved affinity for the A_{2B} and A_3 adenosine receptors and increased affinity for the adenosine A_1 receptor. The affinity of this compound for the adenosine A_{2A} receptor, on the other hand, was reduced indicating that the hydroxyl group contributes to increasing adenosine A_{2A} receptor selectivity (Figure **1.8**).

1.7   Progress on A_{2B} Receptor Research

Despite the great deal of interest in GPCRs, progress in obtaining X-ray structures has been slow, due to challenges involved in GPCR expression, purification, and crystallization. In view of this, the knowledge of the 3D structure of adenosine receptors could be of great benefit in the process of structure-guided drug design. Consequently, since the first crystal structure of a GPCR had been solved in 2000, namely that of bovine rhodopsin [50], many efforts have been undertaken in the field of GPCR modelling, and especially homology modelling studies have been performed. Ivanov et al. [51] described a model of the human adenosine A_{2B} receptor and predicted binding modes for xanthine derivatives.

In 2004 a refined crystal structure of rhodopsin was published [52] and in 2007 the crystal structure of a second GPCR, the human β_2-adrenergic receptor, was made available. The latter showed the same typical features as the rhodopsin structures, but presented individual features at the same time [53]. Most recently, the structure of the human A_{2A} adenosine receptor has been determined [54]. As all crystallized GPCRs were in their inactivated ground states harbouring ligands, the general position of the binding site of this family of GPCRs can be located with good confidence in the upper half of the helical bundle (Figure **1.9**). There is a great need for GPCR structure predictions, which computational methods can help fill.

The sequence identity between the human A_{2A} and A_{2B} adenosine receptor subtypes amounts to 56% i.e. the sequence similarity still remains relatively low, although higher than to bovine rhodopsin (23% identity) or to the human β_2-adrenergic receptor (31% identity). Encouraged by the findings of Forrest, Tang and Honig [55] [56] that homology modelling is able to yield models with acceptable accuracy (2 Å RMSD for Cα-trace in trans-membrane regions) already for template sequence identities of 30%, we applied this approach to our protein of interest based on all available templates. Indeed several examples in the literature suggest that homology modelling is a viable route to conduct e.g. screening experiments by high throughput docking [57] [58] [59].

1.8   Aim of the present thesis

The discovery of the adenosine receptor subtype A_{2B} opened up new possibilities for potential drug treatment for a great variety of pathological conditions such as asthma, chronic inflammation, kidney failure, cardiac diseases and Alzheimer's disease. Therefore, much effort is put on investigating the physiological function of the adenosine A_{2B} receptor subtype and on the identification of selective, high affinity ligands (agonists and antagonists) for therapeutic intervention. Therefore, insight into ligand-receptor interaction is of pivotal importance for designing new ligands with therapeutic potential. In order to study these interactions, three-dimensional structural information about the receptor structure can be most helpful. Therefore, besides the generic objective of complementing the laboratory investigations by insights gained with computational tools, the specific aims of the present study are:

- Design and validation of a ground state 3D-model of the A_{2B} adenosine receptor using molecular modelling

- Studying aspects of the activation process induced in the newly created A_{2B} adenosine receptor model by agonist binding

- Virtual screening of potential ligands using the adenosine A_{2B} receptor model

Thus in chapter 2, we created new, improved and refined homology models for the human adenosine A_{2B} receptor based on the crystal structures of bovine rhodopsin (1U19.pdb), of the human β_2-adrenergic receptor (2RH1.pdb) and of the human adenosine A_{2A} receptor

(3EML.pdb) as templates. As the three-dimensional structure of homology models for proteins with a low percentage of sequence similarity to the template protein are inevitably affected with uncertainties, we integrated extra information during construction of the 3D-model. Thus the modelling and validation process was guided by continually matching the modelling results with those from mutagenesis studies and ligand binding assays.
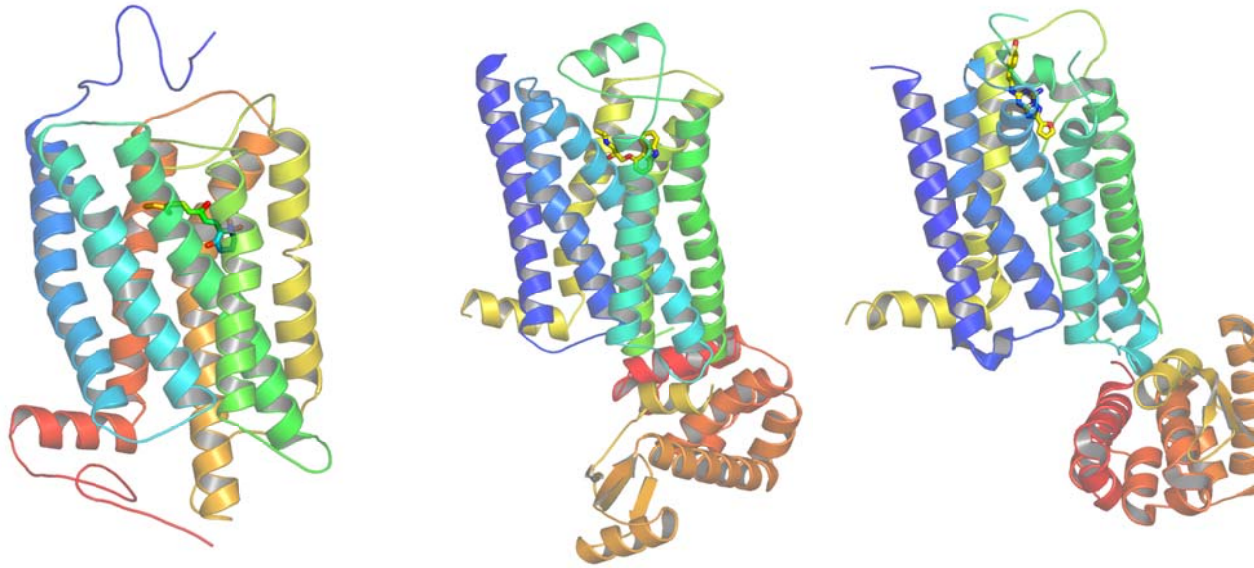
Figure 1.9 X-ray structures of bovine rhodopsin with 11-cis retinal (left), the β_2-adrenergic receptor with carazolol (center) and the adenosine A_{2A} receptor with ZM241385 (right)

In order to address the very first objective, we here describe the methods employed as well as the comparison among the resulting models based on bovine rhodopsin (A_{2B}-I), on the β_2-adrenergic receptor (A_{2B}-II) and on the A_{2A} adenosine receptor (A_{2B}-III). We use well-known A_{2A} and A_{2B} antagonists and agonists as well as mutagenesis data to probe the validity of the models with respect to consistence with experimental evidence from other sources. Additionally, the binding affinity and selectivity of these ligands are investigated.

Chapter 3 focuses on the conformational changes induced by agonist.

In chapter 4 of this work, the A_{2B} homology model based on the adenosine A_{2A} receptor is then used for the search of new antagonists using combined ligand-based approach, flexible

docking, MD simulations and MM-GBSA approaches as well as a database of commercially available chemical entities.

2   Generation of 3D-structure Models

2.1   Introduction

A prerequisite for the understanding of protein-ligand interactions at the molecular level is the knowledge of the 3D structure of the target protein or the ligand-protein complex, respectively. The nature of interacting forces is usually assessed at the level of molecular mechanics or dynamics calculations, which are explained in more detail in section (2.2.6).

X-ray crystallography is the most widely used way to determine high resolution 3D protein structures. Other methods are available to determine 3D structures, but are not always suitable for a biological system for example nuclear magnetic resonance (NMR) has been used to study a wide variety of biological systems. Atomic force microscopy (AFM) can only be used to study the surface features of a protein, and can be utilized to investigate loop flexibility. In addition, electron crystallography can also yield high resolution structures, but because electrons interact more strongly than X-rays this technique can cause mutations or damage to biological systems. Despite of this abundance of techniques, it may be a challenge to characterize structures for a number of reasons. It is difficult to isolate membrane associated proteins from their native environment. The detergent may not interact with a protein in the same way as a cell membrane, causing the protein not to form a functional structure. As cell membranes contain lipids along with cholesterol and other proteins, the target proteins may not orient themselves correctly in the synthetic environment, or form a native structure at all.

Palczewski and his team reported that they had to try multiple solutions because many compounds actually caused structures to collapse or denature [60]. Because of these reasons, crystallization seems to require many years of work before a new crystal structure to be elucidated. Thus homology modelling presents us with a viable alternative route as it is a technique that relies on already existing structural information of another protein and the transfer of this structure to similar amino acid sequences. Due to the immense challenges of the de novo prediction of a protein fold, homology modelling is by far the most important prediction method in this field.

In recent years, the number of fairly reliable 3D-structures of macromolecules (proteins and nucleic acids) determined experimentally (NMR or X-ray) or by homology modelling and deposited in structural databases such as the Protein Data Base (PDB) [61] has been increasing. However, the acquisition of structural information is still a slow and expensive process. Particularly, membrane proteins have been proven difficult to crystallize due to low expression levels and difficulties regarding the crystallization process itself [62]. Therefore, the amino acid sequence of the protein of interest and additional information from the database website are used with different aims such as the prediction of secondary and tertiary structure of the protein and the identification of functional properties.

2.2 Homology Modelling

Homology modelling is the process by which one or more template proteins with known structures, with sequences similar to a protein of interest that lacks a known structure, is used to model the unknown structure. Molecular modelling has become an essential tool in several fields of science, including chemistry, physics, drug discovery, and biochemistry. If the 3D structure of a protein is resolved and the sequence of a related protein of interest is known, the approach of comparative (homology) modelling becomes applicable. In particular, the structural information of the template protein can then be used as a scaffold for the generation of a model of the protein of interest (target protein). Thus knowledge-based approaches were developed to predict the 3D structure of proteins based on experimental data of the 3D structure of homologous reference proteins.

2.2.1   GPCR Template Structures

Bovine Rhodopsin

Since its release in 2000, the 2.8 Å resolution structure of bovine rhodopsin has been successfully used as such a scaffold for the generation of various GPCR homology models [63] [64] [65]. The crystal structure of bovine rhodopsin has been used for 10 years as a template for modelling of GPCRs and because bovine rhodopsin is relatively easy to obtain in high quantities, several crystal structures of its 11 cis-retinal bound

ground state including a retinal Schiff base deprotonated state, have been published during the past decade [50] [66] [67] [68] [52] [69] [70] [71].

Adrenoceptor Structures

The first crystal structure of a nonrhodopsin GPCR for diffusible hormones and neurotransmitters, the human β2-adrenergic receptor bound to the partial inverse agonist carazolol at 2.4 Å resolution was obtained at the end of 2007 using two different approaches to stabilize the receptor protein. In the first approach, an antibody fragment (Fab5) generated in detergent from a monoclonal antibody (Mab5) that binds to the third intracellular loop of the human β2-adrenergic receptor was used to reduce the dynamic nature of this loop, thus facilitating receptor crystallization. The second structure of the human β2-adrenergic receptor was obtained by protein engineering, replacing the IL3 loop with a well-folded soluble protein, T4-lysozyme [53]. Although the position of carazolol in the β2-adrenergic receptor is very similar to that of retinal in rhodopsin, structural differences in the ligand-binding site and other regions highlight the challenges in using rhodopsin as a template model for this large receptor family (Figure **2.1**). With the acquisition of the β2-adrenoceptor's structure the world of GPCR modelling is going to change in particular with respect to more reliable approximations of the ligand binding sites of biogenic amine receptors.
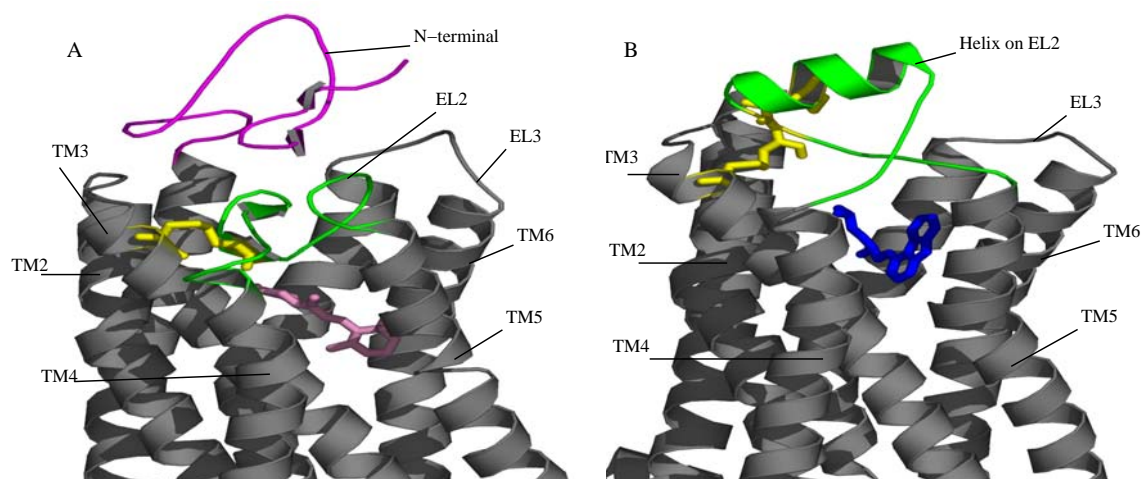
Figure 2.1 Comparison of the extracellular sites of rhodopsin and the β2-adrenergic receptor. (A) EL2 (green) in rhodopsin assumes a lower position in the structure that occludes direct access to the retinal-binding site and forms a small β sheet in combination with the N-terminal region (magenta) directly above the bound retinal

(pink). (B) In contrast, the N terminus is missing from the experimental density in the β_2-adrenergic receptor. EL2 is shown in green and contains a short helical segment and two disulfide bonds (yellow). The intraloop disulfide bond constrains the tip of EL2, which interacts with EL1. The second disulfide bond links EL2 with TM3. The entire loop is held out of the ligand-binding site (carazolol, blue) by a combination of the rigid helical segment and the two disulfide bonds

Another non-rhodopsin GPCR is a mutant version of the 2.7 Å resolution crystal structure of the β_1-adrenergic receptor in complex with the high-affinity antagonist cyanopindolol. The binding mode of cyanopindolol to the β_1-adrenergic receptor and the binding mode of carazolol to the β_2-adrenergic receptor involve similar interactions. A short well-defined helix in cytoplasmic loop two, not observed in either rhodopsin or the β_2-adrenergic receptor, directly interacts by means of a Tyr side-chain with the highly conserved DRY motif at the end of TM3 that is essential for receptor activation. This new adrenoceptor structure was obtained by introducing into the wild-type receptor six point-mutations, whose combination was necessary to stabilize the receptor conformation in a wide range of detergents ideal for crystallization [72].

Adenosine Receptor

Crystallization of a T4-lysozyme fused form of the human adenosine A_{2A} receptor, in complex with a high-affinity subtype-selective antagonist, ZM241385, to 2.6 Å resolution also led to structure determination [54]. Four disulfide bridges are present in the extracellular domain, combined with a subtle repacking of the transmembrane helices relative to the rhodopsin and adrenergic receptor structures.

Bovine Opsin

Sequentially, two crystal structures of ligand-free native bovine opsin have recently been determined [73] [74]. These structures are unique in that they contain some of the structural features that have often been attributed to active GPCR conformations [75].

Generic Features

In general, inactive GPCR structures differ more in the outer TM segments than in the inner TM segments (Figure **2.2**). Furthermore, TM6 and TM7 are the most structurally

conserved helices in inactive GPCR templates, while TM2 and TM5 are the most structurally divergent helices. The extracellular membrane portion of the TMs of the available GPCR templates differs more than their intracellular membrane region. In addition, higher divergence exists in theTM1-4 outer regions of available GPCR crystal structures due to important differences in the mode of binding of different ligands to orthosteric binding pocket sites. In contrast, TM5, TM6, and TM7 exhibited a slightly larger rmsd in the inner membrane side for most of the compared pairs of inactive GPCR structures. This high divergence in the TM5-7 inner parts might be responsible for the recognition of different G proteins, as particularly evident by comparison between the longer TM5-6 helices of the squid rhodopsin and the shorter TM5-6 helices of the bovine rhodopsin. As a result, variations in the individual TM helices revealed by the recent rhodopsin and nonrhodopsin inactive crystal structures appear to affect the ability of a ligand to bind in a correct orientation [76].
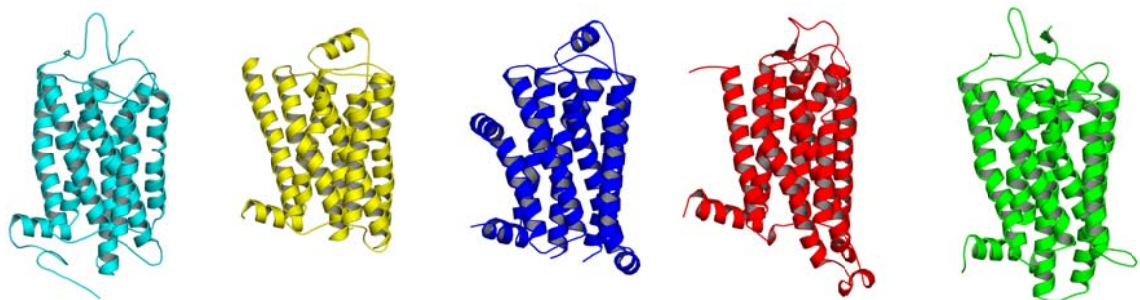
Figure 2.2 Representative inactive GPCR crystal structures. From left to right, bovine rhodopsin, the β$_2$-adrenergic receptor, the β$_1$-adrenergic receptor, the adenosine A$_{2A}$ receptor and opsin (active) are shown in cyan, yellow, blue, red, and green colours, respectively

Concept of This Study

Homology models based on such template structures are supposed to assist a drug discovery process as they offer the possibility to understand ligand-receptor interaction on an atomic level and can bring new stimulus in guiding via database screening methods or de novo design strategies. The steps used to predict the specific role of amino acid residues for the binding of ligands and the regulation of GPCR activity are shown in Figure **2.3**. In detail, the modelling process includes the identification of proteins with known 3D structure that are related to each other and selection of one of

these for the template, identification of structurally conserved regions and structurally variable regions, sequence alignment, geometry optimization and validation of the final structure. The prediction can subsequently be used as guideline for the construction and characterization of point mutations, studies of ligand-receptor interaction, and the design of new leads by application of flexible docking and virtual screening methods.

Based on the three candidate template structures, several variants of a 3D model for the adenosine A_{2B} receptor are to be created. In order to validate the method involved, as well as the models themselves, docking experiments are carried out with well known ligands. As a means to prove the method, these ligands are docked into the crystal structure of the related A_{2A} receptor. For the purpose of testing the models; the approved method is applied to all resulting candidate models. Based on the outcome, the most promising conformation for the subsequent investigation is selected. At the same time, comparison with the A_{2A} results is supposed to point to the amino acid residues responsible for the different pharmacological profiles of both receptor subtypes.
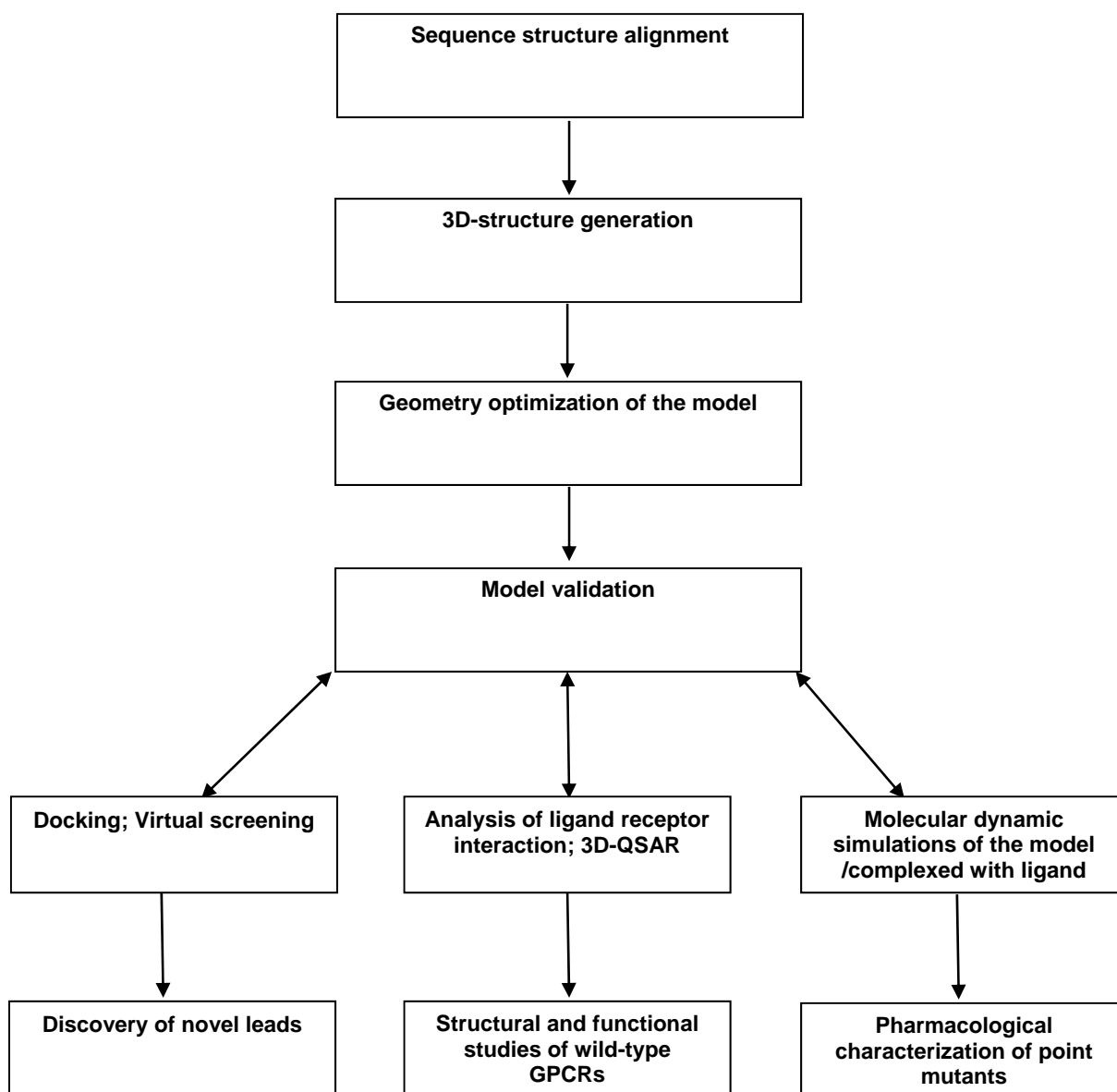
Figure 2.3 Flowchart of steps in homology modelling and possible application of homology models in computational medicinal chemistry and pharmacology

2.2.2   Sequence Alignment

An important step in the homology modelling process is the search for a well suited protein structure as a template for the desired model. Sequence alignment investigations are probably the most common tool to this end. They allow the search for candidate template structures based on sequence similarity to the target sequence. Multiple alignments, i.e. comparisons of several homologous protein sequences allow conclusions about highly conserved, homologous regions and areas of rather insignificant functional residues. In this manner, sequence alignments can be used to find characteristic motifs and conserved residues in protein families and to improve

prediction of secondary structure elements. This information can be used for manually adjusting an automatically created pairwise alignment for an optimal transfer of structured elements/parts.

Commonly automatic sequence alignment tools are used to search for optimal correspondence between the sequences. Most sequence alignment algorithms try to construct the evolutionary conversion of one sequence into another. For this operation homology matrices are used to specify the weight for aligning a particular type of amino acid substitution according to physical and chemical properties and/or statistical and evolutionary probabilities. In cases of different sequence lengths and variations in the locations of conserved regions, gaps are introduced into the alignment. To minimize the number of gaps, a gap penalty function is used.

The original input sequences of the human adenosine receptors and the templates used in this work were retrieved from the Swiss-Prot database [77]. All of these sequence information used for a multiple sequence alignment employing the ClustalW software [78] result in insights about highly and less conserved areas of the target protein. The highly conserved regions are usually related to functionally or structurally important parts of the target protein and therefore have to be found in the template structure. Regions of less conservation are usually not connected to functional or structural importance. Hence, they can be more easily modelled without a template structure. Thus the resulting preliminary alignment was manually refined to incorporate additional experimental evidence and avert gaps within the seven helical segments. Consequently, the alignment was guided by the highly conserved amino acid residues (fingerprint motifs that are shared by the members of this family) including the extracellular disulfide bridge between TM3 and EL2, N1.50, D2.50, the E/DRY motif (D/E3.49, R3.50, and Y3.51), W4.50, the two proline residues P5.50 and P6.50, and the NPXXY motif in TM7 (N7.49, P7.50, and Y7.53) [79]. In this respect is totally consistent with e.g. the multiple alignment of all rhodopsin like sequences published in the GPCR-DB [80]. For the actual alignment used in this study, refer to (Figure **2.4**).
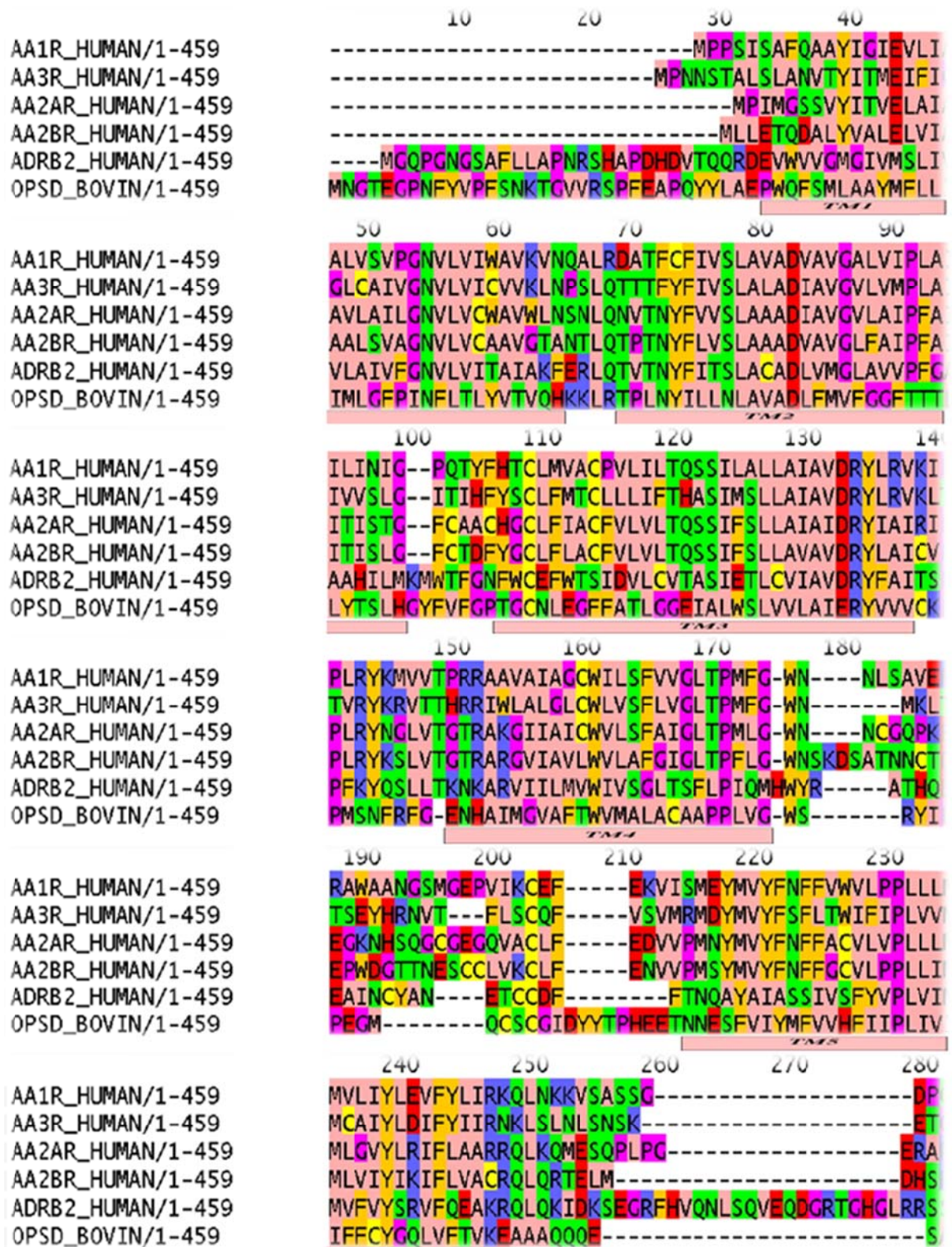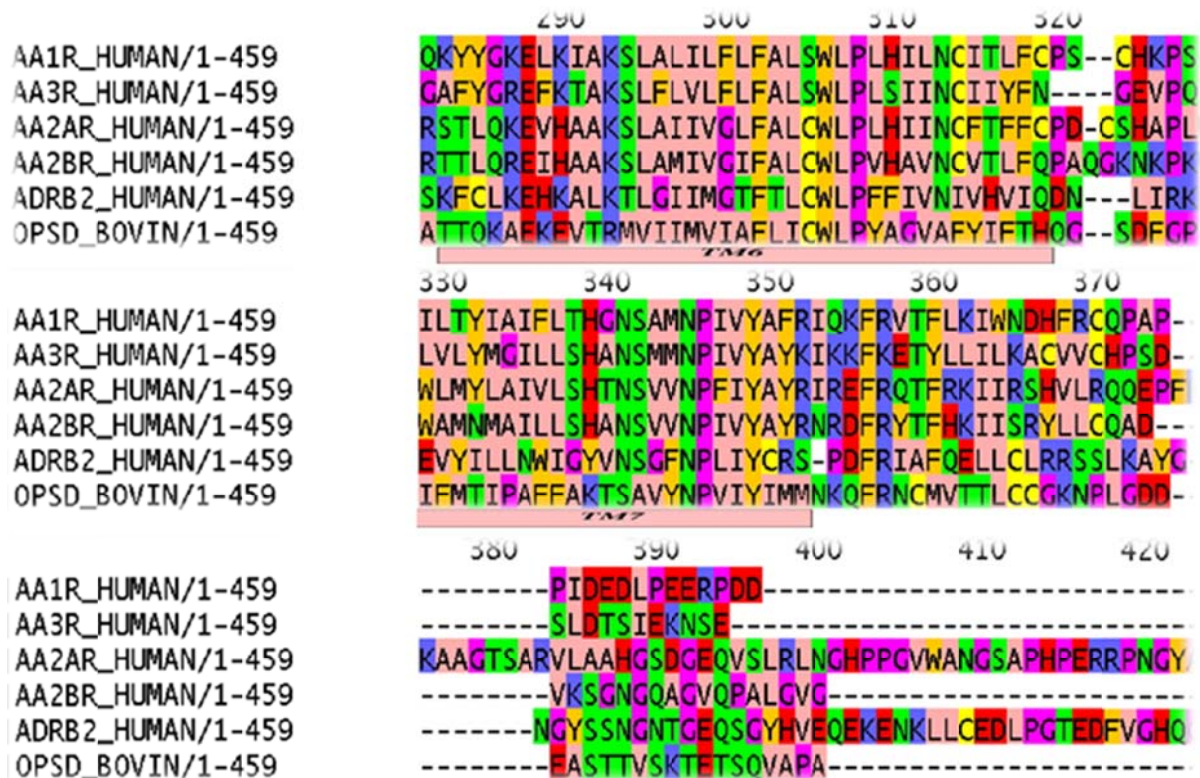
Figure 2.4 Multiple alignment of the human adenosine receptors and the resolved template candidates bovine rhodopsin (POSD_BOVIN) and human β_2-adrenergic receptor (ADRB2_HUMAN) amino acid sequences. Helical parts as evident from the X-ray structures are highlighted and indicated as well

In order to refer to the equivalent residues among different G protein-coupled receptors, we used the numbering system suggested by Ballesteros and Weinstein [81]. The most highly conserved residue in each transmembrane helix was assigned a locant value of 0.50 and this number was preceded by the TM number and followed by the sequence number and the other residues in the helix were given a locant value relative to the sequence number which increases in the direction towards the C-terminal and decreases towards the N-terminal. Information concerning the primary structure of the human adenosine A_{2B} receptor and the subdivision into transmembrane, cytoplasmatic and extracellular domains was obtained from the GPCR Data Bank [82].

2.2.3   3D Structure Creation

Once a reasonable alignment has been found between the template and the target protein, a sequence structure alignment can be carried out in which the backbone atoms of the target protein are arranged identically to that of the template protein. Much more difficult is the generation of non-conserved loop regions that often show little sequence conservation and may diverge in length from the template protein. A common method to obtain coordinates for these regions is carrying out a loop search. Resolved protein structures are searched for a peptide of identical length that can fill the gap in the protein model without introducing large distortions. Alternatively, loops can be generated using de novo strategies (protein threading), where by means of for example simulated annealing energetically favourable loop conformations are generated. The molecular models of the human A_{2B} receptor were generated based on the template structures of bovine rhodopsin, the human β_2-adrenergic receptor and the human adenosine A_{2A} receptor using the homology modelling service Homer [83]. Missing amino sequence parts were replaced by manually inserting glycines to obtain a complete backbone as a first step.

2.2.4   Adding Amino Acid Side-chains

After a sequence structure alignment, structural information is only obtained for the backbone region of the target protein. From statistical analysis of known protein structures it has been observed that amino acid side-chains tend to exist in certain energetically favoured conformations (rotamers). The available conformational space for each side-chain is further reduced by the dependency of the side-chain conformation on the coordinates of the backbone plus neighbouring side-chains. The side-chains still missing were subsequently substituted by the program SCWRL [84] according to the actual target sequence. Additionally, the program allows adopting side-chain placements from the template structure, which is a useful strategy for conserved residues.

2.2.5   System Setup

A particular difficulty with GPCRs in terms of computational complexity relates to the fact that GPCRs are membrane proteins and depend strongly in their conformational stability on their natural surrounding. Hence, the model system of choice would comprise the protein, a membrane patch and layers of water as demonstrated e.g. by

Schlegel et al. [85]. However, we not only intended to create models, but also wanted to study their ligand binding behaviour, therefore we restricted our computations to a system of economic size, which comprised the protein, eventually a bound ligand compound and water caps at the intra- and extra-cellular regions. Thus, the membrane, which would exert most probably non-directed and weak dispersive interactions to the protein, was neglected. We accounted for the limitations inherent to this simplified approach by including experimental evidence where possible.

2.2.6 Energy Minimization and MD Simulations

2.2.6.1 Molecular Mechanics

Molecular dynamics simulation is a valuable tool to study the behaviour of a system in atomic detail that is the position of every atom as a function of time is computed by an algorithm that solves in an iterative fashion Newton's classical equation of motion. In MD simulations force fields are required in order to solve this task as they account for both the (Born-Oppenheimer Approximation) position of nuclei and electrons of each atom considered. Molecular mechanics is one aspect of molecular modelling, as it refers to the use of classical mechanics/Newtonian mechanics to describe the physical basis behind the model and to calculate the potential energy of the system using force fields. This methodology is widely used in several biochemical and biophysical problems, such as conformational analysis of proteins, ligand-receptor interactions and drug design.

2.2.6.2 Force Fields

A force field is a set of parameters and mathematical equations used to describe the properties of atoms and their bonded and non-bonded interactions. The parameters include the definitions of the atomic masses and charges for different atoms as well as the bond lengths, bond angles, and dihedral angles. Together the definitions of the parameters and the equations define the behaviour and potential energy of the system. From a mathematical point of view a force field is a function of potential energy that exclusively depends on the position of the nuclei. The contributions to the potential energy of the molecular system can be subdivided into bonded and non-bonded interactions. Bonded interactions can be further subdivided with regard to the number of particles involved resulting in a term describing bond stretching (two-body

interaction), angle bending (three-body interaction) and a term describing bond rotation (torsion) (four-body interaction). Non-bonded interactions are calculated between all pairs of atoms that are in different molecules or that are in the same molecule but separated by at least three bonds. Non-bonded interactions comprise electrostatic interactions and van der Waals interactions [86].

$$\mathbf{E}_{tot} = \mathbf{E}_{bonds} + \mathbf{E}_{angle} + \mathbf{E}_{dihedral} + \mathbf{E}_{non\text{-}bonded} + \mathbf{E}_{other} \quad \text{(equation 1)}$$

$$\mathbf{E}_{non\text{-}bonded} = \mathbf{E}_{electrostatic} + \mathbf{E}_{van\ der\ Waals} \quad \text{(equation 2)}$$

Where $\mathbf{E}_{other}$ includes terms that are specific for a certain force field

The intramolecular potential energy for bond stretching and angle bending are typically represented by a harmonic potential and the torsion potential is described by a periodic cosine function (equation 1). For calculating the nonbonded interactions the electrostatic interactions are computed based on the Coulomb potential and the Lennard-Jones potential is commonly used for the van der Waals interactions (equation 2).

2.2.6.3   Energy Minimization

A method which minimizes the potential energy is known as energy minimization technique. This technique is used as an optimization of a system's structure to find the local minimum starting from an initial conformation. Energy minimizations result in an optimized arrangement of electrostatic interactions, hydrogen bonding and van der Waals contacts (based on the initial structure). After the sequence structure alignment, the insertion of loop regions and addition of amino acid side-chains, the protein itself is complete in terms of all atoms being present, but there will often remain steric clashes and distorted bonds in the resulting models. Therefore, the goal of an energy minimization is to relax the worst conflicts in the resulting structure and find an energetically more favourable conformation of the system in order to be able to start a simulation.

2.2.6.4 MD Simulations

MD simulations is a powerful method for the validation of a homology model and for obtaining energetically favourable protein model thus allow for structural adaptations within the generated protein model. This technique is also useful for the purpose of generating the global minimum of a protein structure. MD simulations produces a time-dependent ensemble of protein conformations, usually converged to a local energy minimum. The dynamic properties of the trajectory can be analysed to validate the simulation and/or the generated protein model.

In order to carry out an energy minimization, the coordinates of the protein model are required. Based on this information, the potential energy of the system can be calculated thus energy minimization is a prerequisite to later study the protein structure by means of MD simulations thus all models emerging from this procedure were minimized stepwise with respect to the force field energy by using the Amber package [87] (this is a general Molecular Dynamics package to simulate proteins, nucleic acids, sugars and organic molecules) to attain a low energy conformation. The minimization protocol consisted each of 2,400 cycles of the Steepest Descent algorithm followed by 1,400 cycles of the Conjugated Gradient method. Then the three models of the adenosine A_{2B} receptor were subjected to MD simulations at 300 K during 400 ps. The time step of the simulations was 2.0 fs with a cutoff of 10 Å for the non-bonded interactions. The SHAKE algorithm was employed to keep all bonds involving hydrogen atoms rigid. The MD simulations are performed at constant temperature and pressure. During the MD simulations all backbone atoms of the receptor were restrained to their starting positions with a harmonic force constant 2.0 Kcal/(mol $Å^2$).

2.2.7 Model Evaluation

Although all information available has been integrated during the generation of homology models, errors will inevitably occur that reduce the applicability of the models for later purposes i.e. errors in the target-template alignment, errors in loop regions due to lack of structural information and low stereochemical quality. Evaluation takes place in two steps, a formal evaluation and a functional evaluation therefore, the geometrical parameters (bond lengths, bond angles, peptide bond and side-chain ring planarities, chirality, main chain and side-chain torsion angles, and clashes between

non-bonded pairs of atoms) of the created models were evaluated and compared with those obtained for the native structure of the templates using the PROCHECK and PROSAII programs. Although a good stereochemical quality does not guarantee model correctness, it is a prerequisite for a subsequent application of the model. The newly created 3D structures served as receptors for the subsequent docking experiments that are supposed to elucidate the functional validity of the respective models.

2.2.8   Docking Studies

The ability of proteins to bind to another protein or to different ligands in a highly specific manner is an important feature of many biological processes. The characterization of the structure and the energetics of molecular complexes are thus a key factor for understanding biological functions and the energetics often provide the most important and useful link between structure and function of biomolecular systems. Therefore, molecular docking is a key tool in structural molecular biology and computer-assisted drug design. This strategy used to predict the predominant binding mode, and affinity of a ligand with a protein of known 3D structure or homology model. Docking can be used in several ways: for example, to identify possible binding modes for a ligand, and to screen a database [88]. Two aspects are of the most importance for successful computer-aided structure-based drug design: generating protein-ligand configurations (docking), the identification of those binding modes according to the experimental data, and a computational translation of the obtained protein-ligand geometries into approximate estimation of the binding affinity (scoring).

2.2.8.1   FlexX Docking

In molecular docking, one attempts to generate and evaluate a plausible structure of protein-ligand complex. Common to most docking procedures is that only ligand flexibility is considered while the protein receptor is considered rigid. The docking algorithm in FlexX [89] [90] is based on an incremental construction strategy consisting of three phases: In the first phase (base selection), the base fragment of the ligand is identified which is then docked into the active site of the protein (base fragment placement). Finally, the rest of the ligand is then incrementally added to this base fragment placement (complex construction). Upon connecting additional fragments, new interactions are screened and the best partial solutions based on the ranking of a scoring function are hooked up until the ligand is completely constructed.

Ligand flexibility is considered by allowing each fragment to adopt a discrete set of energetically favourable conformations.

The molecular docking of a set of adenosine A_{2A} and A_{2B} antagonists and agonists into a set of receptor models (X-ray structure of A_{2A} and homology models of A_{2B}) was to be performed. Therefore, an automated docking procedure employing the FlexX software and the MD-package Amber were used to create suitable starting structures for subsequent MD simulations of the complexes in an attempt to improve the binding mode and to predict the energetically most favourable binding mode for the respective ligand.

The following outlines our basic strategy in selecting the final conformation of each complex. Firstly, the geometry of the ligands (input for docking program) was optimized by energy minimization using the Amber program. The compounds were automatically docked into the respective binding site, generally yielding several hundred diverse placements of the ligand. Each prediction (i.e. ligand residing in protein binding site) was tested and finally reranked with respect to the force field energy by subjecting the whole system, to an energy minimization. In order to find the most relevant placements, we then performed a clustering analysis, as follows: of all not yet categorized conformations, the most favourable one served as reference for calculating the RMSD to every other conformation. Those conformations with an RMSD of less than 2.0 Å to the current reference conformation where neglected, from the others the one with the lowest value of force field energy became the new reference. This was done until the originally very large set was reduced to only 10-20 diverse binding modes. In our experience it was sufficient to subject only the five most favourable candidates to the time-consuming further analysis of settling the ligand position and estimating the protein-ligand interactions.

Although the interaction energy between the ligand and the receptor may be very sensitive to subtle changes in the binding mode, here a threshold of 2.0 Å was considered appropriate in order to limit the number of conformations needing further analysis, as the dynamic motions during the subsequent MD simulations were supposed to correct minor misplacements. In fact, by crossing over from rigid docking to molecular dynamics we not only switched from the simple empirical scoring function

employed in docking to a more detailed energy function, but also allowed the ligand to accommodate to the protein surrounding and vice versa.

The following procedure for estimating the binding energy comprised a new step of energy minimization (1,500 Steepest Descent steps, followed by 500 of Conjugate Gradient until a convergence of 0.05 kJ mol^{-1} A^{-1} was reached). Then a MD simulations was carried out, i.e. a total of 1 ns were recorded at 300 K, using a distance-dependent dielectric constant of $\varepsilon = 4r$ throughout all simulations in order to account for solvent screening. The MD simulations were performed at 300 K, with a time-step of 1.0 fs. From the latter set of binding modes the candidate with the most favourable binding energy, which at the same time was in agreement with mutagenesis data (Table **2**), was accepted as final placement.

2.2.8.2   Affinity Prediction

The followed strategy in rational drug design depends on whether the 3D structure of the biological target is known or not. If the structure of a target receptor is available, information about the binding-site and principles of protein-ligand interactions can be used to estimate the binding affinity of a given protein-ligand orientation obtained by crystal structure analysis. Accurate and fast scoring is important for both the determination of the correct binding modes from a sample of protein-ligand configurations and the ranking of a large sample of different ligands with respect to their affinity.

If the 3D structure of the target protein is unknown, a good correlation between the experimental and theoretical energies can be used to establish a relationship between molecular structure and biological activity within a series of active compounds. This method does not only explain the relative differences among the observed affinities, but also allows for an affinity prediction of novel compounds [91]. The binding energies between the receptor and the ligand were calculated on the basis of the Linear Interaction Energy approach originally proposed by Åquist and coworkers [92]. Accordingly, the binding free energy is approximated as the difference of the averaged nonbonded energies of the separate ligand and receptor from the nonbonded energy of the receptor-ligand complex: $\Delta G_{bind} = \alpha(\langle E^{elec}\rangle_{bound} - \langle E^{elec}\rangle_{free}) + \beta(\langle E^{vdW}\rangle_{bound} - \langle E^{vdW}\rangle_{free})$, where the nonbonded energy is composed of an electrostatic part (including

polar and nonpolar solvation) as well as a van der Waals part. Both parts may be weighed differently by the factors α and β, which may range from 0.169 to 0.5 in case of α and from 0.016 up to 1.043 for β [93] [94]. The exact values apparently depend on the protein under investigation.

As homology models are being created for lack of structure information, inevitably some uncertainty is inherent to the resulting 3D structures by nature, despite all efforts to compensate for this. Therefore we did abstain from adjusting the parameters α and β such that they would match the experimental binding free energies as closely as possible and did apply $\alpha = \beta = 0.5$, thus neither preferring one nor the other. Therefore, the computed absolute values overestimate the binding affinity at least by a factor of 2-3. Moreover, changes in entropy are not sufficiently taken into account, so that in consequence, the computed interaction energy values cannot be expected to reproduce the experimental binding affinities with numerical exactitude. However, provided that the systematic errors are comparable among the ligands tested, the trend in binding affinity can be assessed by relating our results to observed K_i values via the equation $\Delta G = -RT \ln K_i$, which already would help to distinguish between good and bad ligand candidates.

2.3   Results and Discussion

2.3.1   Homology Modelling

The sequences of all human adenosine receptors were aligned to those of the templates in order to identify the amino acid residues that putatively form the seven transmembrane α-helices of the adenosine A_{2B} receptor. Three homology models were obtained for the adenosine A_{2B} receptor based on published X-ray structures of GPCRs (bovine rhodopsin (1U19.pdb), the β_2-adrenergic receptor (2RH1.pdb) and the human adenosine A_{2A} receptor (3EML.pdb).

Three different models for the adenosine A_{2B} receptor were obtained according to the procedure mentioned in section (2.2.3) using as templates either bovine rhodopsin, yielding the first model A_{2B}-I, an engineered GPCR, the β_2-adrenergic receptor, yielding model A_{2B}-II or the human adenosine A_{2A} receptor, yielding model A_{2B}-III (Figure **2.5**).

The overall sequence identity between bovine rhodopsin and the human A_{2B} receptor amounts to 23%, while that between the β_2-adrenergic receptor and the human A_{2B} receptor amounts to 31%. In contrast, the sequence identity between the human A_{2A} and A_{2B} adenosine receptors amounts to 56%. As stated elsewhere, 30% of sequence identity may be sufficient for creating an acceptable description of the binding site [95]. The mere percentage of sequence identity between target and template, however, is not the only criterion for the final quality of the model. In addition, the coordinates for the helical parts could be transferred to the A_{2B} receptor models A_{2B}-I, A_{2B}-II, and A_{2B}-III with high confidence, as the degree of sequence homology for the TM regions was quite high.

One of the most important anchor points in modelling the individual backbone course of hydrophilic loops is the presence of the disulfide bond between TM3 and EL2, which is highly conserved among all rhodopsin-like receptors [96]. In the obtained models the disulfide bond was formed between Cys78 and Cys171, which was confirmed by mutagenesis studies (S. Hinz, A. Schiedel, C. E. Müller, unpublished results) and corresponds to the Cys110-Cys187 disulfide bond in bovine rhodopsin, the Cys106-Cys191 disulfide bridge in the β_2-adrenergic receptor and the Cys77-Cys166 disulfide linkage in the adenosine A_{2A} receptor respectively. As Figure **2.5** shows, although belonging to the same class, the 3D structures display quite large structural deviations especially in the extracellular and intracellular loops. Therefore the following section will focus on the features of the various templates and the resulting models.
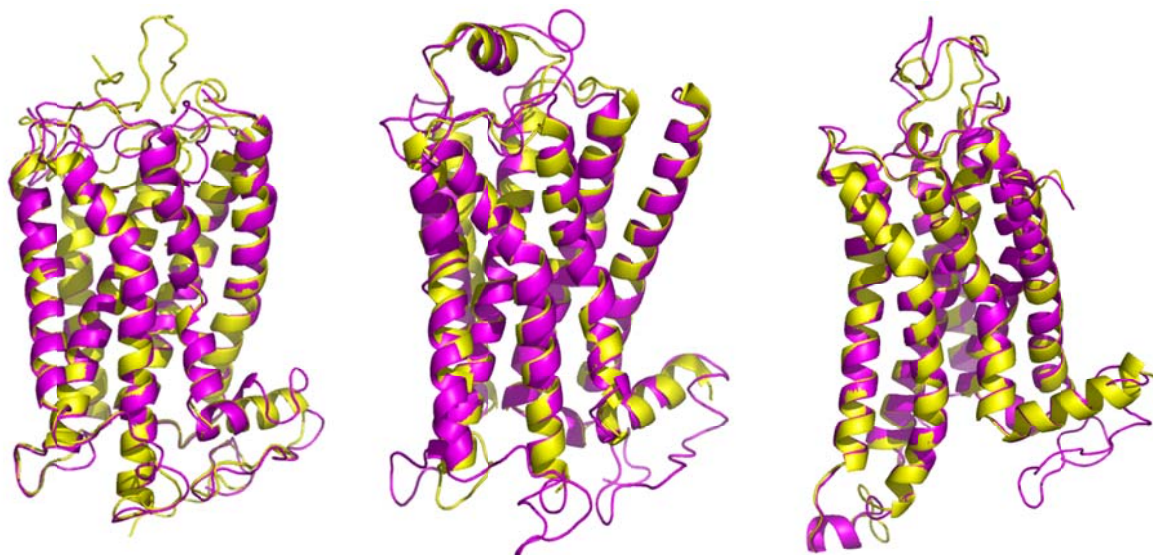
Figure 2.5 The final homology models of the human adenosine A_{2B} receptor (magenta) are shown along with their templates (yellow): The left model, A_{2B}-I, is based on bovine rhodopsin (1U19.pdb), the model in the center, model A_{2B}-II, is based on the β_2-adrenergic receptor (2RH1.pdb), whereas the right one, model A_{2B}-III, is based on the adenosine A_{2A} receptor (3EML.pdb)

2.3.2   Template Description

The most striking difference among the individual template structures is reflected by the resulting models: in the A_{2B}-II model, the extracellular portions of the TM1 and TM3 point away from the center of the receptor, TM4 is twisted away from the center of the receptor, TM5 is closer to the center of the receptor and TM6 is twisted away from the receptor on the cytoplasmic end when compared to A_{2B}-I. Moreover, the A_{2B}-II model has a short helical segment in the middle of the EL2, which is not present in the structure derived from bovine rhodopsin. The largest difference concerns helix 1, which lacks the proline-induced kink found in rhodopsin and thus is comparatively straight [53]. On the other hand, in the A_{2B}-III model most of the structural divergence arises in the extracellular portions of helices I, II, and V, where the variation in the position of helices II, III and V appears to redefine the location of the ligand binding pocket [54].

Criteria for pre-estimating the template quality may be based on the alignment score, the number and distribution of gaps, the length of sequence similarity and conservation

of aligned amino acids as well as the number and length of insertions and deletions. Finally, the quality of the X-ray structures in terms of resolution and authenticity has to be considered as well. The results are summarized in Table **2.1**.

Quality of Alignment

The exactitude of the predictions by comparative modelling greatly depends on the degree of sequence similarity. If the target and the template share more than 50% of their sequences, predictions usually are of high quality. In our case, the alignment scores were 79.0 bits (193) for bovine rhodopsin, 96.7 bits (239) for the β_2-adrenergic and 267 bits (683) for the adenosine A_{2A} receptor. The gap ratio in the alignment of the human adenosine A_{2B} receptor with the β_2-adrenergic receptor was slightly worse (26/217 = 11%) than that with bovine rhodopsin (32/302 = 10%) but with the adenosine A_{2A} receptor (10/215 = 4%) it was considerably much better (obtained by using the BLAST program) [97].

Quality of X-ray Crystal Structures

Concerning the quality of the crystal structures as the source of coordinates, we must consider that in order to facilitate the growth of diffraction-quality crystals, the human β_2-adrenergic was modified by inserting T4-lysozyme. However, according to Rosenbaum et al. [98] the engineered receptor did retain its basic functionality despite the structural modification: the agonist binding affinities were slightly elevated; the antagonist binding affinities remained almost unchanged. Thus, although displaying an engineered protein, the crystal structure represents a functional protein. Said 3D structure was solved at 2.4 Å resolution and in the presence of the antagonist carazolol, which points to the potential location of the ligand binding site. Yet, the N-terminus of the β_2-adrenergic receptor, especially the residues 1-28 and the majority of the C-terminus are not included in the crystal structure of the β_2-adrenergic receptor [53]. Conversely, the X-ray structure of bovine rhodopsin contains the complete receptor, harbouring a retinal moiety, at a slightly better resolution of 2.20 Å with a similar R-value of 0.200 [52]. (R-value is the measure of the quality of the atomic model obtained from the crystallographic data. When solving the structure of a protein, the researcher first builds an atomic model and then calculates a simulated diffraction pattern based on

that model. The R-value measures how well the simulated diffraction pattern matches the experimentally-observed diffraction pattern).

The structure of the adenosine A_{2A} receptor was resolved at 2.6 Å resolution with a R-value 0.198. According to Forrest et al. [56], a resolution of 2.5 Å implies that backbone as well as side-chain atoms are well resolved with an accuracy of ±0.4 Å for the atomic positions. Thus all potential template structures are of comparable and supposedly sufficient quality.

Based only on the sequence relations the structure of the adenosine A_{2A} receptor would score highest as a template. However, the sequence similarity might even turn out as a disadvantage, as the receptor was cocrystallized with ZM241385 and thus was accommodated to exactly this compound. Since we start with rigid docking, the binding site of a quite flexible receptor adapted to a given compound (or to none at all) might not be capable of accepting compounds of a different layout, at least this was found for protein kinases when testing crystal structures versus homology models [99] [100]. Considering this, as well as the authenticity and resolution of the crystal structures, the crystal structures of rhodopsin and the β_2-adrenergic receptor appear suited as well. Thus, at this point all crystal structures had to be considered as appropriate template structures for creating a model of the adenosine A_{2B} receptor (Table **2.1**).

2.3.3   Evaluation of the Predicted Models

The formal validation of the created models was done with PROCHECK [101] [102] and PROSAII [103] to rule out gross errors, i.e. checking only the plausibility of the main chain and side-chain conformations with respect to allowed torsions, the absence of D-amino acids or *cis*-peptide conformations in each residue within the models. Whether the final models indeed do possess a realistic geometry and exert a certain predictive power was finally assessed by further docking and MD studies.

PROCHECK Analysis

Accordingly, the plausibility of the final models was evaluated by means of Ramachandran's plots. As shown in Figure **2.6**, all helical amino acids are located in the region favouring a right-handed α-helix. Only 0.7% of all residues were in a sterically disallowed region in model A_{2B}-I, 1.7% of the respective residues were

located in the disallowed region in model A$_{2B}$-II, while 0.7% of the respective residues were located in the disallowed region in model A$_{2B}$-III. In all cases these residues are located in loop segments, thus not affecting the core region of the models and therefore do not have to be corrected. The crystal template structures themselves did display 0.7%, 0% and 0% of residues in disallowed regions in case of rhodopsin, the β$_2$-adrenergic receptor and the A$_{2A}$ receptor, respectively (Table **2.1**).

Table 2.1 Quality of crystal structure templates

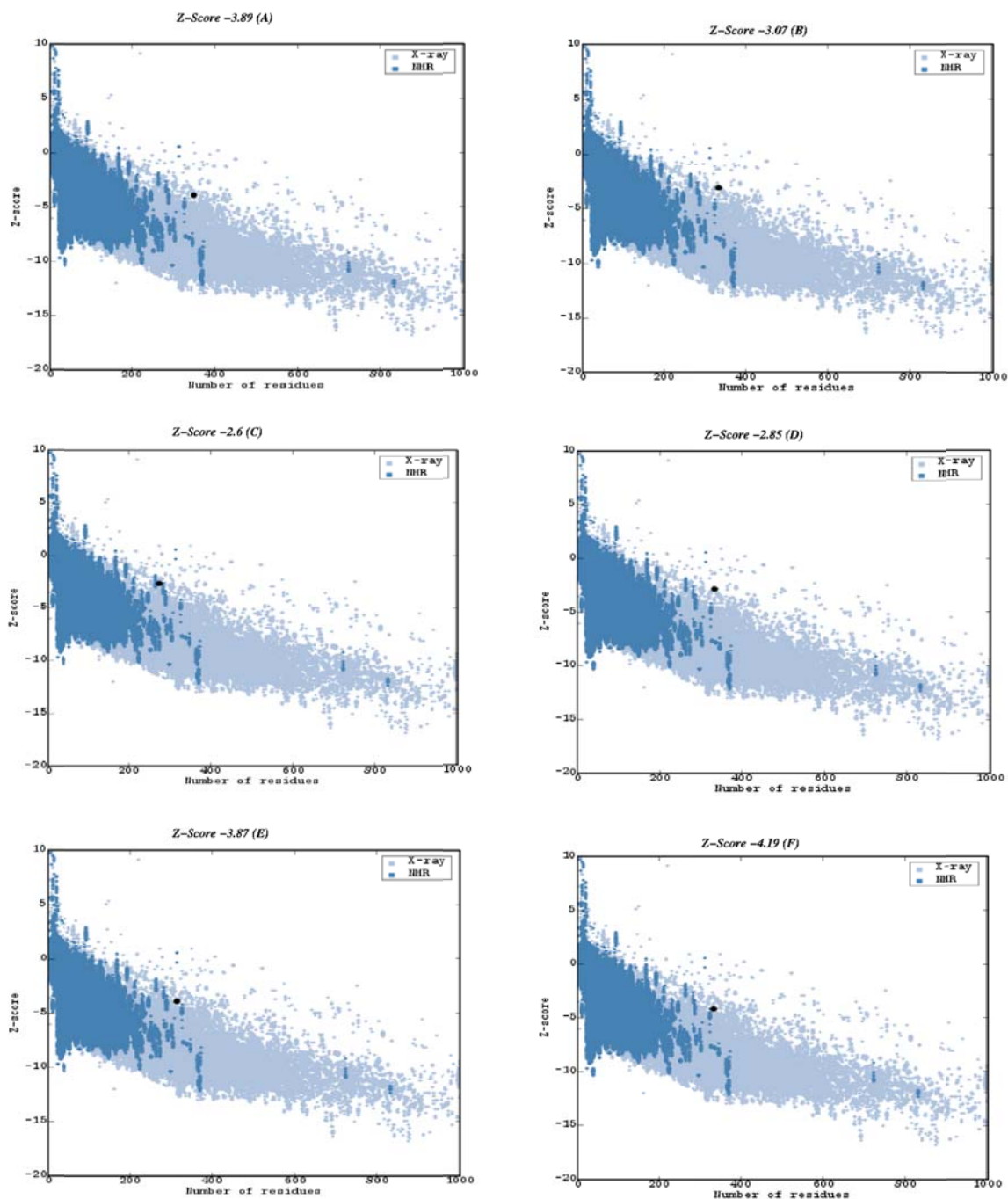|	Bovine rhodopsin	β$_2$-adrenergic receptor	Adenosine A$_{2A}$ receptor
Sequence identity	23%	31%	56%
Alignment score	79.0	96.7	267
Gap ratio	10%	11%	4%
Resolution of X-ray structures	2.2 Å	2.4 Å	2.6 Å
Cocrystallized ligand	11 cis-retinal	Carazolol	ZM241385
PROSAII analysis (Z-score)	-3.89	-2.6	-3.87
Procheck analysis (disallowed region)	0.7%	0.0%	0.0%
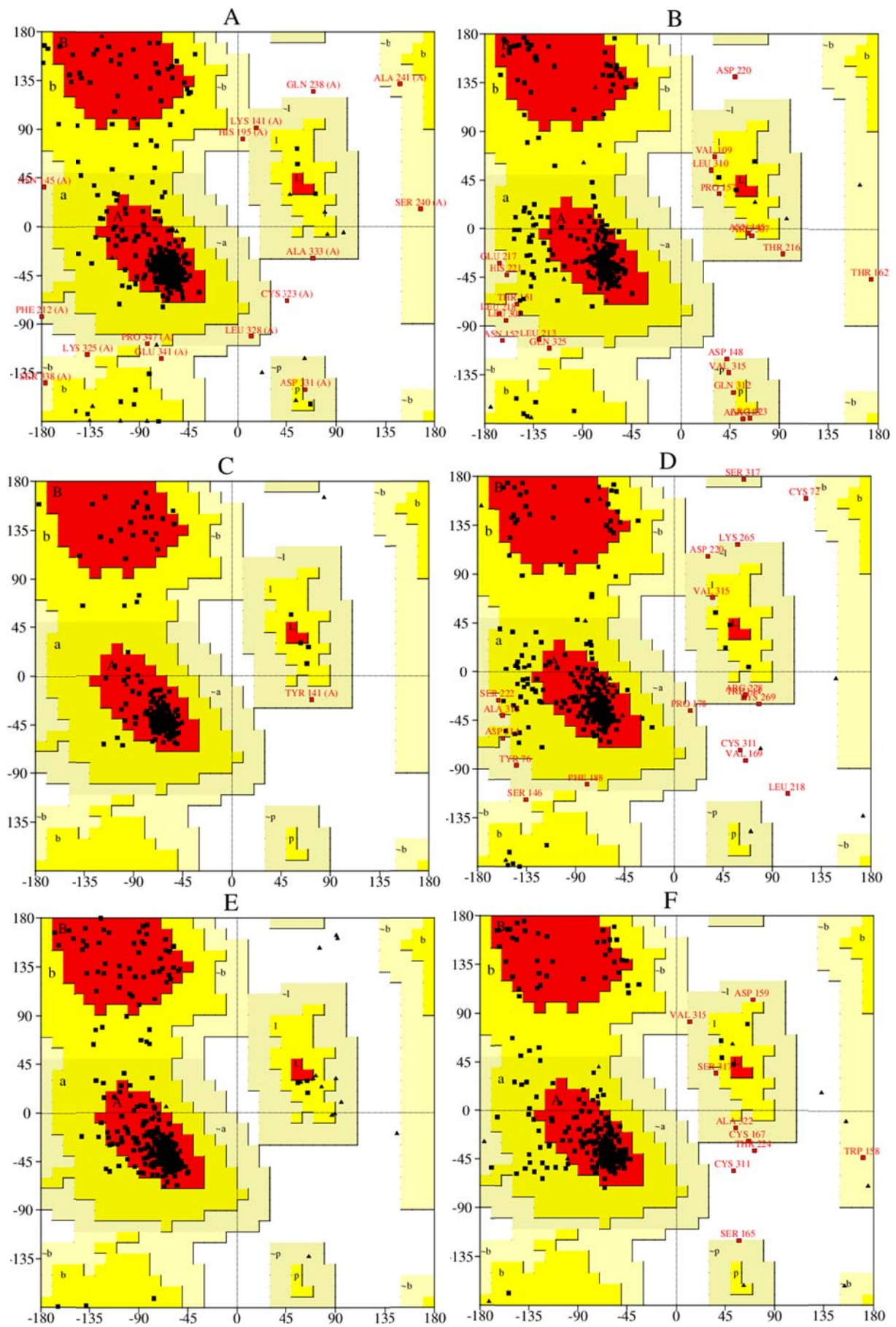
Figure 2.6 Ramachandran plots of rhodopsin (A), model A_{2B}-I (B), the β_2-adrenergic receptor (C), the model A_{2B}-II (D), the human adenosine A_{2A} receptor (E), and the model A_{2B}-III (F). The most favoured regions are coloured red, additional allowed, generously allowed and disallowed regions are indicated as yellow, light yellow and white fields, respectively. Residues marked with red squares have a bad conformation, which usually disappears during minimization and/or dynamics simulation

PROSAII Analysis

The Z-score computed by PROSAII [103] indicates the overall model quality, and its value for the respective model is related to the Z-scores of all experimentally determined protein structures in the current database indicating whether the Z-score of the particular structure is within the range of reasonable scores (Figure **2.7**). This plot shows the local model quality by plotting energies as a function of amino acid sequence position. In general, positive values correspond to problematic parts of the input structure. As a result, the bovine rhodopsin template shows a Z-score of -3.89 and the deduced model (A_{2B}-I) shows a Z-score of -3.07, the β_2-adrenergic receptor shows a Z-score of -2.6 and the derived model (A_{2B}-II) has a Z-score of -2.85, while the A_{2A} receptor shows a Z-score of -3.87 and the derived model (A_{2B}-III) has a Z-score of -4.19. These values indicate that the structural average for the second generation quality control values is within a normal range. Therefore all final refined models did pass the formal evaluation and need to be considered as suitable for further studies.

Figure 2.7 The Z-scores of the A$_{2B}$ receptor models and the templates (bovine rhodopsin (A), the model A$_{2B}$-I (B), the β$_2$-adrenergic receptor (C), the model A$_{2B}$-II (D), the adenosine A$_{2A}$ receptor (E), and the model A$_{2B}$-III (F)

Firstly, a qualitative comparison of the common as well as of the individual structural features of all models was performed. The backbone root mean square deviation (RMSD) (The root mean square deviation measures the difference between Cα atom positions between two proteins. The smaller the deviation, the more spatially equivalent
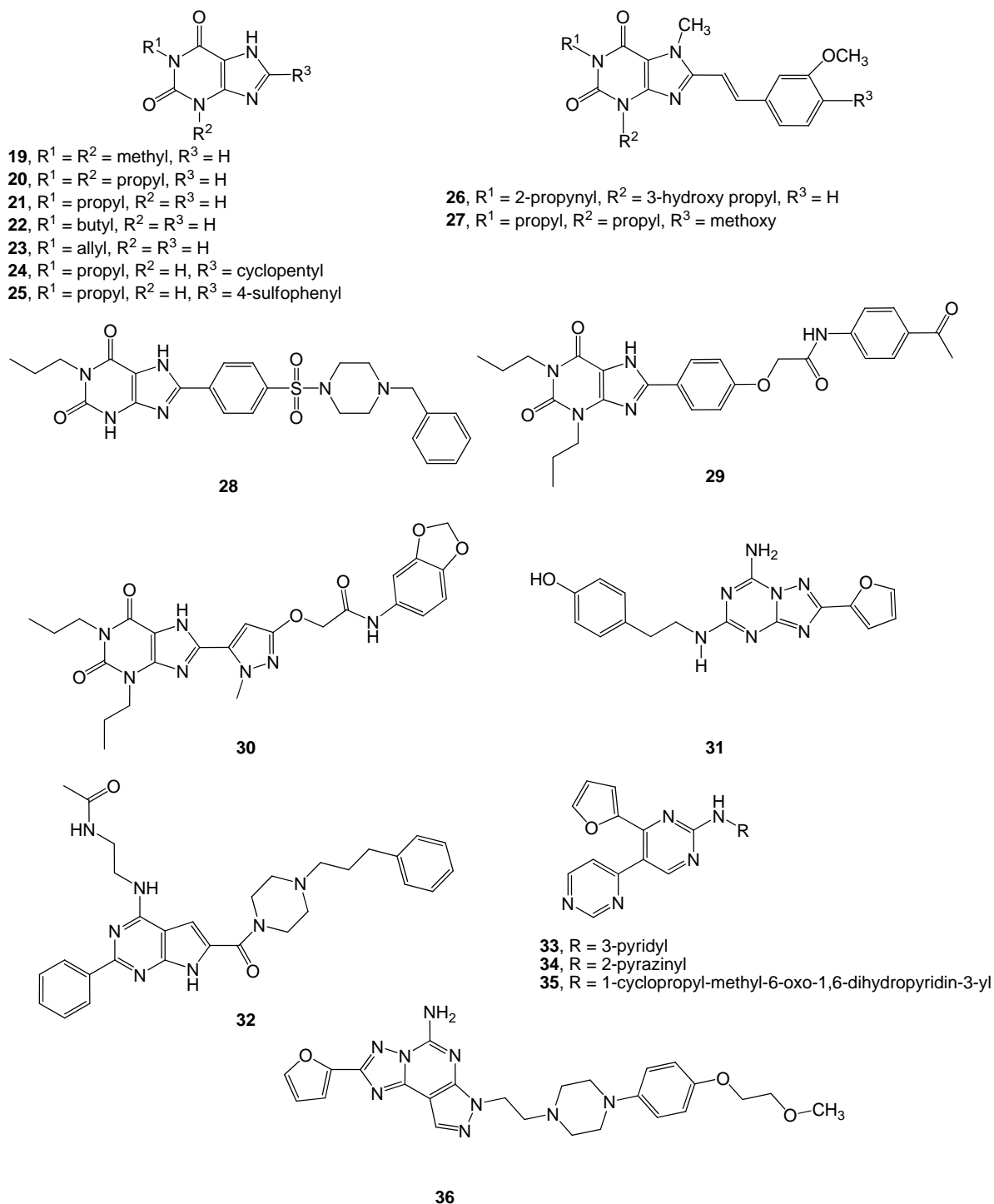
the two proteins are) of the created models relative to the corresponding residues of the X-ray structures was calculated as a measure of structure similarity. As shown in Figure **2.5**, the trans-membrane parts, where the sequences match best, superimpose perfectly, whereas the backbone course of the extracellular and intracellular loop regions differ significantly from the original. This is most noticeable for the rhodopsin based model, as the N-terminus of the A_{2B} receptor is much shorter. Apart from a different arrangement of the helices, all models vary largely in the backbone course of EL2. While for the model A_{2B}-I a β-sheet conformation was assumed, the A_{2B}-II model inherited a short helix from the $β_2$-adrenergic receptor in this section. On the other hand, the A_{2B}-III model lacks the prominent secondary structural elements in EL2, such as β-sheet and α-helix, which were observed in the rhodopsin and $β_2$-adrenergic-based models.

2.3.4   Docking Study Results

With the aim of further validation of model quality, eventual selection of the best model and understanding the binding behaviour in terms of affinity as well as selectivity, we carried out several docking studies for a set of ligands as detailed in the methods section (2.2.8.1), and correlated the results to experimental evidence i.e. binding and mutation studies. The template structures accommodate their inactivating ligands geocentrically in a comparable position, i.e. in the outer half of the helix bundle. Therefore, the binding site of the models was transferred from the template structures to the models assuming that their mechanism of operation would be very similar.

Based on published studies, we collected a series of compounds to test the models of the human adenosine A_{2B} receptor (Figures **2.8**, **2.9**). These compounds comprise 18 antagonists, as well as 7 agonists, addressing the inactive receptor state as well as the activated receptor conformation, as we wanted to exploit the predictive power of our model and methods, respectively. In detail, we included compounds selective for the A_{2A} or the A_{2B} receptor subtypes besides unselective ones, xanthines as well as and non-xanthines, in order to identify the individual key features of the adenosine A_{2B} receptor that would allow to control it separately from the other subtypes and to be able to develop selective ligands by rational drug design. Most of the antagonist compounds

investigated (**19-36**) are based on xanthine scaffolds (**19-30**), while other ligands show non-xanthine structures (**31-36**).

19, R¹ = R² = methyl, R³ = H
20, R¹ = R² = propyl, R³ = H
21, R¹ = propyl, R² = R³ = H
22, R¹ = butyl, R² = R³ = H
23, R¹ = allyl, R² = R³ = H
24, R¹ = propyl, R² = H, R³ = cyclopentyl
25, R¹ = propyl, R² = H, R³ = 4-sulfophenyl

26, R¹ = 2-propynyl, R² = 3-hydroxy propyl, R³ = H
27, R¹ = propyl, R² = propyl, R³ = methoxy

28

29

30

31

32

33, R = 3-pyridyl
34, R = 2-pyrazinyl
35, R = 1-cyclopropyl-methyl-6-oxo-1,6-dihydropyridin-3-yl

36

Figure 2.8 First set of compounds: Antagonists. Nonselective antagonists (**19-24**) and selective antagonists for the A$_{2A}$ receptor (**26**, **27**, **31**, **36**) and selective antagonists (**25**, **28-30**, **32-35**) for the A$_{2B}$ receptor (**19**, theophylline; **20**, 1,3-dipropylxanthine; **21**, 1-

propylxanthine; **22**, 1-butylxanthine; **23**, 1-allylxanthine; **24**, 1-propyl-8-cyclopentyl-xanthine; **25**, PSB-1115; **26**, MSX-2; **27**, istradefylline; **28**, PSB-601; **29**, MRS-1706; **30**, MRE-2029F20; **31**, ZM241385; **32**, OSIP339391; **33**, **34**, and **35**, 2-aminopyrimidine derivatives; **36**, preladenant)
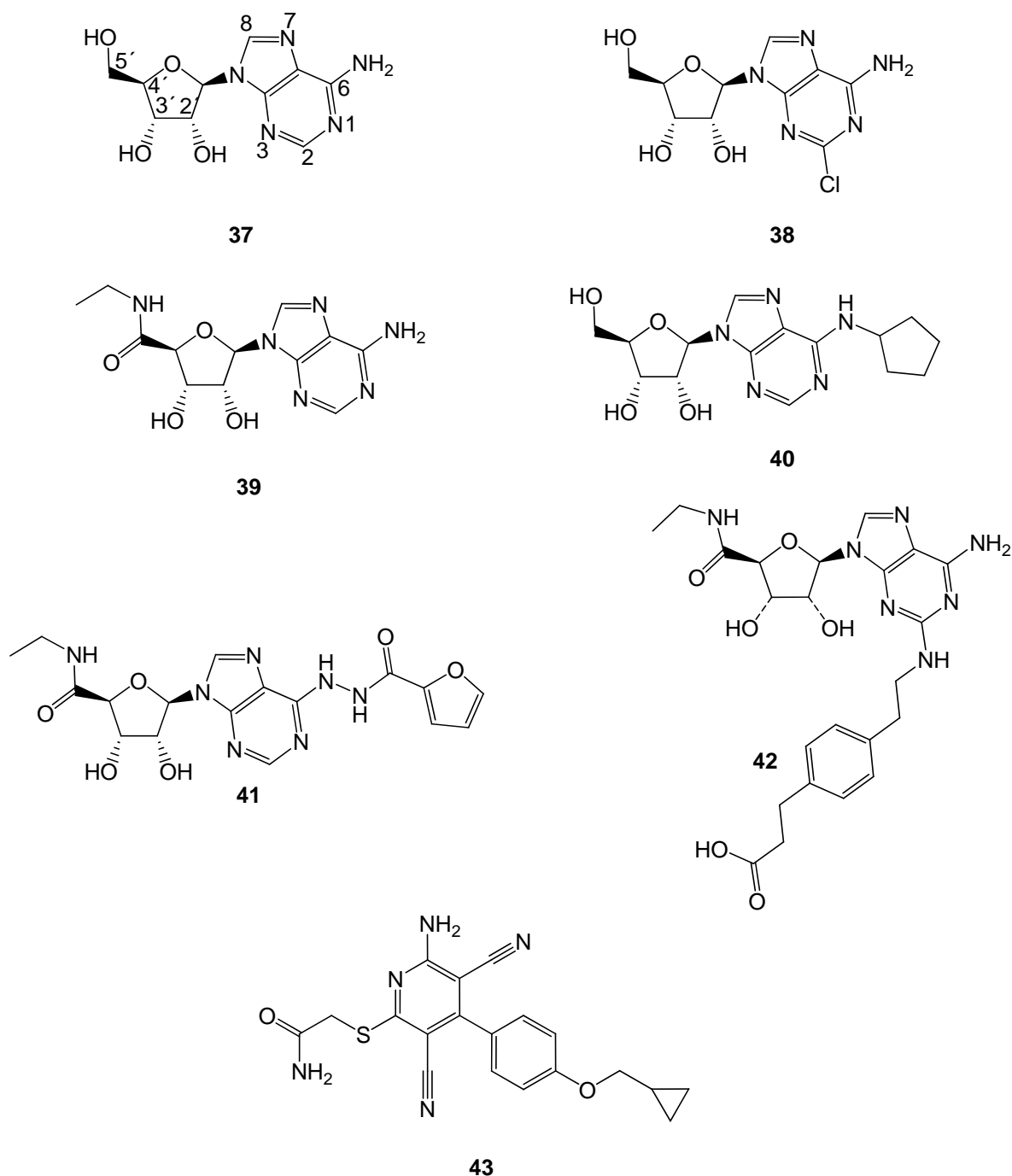

Figure 2.9 Second set of compounds: Agonists. Nonselective agonists (**37-41**), selective agonist for the A$_{2A}$ receptor (**42**) and selective agonists (**43**) for the A$_{2B}$

receptor (**37**, adenosine; **38**, CADO; **39**, NECA; **40**, CPA; **41**, substituted NECA; **42**, CGS21680; **43**, BAY-60-6583)

2.3.5   Docking of ligands into the adenosine A$_{2A}$ receptor

Redocking of ZM241385 into the adenosine A$_{2A}$ receptor

In order to check the efficiency of the method employed for creating suitable binding modes as described in the method section, we performed molecular redocking of ZM241385 [104] (compound **31** in Figure **2.8**) into the crystal structure of the A$_{2A}$ receptor. As a result, the binding mode of ZM241385 with the A$_{2A}$ receptor is similar to the reference of the crystal structure (RMSD of 0.6 Å) where ZM241385 binds in an extended conformation and its orientation is almost perpendicular to the membrane plane, co-linear with transmembrane helix VII and interacting with both EL2 and EL3. In both structures, the bicyclic triazolotriazine core of the ligand is anchored by an aromatic stacking interaction with Phe168, aliphatic hydrophobic interactions with Ile274, Met177, Ile252, Met270, and Met174 and a hydrogen bonding interaction with Asn253.
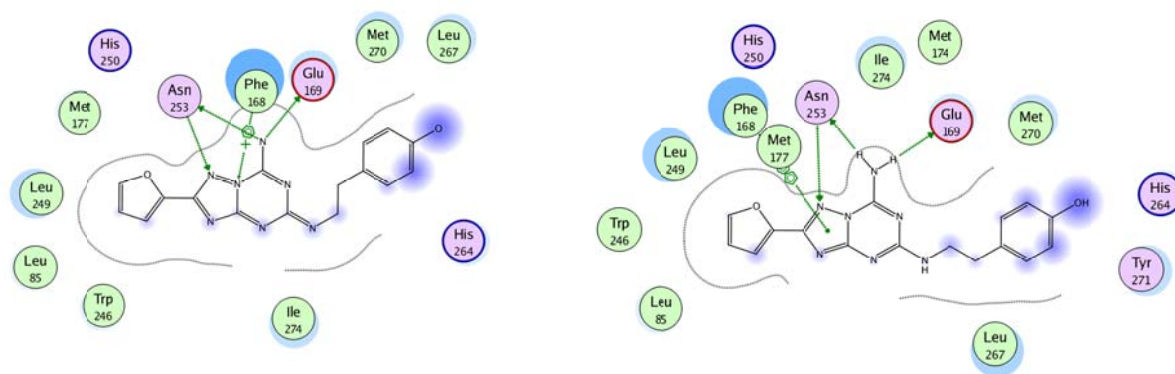
Figure 2.10 Comparison of the predicted binding modes for ZM241385 with X-ray structure (left) and redocking ligand with the A$_{2A}$ structure (right). Showing hydrogen bonding and aromatic stacking interactions

Furthermore, Glu169 interacts with the exocyclic amino group, and the phenolic hydroxyl group forms a hydrogen bonding interaction with a water molecule. Also, the phenyl ring (this moiety appears to be mobile within the reference receptor) forms hydrophobic interactions with Leu267, Leu167, Tyr271 and His264. The furan ring is

hydrogen-bonded to Asn253 and located in the hydrophobic pocket formed by His250, Leu85, Val84, and Leu249. Additionally, the furan ring is roughly 3.3 Å away from the highly conserved Trp246. We therefore conclude that indeed our docking and selection procedure is able to successfully produce reasonable binding modes (Figure **2.10**).

Several antagonists were docked into the A$_{2A}$ crystal structure (MSX-2, Istradefylline, Preladenant, MRS-1706, MRE-2029F20 and PSB-601)

In order to further assess the reliability of the method for estimating binding affinities. According to the experimental data MSX-2, Istradefylline, and Preladenant are A$_{2A}$ selective antagonists and display high binding affinities with K$_i$ values of 5.0 nM, 13.0 nM, and 1.1 nM for the A$_{2A}$ receptor, whereas MRS-1706, MRE-2029F20 and PSB-601 are A$_{2B}$ selective antagonists and show K$_i$ values of 112 nM, >1000 nM, and 484 nM in the A$_{2A}$ receptor. Based on mutagenesis data, a common binding mode for the compounds sharing a xanthine scaffold moiety is expected. As the binding affinities range from high to low, we anticipate finding the overall trend reflected in the calculated values. Indeed, all predictions display very similar placements of the xanthine moiety, which also coincides with the bicyclic core of ZM241385. The common interaction pattern involves Asn253 and Phe168.

In detail, the placement of the antagonist MSX-2 [105] in the A$_{2A}$ X-ray structure (compound **26** in Figure **2.8**) illustrated in Figure **2.11** also shows a hydrogen bonding interaction between the carbonyl group at the 2-position of the ligand and Thr88, even though it is not maintained along the whole MD trajectory. The hydroxyl moiety of the ligand is stabilized by a hydrogen bonding interaction with the unprotonated nitrogen atom of His278 and the amino group at the 9-position of the ligand interacts with a water molecule. In addition, the methoxy oxygen atom of the ligand interacts with the backbone amino group of Phe168. Besides, the styryl moiety of the ligand is located in the hydrophobic pocket formed by Ala63, Ile66, and anchored by an aromatic stacking interaction with Tyr271.
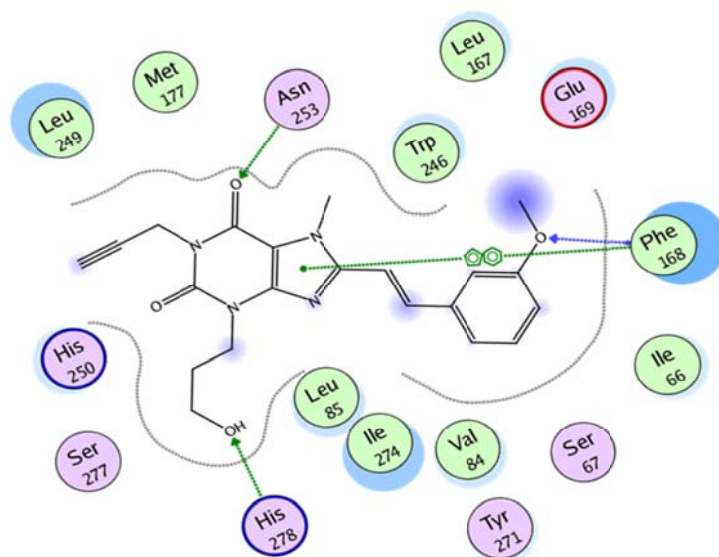
Figure 2.11 Predicted binding mode for MSX-2 with the adenosine A$_{2A}$ receptor. Showing hydrogen bonding and aromatic stacking interactions

The xanthine moiety of the ligand is commonly oriented as it gives an aromatic stacking interaction with Phe168 and the lipophilic cage made up of Met177, Ile252, Leu249, Ala273, Met270, Ile274, Met174, and Trp246. Moreover, the propargyl moiety at the 1-position of the ligand is bordered by Asn181, Val186, Leu85, and His250. Furthermore, the propyl moiety of the ligand is located inside the pocket formed by Ala59, Val55, Val84, Ile60, Leu87 and Val275, whereas the methyl moiety of the ligand is placed in the pocket formed by Leu167, Gly69, His264, and Leu267.

The final result for istradefylline [106] in the A$_{2A}$ X-ray structure (compound **27** in Figure **2.8**) follows the general pattern observed for MSX-2. As before, the hydrogen bonding and lipophilic interactions are maintained. However, the methoxy oxygen atom of the ligand forms a hydrogen bonding interaction with Tyr271 (Figure **2.12**).
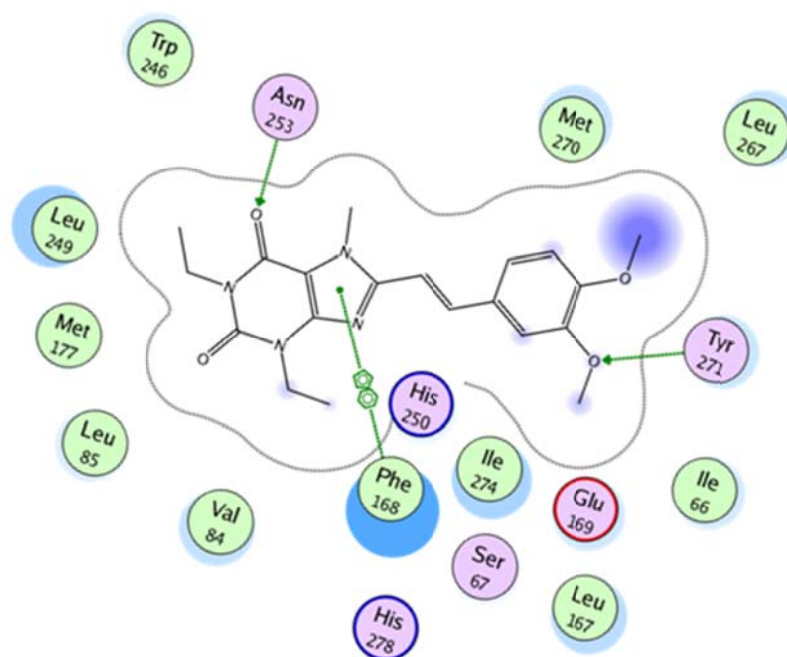
Figure 2.12 Predicted binding mode for istradefylline with the adenosine A_{2A} receptor. Showing hydrogen bonding and aromatic stacking interactions

The obtained result for the non-xanthine antagonist preladenant [107] in the A_{2A} X-ray structure (compound **36** in Figure **2.8**) is virtually the same as that of ZM241385, where the bicyclic and tricyclic moieties of these two ligands reside in a similar position. Additionally the two oxygen atoms of the methoxyethoxy moiety of the ligand interact with two water molecules and the methoxy oxygen atom is predicted to be in proximity to Asn154. Furthermore, the amino group at the 4-position of triazole moiety of the ligand constitutes water-mediated interactions with Ile80 and Ala81.
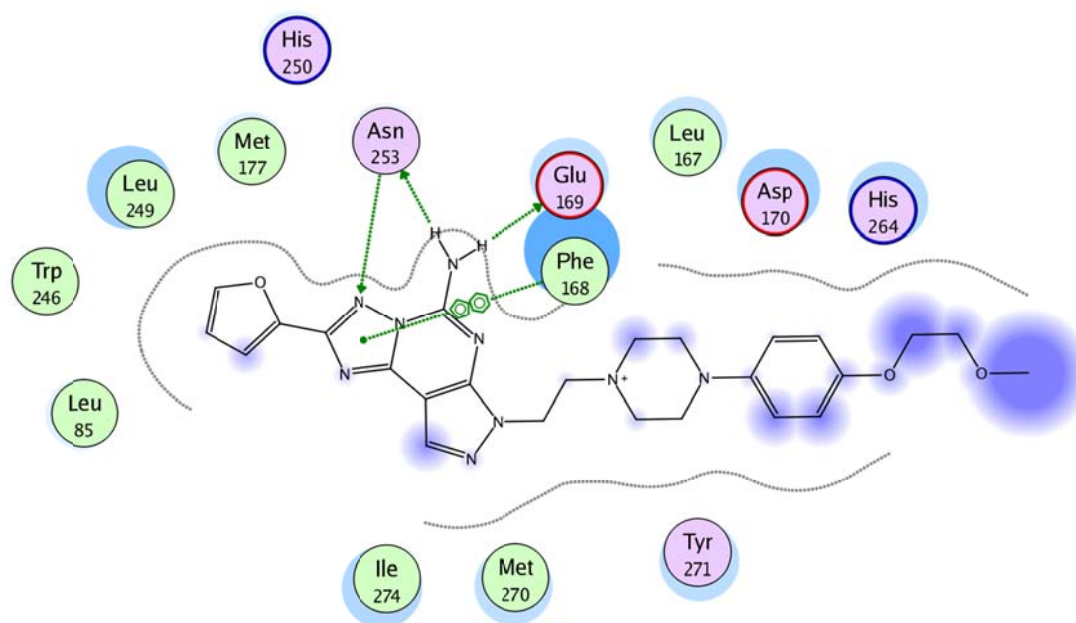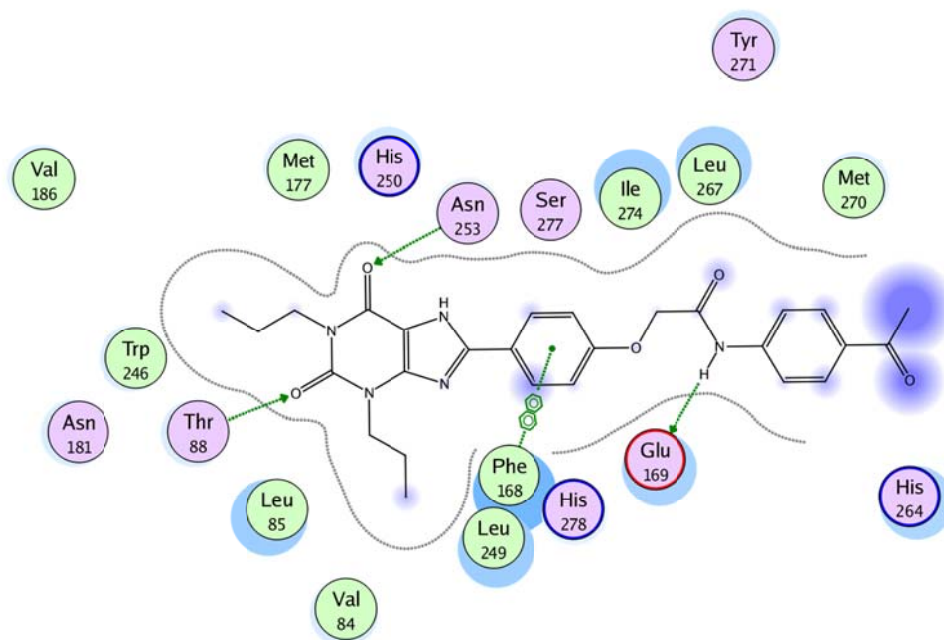
Figure 2.13 Predicted binding mode for preladenant with the adenosine A_{2A} receptor. Showing hydrogen bonding and aromatic stacking interactions

Besides, Tyr271 is located near the amino group at the 1-position of the piperazine moiety of the ligand at the same time, His264 is placed near the amino group at the 4-position of the piperazine moiety of the ligand which is believed to be critical for binding and contributes to an increase in the affinity of the ligand. In addition, the phenyl moiety of the ligand makes favourable hydrophobic interactions with Leu267, Leu167, and Val171. The tricyclic structure of the pyrazolotriazolopyrimidine, the presence of the furan ring, the exocyclic 5-amino group, and the aryl-alkyl substituent on the nitrogen at the 7-position are probably essential for both affinity and selectivity for the A_{2A} receptor. Also, because of the existence of additional hydrogen bonding and desirable interactions, preladenant has higher affinity towards the A_{2A} adenosine receptor than the other ligands (Figure **2.13**).

In the most favourable location we found for MRS-1706 [38] in the A_{2A} X-ray structure (compound **29** in Figure **2.8**) is that again the Asn253 side-chain forms a hydrogen bonding interaction with the carbonyl group at the 6-position of the ligand. However, the NH group at the 7-position of the ligand is located far away from Asn253. The amino group at the 9-position of the ligand is involved in a hydrogen bonding interaction with a water molecule.

Figure 2.14 Predicted binding mode for MRS-1706 with the adenosine A_{2A} receptor. Showing hydrogen bonding and aromatic stacking interactions

Additionally, Thr88 forms a hydrogen bonding interaction with the carbonyl group at the 2-position of the ligand and Glu169 forms a hydrogen bonding interaction with the amino group of the phenoxyacetamide moiety of the ligand. The propyl group at the 1-position is located inside the hydrophobic pocket formed by Val186, Phe182, Thr88, Leu85, Gln89, Ile135 and Ile92. Likewise the propyl group at the 3-position is in contact to Ala59, Val55, His278 and Val84. Moreover, the phenylxanthine moiety of the ligand is involved in hydrophobic interactions with Ile66, Ala63, Ile274, Leu249, His250, Ala81, Met177 and Trp246 and stabilized by an aromatic interaction with Phe168. Besides that, the carbonyl oxygen atom of the acetyl group of the ligand forms water-mediated interactions with His264 and Asp170. Furthermore, the acetylphenyl group of the ligand is predicted to be involved in an aromatic stacking interaction with His264 and located inside the pocket formed by Leu167, Met270, Leu267 and Tyr271 (Figure **2.14**).

Table 2.2 Effects of mutation of single amino acids in adenosine A_{2A} and A_{2B} receptors on antagonist and agonist binding and/or function

| A_{2A}	Effect	A_{2B}	Effect
E13 [1.39]	Q: slight reduction of Ag but not Ant affinity [108]	V11 [1.36]	NC for Ag [15]
V84 [3.32]	A/D: loss of Ag & Ant radioligand binding, L: slight increase in Ag & decrease in Ant affinity [109]	A12 [1.37]	NC for Ag [15]
T88 [3.36]	A/S/R/E: substantial decrease in Ag but not Ant activity [110]	N36 [IL1]	NC for Ag [111]
Q89 [3.37]	A: slight increase in Ag and Ant activity, D: slight increase in Ag but not Ant affinity, N/S/L: marginal changes in ligand binding, H/R: Ant binding affected [110]	T42 [2.39]	Decrease in Ag activity (4.9 fold) [111]
S90 [3.38]	A: marginal changes in ligand binding [110]	V54 [2.51]	Decrease in Ag activity (6.3 fold) [111]
S91 [3.39]	A: marginal changes in ligand binding [110]	L58 [2.55]	NC in Ag [15]
E151 [EL-2]	A/Q/D: loss of Ag and Ant binding, ~1000-fold decrease in Ag potency [112]	F59 [2.56]	No specific binding and no cAMP production [15]
E169 [EL-2]	A: loss of Ag and Ant binding, ~1000-fold decrease in Ag potency, Q: gain in Ag affinity	F84 [3.31]	Decrease in Ag activity (3.1-6.5 fold) [111]

	[112]		
D170 [EL-2]	K: NC in ligand binding [112]	S91 [3.38]	NC in Ag [111]
P173 [EL-2]	R: NC in ligand binding [112]	N273 [7.36]	NC for Ant, NC for Ag except for CGS21680 (decrease of 3.2 fold) and other 2-substituted adenosines [15]
F180 [5.41]	A: minor changes in ligand binding [113]		
N181 [5.42]	S: modest reduction of Ag binding [113]		
F182 [5.43]	A: loss of Ag and Ant binding, Y, W: modest reduction of Ag binding [113]		
H250 [6.52]	A: loss of Ag and Ant binding, no Ag activity in functional assays, F, Y: modest reduction of Ag binding; no effect on Ant binding, N: slight increase in Ag affinity, minor changes in Ant affinity [109] [113]		
N253 [6.55]	A: loss of Ag and Ant radioligand binding [113]		
C254 [6.56]	A: minor changes in ligand binding [113]		
F257 [6.59]	A: loss of Ag and Ant radioligand binding [113]		

C262 [EL-3]	G: NC in radioligand binding [112]		
I274 [7.39]	A: loss of Ag and Ant binding, 30-fold decrease in Ag potency [113]		
S277 [7.42]	A: substantial decrease in only Ag activity and potency, T/C/N/E: marginal changes in binding [109] [112]		
H278 [7.43]	A: loss of Ag and Ant binding; 300-fold decrease in Ag potency, Y: modest reduction of Ag binding; NC on Ant binding, D/E: marginal changes in binding [113] [114]		
S281 [7.46]	A: loss of Ag and Ant radioligand binding; no Ag activity in functional assay, T: enhanced activity for Ag, N: marginal changes in ligand binding [113] [114]		

Ag, agonist; Ant, antagonist; NC, no change

The result from our docking study of MRE-2029F20 [37] with the A$_{2A}$ receptor (compound **30** in Figure **2.8**) is that both, the hydrogen bonding interaction between Asn253 and the carbonyl group at the 6-position of the ligand as well as the hydrogen bonding interaction between the carbonyl group at the 2-position of the ligand and Thr88 are lost due to unfavourable interactions and the steric effect induced by the bulky fragment of the ligand. The carbonyl group of the oxyacetamide moiety of the ligand is hydrogen-bonded to the backbone amino group of Asp170. At the same time, the amino group of the oxyacetamide moiety of the ligand forms a hydrogen bonding interaction with a water molecule. The pyrazolylxanthine moiety of the ligand is located inside the pocket similar to that of the phenylxanthine moiety of MRS-1706. In

addition, the methylenedioxyphenyl moiety of the ligand is surrounded by Asp170, Glu169, Thr256, Leu167, His264 and Leu267 (Figure **2.15**).
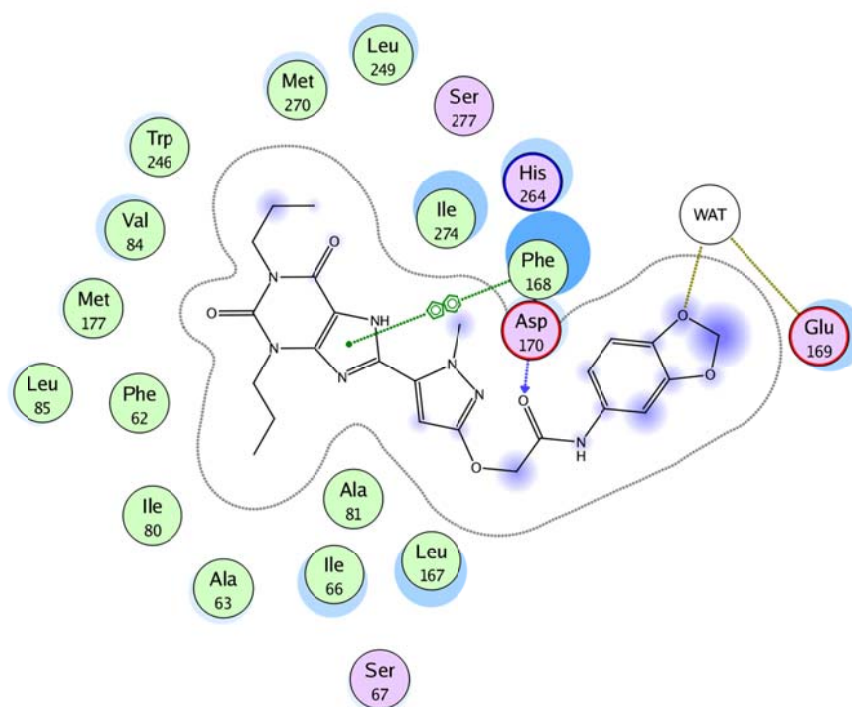
Figure 2.15 Predicted binding mode for MRE-2029F20 with the adenosine A_{2A} receptor. Showing hydrogen bonding and aromatic stacking interactions

The obtained binding mode for PSB-601 [115] in the A_{2A} X-ray structure (compound **28** in Figure **2.8**) suggests that the arrangement of the ligand is similar to that of MRS-1706. The interaction between Asn253 and the carbonyl group at the 6-position is present however, the interaction between Asn253 and the NH group at the 7-position of the ligand is lost. The Thr88 side-chain forms a hydrogen bonding interaction with the carbonyl group at the 2-position of the ligand. The lipophilic interaction is maintained and adopted the same cavity in the active site similar to that of MRS-1706 (Figure **2.16**). The predicted binding rank of MRS-1706 and PSB-601 with the A_{2A} receptor is consistent with the experimental results. According to the predicted binding modes of the complexes, the residues in the active site of MRS-1706 and PSB-601 give similar contribution for the A_{2A} adenosine receptor. This is reasonable because the active sites of the complexes have similar residues and volume. However, MRS-1706 [K_i= 112 nM] binds to the active site and has additional interactions. Moreover, Leu85, Asn181, and His278 are close to the active site and could be responsible for increasing affinity but PSB-601 [K_i= 484 nM] did not bind so well.
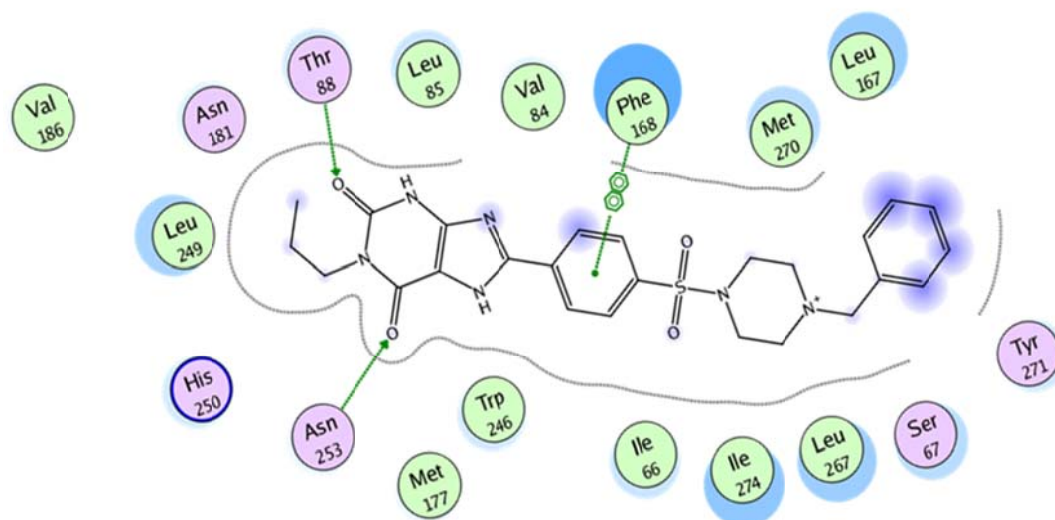
Figure 2.16 Predicted binding mode for PSB-601 with the adenosine A$_{2A}$ receptor. Showing hydrogen bonding and aromatic stacking interactions

Summarizing the obtained docking results with antagonists in complex with the A$_{2A}$ X-ray structure, the outcome indicates that all xanthine and nonxanthine type antagonists have similar binding mode patterns and the above results are in a good agreement with the experimental data collected in Table **2.2**. By combining the docking results from the above discussed antagonists, we were able to extract some residues, which could be essential for different ligands to bind potential A$_{2A}$ antagonists. Apparently, Val84, Glu169, His250, Asn253, His278, Phe182, Glu151, Ile274 are involved in the antagonist recognition. Moreover, the hydrophobic interaction domains located at the binding pocket are supposed to importantly contribute to the binding affinity of A$_{2A}$ antagonists. In summary, it is reasonable to suggest that Ile80, Leu249, Ile252, Met270, Ala59, Leu167, Asn154, His264, Leu267, and Tyr271 could be responsible for the selectivity of adenosine A$_{2A}$ receptor ligands.

Free energy decomposition involving the MM-GBSA method has been developed to investigate the binding modes in detail at the atomic level. The per-atom contributions can be summed over atom groups such as residues, backbones and side-chains, to obtain their contributions to the total binding free energy (Table **2.3**) (more details see chapter **4** section **4.2.4.3**).

Table 2.3 Interactions energies (in kcal mol $^{-1}$) between the A$_{2A}$ antagonists and the important residues based on the energy decomposition analysis MM-GBSA

Residue/ A$_{2A}$	ZM241385	MSX-2	Istradefylline	Preladenant	MRS-1706	MRE-2029F20	PSB-601
Asn253	**-7.6**	**-4.9**	**-5.1**	**-7.2**	-2.1	-1.2	-1.7
Glu169	**-9.3**	-3.0	-3.0	**-10.9**	**-5.2**	**-4.9**	-0.1
Phe168	-4.5	-5.6	**-6.4**	**-8.1**	-5.0	**-9.4**	**-6.2**
Leu249	**-3.8**	**-4.6**	**-4.1**	**-4.0**	-3.3	-2.1	-2.8
Trp246	-0.5	**-1.9**	**-1.2**	-0.7	**-1.6**	-0.9	**-2.5**
Leu85	-1.0	-1.0	**-1.1**	-1.0	**-3.7**	**-1.2**	**-2.3**
His250	-0.5	**-2.0**	**-1.0**	-0.7	**-1.7**	-0.2	**-1.4**
Val84	-0.5	-1.8	**-2.3**	-0.4	**-1.9**	**-2.9**	**-1.9**
Thr88	-0.1	**-0.3**	-0.1	-0.2	**-4.7**	**-0.2**	**-3.3**
His278	-0.0	**-3.2**	**-0.7**	-0.0	**-1.6**	**-0.6**	-0.2
Met177	-1.8	**-2.2**	**-1.9**	**-1.9**	**-1.9**	-1.0	-1.7
Phe255	-0.0	-0.0	-0.0	-0.0	-0.0	-0.0	-0.0
Ile252	**-0.6**	-0.2	-0.2	**-0.5**	-0.1	-0.1	-0.2
Ala63	-0.1	**-0.4**	**-0.6**	-0.1	-0.1	**-1.4**	**-0.2**
Leu269	-0.1	-0.1	-0.1	-0.1	-0.1	-0.0	**-0.2**
His264	**-1.0**	-0.3	-0.3	**-1.4**	**-1.5**	**-1.8**	-0.4

Leu267	**-2.3**	-0.3	**-1.0**	-0.5	**-2.1**	**-1.0**	**-1.5**
Tyr271	**-1.0**	-0.5	**-1.7**	**-1.3**	-0.5	-0.5	**-0.9**
Ala265	-0.1	-0.1	-0.0	-0.1	-0.1	-0.1	-0.0
Ser263	-0.0	-0.0	-0.0	-0.0	-0.0	-0.0	-0.0
Pro266	**-0.1**	-0.0	-0.0	**-0.1**	-0.0	-0.0	**-0.1**
Leu167	-0.6	**-2.0**	-1.7	**-2.8**	-1.9	**-3.9**	**-2.7**
Asp170	-0.2	-0.2	**-0.3**	**-3.8**	-0.2	**-1.9**	-0.2
Ser67	-0.2	**-0.7**	**-1.1**	-0.2	-0.1	**-0.7**	**-3.5**
Ala165	-0.0	-0.0	-0.0	-0.1	-0.0	-0.0	-0.2
Ala81	-0.2	-0.2	-0.5	-0.2	-0.2	**-1.3**	-0.3

The most significant interactions are highlighted in bold in order to emphasize the respective interaction patterns

Docking of agonists (NECA, BAY-60-6583 and CGS21680) into the A$_{2A}$ receptor in order to study performance of receptor structure with agonists

The obtained result for NECA [29] in the A$_{2A}$ X-ray structure, an analogue of the native agonist (compound **39** in Figure **2.9**) is that the amino group at the 6-position of NECA is involved in hydrogen bonding interactions with Asn253 and Glu169. In addition, the amino group at the 7-position of NECA forms a hydrogen bonding with a water molecule. Thr88 is predicted to be hydrogen bonded with the amino group of the ligand amide moiety. Additionally, the 3'-hydroxyl group of the ligand forms water-mediated interactions with Ala59 and Ile80, while the 2'-hydroxyl group of NECA constitutes water-mediated interactions with Ile80 and Ala81. At the same time, the carbonyl group at the 5'-position of NECA forms a hydrogen bonding interaction with Ser277. Moreover, His278 is located at a distance of 4.65 Å from the 5'-amino group of NECA. The adenine moiety of NECA is stabilized by an aromatic stacking interaction with Phe168 and hydrophobic interactions with Trp246, Met270, Met174, Met177, Leu85,

Leu249, His250, Ile252, Ala273, and Ile274. Furthermore, the ribose moiety of NECA is surrounded by Ala81, Ile66, Val84, Ala63, and Thr88 (Figure **2.17**).
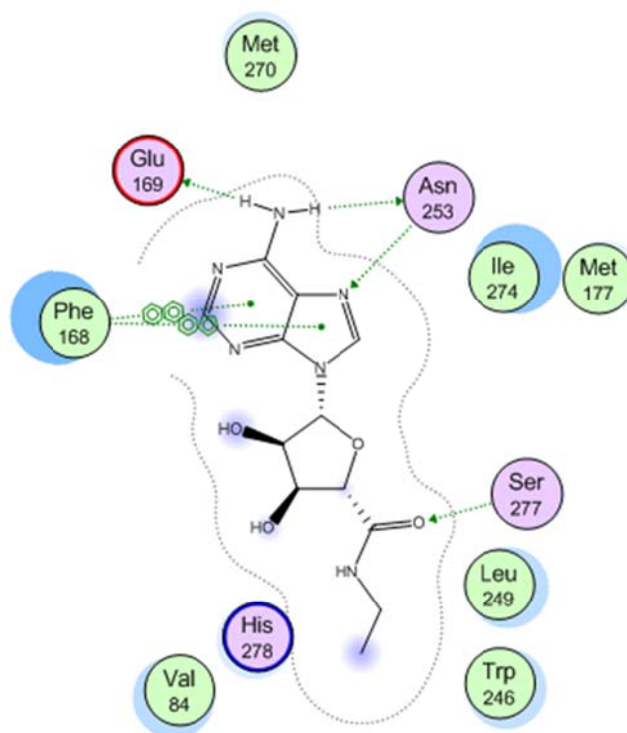
Figure 2.17 Predicted binding mode for NECA with the adenosine A$_{2A}$ receptor. Showing hydrogen bonding and aromatic stacking interactions

The adenosine A$_{2A}$ selective agonists usually contain a bulky substituent in the 2-position of the adenine ring of NECA. Also, some analogs of NECA substituted in the 2-position of the adenine ring by an alkyl group as well as an aromatic or heteroaromatic ring showed high potency at the adenosine A$_{2A}$ receptor. For example, CGS21680 was shown to be a selective agonist for the A$_{2A}$ adenosine receptor. It is observed that the substitution at the 2-position of the A$_{2A}$ agonist ligands is surrounded by amino acid residues located not only in the TMs of the receptor, but also in the EL2 and EL3. The proposed binding mode of CGS21680 [116] in the A$_{2A}$ X-ray structure, a NECA-derivative (compound **42** in Figure **2.9**) is that the amino group at the 6-position of the ligand is involved in hydrogen bonding interactions with the carbonyl oxygen atom of Asn253 and Glu169. Additionally, the 3'-hydroxyl group of the ligand forms water-mediated interactions with Ile80 and Ala81, while the 2'-hydroxyl group of ligand constitutes a water-mediated interaction with Ala81. Thr88 is predicted to be hydrogen bonded with the amino group of the ligand amide moiety.

The carbonyl group at the 5'-position of the ligand forms a hydrogen bonding interaction with Ser277. The adenine moiety of the ligand is stabilized by an aromatic stacking interaction with Phe168 and hydrophobic interactions with Leu85, Met270, Met174, Met177, Thr256, Leu249, His250, Ile252, Ala273, and Ile274. Furthermore, the ribose moiety of the ligand is surrounded by Trp246, Leu85 and Ala63. The N-alkyl chain of the ligand can be located inside the pocket formed by Val84, Leu87, Val55, Ala59 and Ile60. The hydroxyl group as well as carbonyl group of the carboxylate moiety of the ligand are formed water-mediated interactions with Asp170 and His264. In addition, the side-chain of Tyr271 is observed in proximity to the hydroxyl group of the carboxylate moiety of the ligand. The phenylethyl moiety of the ligand shows an aromatic stacking interaction with Tyr271 and aliphatic hydrophobic interactions with Leu267, Leu167, Ala63 Gly69 and Ile66, a pocket that contributes to an increase in the affinity and selectivity of the ligand with the A_{2A} adenosine receptor (Figure **2.18**).
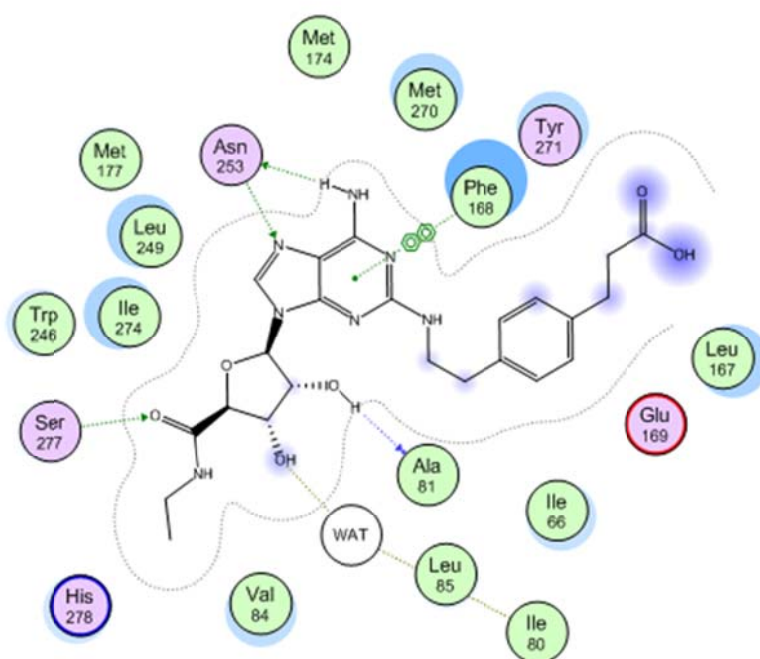
Figure 2.18 Predicted binding mode for CGS21680 with the adenosine A_{2A} receptor. Showing hydrogen bonding and aromatic stacking interactions

Initially, we tried to place the A_{2B} agonist BAY-60-6583 [34] into the putative A_{2A} binding site. However, undesirable steric effects, resulting from the absence of sufficient free space to accommodate the ligand, were observed. The obtained result of

molecular docking of BAY-60-6583, a non-adenosine agonist, suggests that the amino group at the 6-position of BAY-60-6583 (compound **43** in Figure **2.9**) forms hydrogen bonding interactions with the amide oxygen atom of Asn253 and the backbone carbonyl group of Met177, additionally Val178 and Phe182 are closer to this moiety.

The side-chain of Asn181 and the backbone carbonyl group of Leu85 form hydrogen bonding interactions with the amino group of the sulfanylacetamide moiety of the ligand, and the sidechains of Ile92 and Ile135 are located near the amino group of the sulfanylacetamide moiety of the ligand. Furthermore, Gln89 forms a water-mediated interaction with the carbonyl group of the sulfanylacetamide moiety of the ligand. Besides, the cyano group at the 3-position of the ligand is located at a distance of 3.09 Å from Thr88. The phenylpyridine moiety is located inside the hydrophobic pocket formed by Val84, Leu85, Met174, Phe168, Met177, His250, Leu249, Trp246, and Val186, while the cyclopropyl residue is surrounded by Ile66, Ala63, Ala59, Phe62, Ala81, Ile80, Cys82, Ile274, and His278.

Summarizing A_{2A} receptor results; our study has confirmed that the interaction with Asn253 is crucial, which is suggested by mutagenesis studies to be of great importance for this receptor subtype. Moreover, it was assumed that the presence of His250 is required in the binding pocket but a hydrogen bonding is not necessary. In addition, the results of molecular docking are in a good agreement with mutagenesis data (Table **2.2**) for the human adenosine A_{2A} receptor subtype. Moreover, the results of site-directed mutagenesis of the adenosine A_{2A} receptor suggested that Phe182$^{5.43}$, His250$^{6.52}$, Asn253$^{6.55}$, His278$^{7.43}$, Glu13$^{1.39}$, Ile274$^{7.39}$, Val84$^{3.32}$, Thr88$^{3.36}$, Gln89$^{3.37}$, Glu151^{EL-2}, Glu169^{EL-2}, Ser277$^{7.42}$ and Ser281$^{7.46}$ are the most important for binding of agonists. The mainly aromatic amino acids of the lipophilic part of the pocket located in the TM2, TM7, EL2 and EL3 seem to be responsible for the affinity and selectivity of the adenosine A_{2A} receptor. In particular, this moiety is consisted of several aromatic and hydrophobic amino acid residues, such as His264, Tyr271, Leu267, Leu167, and Ile66. Therefore, the docking of CGS21680 shows that the selectivity of this ligand could be due to the presence of His264, Tyr271, Leu267, Leu167, Asp170 and Ile66. These findings may provide a possible explanation for the higher selectivity of this agonist for the A_{2A} adenosine receptor in comparison to the A_{2B} receptor. Therefore, the results from our molecular docking of the agonists showed that the results are in accordance

with experimental data and Val84, Thr88, Gln89, Glu169, Asn181, Phe182, His250, Asn253, Ile274, Ser277, and His278 are essential for A$_{2A}$ agonist docking and the selectivity of the A$_{2A}$ receptor could be due to the presence of Ile80, Leu249, Ile252, Ala59, His264, Tyr271, Leu267, Leu167, Asp170 and Ile66.

2.3.6   Probing of the adenosine A$_{2B}$ models by docking of selected antagonists (theophylline, ZM241385, MRS1706, and PSB-601) and selection of the most suitable model for further studies

The obtained binding mode for the most simple, known antagonist theophylline [35] (compound **19** in Figure **2.8**) in the A$_{2B}$-I model suggests that the Asn254 side-chain forms hydrogen bonding interactions with the carbonyl group at the 6-position and the NH group at the 7-position of the xanthine ring. In addition, the Gln90 side-chain fixes the ligand by another hydrogen bonding interaction to the carbonyl oxygen atom at the 2-position of the xanthine ring and the amino group at the 9-position of the xanthine ring interacts with a water molecule.

Furthermore, the methyl group at the 1-position is stabilized by lipophilic interactions with Val191, and Phe187, while the methyl group at the 3-position can interact with Thr89, Ile136, and Leu86. The xanthine moiety of the ligand forms an aromatic stacking interaction with Phe173 and lies inside the pocket formed by Leu172, Val183, His250, and Trp247. The binding mode in the A$_{2B}$-II model is generally the same as in the A$_{2B}$-I model, except that Asn186 forms a water-mediated interaction with the carbonyl group at the 6-position of the ligand. However, in the A$_{2B}$-III model the carbonyl oxygen atom at the 2-position of the xanthine ring interacts with a water molecule (Figure **2.19**).

The obtained binding mode of ZM241385 [104] (compound **31** in Figure **2.8**) with the A$_{2B}$-III model allowed us to propose that the bicyclic triazolotriazine core of ZM241385 is stabilized by an aromatic stacking interaction with Phe173, aliphatic hydrophobic interactions with Val250, Met272, Met179, Val253, Met182, and Ile276, and hydrogen bonding interactions with Asn254 and Glu174 (conjugated hydrogen bonding from Thr257 through Glu174 and Asn254 to the exocyclic amino group), which interacts with the exocyclic amino group.

Furthermore, Asn254 interacts with the furan oxygen atom and the amino group at the 1-position of the triazolotriazine moiety of the ligand. At the same time, the furan oxygen atom is in proximity to the backbone amino group of Asn186. In addition, the furan ring is stabilized by hydrophobic interactions with Leu86, His251, and Val85, and the furan ring is approximately 4.3 Å away from the highly conserved Trp247. Moreover, the phenolic hydroxyl group forms a hydrogen bonding with the backbone carbonyl group of Ser68 and the phenyl ring forms hydrophobic interactions with Ile67, Gly70, and Leu172. Furthermore, Lys269 is located near the phenol moiety of the ligand (Figure **2.19**).

The most favourable position of the phenyl ring of ZM241385 was surrounded by Leu267, Tyr271, and His264 of the A_{2A} receptor, however, this most favourable arrangement of the phenyl ring of ZM241385 inside the A_{2A} receptor has two serious drawbacks in comparison to the binding mode obtained for the A_{2B} receptor. Firstly, in the A_{2B} receptor the phenyl ring of the ligand was located near Lys269, which resulted in unfavorable interactions. Second, because of the large distance Lys269 was unable to form the very important interaction with the phenyl ring of the ligand. These results might provide an explanation for the considerable difference between the K_i values of ZM241385 determined for the A_{2A} [0.8 nM] and A_{2B} [50 nM] and Leu267, Tyr271, His264, Leu249, and Ile252 could be responsible for increasing the affinity towards the adenosine A_{2A} receptor. The binding modes for the A_{2B}-I and A_{2B}-II models are similar to that of A_{2B}-III model however, in the A_{2B}-II model His280 is directly involved in a hydrogen bonding interaction with the phenolic hydroxyl group of the ligand.

The placement of MRS-1706 [38] (compound **29** in Figure **2.8**) in the model A_{2B}-II is that the Asn254 side-chain forms hydrogen bonding interactions to the carbonyl group at the 6-position and the NH group at the 7-position of the ligand. In addition, the Gln90 side-chain constitutes a hydrogen bonding interaction with the carbonyl oxygen atom at the 2-position of the ligand. Besides that the backbone amino groups of Phe173 and Glu174 form hydrogen bonds with the carbonyl oxygen atom of the phenoxy acetamide moiety of the ligand. The propyl group at the 1-position is located inside the hydrophobic pocket formed by Val183, Phe187, Val191, and Cys190. Likewise the propyl group at the 3-position is in contact to Thr89, Leu86, Ile136, and Pro140.

Moreover, the xanthinephenyl moiety of the ligand is involved in hydrophobic interactions with Phe173, Val250, Met272, Ile276, Val253, and Trp247.

The phenyl ring of the phenoxy acetamide moiety of the ligand resides in the hydrophobic pocket formed by Leu172 Trp270, and the lipophobic part of Lys269 and makes favourable cation-π interactions with Lys170 and Lys267. The obtained position of MRS-1706 in the A_{2B}-I and A_{2B}-III model is similar to that in the previous one, except that in the A_{2B}-I model Glu14, Asn186, and His280 are directly involved in an interaction (Figure **2.19**).

The obtained binding mode for PSB-601 [115] (compound **28** in Figure **2.8**) in the model A_{2B}-III suggests that the Asn254 side-chain forms hydrogen bonding interactions with the carbonyl group at the 6-position and the NH group at the 7-position of the ligand. Besides that, the backbones of Glu174, Phe173 and a water molecule form hydrogen bonding interactions with the sulfonyl group of the ligand. Furthermore, the backbone amino group of Asn175 is in proximity to the sulfonyl group of the ligand (Table **2.5**).

In addition, the amino group at the 9-position of the ligand is involved in a hydrogen bonding interaction with a water molecule. Additionally, the propyl group at the 1-position of the ligand is located inside the hydrophobic pocket formed by Leu86, Val85, Thr89, His251, and Val191. The phenylxanthine moiety of the ligand is stabilized by an aromatic stacking interaction with Phe173 and located inside the pocket formed by Ala64, Ile67, Met179, Ile276, His280, Met182, Val250, and Trp247. Moreover, the benzylpiperazine moiety of the ligand is surrounded by Leu172, Lys265, Pro268, Met272, and Lys269. As before, the binding modes for the A_{2B}-I and A_{2B}-II models are similar to that of the A_{2B}-III model, however, in the A_{2B}-I model Leu81, Lys170, Asn186 and His280 are directly involved in interactions (Figure **2.19**).

Comparison of all models

Of the investigated models, A_{2B}-I and A_{2B}-II yielded concordantly the same binding modes, which overlap significantly with the location of binding site found in the adenosine A_{2A} receptor. However, A_{2B}-III has a different binding mode where the ligands bind in an extended conformation and its orientation is almost perpendicular to

the membrane plane and co-linear with transmembrane helix VII. As a next step, to assess the relevance of the individual models, the complex properties were not only investigated with respect to the sterical and electronic aspects of the binding modes, but in addition the estimated binding affinities were taken into account. As shown in Table **2.4** the calculated free binding energies ΔG for the A_{2B}-I, A_{2B}-II and A_{2B}-III models are similar. In summary, all models perform equally well, quantitatively, i.e. in terms of relative binding affinities, the results were equivalent. However, qualitatively, i.e. in terms of predicted binding modes they were different. Therefore, in order to make a decision, other criteria namely the template features mentioned in section (2.3.2), where taken into account too. Thus, for further studies we chose model A_{2B}-III which is the one with the highest sequence identity (56%), the lowest rmsd value (relative to the adenosine A_{2A} receptor), the most favourable gap ratio, and the obtained results for the A_{2B} receptor are in accordance with experimental data where His280 might not be important for ligand binding but for maintaining the global receptor architecture (S. Hinz, A. Schiedel, C. E. Müller, unpublished results). In order to validate this model further, we subsequently compared the binding modes and affinities of a larger set of compounds with experimental data.
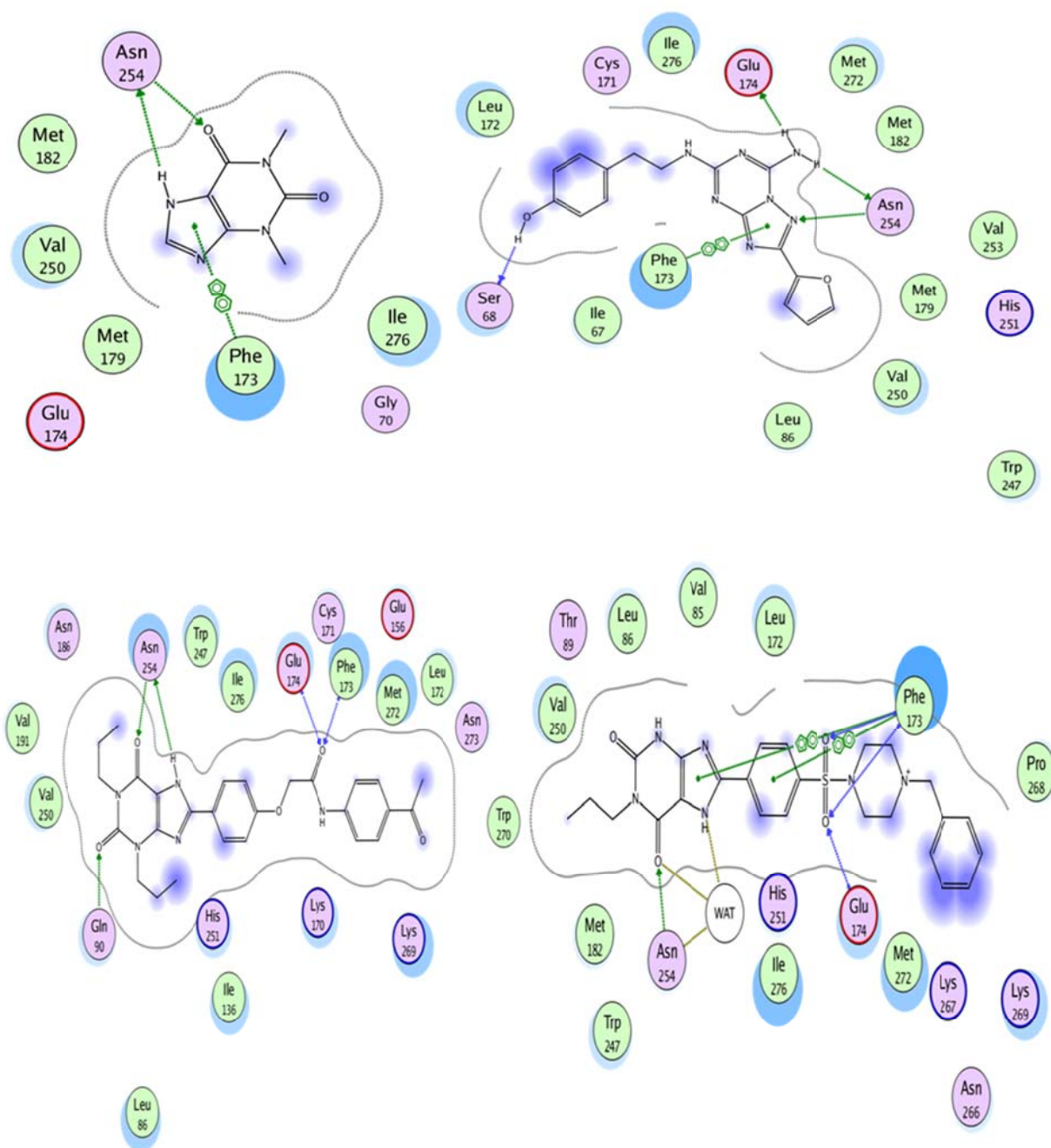
Figure 2.19 Predicted binding modes for theophylline in model A$_{2B}$-I (top left), ZM241385 in model A$_{2B}$-III (top right), MRS-1706 in model A$_{2B}$-II (bottom left) and PSB-601 in model A$_{2B}$-III (bottom right). Shown are hydrogen bonding and aromatic stacking interactions

Table 2.4 The calculated ΔG free energy of binding and binding affinities for all models

Ligand	Calculated ΔG (A$_{2B}$-I) [kcal mol^{-1}]	Calculated ΔG (A$_{2B}$-II) [kcal mol^{-1}]	Calculated ΔG (A$_{2B}$-III) [kcal mol^{-1}]
Theophylline [35]	-48.0 ± 0.6	-45.0 ± 1.2	-48.1 ± 1.0
ZM241385 [104]	-80.0 ± 3.0	-80.0 ± 1.0	-86.1 ± 4.0
MRS-1706 [38]	-114.0 ± 3.3	-99.1 ± 4.1	-115.0 ± 3.0
PSB-601 [115]	-100.0 ± 2.0	-94.0 ± 1.0	-106.0 ± 4.0
RMSD [Å]	3.25	3.29	0.8

RMSD with respect to the X-ray structure of A$_{2A}$

2.3.7 Docking of a larger set of compounds to A$_{2B}$-III

In order to cover a wider range of ligands, we studied some smaller and more weakly binding ligands as well. The obtained results for 1,3-dipropylxanthine, 1-propyl-xanthine, 1-butylxanthine, and 1-allylxanthine [35] (compounds **20**, **21**, **22** and **23** in Figure **2.8**) suggest that the Asn254 side-chain consistently forms hydrogen bonding interactions with the carbonyl oxygen atom at the 6-position and the NH group at the 7-position of the xanthine ring. Furthermore, a water molecule forms a hydrogen bonding interaction with the carbonyl oxygen atom at the 2-position of the xanthine ring. The substituted group at the 1-position is located inside the binding pocket formed by Leu86, Thr89, and Val85, while the substituted group at the 3-position is involved in ligand binding via interaction with Ile67, Ala82, Ile276, and Ala64. The xanthine moiety is stabilized by an aromatic stacking interaction with Phe173 and located inside the pocket formed by Met182, His251, Trp247, Val250, Val253, Met272, and Met179.

According to the computed binding mode for 1-propyl-8-cyclopentylxanthine [35] (compound **24** in Figure **2.8**) the Asn254 side-chain forms two hydrogen bonding

interactions, one to the carbonyl oxygen atom at the 6-position and the other one to the NH group at the 7-position of the xanthine ring. In addition, a water molecule stabilizes the ligand's position by a hydrogen bonding interaction with the amino group at the 3-position of the xanthine ring. The propyl group at the 1-position is located inside the binding pocket formed by Val85, Leu86, Val191, and Thr89. The xanthine moiety is stabilized by an aromatic interaction with Phe173 and lies inside the pocket formed by Ala82, trp247, Val250, His251, Met179, and Met182. Furthermore, the cyclopentyl ring is surrounded by Val253, Ala275, Ile276, and Met272.

The proposed binding mode for PBS-1115 [40] in A_{2B}-III model (compound **25** in Figure **2.8**) is much the same to that of 1-propyl-8-cyclopentylxanthine. Additionally, the sulfonate function of the ligand is stabilized by interactions with the sidechains of Asn266, Thr257, and the backbone amino group of Lys267. The results are in agreement with mutagenesis data for the closely related human adenosine A_{2A} receptor subtype (Table **2.2**) and are consistent with SAR of a series of sulfonamide derivatives of PSB-1115 bearing a large variety of substituents [115].

The result from our docking study with MRE-2029F20 [37] compound **30** in Figure **2.8**) was that the Asn254 side-chain directly interacts with the xanthine moiety of the ligand as before. In addition, a water molecule is involved in a hydrogen bonding interaction with the amino group at the 9-position of the ligand. The propyl group at the 1-position is stabilized by lipophilic interactions to Leu86, Val191, Met182, and Thr89, while the propyl group at the 3-position is neighbouring the residues Ala60, Val85, Ala82, His280, and Ala64. The carbonyl group of the oxyacetamide moiety of the ligand is hydrogen-bonded to the backbone amino groups of Glu174 and Phe173. At the same time, the amino group of the oxyacetamide moiety of the ligand forms a hydrogen bonding with a water molecule. The pyrazolylxanthine moiety of the ligand is located inside the pocket formed by Ile67, Met179, Trp247, Val250, Ile276, His251, and Met272 and stabilized by an aromatic interaction with Phe173. In addition, the methylenedioxyphenyl moiety of the ligand is surrounded by lipophilic groups of Leu172 and by polar groups of Asn175, Thr257, and Gln263.

The molecular docking performed for the 4'-furan-2-yl-N-pyridin-3-yl-4,5'-bipyrimidin-2'-amines as potent and selective adenosine A_{2B} receptor antagonist [46]

(compounds **33**, **34**, and **35** in Figure **2.8**) suggests that Asn254 is involved in an interaction with the furan oxygen atom and the amino group at the 2'-position of the ligand and the furan moiety of the ligand is located in the pocket formed by Thr89, His251, Val191, and Leu86. Additionally, the nitrogen atom of the pyridine moiety of the ligand is stabilized by hydrogen bonding interaction with Thr257 and hydrophobic interactions with Val253 and Met272. The nitrogen atom at the 1'-position of the ligand forms a hydrogen bonding interaction with a water molecule. Furthermore, the nitrogen atom at the 1-position of the pyrimidine moiety of the ligand is potentially kept in its position by a hydrogen bonding interaction with the protonated nitrogen atom of His280. In addition, the bipyrimidine moiety of the ligand is anchored by an aromatic stacking interaction with Phe173 and located in the hydrophobic pocket formed by Ala60, Ala64, Trp247, Val250, Met182, Met179, Ala275, Vla85, Ala82, and Ile67. The obtained binding modes are comparable for all three members of this type of antagonists (Figure **2.20**).
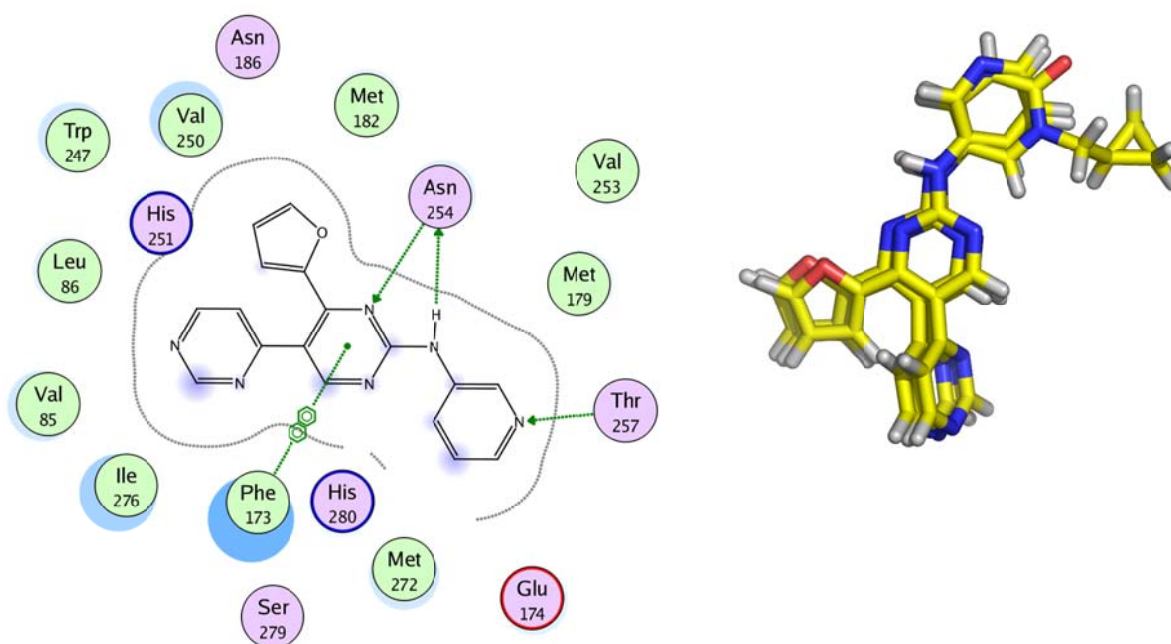
Figure 2.20 binding mode for 33 (left). Showing hydrogen bonding and aromatic stacking interactions. And the superposition of final ligand placements for the non-xanthine antagonists (right)

The obtained binding mode for OSIP339391 [48] in A_{2B}-III (compound **32** in Figure **2.8**) shows that the amino group attached to the heterocycle is involved in a hydrogen

bonding interaction with Asn254 and the carbonyl group of the acetamide moiety of the ligand is hydrogen bonded to Thr257, and Asn266 is located in proximity to the carbonyl group of the acetamide moiety of the ligand. Furthermore, the phenyl moiety of the ligand is stabilized by an aromatic interaction with Trp247 and involved in hydrophobic interactions with Leu86, His251, Met182, Val85, and Thr89 however, the pyrrolopyrimidine moiety of the ligand is stabilized by an aromatic interaction with Phe173 and located inside the pocket formed by Val253, Ala275, Met272, Val250, Ile67, Ala64, Ala82, and Ile276. In addition, the methyl moiety of the ligand is placed in the cage formed by Met179 and Thr257. The piperazinylpropylphenyl moiety of the ligand is occupied by a hydrophobic residue such as Leu172. Additionally, the cationic sideshain of Lys269 is involved in cation-π interaction with the propylphenyl moiety of the ligand. In particular, this interaction could be suggested to provide significant stability at the solvent-exposed surface of a protein (Figure **2.21**).
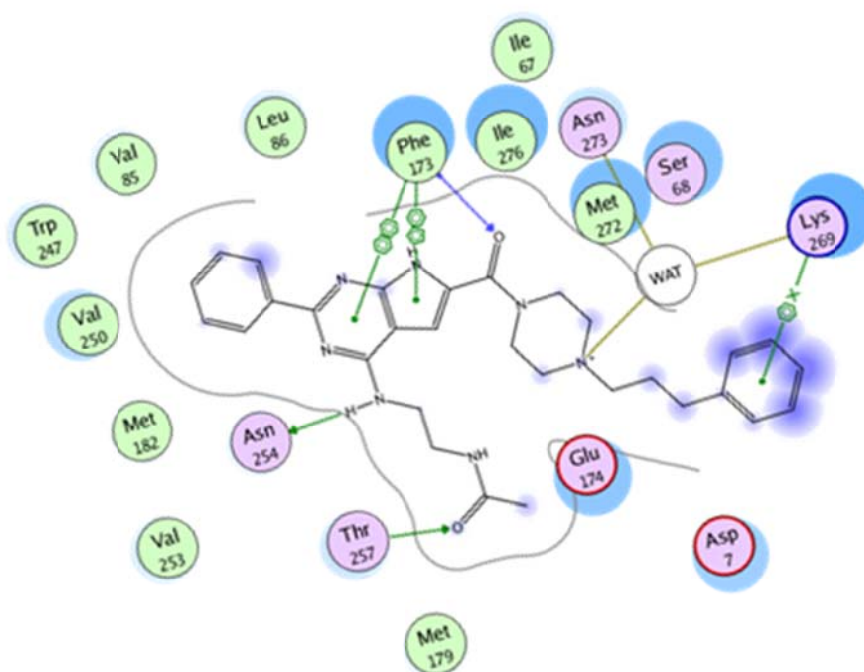
Figure 2.21 Predicted binding mode for OSIP339391. Showing hydrogen bonding, aromatic stacking and aromatic-cation interactions

The obtained binding modes of MSX-2 [105] and Istradefylline [106] (compounds **26** and **27** in Figure **2.8**) into the A$_{2B}$ receptor is similar to that of the A$_{2A}$ receptor where the corresponding residues show the same hydrogen bonding and hydrophobic

interactions. In the adenosine A_{2A} receptor the styryl moiety of the ligands are anchored by an aromatic stacking interaction with Tyr271 and hydrophobic interactions with Leu267, and His264. However, the corresponding residues Asn273, Lys269, and Asn266 of the A_{2B} receptor are located within 7 Å from the styryl moiety of the ligand thus unable to connect to this moiety of the ligands (Figure **2.22**).
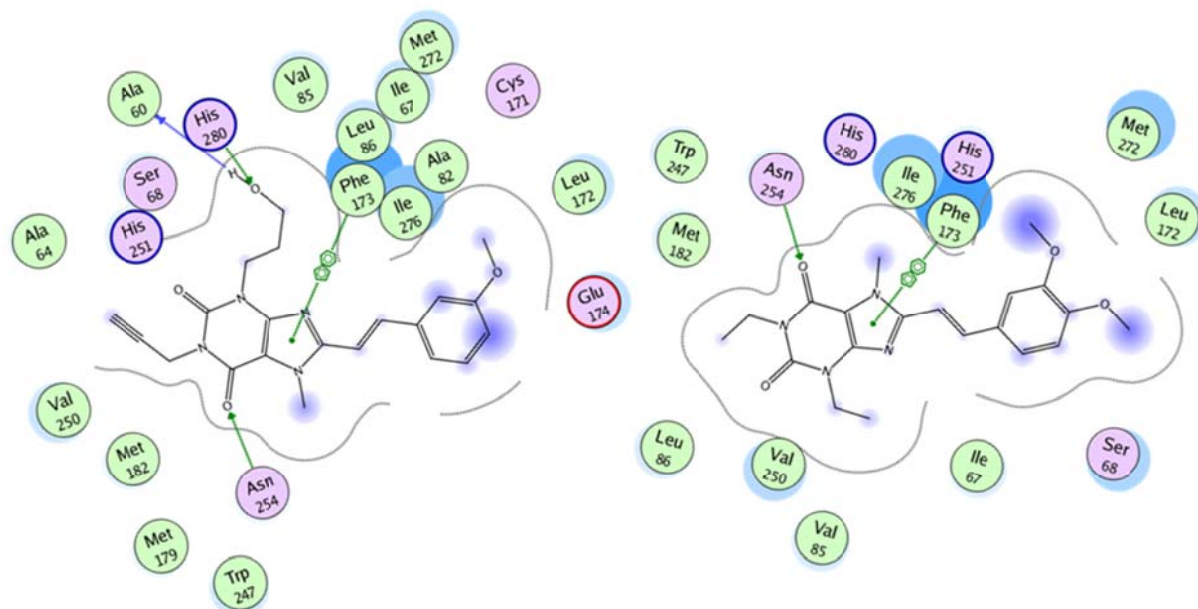
Figure 2.22 Predicted binding modes for MSX-2 (left) and Istradefylline (right). Showing hydrogen bonding and aromatic stacking interactions

The obtained result from molecular docking of preladenant [107**]** (compound **36** in Figure **2.8**) with the A_{2B} receptor is comparable to that of the A_{2A} receptor, while the corresponding residues Glu174, Asn273, Lys269, and Asn266 in the case of the A_{2B} subtype, are far away, thus avoiding any favourable interactions (Figure **2.23**).
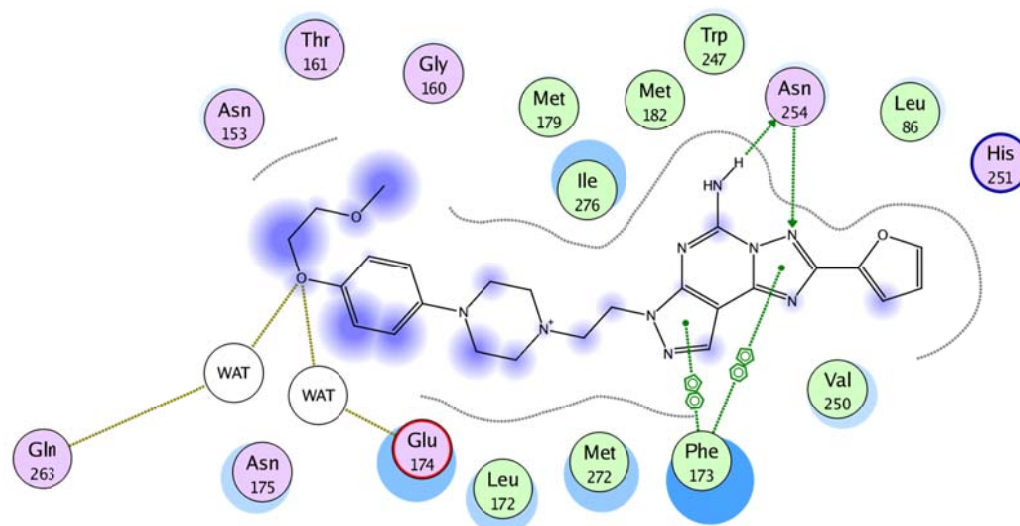
Figure 2.23 Predicted binding mode for preladenant. Showing hydrogen bonding and aromatic stacking interactions

Table 2.5 Interaction energies (in kcal mol $^{-1}$) between the A_{2B} antagonists and the important residues based on the energy decomposition analysis MM-GBSA

Residue/ A_{2B}	ZM241385	MSX-2	Istradefylline	Preladenant	MRS-1706	MRE-2029F20	PSB-601
Asn254	**-6.9**	-2.3	**-4.6**	**-6.1**	-3.8	**-4.7**	-4.2
Glu174	**-8.2**	-1.2	-0.7	**-4.4**	**-4.9**	**-5.2**	-3.2
Phe173	-5.7	-6.0	-6.4	**-6.6**	**-6.6**	**-7.7**	-7.7
Val250	-2.5	**-2.8**	**-2.7**	-2.3	**-3.0**	**-3.1**	-2.4
Trp247	-0.7	-0.9	**-1.5**	-0.8	**-1.9**	**-1.8**	**-1.9**
Leu86	-1.0	**-1.4**	**-1.5**	-1.0	**-1.3**	**-1.4**	-1.2
His251	-0.7	-0.7	**-0.9**	-0.5	**-1.8**	**-1.6**	**-1.2**
Val85	-0.3	**-4.4**	**-2.0**	-0.6	**-1.4**	**-1.7**	-1.1
Thr89	-0.2	**-0.5**	-0.2	-0.3	**-0.8**	**-0.6**	**-0.6**
His280	-0.0	**-2.1**	**-0.8**	-0.1	**-1.5**	**-0.8**	-0.2
Met182	-1.7	**-2.1**	**-2.5**	-1.8	**-1.9**	**-1.9**	**-2.1**

Val256	-0.0	-0.0	-0.0	-0.0	-0.0	-0.0	**-0.1**
Val253	**-0.7**	**-0.4**	-0.3	**-0.5**	-0.2	-0.2	**-0.5**
Ala64	-0.1	**-1.3**	**-0.5**	-0.1	**-0.8**	**-0.5**	-0.2
Ala271	-0.1	-0.1	-0.1	-0.1	-0.1	-0.0	**-0.3**
Asn266	-0.0	-0.1	-0.1	**-0.6**	-0.2	-0.2	**-2.0**
Lys269	-0.2	**-0.4**	**-0.4**	-0.2	-0.1	-0.1	**-2.1**
Asn273	-0.1	-0.1	-0.2	-0.1	-0.1	-0.2	-0.2
Lys267	-0.1	**-0.3**	-0.1	-0.1	-0.1	-0.1	**-0.4**
Lys265	-0.0	**-0.2**	-0.0	-0.1	-0.0	-0.0	**-0.2**
Pro268	-0.0	-0.0	-0.0	-0.1	-0.0	-0.0	-1.0
Leu172	**-2.8**	-1.9	-2.1	**-2.8**	**-4.5**	**-4.5**	**-3.4**
Asn175	-0.1	-0.1	-0.1	**-2.0**	**-4.3**	**-2.5**	-0.2
Ser68	**-1.7**	**-0.8**	**-1.3**	-0.1	**-0.4**	-0.1	-0.3
Lys170	-0.2	**-0.3**	-0.1	-0.1	-0.1	-0.1	-0.1
Ala82	-0.1	**-1.6**	**-0.4**	-0.2	-0.2	**-0.6**	-0.2

The most significant interactions are highlighted in bold in order to emphasize the respective interaction patterns

So far, the results of the docking analysis of the antagonists of the adenosine A_{2B} receptor display a common binding mode for the xantine and nonxanthine derivatives which is very similar to that of the binding mode of the adenosine A_{2A} receptor. In addition, considering the close relationship of the A_{2A} and A_{2B} adenosine receptor subtypes, the results may be correlated to the mutagenesis data published for the much better characterized A_{2A} subtype (Table **2.2**), which in fact confirms the relevance of the identified interaction partners. Moreover, the structural findings are accompanied by energetic aspects. In Table **2.6** the observed binding energies ΔG for each complex are listed. The experimentally measured values ranged from -6.8 to -12.5 kcal·mol^{-1}. As

shown in Figure **24**, the computed values reflect the overall trend, but overestimate the ΔG-values by a factor of five (due to the chosen prefactors as mentioned in the methods section).

Table 2.6 K_i values from experimental measurements, absolute free binding energies calculated from K_i values, and computed values of ΔG [kcal mol^{-1}] for all antagonist ligands tested in the present study

	Ligand	Experimental K_i value [nM]	Experimental ΔG [kcal/mol]	ΔE_{ELE}	ΔE_{VDW}	calc. ΔG [kcal/mol]
1	Theophylline [35]	9070	-6.8 ± 0.1	-26.3 ± 2.0	-21.8 ± 1.6	-48.0 ± 1.0
2	1,3-Dipropylxanthine [35]	1110	-8.00 ± 0.2	23.4± 0.9	-30.7 ± 0.5	-54.0 ± 0.4
3	1-Propylxanthine [35]	360	-8.6 ± 0.1	-30.6± 0.7	-24.4 ± 0.8	-54.9 ± 1.1
4	1-Butylxanthine [35]	421	-8.6 ± 0.1	-33.7± 1.1	-25.3 ± 1.0	-59.0 ± 0.5
5	1-Allylxanthine [35]	461	-8.5 ± n.a.	-27.5 ± 2.0	-24.3± 1.6	-51.8 ± 1.7
6	1-Propyl-8-cyclopentylxanthine [35]	34.4	-10.0 ± 0.2	-31.7 ± 1.7	-35.9 ± 1.1	-67.6 ± 1.1
7	PSB-1115 [40]	53.4	-9.8 ± 0.2	-31.3± 4.6	-41.4 ± 1.7	-72.7 ± 4.2
8	MRS-1706 [38]	1.39	-11.9 ± n.a.	-47.9 ± 3.1	-66.8± 2.1	-114.7 ± 2.8
9	MRE-2029F20 [37]	5.5	-11.1 ± n.a.	-39.1 ± 2.5	-61.7 ± 2.6	-100.8 ± 2.8

10	PSB-601 [115]	3.6	-11.3 ± 0.1	-50.8± 3.4	-55.1± 1.9	-105.9 ± 3.5
11	2-aminopyrimidine derivative [46]	17	-10.4 ± 0.2	-29.6± 1.8	-41.9 ±1.3	-71.4± 0.7
12	2-aminopyrimidine derivative [46]	116	-9.3 ± 0.1	-26.2 ± 0.8	-40.7 ±0.7	-66.9± 1.3
13	2-aminopyrimidine derivative [46]	119	-9.3 ± 0.2	-18.8 ± 1.5	-46.8 ± 1.5	-65.6 ± 1.8
14	Osip339391 [48]	0.5	-12.5 ± 0.1	-53.0 ± 1.4	-61.6 ± 2.7	-114.7 ± 3.4
15	ZM241385 [104]	5.8	-11.0 ± 1.3	-43.9 ± 3.2	-42.1 ± 1.5	-86.1 ± 3.6
16	MSX-2 [105]	10	-10.8 ± n.a	-32.7 ± 2.3	-50.7 ± 1.2	-83.4 ± 1.2

Figure 2.24 Correlation of experimental binding free energies ΔG and calculated ΔG values
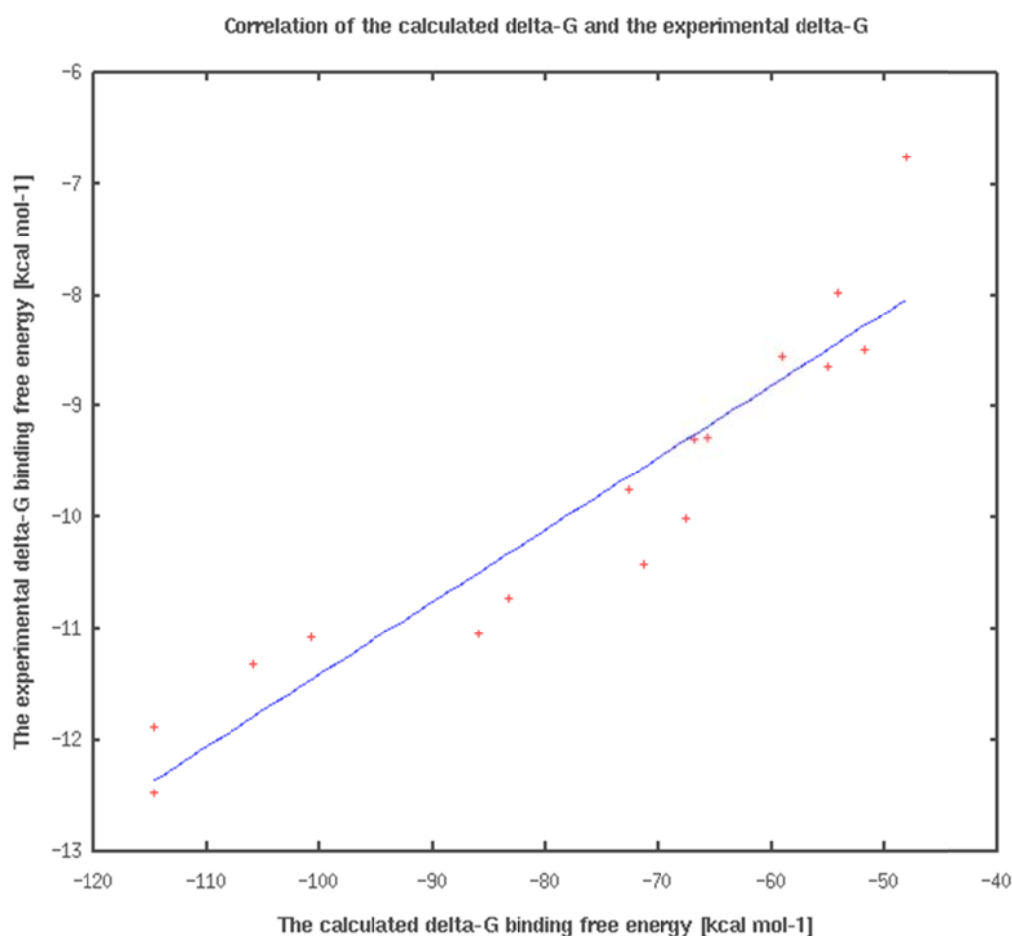
Docking of agonists in A₂B-III

The resulting binding mode of the native agonist adenosine [117] (compound **37** in Figure **2.9**) implies that the amino group at the 6-position of adenosine forms a hydrogen bonding interaction with the carbonyl oxygen atom of Asn254 (conserved among all adenosine receptor subtypes). Likewise, the 3'-hydroxyl group of the ligand is involved in a water-mediated interaction with Ala60 and located at a distance of 3.69 Å from His280. Additionally, the 2'-hydroxyl group of adenosine constitutes a water-mediated interaction with the backbone carbonyl group of Leu81. The 5'-hydroxyl group might form a hydrogen bonding interaction with Ser279 (located at a distance of 3.3 Å). The adenine moiety is located in the hydrophobic pocket formed by Met179, Met182, Val253, Val250, His251, Ile276, and Trp247 and stabilized by an aromatic stacking interaction with Phe173. Also, the ribose moiety is surrounded by Ala60, Ala64, Ile67, Ala82, Val85, Leu86, and Ile61.

The obtained result for the binding mode of 2-chloroadenosine [118] (CADO, compound **38** in Figure **2.9**) is similar to that of the above-mentioned adenosine.

The obtained result from molecular docking study of NECA [29] (compound **39** in Figure **2.9**) is similar to that of adenosine; additionally, the 2'-hydroxyl group of NECA forms water-mediated interactions with the backbone carbonyl groups of Ala82 and Leu81. At the same time, the carbonyl group at the 5'-position of NECA forms a hydrogen bonding interaction with Ser279 (Figure **2.25**). As shown in Table **2.7**, the calculated free energy of binding ΔG for the A_{2A} crystal structure is much higher than for the A_{2B} model and the electrostatic interactions appeared to be mainly responsible for affinity.
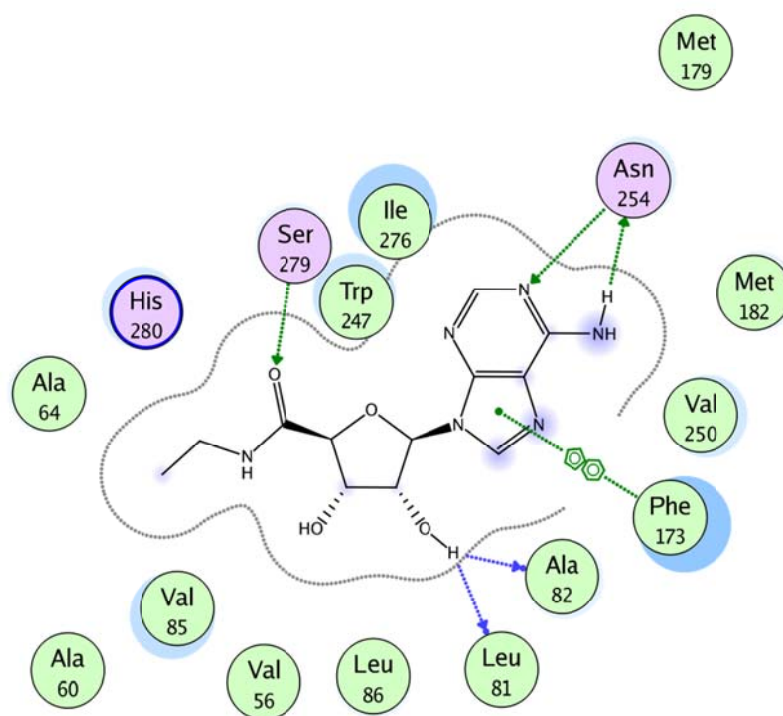
Figure 2.25 Predicted binding mode for NECA. Showing hydrogen bonding and aromatic stacking interactions

Table 2.7 The calculated ΔG free energy of binding and binding affinities for both the A_{2A} crystal receptor and A_{2B} model

Agonist	Calculated ΔG (A_{2A}) [kcal mol^{-1}]	Calculated ΔG (A_{2B}) [kcal mol^{-1}]
NECA	-94.92 (ELE= -59.86, VDW= -35.07)	-79.25 (ELE= -39.55, VDW= -39.71)

The higher affinity of NECA towards the adenosine A_{2A} as compared to the A_{2B} receptor most likely can be explained by the following points. Firstly, molecular docking of the A_{2A} and A_{2B} adenosine receptors has detected that the amino group at the 6-position of NECA was hydrogen bonded to $Asn^{6.55}$ conserved among all adenosine receptor subtypes. In the A_{2A} adenosine receptor, Glu169 is involved in an interaction with the ligand, while in the A_{2B} model the corresponding Glu174 is located at a large distance of 6.6 Å from the amino group at the 6-position of NECA. In addition, the 3'-hydroxyl group of the ligand forms water-mediated interactions with Ala59 and Ile80 and the amino group at the 7-position of the NECA forms a hydrogen bonding with a water molecule. These interactions were not observed for the A_{2B} model. This fact is reflected by the less favorable electrostatic interaction energy for NECA in the A_{2B} receptor model as given in Table **2.7**.

Secondly, The A_{2A} adenosine receptor has a larger volume of the hydrophobic pocket than the A_{2B} receptor. The size of this hydrophobic pocket of the A_{2A} receptor is large enough to accommodate the ligand which could contribute to increase of the A_{2A} affinity. However, in the A_{2B} receptor, the size of the pocket has a higher degree of conformational flexibility, decreasing the relative stability of the complex.

Thirdly, on the other hand, the A_{2B} receptor agonist was located slightly deeper inside the receptor than the A_{2A} adenosine receptor. These particular features of the A_{2A} adenosine receptor combined with the obtained binding mode allow us to propose an explanation of the high affinity of NECA at this subtype in comparison to the A_{2B} adenosine receptor subtype.

N^6-Cyclopentyladenosine (CPA [118], compound **40** Figure **2.9**) is an agonist, which in contrast to the previous ones, carries a bulky substituent at its 6-position. The predicted binding mode for CPA indicates that the cyclopentyl moiety at the 6-position of the ligand is located inside a pocket formed by several amino acid residues. In particular, Met179, Ala275, Val253, Thr257, Val250, and Met272 are arranged within 3.5 Å around the cyclopentyl ring of CPA. Additionally, the hydroxyl group of the ligand at the 3'-position forms a water-mediated interaction with Leu81 (Figure **2.26**). The docking results of adenosine, NECA and CPA are in accordance with published data regarding the binding modes of the adenosine receptor agonists [119].
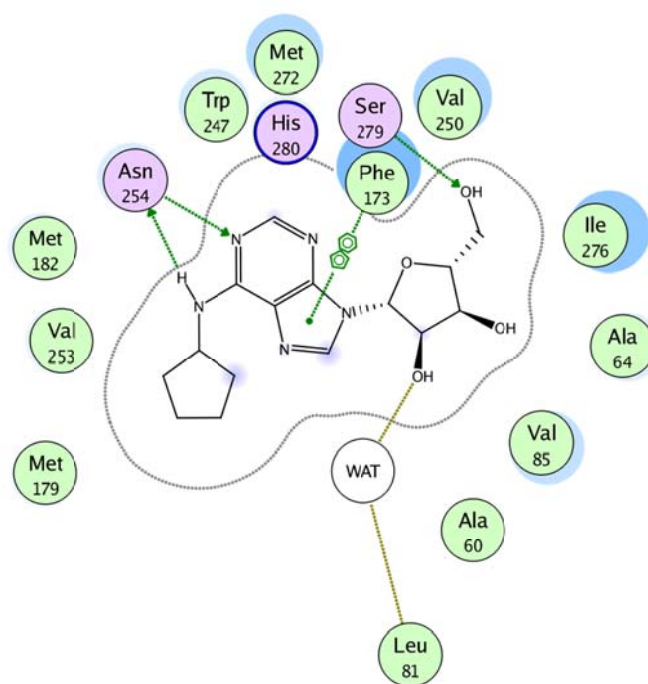
Figure 2.26 Predicted binding mode for CPA. Showing hydrogen bonding and aromatic stacking interactions

The N[6]-substituted NECA derivative [30] (compound **41** in Figure **2.9**) nicely fits inside the TM regions of the model of the A_{2B} receptor. This agonist shows many hydrophilic interactions and interacts in the same manner as NECA (Figure **2.27**). In addition, the furan moiety of the ligand is in contact with Met272, Ala271, Ala275, Val253, Val250, Met179, and the lipophobic part of Lys267 which is in agreement with mutagenesis studies demonstrating that the said residues exert an effect on agonist affinity (Table **2.2**).
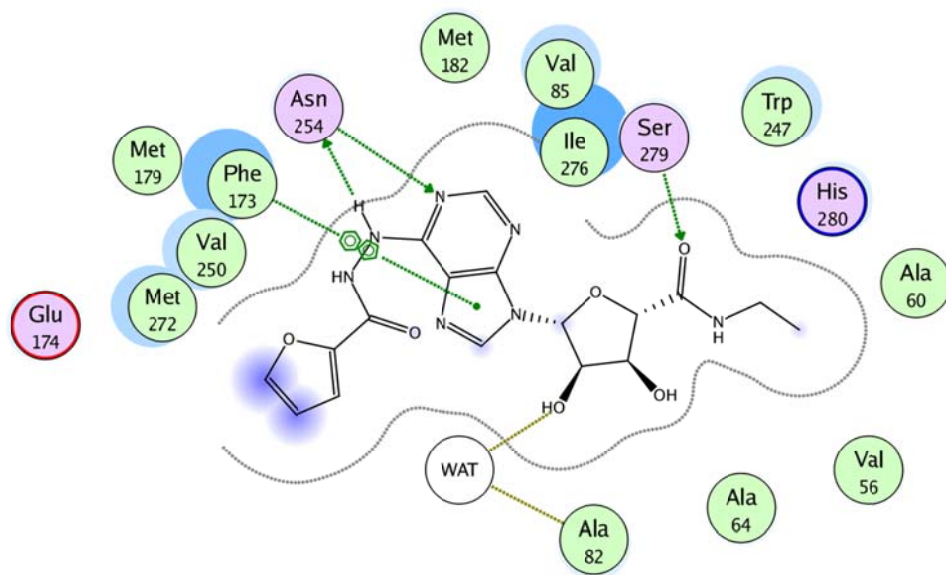
Figure 2.27 Predicted binding mode for NECA derivative. Showing hydrogen bonding and aromatic stacking interactions

The interaction pattern obtained for the non-nucleosidic A_{2B}-selective agonist BAY-60-6583 [34], which (apart from having a planar heterocyclic core) only distantly resembles the native agonist adenosine or its derivatives (compound **43** in Figure **2.9**) suggests that the amino group at the 6-position of BAY-60-6583 forms a hydrogen bonding interaction to the amide oxygen of Asn254. At the same time, the protonated nitrogen atom of His251 is involved in a hydrogen bonding interaction with the carbonyl group of the sulfanylacetamide moiety of the ligand. Furthermore, the amide side-chain of Asn186 makes a hydrogen bonding interaction with the amino group of sulfanylacetamide moiety of the ligand, even though it is not maintained along the whole MD trajectory. Also, Gln90 is observed in proximity to the amino group of sulfanylacetamide of the ligand (3.3 Å).

The oxygen atom of the cyclopropylmethyl-phenyl ether of the ligand is within a hydrogen bonding distance of the protonated nitrogen atom of His280 and Ser279 is predicted to be in proximity to the oxygen atom of the cyclopropylmethyl-phenyl ether. The cyano group at the 3-position of the ligand is involved in a hydrogen bonding interaction with Thr89. The cyano group at the 5-position of the ligand forms a water-mediated hydrogen bonding interaction.

The phenylpyridine moiety of the ligand is stabilized by an aromatic stacking interaction with Phe173 and located inside in the hydrophobic pocket delimited by Leu86, Met182, Met179, Ala275, Val253, Phe243, Phe187, Val250, Ile276, Val85, and Trp247, while the cyclopropyl residue is surrounded by Leu81, Ile67, Ala82, Phe63 and Ala64 (Figure **2.28**).
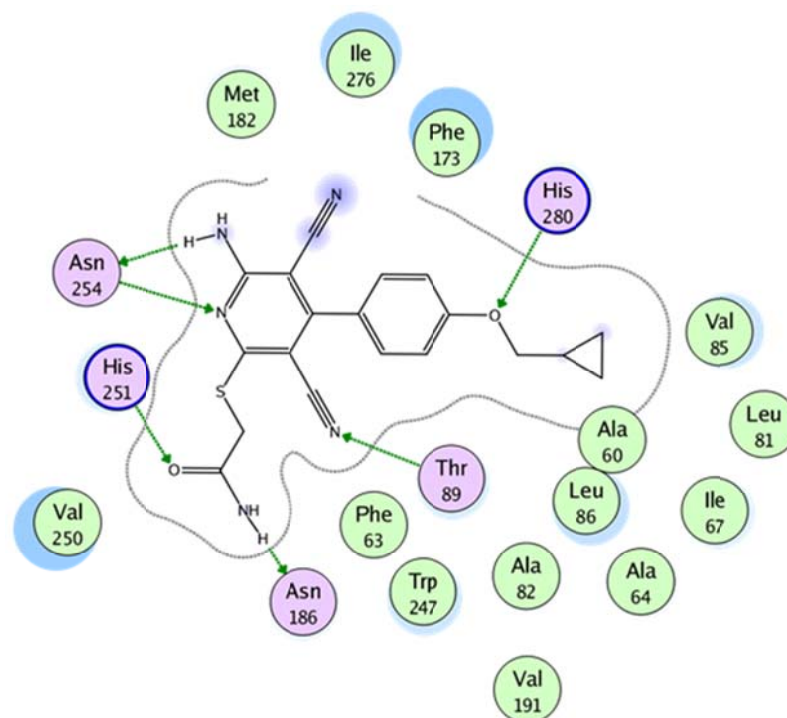
Figure 2.28 Predicted binding mode for BAY-60-6583. Showing hydrogen bonding interactions

Summarizing here, we may say, that the adenosine agonists, which have a similar (purine) ring structure as the xanthine antagonists (even though the interaction pattern is inverted), analogously present a common binding pattern. As key residues again Asn254 was identified, but now His280 is also constantly involved in contacting the ribose moiety, which appears to be essential for the agonistic character of the compounds investigated so far. The residue of the template structure bovine rhodopsin that corresponds to His280 is Lys296, which is the one that carries the covalently bound cis-trans retinal. This implies that His280 might be directly involved in or even triggers the receptor activation mechanism.

Again, the geometrical observations were complemented by estimating the strength of the ligand–receptor interactions. The difficulty here was, however, that the agonist effects were measured by functional assays which yield EC_{50} values. Those cannot

unambiguously be converted to K_i-values, since they depend very much on test conditions, in particular receptor density. Results from radioligand binding studies of agonists versus an agonist radioligand (labelling the high-affinity state of the receptor) would be ideal for the calculations, but such data are not available since an agonist radioligand has not yet been developed for A_{2B} receptors. Table **2.8** lists the EC_{50} values obtained in cAMP assays along with computed ΔG values. Since the data were taken from different studies, they can only provide a very rough estimate of compound activity.

Table 2.8 EC_{50} values and computed ΔG values for all agonists tested (EC_{50} values for NECA and BAY-60-6583 are from S. Hinz, A. Schiedel, C. E. Müller, unpublished results).

	Ligand	EC_{50} [nM]	Calculated ΔG [kcal mol^{-1}]
1	Adenosine [117]	23500	-65.06
2	CADO [118]	24000	-64.64
3	NECA [29]	83.5	-76.01
4	CPA [118]	18600	-67.84
5	NECA derivative [30]	82	-87.28
6	BAY-60-6583 [34]	42.4	-96.11

According to (Table **2.8**) the calculations for the adenosine and non adenosine agonists reproduced the experimentally observed trends to some degree.

Our results contradict the binding modes reported previously in the literature by Ivanov et al. [51], who postulated binding modes for xanthine derivatives that differ significantly from the positions we propose. This is mainly due to an alternate choice of the location of the binding site. Our choice of the binding center relies on the evidence

given by the positions of the cocrystallized ligands bound to their template structures, retinal bound to rhodopsin, carazolol bound to the β_2-adrenergic receptor, and ZM241385 bound to the adenosine A_{2A} receptor. The residues identified by our procedure as part of the binding pocket indeed turned out to be relevant for ligand binding in mutagenesis studies for either the A_{2B} receptor directly or the closely related adenosine A_{2A} receptor. Our approach finally allowed us to outline the general trend between the experimentally observed and the computed binding behaviour. The final correlation of the calculated binding affinities with experimental findings justifies in retrospect our initially made, severely simplifying assumption that the natural membrane environment is dispensable, at least for the limited purpose of this application. Recently, the crystal structure of opsin was published, which displays structural features that are attributed to an active GPCR state [74]. Like our receptor model in complex with the agonist, the opsin shows prominent structural changes in the conserved E(D)RY region.

2.4   Conclusions

We have developed and compared a novel 3D model of the human adenosine A_{2B} receptor, based on the highest resolution structures of bovine rhodopsin, of the β_2-adrenergic receptor and of the recently adenosine A_{2A} receptor, incorporating information from mutagenesis studies at the same time. Also, based on the results obtained, possible explanations for the selectivities of the adenosine A_{2A} and A_{2B} receptors were described.

In the course of combined docking and MD simulation studies the model has been thoroughly investigated; the structural effects of ligand binding have been examined on the basis of hydrogen bonds, lipophilic interactions and binding energies in the final complexes obtained from automatic ligand placement and structural refinement. For antagonists, which address the inactive state of the receptor, the outcome was generally in concordance with experimentally conducted binding studies, for agonists, that trigger/require significant changes in the conformation of the receptor, the results were also plausible. Thus, for the receptor ground state the final model not only integrates without any contradictions sequential and structural information, as well as evidence from site-directed mutagenesis and binding studies, rendering a quite plausible model for ligand receptor interactions. Given the profile of sequence similarity, which is

highest in the trans-membrane parts, we may consider the helical bundle as comparatively very well characterized in contrast to the intra- and extracellular loop regions. The major part of the binding site is made up by the trans-membrane helices; however the exact structure of the second extracellular loop, which may also be involved in ligand binding, is still quite uncertain. We have made suggestions on the potential structure of this part, which will require further confirmation.

Nevertheless, the results of the present study provide valuable information concerning the optimal structural requirements for selective antagonist and agonist recognition by the human adenosine A_{2B} receptor. Most of the amino acid residues covering the putative binding sites are conserved among the four adenosine receptor subtypes. Asn254, His280, Trp247, Leu86, and Ile276, which are common to all subtypes, are believed to play an important role in the binding of both agonists and antagonists. In order to design new, receptor subtype-selective ligands, we need to target the non-conserved amino acid residues that point to the center of the trans-membrane part according to the present study, namely Asn273, Leu81, Lys170, Val256, Ala271, Asn266, Lys269, Lys267 and Val250. These residues are in proximity to the ligand, but specific for the A_{2B} receptor. The actual behaviour of compounds designed on these predictions will help to confirm and optimize the presented receptor model.

3   Conformational Changes induced by Agonist

3.1   Introduction

The binding of agonists stabilizes or induces active states of GPCRs, representing specific conformations which are recognized by heterotrimeric G proteins through interactions with the intracellular domains. Analysis of several GPCR mutants has indicated that the TM pocket close to the extracellular region forms the binding site for ligands, while the intracellular loops mediate receptor G protein coupling [120]. The activation of a GPCR is commonly described in terms of a ternary complex involving the hormone (in general: ligand), the receptor and the trimeric G protein [121]. **Agonists** are defined as ligands that fully activate the receptor. **Partial agonists** induce submaximal activation of the G protein even at saturating concentrations. **Inverse agonists** inhibit basal activity. **Antagonists** have no effect on basal activity, but competitively block access of other ligands. The term "efficacy" is used to describe the effect of a ligand on the functional properties of the receptor thus the efficacy of a given drug may vary depending on the signalling pathway being examined [122].

It is assumed that a receptor molecule exists in a conformational equilibrium between the active and the inactive biophysical states. In these conditions, the binding of full or partial agonists, as well as the specific interaction with the G protein may shift the equilibrium toward the active receptor states. GPCR ligands are classified according to their influence on this equilibrium and the efficacy of ligands reflects their ability to alter the equilibrium between these two states. Full agonists bind to and stabilize the active conformation, while inverse agonists bind to and stabilize the inactive conformation. Partial agonists have some affinity for both the inactive state and the active state and are therefore less effective in shifting the equilibrium towards the active state. Antagonists do not affect the equilibrium [123].

In spite of the remarkable diversity of ligands and ligand binding domains in the family of GPCRs, there is also considerable evidence for a common mechanism of activation. When comparing GPCR sequences, GPCRs are most similar at the cytoplasmic ends of the TM segments adjacent to the second and third cytoplasmic domains, the regions known to interact with cytoplasmic G proteins [124]. Since the crystal structures of activated GPCRs are not

yet available, computational methods and biophysical techniques have been used to predict the structures of GPCR active states.

Activation of GPCRs is initiated by conformational changes in the TM helices and the intra- and extracellular loops induced by agonist binding. All GPCR structures show the same overall fold with little differences in TM helix arrangement. Small variations are seen as receptor specific features. Among the different receptor conformations observed in these structures, the difference between rhodopsin and opsin is the largest. In the following a set of most typical structural motifs that alter their arrangement upon activation is presented:

Most prominent among the conformal changes are the TM6/TM5 helix motion, breakage of the "ionic lock" between TM3 (E(D)RY motif) and TM6, breakage of the electrostatic interaction between Tyr306 and Phe313 (NPxxY(x)5,6F motif), and reorganization of some amino acid side-chains in the retinal binding pocket. An explanation might be that rhodopsin represents a maximally inactivated GPCR, whereas the opsin structure might be close to an active conformation.

In addition, a rotation of the $Trp^{6.48}$ "toggle switch" would occur upon activation of the receptor [53]. Moreover, the TM region is stabilized by two sets of interhelical hydrogen bonding interactions involving residues that are conserved among the members of the human adenosine receptor family. For example, a hydrogen bonding interaction between the side-chains of $Glu^{1.39}$ and the highly conserved $His^{7.43}$ will facilitate antagonist binding. Another residue, $Asp^{2.50}$, is in the network among the highly conserved amino acid residues, $Asn^{7.45}$, $Ser^{7.46}$, and $Asn^{7.49}$, which also form hydrogen bonds to $Ser^{3.39}$ [125]. The occurrence of these hydrogen bonding interactions in our model supports the validity of the structure. The next paragraphs present the special features of the single motifs in more detail, based on experimental evidence from GPCRs other than the A_{2B} adenosine receptor. We therefore monitored a possible activation process of the human A_{2B} receptor during simulation by observing the structural characteristics of these relevant motifs.

Changes in E(D)RY motif

A set of intermolecular interactions involving a group of highly conserved amino acid residues throughout the members of the GPCR superfamily and located at the cytoplasmic sides of helices TM3 ($Arg^{3.50}$), part of the highly conserved (D/E)RY motif, and TM6

(Glu$^{6.30}$), have been suggested to form part of a general activation mechanism for all members of the family. These interactions are often referred to as "ionic lock", which were proposed to stabilize TM3 and TM6 in their inactive conformation by restraining the motion of certain domains [126]. Thus its disruption was believed to be one of the critical events in the activation process (Figure **3.1**).
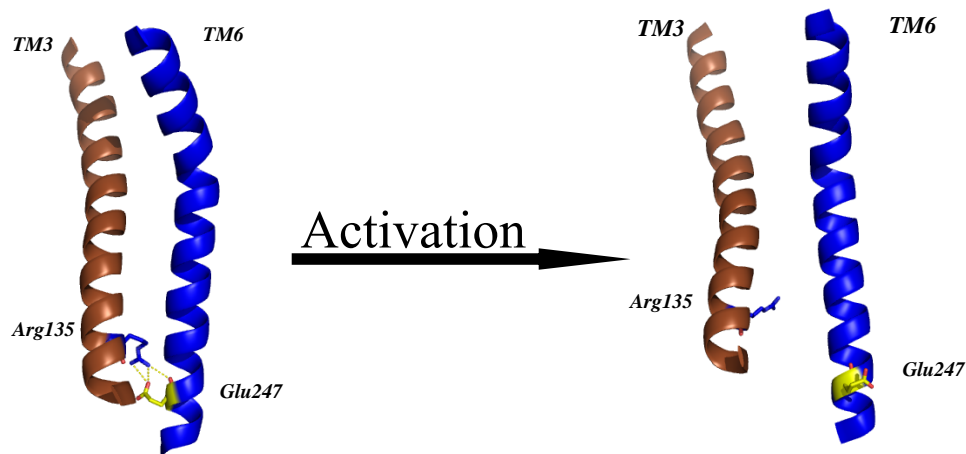
Figure 3.1 Intact (bovine rhodopsin) and disrupted (opsin) ionic lock. The interaction is depicted via dashed yellow lines. In the receptor structures, only the TM3 and TM6 domains are shown

Moreover, the spontaneous disruption of such interactions acts as a molecular switch that, in some cases, can lead to the active form of the receptor that is able to bind to the G protein with high affinity, favouring its activation. As a result, the intracellular sides of TM3 and TM6 are separated. These preliminary experiments were supported by the newly solved crystal structures of opsin showing no interaction between the above-mentioned residues as well as an extended helical conformation of TM6 in the intracellular side [74]. Recently, Shaw et al. showed that the distance between the Cα atoms of Arg$^{3.50}$ and Glu$^{6.30}$ and the minimum distance between the guanidine nitrogen atoms of Arg$^{3.50}$ and the carboxylate oxygen atoms of Glu$^{6.30}$ are indicative for the activated/inactivated state of the human β$_2$-adrenergic receptor. We therefore monitored the possible activation process of the human A$_{2B}$ receptor by means of these parameters [127].

In the human β$_2$-adrenergic receptor, conformational changes of the "ionic lock" during activation of the receptor by agonists have been demonstrated by fluorescence spectroscopic studies [128]. The data are in agreement with a broken "ionic lock" as seen in the opsin structure. However, the structures of β-adrenergic receptors and the human A$_{2A}$ adenosine

receptor in their ligand-bound state (antagonist cyanopindolol, β_1-adrenergic receptor; partial inverse agonist carazolol, β_2-adrenergic receptor; antagonist ZM241385, A_{2A} adenosine receptor) show relative to inactive rhodopsin and active opsin already a partially broken "ionic lock". The distance between TM3 and TM6 and thus between $Arg^{3.50}$ and $Glu^{6.30}$ is increased. $Glu^{6.30}$ (the equivalent to Glu247 of opsin) is completely released from $Arg^{3.50}$, but the intrahelical interaction between $Glu^{3.49}$ and $Arg^{3.50}$ of the E(D)RY motif is still intact. The partially broken "ionic lock" facilitates further TM6 motion and may explain why the antagonist-bound GPCRs (β_1-adrenergic receptor, β_2-adrenergic receptor and A_{2A} adenosine receptor) display some basal activity but do not feature the completely active conformation of the receptors [129]. In contrast, rhodopsin ground state structures (bovine and squid) show the full "ionic lock" which firmly stabilizes the inactive receptor state (Figure **3.2**).
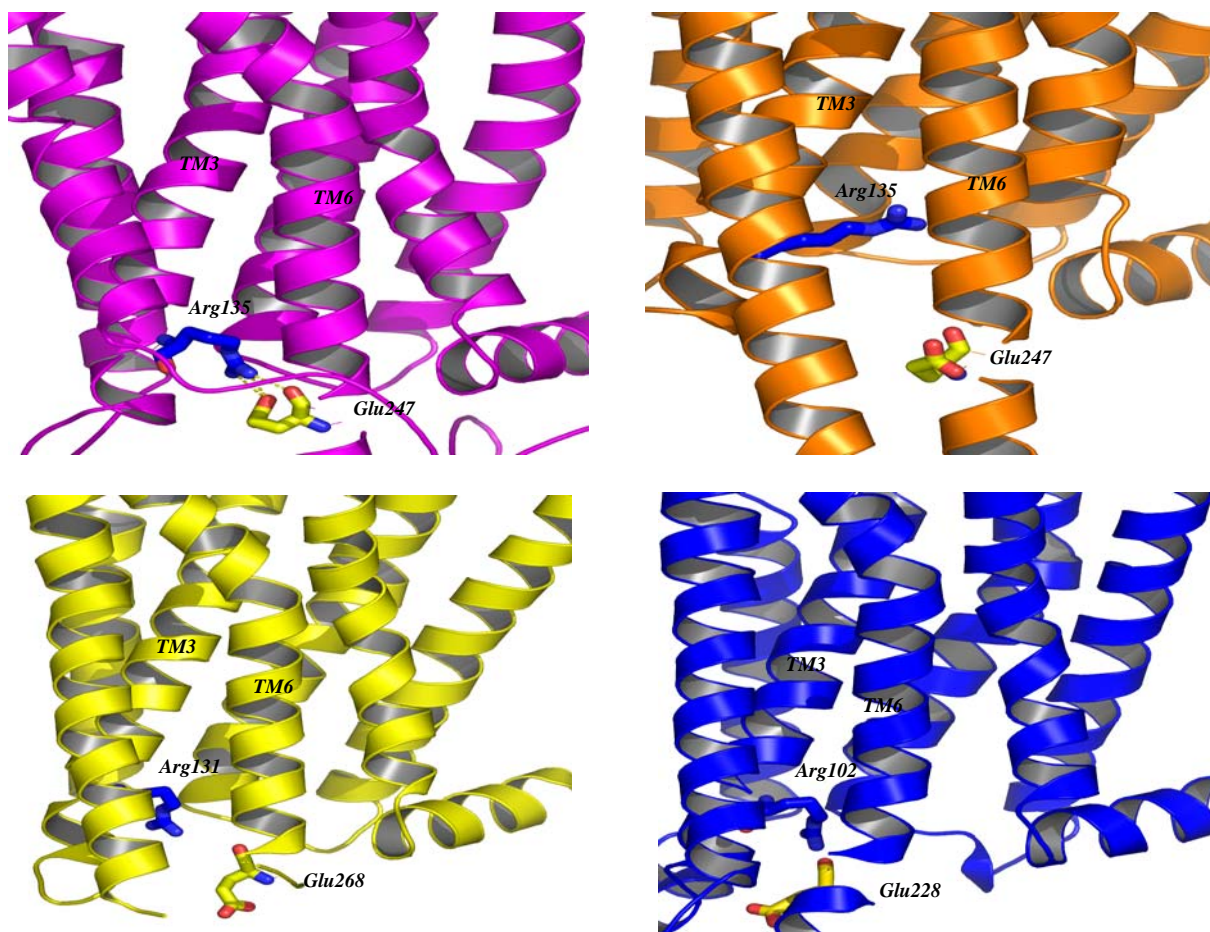
Figure 3.2 Comparison of GPCRs containing the E(D)RY motif. Structures are presented as cartoon and show rhodopsin (magenta), opsin (orange), the β_2-adrenergic receptor (yellow) and the A_{2A} adenosine receptor (blue), respectively

Changes in NPxxY(x)5,6F motif

Besides the E(D)RY motif, most GPCRs contain the NPxxY motif in TM7 or an NPxxY(x)5,6F motif, with the additional Phe residue in TM8. The NPxxY(x)5,6F motif was identified like the E(D)RY motif to be an important element for the interaction of activated GPCRs [130]. Biochemical and biophysical studies indicated that a structural rearrangement of the NPxxY(x)5,6F motif occurs upon receptor activation [131] [132]. As seen in Figure **3.3**, a large structural change of the NPxxY(x)5,6F motif is also found in the opsin structure. In rhodopsin an aromatic stacking interaction between the aromatic side-chains of Tyr306 and Phe313 is observed. This interaction is broken in the opsin structure because of the TM6 tilt outward of the helix bundle, allowing the Tyr306 side-chain to rotate into the helix bundle. Tyr306 thereby blocks TM6 from moving back toward TM3 to adopt an inactive conformation corresponding to the rhodopsin ground state.

Like the E(D)RY motif, the NPxxY(x)5,6F motif is part of a functional domain. In the rhodospin ground state, and analogously in other GPCR structures, Asn302 ($Asn^{7.49}$ in TM7) forms a hydrogen bonding network with Asn55 ($Asn^{1.50}$) and Asp83 ($Asp^{2.50}$) in the protein interior whereas in the cytoplasmic domain Tyr306 ($Tyr^{7.53}$) and Phe313 ($Phe^{7.60}$; on cytoplasmic TM8) are tethered by an aromatic stacking interaction. The network includes water molecules used to link the TMs. In the known GPCR structures, water clusters were identified which extend from the ligand binding pocket to the cytoplasmic surface of TMs [133]. Waters are often bound to highly conserved residues ($Asn^{1.50}$, $Asp^{2.50}$, $Asn^{7.49}$ and $Tyr^{7.53}$) and are part of functionally important domains "toggle switch" which enables to modulate the bent angle of TM6 around the highly conserved proline [134] [135] and the NPxxY(x)5,6F motif (Figure **3.3**).
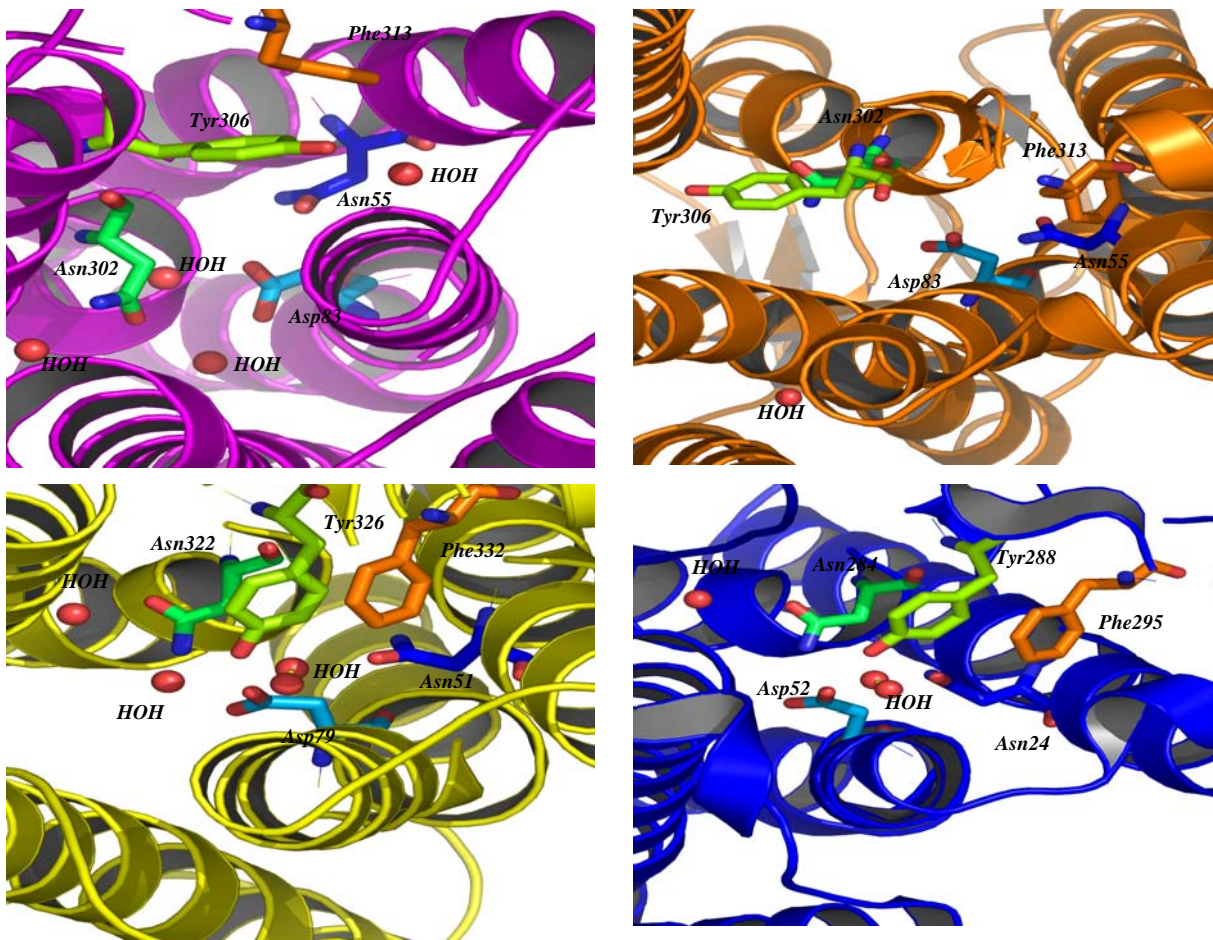
Figure 3.3 Structural changes in the NPxxY(x)5,6F region of rhodopsin (magenta), opsin (orange), the β₂-adrenergic receptor (yellow) and the A$_{2A}$ adenosine receptor (blue), respectively. The side-chains of the NPxxY(x)5,6F residues Tyr$^{7.53}$ and Phe$^{7.60}$ are shown as stick models. In rhodopsin, an aromatic stacking interaction between Tyr$^{7.53}$ and Phe$^{7.60}$ is presented. However, in opsin, the aromatic stacking interaction between Tyr$^{7.53}$ and Phe$^{7.60}$ is not presented and Tyr$^{7.53}$ is rotated inside the helix bundle to stabilize TM6 in its outward position. The water molecules found in the crystal structures are presented as red spheres and mediate the interhelical interactions between TM1, TM2 and TM7 (Asn$^{1.50}$, Asp$^{2.50}$, Asn$^{7.49}$)

A water cluster in GPCR structures

Another common feature of the available high-resolution crystal structure models of class A GPCRs includes similar water clusters in interhelical cavities. These cavities might be able to form a long hydrogen bonding network between TM1-TM3 and TM6-TM7 extending from the transmembrane helical bundle to the cytoplasmic surface [136] [53] [52] [54] and thus these water molecules are likely to be as important to proper receptor function as the

conserved residues. The hydrogen bonding network is usually extended from the toggle switch residue (Trp265 in rhodopsin, Trp274 in squid rhodopsin and Trp286 in the β_2-adrenergic receptor, except His278 in the A_{2A} adenosine receptor) to the NPxxY(x)5,6F motif as shown in Figure **3.4**. A water molecule is coordinated to the indole nitrogen atom of the toggle switch $Trp^{6.48}$ residue, likely to maximize the proline-induced kink ($Pro^{6.50}$) in TM6 and to facilitate helix movements [133]. TM3/TM6 movement upon receptor activation may rearrange water molecules in the hydrogen bonding network. It is likely that this network, which interacts with a number of highly conserved amino acids, may be important in transmitting structural changes from the ligand-binding pocket to distal sites.
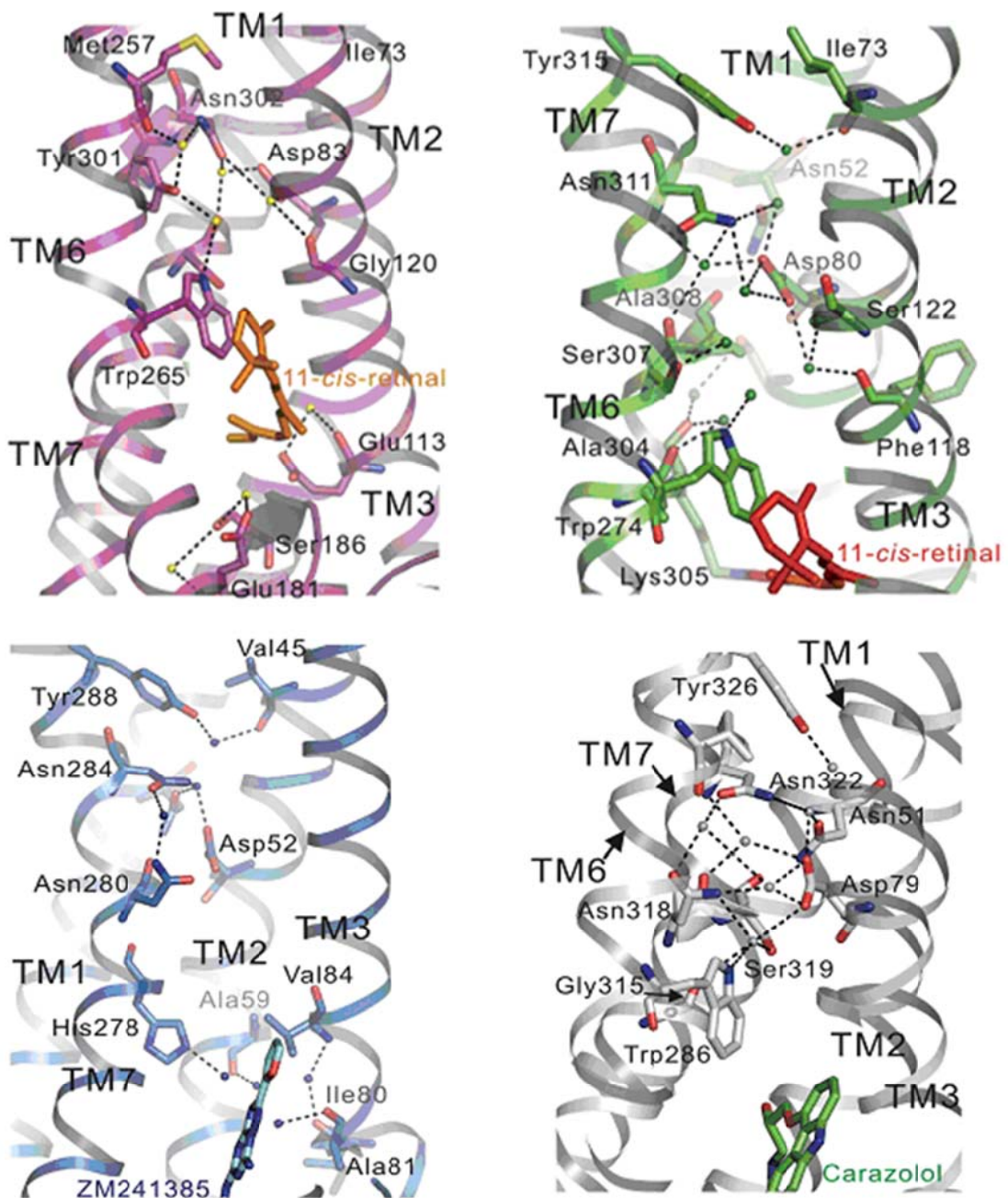
Figure 3.4 Comparison of interhelical water clusters in GPCR structures. Overall structures of GPCRs and water clusters in interhelical cavities are presented as cartoon models. Color code: bovine rhodopsin (magenta), Squid rhodopsin (green), the A_{2A} adenosine receptor (blue) and the β_2-adrenergic receptor (grey). Residues coordinated to water molecules are shown as stick models. Water molecules are presented as yellow (bovine rhodopsin), forest (squid rhodopsin), dark blue (the A_{2A} adenosine receptor) and grey (the β_2-adrenergic receptor) sphere models, respectively. Ligands in the different GPCR models are presented as stick model. Dotted lines indicate hydrogen bonds between coordination partners

Conformational changes in extracellular domains

When a GPCR is activated, structural changes occur in the cytoplasmic G protein-coupling domains linking the presence of an extracellular signal to an intracellular response. These changes have been characterized for several receptors, including rhodopsin and the β_2-adrenergic receptor. In rhodopsin, EL2 forms a structured cap over the covalently bound ligand retinal and interacts with the TM segments involved in activation. Recent solid-state NMR data show that light activation of rhodopsin also induces conformational changes in EL2 and there is a rearrangement in the hydrogen-bonding networks connecting EL2 with the extracellular ends of transmembrane helices TM4, TM5 and TM6 [137]. In addition, the EL2 of the β_2-adrenergic receptor connecting TM4 and TM5 forms a two turn α-helix that is displaced away from the ligand-binding site entrance (Figure **3.5**). Two disulphide bonds stabilize EL2, one within the loop and one to the end of TM3. A salt bridge formed by Lys305$^{7.32}$ and Asp192^{EL2} connects EL3–TM7 to EL2.
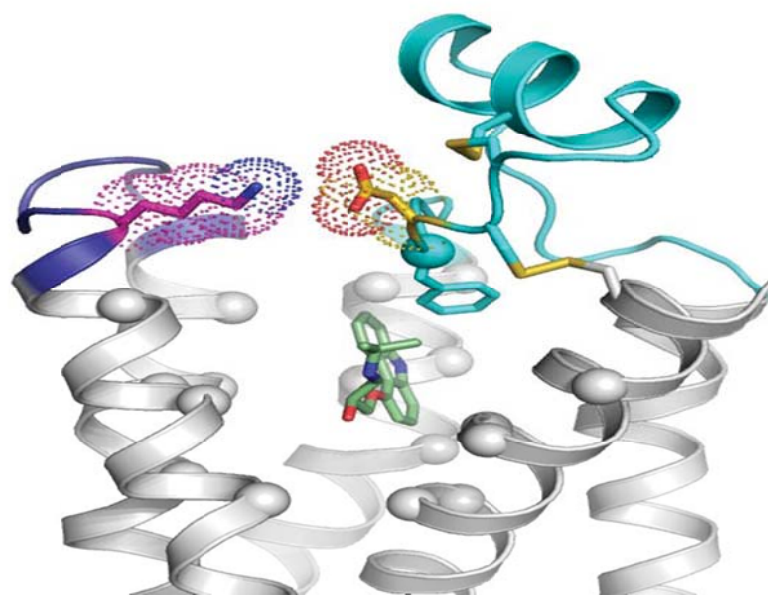
Figure 3.5 Extracellular domains of carazolol-bound β₂-adrenergic receptor. The extracellular domains of the β₂-adrenergic receptor showing EL2 (cyan), EL3 (dark blue), Lys305 (magenta), Asp192 (yellow) and the inverse agonist carazolol (green). Spheres indicate the Cα of residues in direct contact with carazolol (at least one atom within 4 Å distance). Disulphide bonds are shown as yellow sticks. TM1 and TM2 have been removed for clarity. Asp192 and Lys305 form the salt bridge observed in the crystal structure [138]

Carazolol is an inverse agonist that binds in the orthosteric pocket of the β₂-adrenergic receptor formed by TM3, TM5, TM6 and TM7. The only direct interaction between the extracellular domains and carazolol is through an aromatic interaction with Phe193^{EL2}. Given these specific associations between extracellular domains, the orthosteric ligand-binding site and TMs involved in activation and consequently, the β₂-adrenergic receptor extracellular domains and the associated salt bridge rearrange on activation [139]. The NMR data of this study suggested that the salt bridge (Lys305 and Asp192) is weakened in the β₂-adrenergic active state.

3.2   Material and Methods

3.2.1 Model construction

An initial 3D model of the human adenosine A$_{2B}$ receptor is generated by homology modelling using the X-ray structure of the adenosine A$_{2A}$ receptor in its inactive conformation as a template (for details see chapter **2**).

3.2.2 Docking of A$_{2B}$ receptor agonist and antagonist

A$_{2B}$ agonists are expected to bind with high affinity to a different conformational state of the receptor than antagonists or inverse agonists. In addition, agonists might effect a conformational change upon binding to an inactive receptor conformation by simply disrupting existing interactions, thereby favouring a new set of interactions that stabilize a new conformational state. Therefore, we selected compounds showing opposed pharmacological profiles. Thus an antagonist, PSB-603 (**10**) and an agonist, BAY-60-6583 (**3**) have been docked into the putative binding site of the A$_{2B}$ model representing the inactive and active receptor states, respectively.

PSB-603 [41] belongs to the large series of A_{2B} xanthine ligands, with high potency and specificity across species (including rodents and humans). It displays a K_i value of 0.553 nM for binding to the human A_{2B} adenosine receptor. In contrast, BAY-60-6583 [34] represents a non-nucleosidic A_{2B}-selective partial agonist. The latter compound is very selective for the adenosine A_{2B} receptor with a low EC_{50} value of 3–10 nM for the human adenosine A_{2B} receptor and, contrarily, high EC_{50} values of > 10 μM for the A_1, A_{2A} and A_3 receptor subtypes, characterized by CHO cells in a gene-reporter assay expressing recombinant human receptors in high density. The ligands are shown in Figure **3.6**.
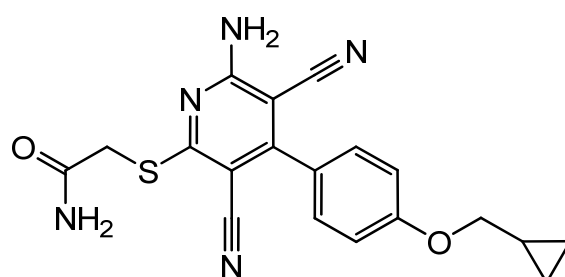
3

BAY-606583 [34]

hA_1 > 1000 nM
hA_{2A} > 1000 nM
hA_{2B} = 3-10 nM
hA_3 > 1000 nM

10
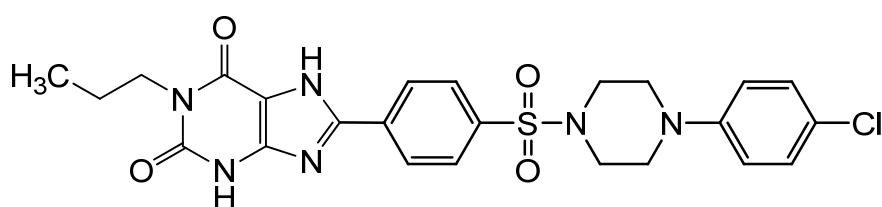
PSB-603 [41]

hA_1 > 10,000 nM
hA_{2A} > 10,000 nM
hA_{2B} = 0.553 nM
hA_3 > 10,000 nM

Figure 3.6 Compounds docked into the binding site of the A_{2B} receptor model in order to stabilize the inactive conformation (PSB-603) or induce conformational change (BAY-606583)

The selected ligands were docked into the binding site of the fully inactive form of the A$_{2B}$ model using an automated docking procedure employing the FlexX software. The complexes were reoptimized at the same place as described in chapter **2**.

3.2.3 Molecular systems

Nowadays, the commonly accepted surrounding for carrying out MD simulations of membrane proteins is the use of the phospholipid bilayer solvated by water under periodic boundary conditions to provide the optimum environment. This environment is assumed to be a reasonable approximation of the natural lipid bilayer, as it has been shown to conserve functional properties of the receptor (Figure **3.7**). The following briefly outlines the setup-procedure for creating the final system for MD simulations.

The receptor-ligand complexes were embedded in an explicit bilayer membrane consisting of 1-palmitoyl-2-oleoyl-*sn*-glycero-3-phosphatidylcholine (POPC) molecules. Starting coordinates of an equilibrated membrane with 200 lipid molecules were obtained from http://www.lrz.de/~heller/membrane/membrane.html. published by Heller et al. [140]. A cylindrical hole was made in the center of the bilayer in such a way that α-helices of the receptor were oriented approximately parallel to the hydrocarbon chains of the phospholipids. After that all phospholipids within a radius of 2 Å around the receptor were deleted. Subsequently water and chlorine counter ions were added to neutralize the system. Water molecules placed inside the phospholipid membrane were removed manually.
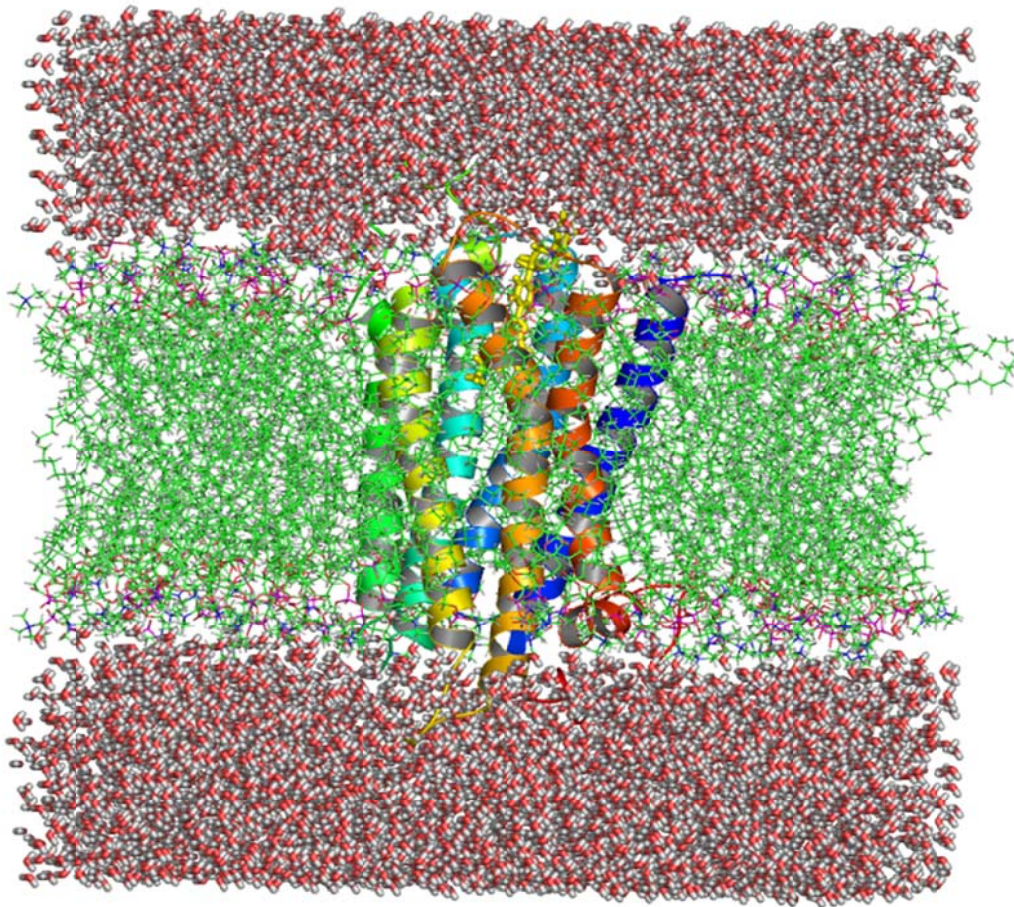
Figure 3.7 Illustration of the complete simulation system containing 55031 atoms in total. The A_{2B} model is shown in cartoon, embedded in a POPC lipid bilayer. The complex system contains PSB-603 (yellow), lipids in green (lines) and water in red (sticks)

3.2.4 Molecular dynamic simulations

Molecular dynamic simulations were carried out by running a) an energy minimization procedure followed by b) a position restrained MD, c) equilibration and finally d) production run.

a) Prior to MD simulations, three stages of minimization were carried out for the following reason: Setting up such enormously big systems (55031 atoms in case of PSB-603, 55020 atoms in case of BAY-606583) invariably leads to close contacts in the initial positions of the atoms. These are associated with extremely high repulsive forces and thus accelerate the involved atoms accordingly. The consecutively large displacements very quickly distort the

overall spatial arrangement of atoms leading to erroneous abortion of the simulation. Careful, multistage energy minimization is one method that helps to relieve close contacts and ensure stable simulation.

In the first stage, we kept the atoms of protein, ligand and phospholipids harmonically tethered to their starting positions with a constraint force of 100 Kcal/(mol Å^2) and we just minimized the positions of the water molecules including ions; then in the second stage, we minimized the phospholipids-water system, again applying a constraint force of 100 Kcal/(mol Å^2) to the protein. Finally in the last stage all atom positions are fully minimized without any constraints and allowed everything to relax. The three minimization stages consisted of 5000 steps each, in which the first 1000 were using the Steepest Descent algorithm and the last 4000 steps were applying Conjugate Gradient minimization method. This is slightly more than necessary, since minimization prior to classical molecular dynamics is used only to relieve bad contacts found in the initial configuration.

b) MD dynamics runs were performed using the previously optimized structure. The time step of the simulations was 2.0 fs with a cutoff of 10 Å for the non-bonded interactions. The SHAKE algorithm was employed to keep all bonds involving hydrogen atoms rigid. A constant-volume simulation was carried out for 70 ps, during which the temperature was raised from 10 to 310 K (using the Langevin dynamics method); then the constant pressure MD were carried out at 310 K. During the constant pressure MD all the Cα-atoms of the receptor were restrained to their starting positions with a harmonic force constant that decreased from 5 to 2 Kcal/(mol Å^2) in 10 ns and from 2 to 0.5 Kcal/(mol Å^2) in 10 ns.

c) Continue at constant pressure until the density equilibrated and during which there were no constraints.

d) In the production runs, a constant pressure of 1 atm and a constant temperature of 310 K were applied.

3.3   Results and discussion

As stated before, rhodopsin-like GPCRs share a large number of conserved sequence patterns. For example, the most conserved residues in each TM are: N1.50, D2.50, R3.50, W4.50, P5.50, P6.50, and P7.50. Furthermore, the packing of the TM domain in the A$_{2B}$

model based on the adenosine A_{2A} crystal structure shows the typical interactions characterizing the stabilization of the inactive state of the adenosine A_{2A} crystal structure. The A_{2B} model (described in chapter **2**) suggests that the inactive state is stabilized by several typical interactions that are supposed to be broken during the activation process. These are:

- a salt bridge (ionic lock) formed by two highly conserved amino acid residues, $Arg103^{3.50}$ (DRY consensus motif in TM3) and $Glu229^{6.30}$ (cytoplasmic part of TM6),

- a hydrogen bonding network mediating interactions between TM1 ($Asn25^{1.50}$), TM2 ($Asp53^{2.50}$) and TM7 ($Asn286^{7.49}$),

- interhelical hydrogen bonding interactions stabilizing the TM region involving residues that are conserved among the adenosine receptor subtypes, e.g., the hydrogen bonding interactions between TM1 ($Glu14^{1.39}$) and TM7 ($His280^{7.43}$),

- a salt bridge stabilizing the course of the EL2 and EL3. For example, the side-chain of $Lys267$ is potentially linked with the side-chain of $Glu174^{EL2}$.

MD simulations have been carried out for an antagonist bound receptor as well as for an agonist bound receptor in order to study two aspects: The antagonist-complex is supposed to demonstrate whether these structural features indeed are stable and characteristic for the inactive state. The agonist-complex should be suitable to study a ligand-induced process of conformational change that leads to a possibly active receptor conformation.

Equilibration of the adenosine A_{2B} receptor in a phospholipid bilayer

Our aim was to look for differences in the behaviour of the adenosine A_{2B} receptor model in the presence of an agonist or an antagonist. First we had to ensure equilibration of the receptor model in the bilayer. Thus we took the change of total energy as the main criterion. The biggest decline in energy occurred after the first 21 nanoseconds which can be attributed to the relaxation of the protein after removal of position restraints. Afterwards the change is accompanied by a period of decrease in total energy. It was shown that the ionic lock is not present in the inactive crystal structure of the human adenosine A_{2A} receptor. This absence could result from the crystallization procedure, but could also suggest that the ionic lock is not a general constitutive activity-reducing interaction for family A GPCRs which could

indicate that the inactive state of the A_{2B} receptor model which is characterized by the decrease in total energy more than the active state shows the characteristic of a partially activated state similar to the simulated A_{2A} receptor [141] (Figure **3.8**). After 30 ns no further change in total energy could be observed in both complexes, thus the following period i.e $\approx$ 10 ns were used for analysis.
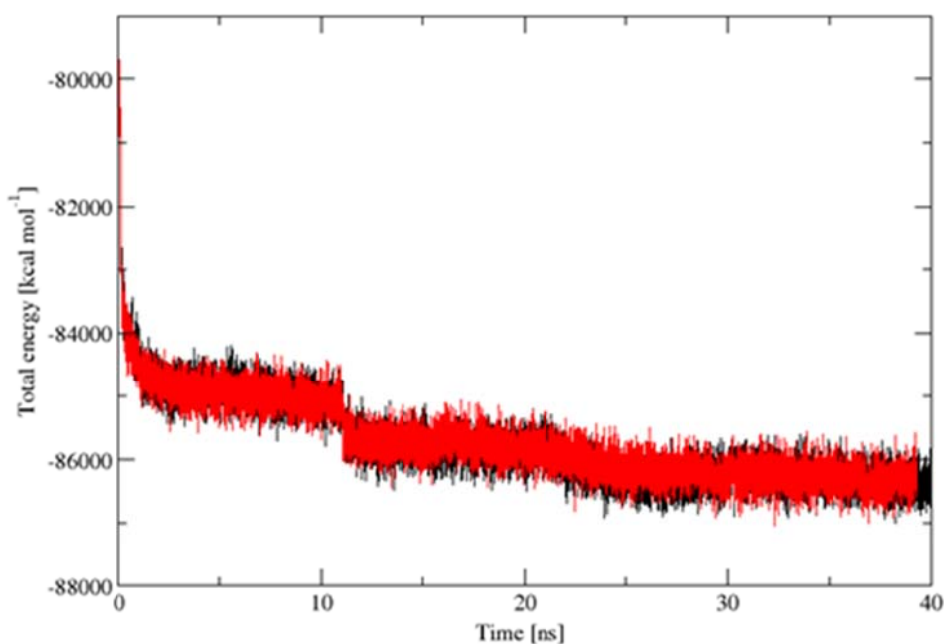
Figure 3.8 Total energy plotted versus time for PSB-603 (black) and BAY-60-6583 (red)

In addition, the root mean square deviation (RMSD) of the backbone atoms is also an important criterion for the convergence achieved by MD simulations. As shown in Figure **3.9**, the RMSD with respect to the starting structure reached stability and after 30 ns no significant change in the RMSD value was observed. These results suggested that different, but relatively stable conformations of the A_{2B} model with the antagonist and agonist were discovered through the MD simulations.
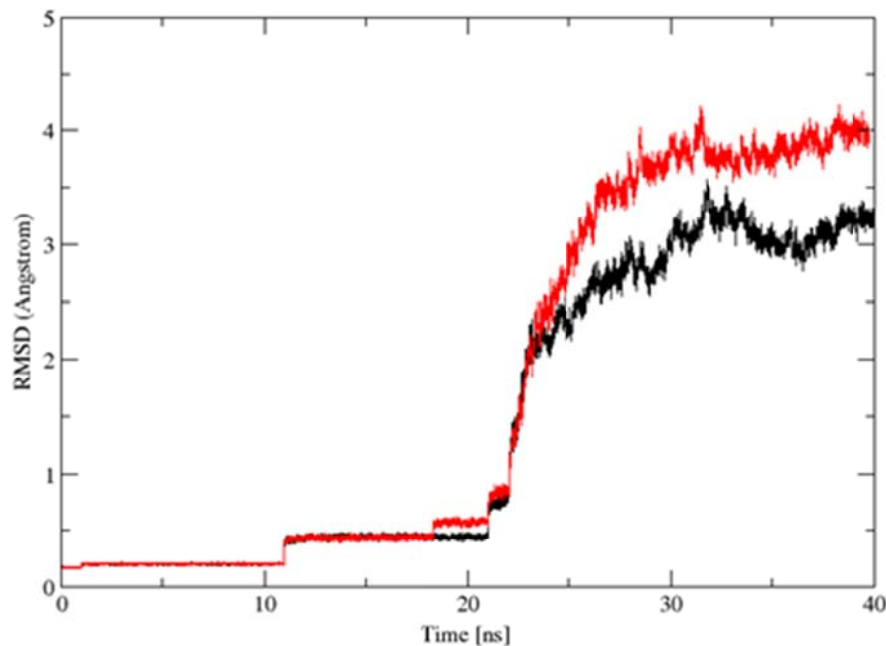
Figure 3.9 RMSD of the backbone atoms observed during the simulation of A_{2B} model with PSB-603 (black) and BAY-60-6583 (red) plotted versus time

Changes in E(D)RY motif

We compared the resulting, putatively active state model with the inactive state model and observed the mentioned conformational switches in the adenosine A_{2B} model, namely, the ionic lock between Arg103 on TM3 and Glu229 on TM6. Upon antagonist binding, the A_{2B} model adopted a conformation with the ionic lock formed between the intracellular ends of TM3 and TM6. Apparently, the inactive state is stabilized by the presence of the ionic lock interaction, which was monitored by the distance between the guanidine nitrogen atoms of Arg103$^{3.50}$ and the carboxylate oxygen atoms of Glu229$^{6.30}$. As shown in Figure **3.10**, after releasing the constraints, the Arg103-Glu229 distance apparently reaches stable levels, 3.4 Å for the antagonist complex which could be an indicative of the inactive state. However, the agonist complex showed a higher distance than 8.8 Å, and the ionic lock was disrupted during the whole simulation.
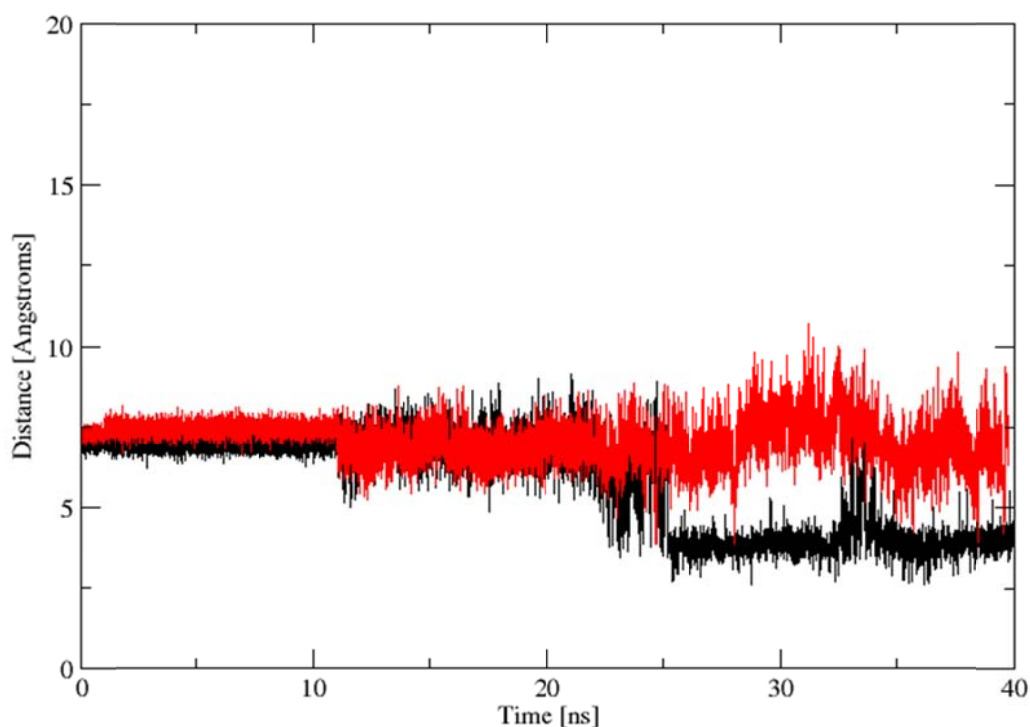
Figure 3.10 The distance between Arg103 and Glu229 with PSB-603 (black) and BAY-60-6583 (red) plotted versus time

In addition, we consistently observed a rearrangement of conserved hydrophobic residues at the interface of helices 3, 5, and 6 that permitted stable ionic lock formation. These results support the hypothesis that the ionic lock stabilizes the inactive conformation of the receptors.

In the agonist-containing complex the disruption of the ionic lock between Arg103$^{3.50}$ and Glu229$^{6.30}$ leads to the movement of the cytoplasmic end of TM6 away from TM3. In the predicted active state conformation, the ionic lock is readily broken and the distance between Arg103$^{3.50}$ and Glu229$^{6.30}$ side-chains is increased (Figure **3.11**).
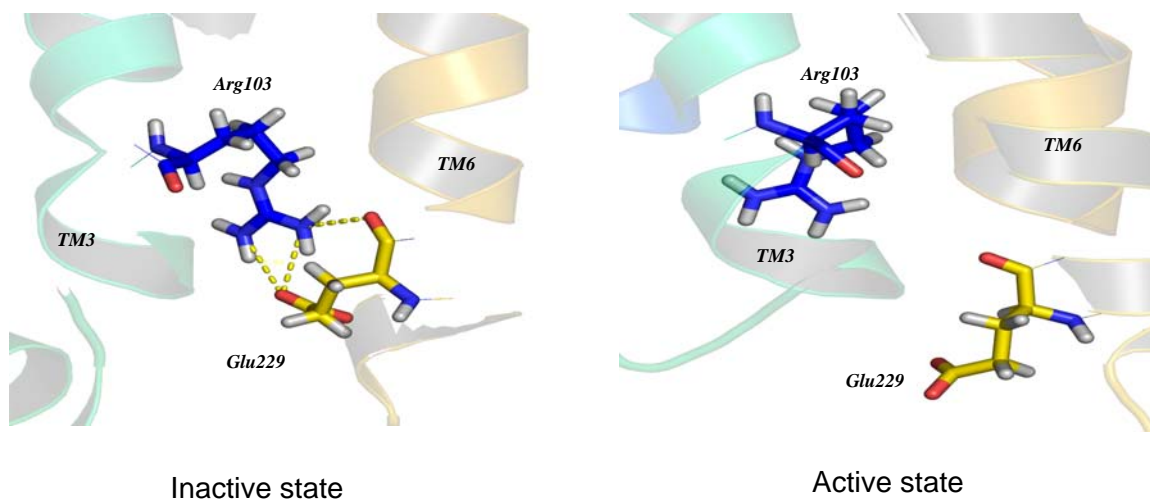
Figure 3.11 Conformational switches in the A$_{2B}$ model at the ionic lock with antagonist (left) and agonist (right)

Rearrangement of interhelical hydrogen bonding

The network of hydrogen bonding interactions is suggested to stabilize the inactive state involving the TM domains. The hydrogen bonding interactions between the side-chains of the highly conserved Asn25, Asp53 and Asn286 in the A$_{2B}$ receptor model stabilize TM1, TM2 and TM7 and facilitate antagonist binding. In the inactive stabilized conformation, the interactions are observed between the residues of Asn25, Asp53 and Asn286, unlike in the active structure of the A$_{2B}$ model. However, the hydrogen bonding interactions between Asp53$^{2.50}$ and Asn286$^{7.49}$ remain similar to the inactive state of the A$_{2B}$ model (Figure **3.12**).
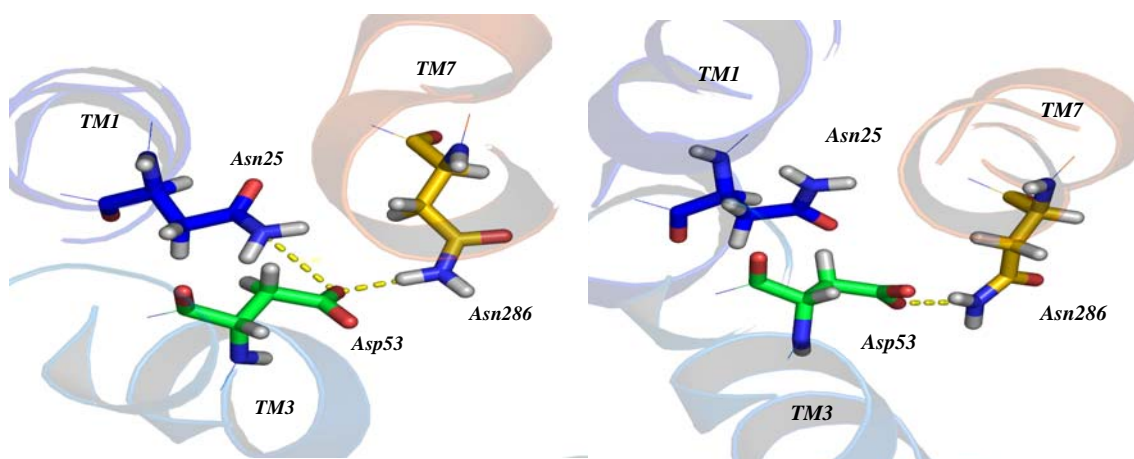
Figure 3.12 Conformational switches in the A$_{2B}$ model at the highly conserved Asn25, Asp53 and Asn286 with antagonist (left) and agonist (right)

Besides disulfide bridges formed by the two Cys residues located in EL2 and at the beginning of TM3, the DRY/ERY motif at the end of TM3 and an extended motif consisting of the NPxxY motif in TM 7. In the adenosine A_{2B} receptor, the adenosine receptors share a salt bridge between the side-chains of Glu14$^{1.39}$ and the highly conserved His280$^{7.43.}$ This potential salt bridge is a common feature in adenosine receptors but is not present in rhodopsin and the β_2-adrenergic receptor. Salt bridges have been suggested to form an intramolecular constraint to keep receptors in an inactive conformation or alternatively to be involved in ligand binding (Figure **3.13**). In addition, as shown in Figure **3.14** the distance between Glu14 and His280 is increased with agonist and decreased with antagonist.
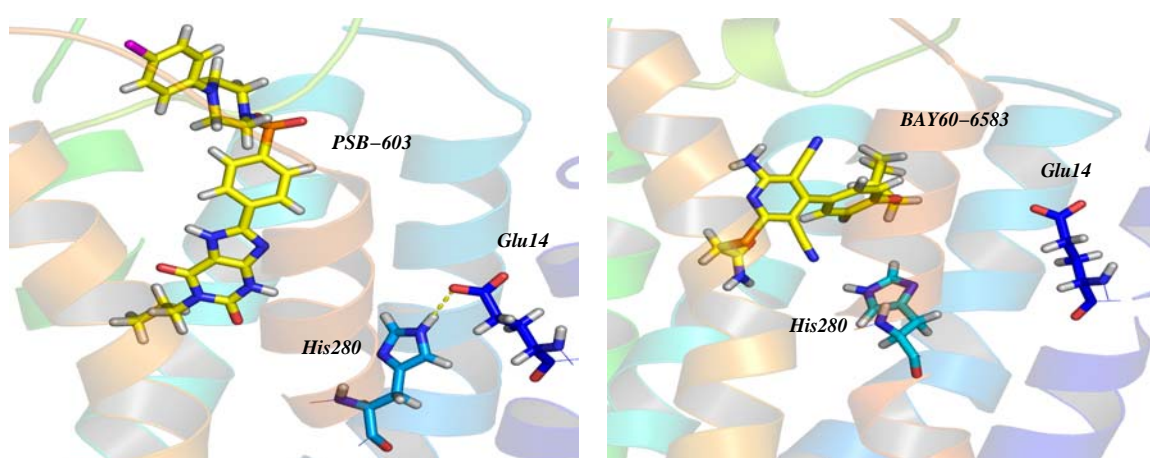
Figure 3.13 Conformational switches in the A_{2B} model at a salt bridge between the side-chains of Glu14$^{1.39}$ and the highly conserved His280$^{7.43}$ with antagonist (left) and agonist (right)
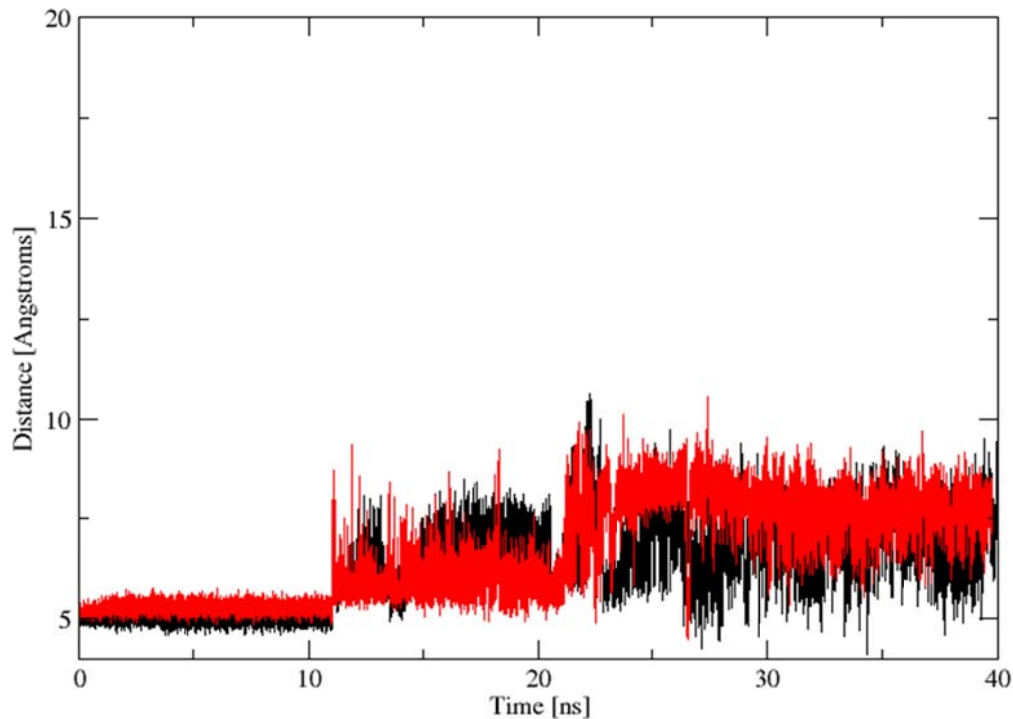
Figure 3.14 The distance between the Glu14 and His280 with PSB-603 (black) and BAY-60-6583 (red) plotted versus time

Changes in NPxxY(x)5,6F motif

As shown in Figure **3.15** and **3.16**, in the inactive state, the Tyr290 is wedged between TM3 and TM6, enabling tight packing between TM3 and TM6 by forming a hydrogen bonding interaction with Asn286 and Asp53. Also the Tyr290 is involved in aromatic stacking interactions with Phe297 and Phe301 which are stabilizing the inactive state, whereas in the active state, the Tyr290 side-chain is rotated from between TM3 and TM6 to the lipid-exposed side of helix 6. Taken together, our simulation results and the crystal structure of the adenosine A_{2A} receptor suggest that the rotation of Tyr290 and rearrangement of neighbouring conserved residues may be a key step along the activation pathway of the adenosine A_{2B} receptor.
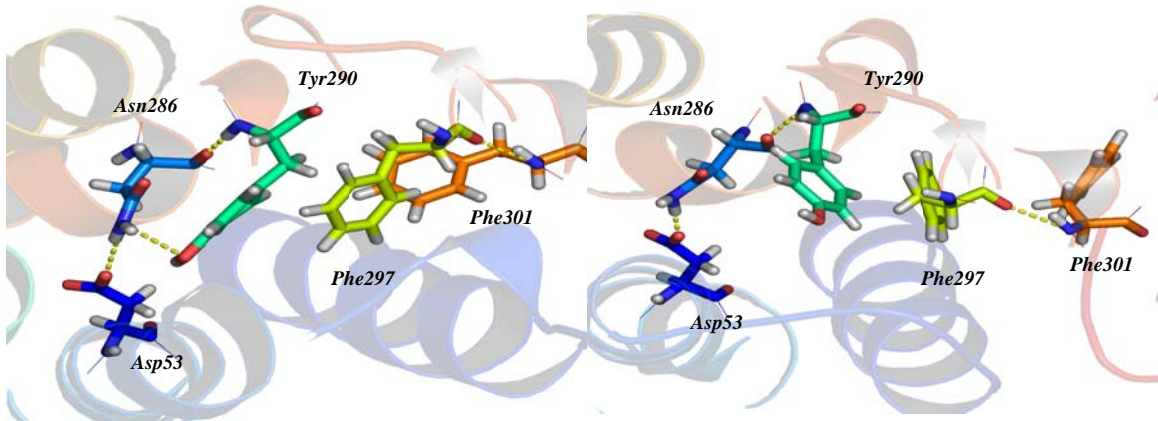
Figure 3.15 Conformational switches in the A_{2B} model at NPxxY(x)5,6F motif with antagonist (left) and agonist (right). In the inactive model, Tyr290 is involved in an aromatic stacking interaction with Phe297 and Phe301, and Tyr290 is involved in interhelical interaction with Asn286. However, in the active form, the electrostatic interaction between Tyr290 and Phe297 is broken and Tyr290 is rotated inside the helix bundle to stabilize TM6 in its outward position
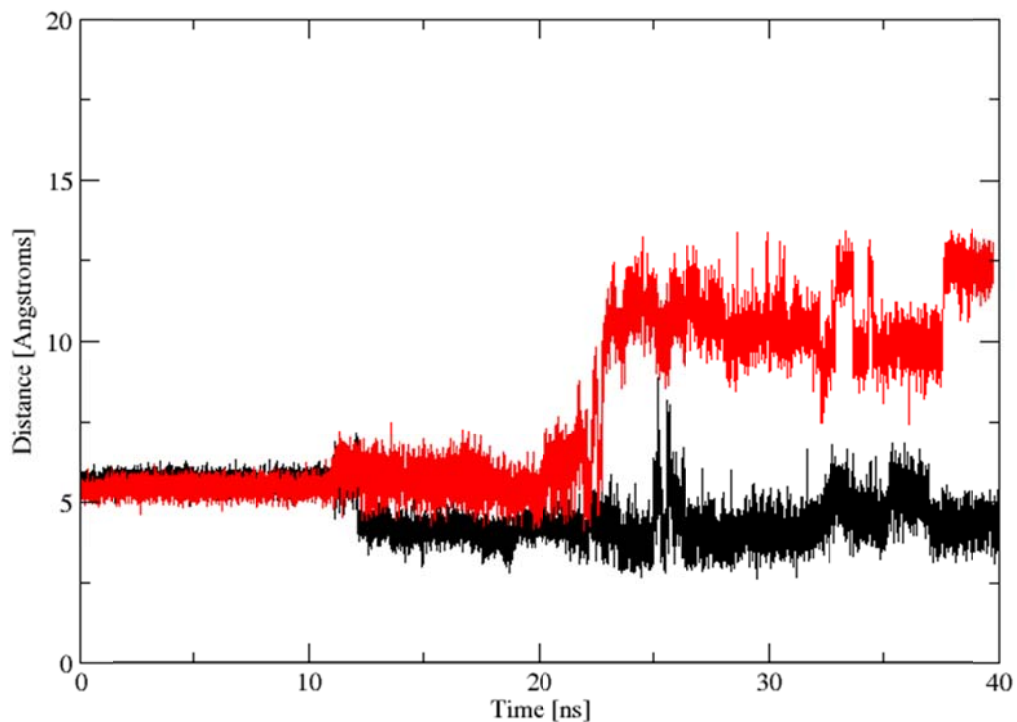
Figure 3.16 The distance between Asn286 and Tyr290 with PSB-603 (black) and BAY-60-6583 (red) plotted versus time. The distance is stable with antagonist and increased with agonist

A water cluster in GPCR structures

Inspection of several high resolution crystal structures of family A GPCRs reveals a set of conserved water molecules, which are also present in the adenosine A_{2A} receptor. Interactions mediated by these ordered waters in the transmembrane core that make contacts with highly conserved residues suggest that they are likely to play an important role in stabilizing TMs. Therefore, structural water molecules may act as indispensable groups for proper protein function. In the case of activation of GPCRs, water likely imparts structural plasticity required for agonist-induced signal transmission [142]. Waters are often bound to highly conserved residues and are part of functionally important domains for example, the "toggle switch" which enables to modulate the bend angle of TM6 around highly conserved proline [134] [135] and the NPxxY(x)5,6F motif, likely to maximize the proline-induced kink ($Pro^{6.50}$) in TM6 and to facilitate helix movements. As a result, in the inactive A_{2B} structure, the indole nitrogen of the Trp247 forms a water-mediated hydrogen bonding interaction with Asn282 of the conserved NPxxY motif in TM7. In the active form, the A_{2B} model did not contain any water molecules, thus this hydrogen bonding interaction is disrupted in the active-state model when the flipping of the Trp247 rotamer is triggered by agonist docking (Figure **3.17**).
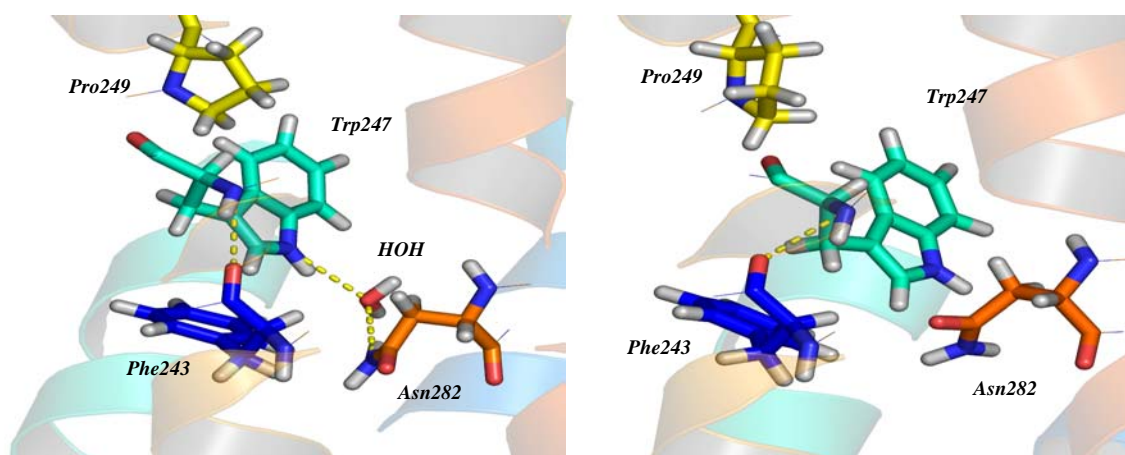
Figure 3.17 Comparison of interhelical water in the A_{2B} model at NPxxY(x)5,6F motif with antagonist (left) and agonist (right)

Conformational changes in the extracellular loops

The most obvious change in the active receptor conformation occurred in the EL2. In the active structure of the A_{2B} model, this loop forms a beta sheet between the EL1 and EL2 which is essentially identical to that observed in the crystal structure of the A_{2A} receptor. Furthermore, the X-ray structure of the adenosine A_{2A} receptor in the inactive state and the A_{2B} model derived from this template contain a short helical segment in EL2 that is not persistent in the active structure. In addition, Glu174 and Lys267 are oriented towards each other and potentially form a salt bridge in the inactive state. However, in the active state, these residues are oriented in opposite directions (Figure **3.18**). Moreover, the EL2 and EL3 are inserted more into the TM domains.
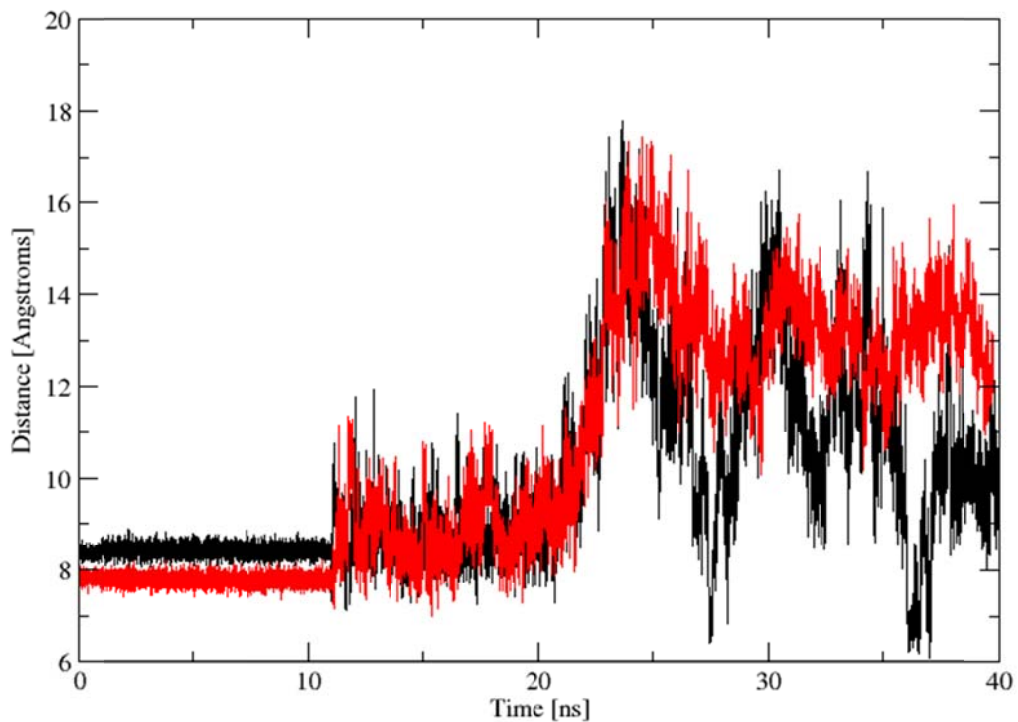
Figure 3.18 The distance between the Lys267 and Glu174 with PSB-603 (black) and BAY-60-6583 (red) plotted versus time. The distance is increased with agonist and decreased with antagonist

Conformational changes in Trp247

The rotamer Trp247$^{6.48}$ on the TM6 could potentially switch to a different conformation upon activation. Figure **3.19** and **3.20** show the torsional angles $\chi 1$ and $\chi 2$ of Trp247 in the A_{2B} model with antagonist and agonist, respectively. It is obvious that the presence of an antagonist stabilizes the starting conformation of Trp247. Also in the inactive state, the indole

nitrogen of the Trp247 forms a water-mediated hydrogen bonding interaction with Asn282 of the conserved NPxxY motif in TM7. This hydrogen bonding is disrupted in the active state model. Also the presence of an agonist does not stabilize the starting conformation of Trp247.
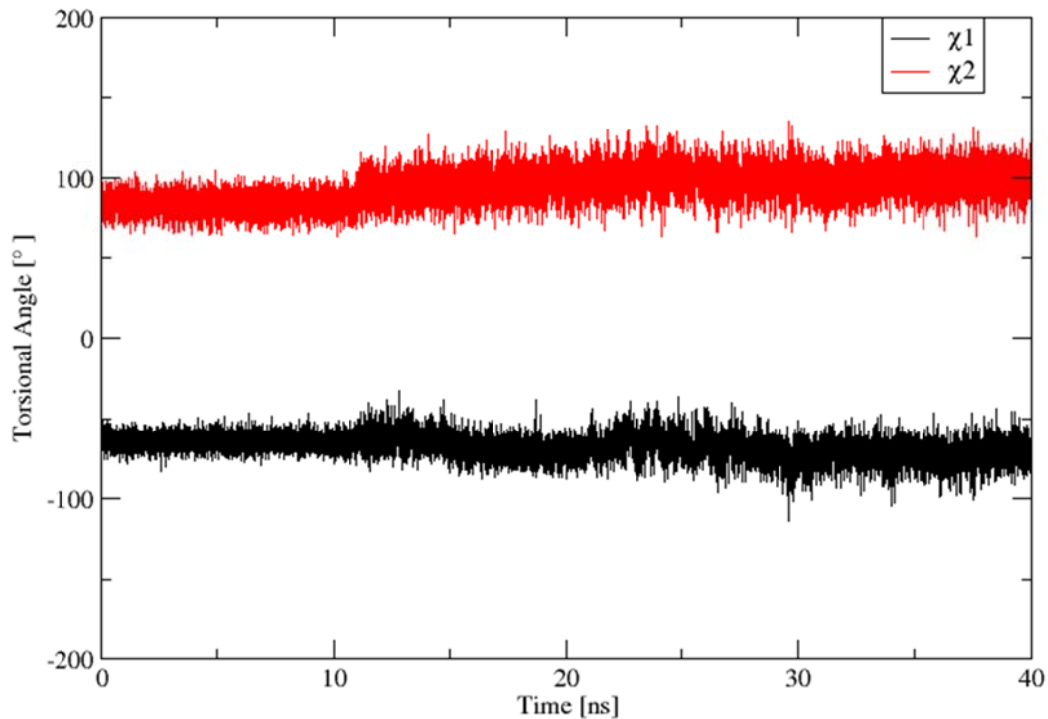
Figure 3.19 Torsional angles χ1 and χ2 of Trp 247 receptor with PSB-603 plotted versus time
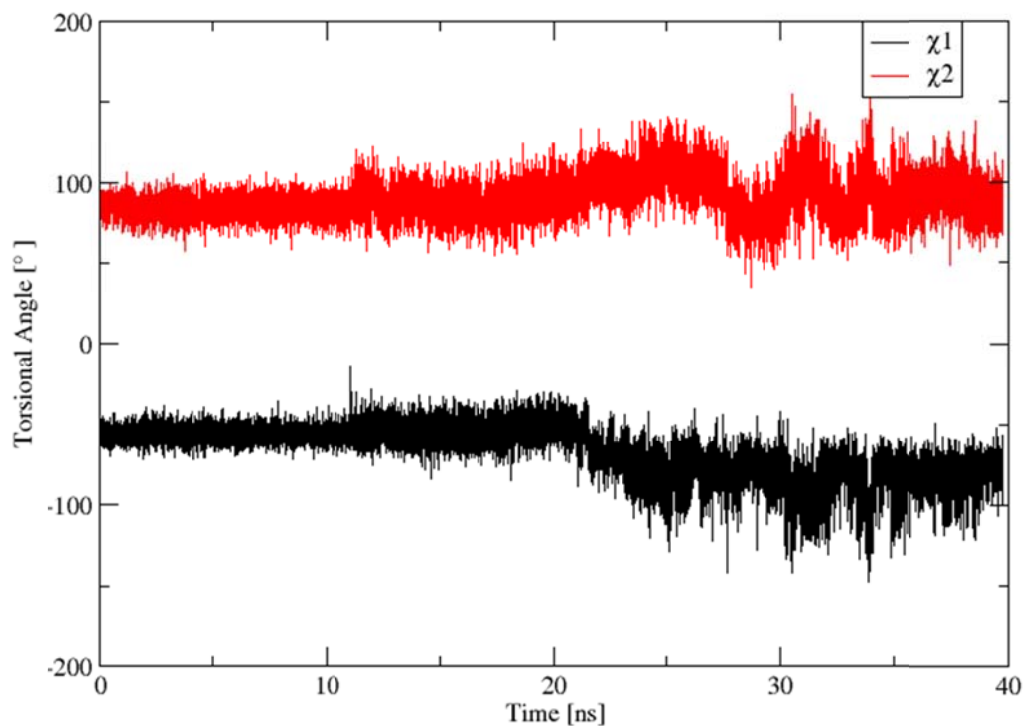
Figure 3.20 Torsional angles χ1 and χ2 of Trp 247 receptor with BAY-60-6583 plotted versus time

Movement and rotation of TM6 upon receptor activation

The last conformational change during the receptor activation is a rotational motion of TM6 (see introduction). In the A_{2B} model of the fully active state, this movement allows a small rearrangement of the helical segments and the intra- and extracellular loops compared to the inactive state. In particular, the EL2 and EL3 loops are inserted more into the TM domains. Once more, this rearrangement of EL2 seems to be important for A_{2B} receptor activation (Figure **3.21**).
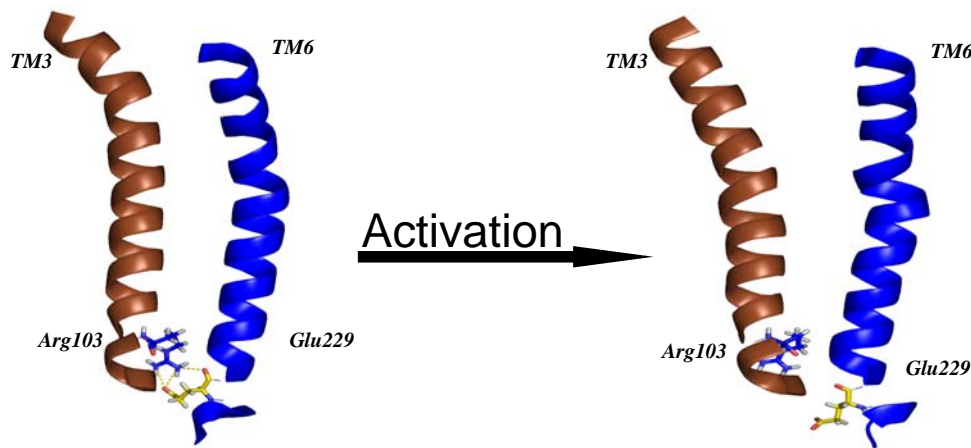
Figure 3.21 Intact (inactive) and disrupted (active) ionic lock. The interaction is depicted via dashed yellow lines. In the receptor structures, the TM3 and TM6 domains are highlighted

With respect to the putative binding site of the A_{2B} model, residues such as Leu81 and Leu86 in TM3, Met182 and Met179 in TM5 as well as Ile276 and Asn273 in TM7 are similarly oriented in different states. However, three important residues, Trp247, Val250 and His251, show another orientation in the active model compared to the model of the inactive state and this difference could be due to the rotation of TM6.

3.4 Conclusions

The molecular modelling together with MD simulations of the A_{2B} model in a phospholipid bilayer indicated characteristic differences between agonists and antagonists, which correlated well with known experimental results. In addition, they provided insight into the

conformational preferences and binding requirements for agonists and antagonists at the adenosine A$_{2B}$ receptor.

Furthermore, the A$_{2B}$ receptor model in different states suggests conformational differences and important collective changes of TM domains and the intra- and extracellular loops during the activation process. This model also helps in understanding the different interactions of typical antagonists and agonists with a largely overlapped binding site. The analysis of the putative receptor-ligand interactions has shown that part of the highly conserved (D/E)RY motif, changes in the NPxxY(x)5,6F motif, separation of the intracellular sides of TM3 and TM6 as well as conformational changes in the extracellular loops are suggested to form the activation mechanism for the A$_{2B}$ receptor. Our results also demonstrated a critical role for Glu14 and Asn25 in **TM1**, Asp53 in **TM2**, Arg103 in **TM3**, Glu229 and Trp247 in **TM6**, and His280, Asn282, Asn286 and Tyr290 in **TM7** as anchor sites in agonist binding and receptor activation. In addition, our study suggests a structural conformation for direct contribution of these interactions in the conformational changes of the ligand binding pocket, and their role in differentiation between agonistic and antagonistic effect of the adenosine A$_{2B}$ ligands. The results are consistent with other experimental results for family A GPCRs. Thus, our findings suggest that the conformational changes associated with adenosine A$_{2B}$ receptor activation are similar to other GPCRs and indicate a shared mechanism of GPCR activation.

4 Virtual (in silico) screening of ligands for the adenosine A$_{2B}$ receptor

4.1 Introduction

It is commonly accepted that there are several subsequent steps in the drug discovery process; including disease selection, target hypothesis, lead compound identification (screening), lead optimization, pre-clinical trial, clinical trial and pharmacological optimization. Traditionally, these steps are carried out sequentially, and if one of the steps is slow, the entire process is delayed. Because it is not possible to speed-up clinical trials, it seems that the only way to accelerate the process is to act on the preclinical steps. Among the various techniques used to facilitate hit identification, high throughput screening (HTS) represents probably the most investigated one. The perspective of screening millions of compounds on a target can be powerful to identify hits [143].

Virtual screening has become an integral part of the drug discovery process in recent years. Virtual screening uses computer-based methods to discover new ligands on the basis of biological structures. Therefore, in silico screening is perhaps the cheapest technique, faster than experimental synthesis and biological testing and a way to identify new lead compounds. Virtual, or "in silico" screening is a tool for selecting compounds by evaluating their desirability in a computational model [143]. The desirability comprises high potency, selectivity towards the target protein, appropriate pharmacokinetic properties, and favorable toxicology.

Virtual screening assists the selection of compounds for screening libraries and compounds from external vendors. The strategy of applying in silico screening is to bring a more focused approach to the wet-lab experiments using pharmacophore searches of 3D databases, homology searching and docking. Some important points to be considered for virtual screening are: the availability of the compounds to be screened against the receptor, the knowledge about the structure of the receptor and the receptor ligand interactions, and the knowledge about drugs and drug characteristics [144]. Virtual screening allows the scope of screening to be extended to external databases. The major benefits of virtual screening are: increasingly diverse hits can be identified potentially leading to more diverse lead compounds.

In silico screening of compounds for GPCRs activity can be performed by two approaches: The first is "structure-based screening", which requires knowledge of the 3D structure of the target protein's binding site to prioritize compounds by their likelihood to bind to the protein; and the second is "ligand-based screening", where no information on the protein is necessary. Instead, one or more compounds that are known to bind to the protein are used as a structural query [145] [146] and a compound's similarity to certain query features determines the likelihood for high affinity towards the particular receptor.

So far ligand-based methods are the main technique used to design drugs for the GPCR family because of the limited availability of structural data about GPCRs. The strategy is to use information provided by compounds that are known to bind to the desired target and to use these data to identify other molecules in the databases with similar properties [147] [148] in order to improve the biological activity. These methods are based on analysis of sets of ligands with known biological activity. This can be done by a variety of methods, including similarity and substructure search, clustering, quantitative structure-activity relationships (QSAR) (which is effective for development of close analogues of known compounds), pharmacophore matching (which represents a set of points in space with the certain properties and distances between them) or three-dimensional shape matching (which takes into account spatial structure of compounds).

Structure-based drug design is one of several methods in rational drug design and pharmaceutical research. In structure-based screening, it is assumed that the 3D structure of the target is known either by X-ray crystallography, NMR experiments or predicted by homology modeling [149] [150] [151]. When an X-ray structure or 3D homology model of a receptor is known, then receptor-based approaches can be used to screen compound collections virtually. The basic approach in structure-based virtual screening is to identify the binding pose of each small molecule in a test library (docking), and from that identify the free energy of binding of that molecule (scoring). The set of hit compounds is then predicted by sorting all compounds in the test library by this score and deciding on a threshold score. Compounds scoring better than this threshold are regarded as hits, and are evaluated further. This is analogous to experimental HTS, where the percent inhibitions obtained from HTS serve the same role as the score in structure-based virtual screening [152]. The virtual screening method is fast and allows identifying possibly active compounds with a completely

different scaffold than the existing compounds, and it is thus a valuable tool in finding novel drug candidates.

In fact, the use of 3D GPCR structural models in drug design and structure-based virtual screening studies has increasingly emerged in recent literature. The homology models among these studies were reliable enough to retrieve known antagonists via structure-based virtual screening from several compound databases [151] [153] [154] [155] [156]. In order to develop more active novel compounds for the adenosine A_{2B} receptor, the strategy used to reduce the number of promising compounds in this study, which employs ligand-based (filtering and fingerprint) and receptor-based (docking) approaches is shown in Figure **4.1**.
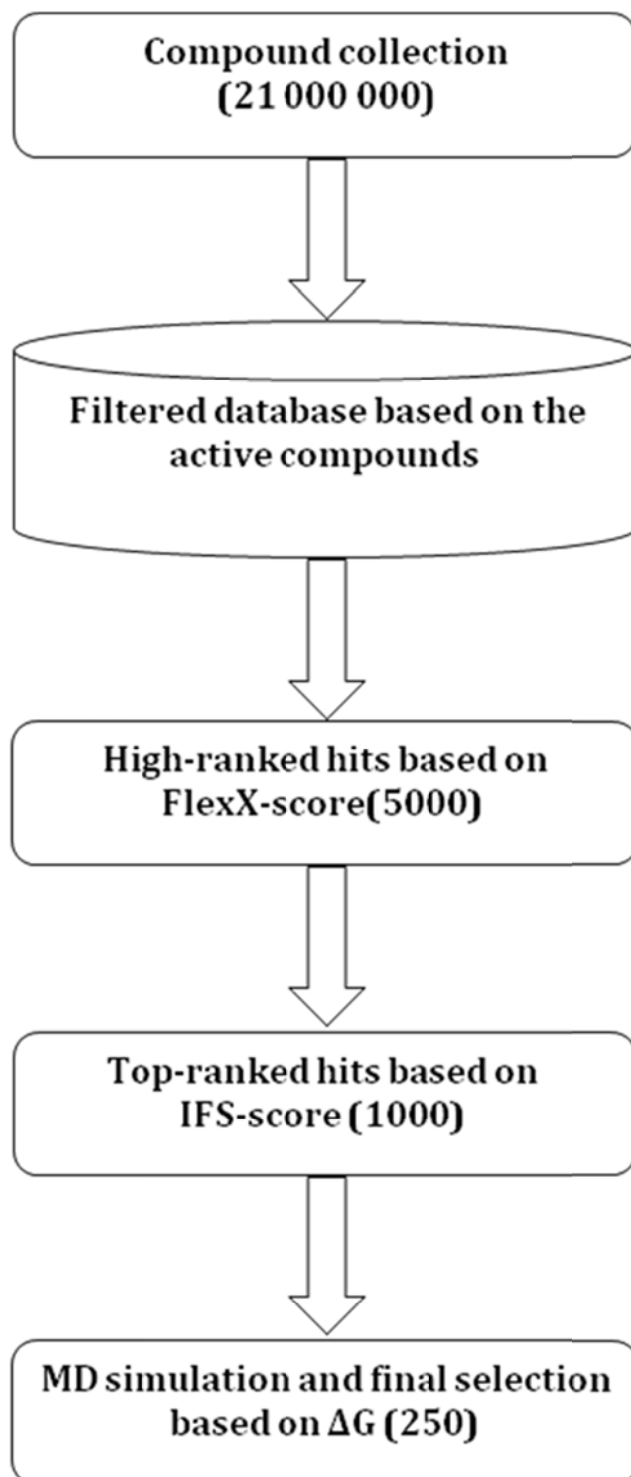
Figure 4.1 A pictorial description of the workflow of a virtual screening run against the A_{2B} receptor model. The initial database comprised about 21 000 000 entries. In the first selection step, putative ligands (800,000) were chosen based on molecular similarity with known antagonist ligands (55). Subsequently flexible docking to the target protein served as sequential filters to reduce the initial set to about 5000 prospective entries. On the basis of the

resulting scoring and ranking of the selected hits the top 5000 compounds were selected for FlexX-score and the top 1000 compounds were selected for the interaction fingerprint based similarity (IFS) evaluation to control the performance of our strategy. A final set of top 250 compounds were selected for computing free energy of binding (ΔG) using MD simulations

In the present study, we report on the development of a structure-based virtual screening protocol for A_{2B} antagonist discovery. The protocol is based on the 3D homology structural model of the human adenosine A_{2B} receptor which was generated using homology modeling based on the adenosine A_{2A} receptor as a template (as described in chapter **2**, in section **2.2.2**). The performance of the screening model was further improved by retaining several highly structured water molecules (three water molecules based on the A_{2A} template) in the binding site and refining the side-chains in the binding pocket similar to structure-based discovery based on the X-ray structure of the A_{2A} receptor [157]. Prototypic A_{2B}-antagonist complexes were first constructed through flexible docking and MD simulations on the basis of important binding residues derived from site-directed mutagenesis data. The generated complexes were then used to examine the potential binding pocket for the A_{2B}-selective antagonists. In addition, the predicted binding pocket was further evaluated in terms of its ability to identify more known A_{2B} antagonists (see chapter **2**, in section **2.3.7**). The optimized model was used for virtual screening of more than 21 million commercially available lead-like and drug-like compounds in the ZINC database [158].

In virtual screening, large compound libraries of molecules are docked into the target structure. These databases contain unwanted and unnecessary compounds, which have undesirable or some other toxic effects. The large database is filtered and reduced from a few millions to a few hundreds for increasing the chances of finding new ligands. Thus, virtual screening was performed using FTrees [159] [160] available from BioSolveIT GmbH (http://www.biosolveit.de/), to identify compound molecules that satisfy the chemical and the geometrical requirements. Subsequently, the A_{2B} structure-based virtual screening protocol was established using the FlexX-docking program. In this developed protocol, FlexX-Score and the interaction fingerprint based similarity were used to rescore binding energies of the hits screened from the testing compound database by FlexX docking into the A_{2B} homology model. The final candidate compounds were selected based on free energy of binding (ΔG).

Therefore, our present A_{2B} structure-based antagonist virtual screening studies will allow us to establish an alternative approach for lead discovery of A_{2B} antagonists.

4.2   Material and Methods

4.2.1   Homology model preparation

Often, the X-ray crystal structure of the therapeutic target is not available, but the 3D structure of a homologous protein will have been determined. Depending on the degree of homology between the two proteins, it may be useful to model the structure of the unknown 3D protein based on the known structure. So, in absence of an experimental protein structure, a homology model may be used for docking and structure-based design. Since the adenosine A_{2B} receptor does not have an experimental 3D structure available yet, the 3D structure of the A_{2B} homology model has been constructed based on the crystal structure of the adenosine A_{2A} receptor as structural template using a comparative protein structure prediction method and further refined by MD simulations for use in a docking/screening study. This receptor belongs to the family of GPCRs, which represents one of the most important pharmaceutical drug target classes.

The homology model was then employed to analyze the A_{2B} structure regarding 7TM helical bundle, interhelical hydrophobic interactions, interhelical hydrogen bonding networks, conserved residues and motifs, and a possible disulfide bond between residues Cys78 and Cys171. The first step in the calculation of a ligand-supported homology model was to select a set of appropriate reference ligands. The active compounds belonged to five different scaffold classes. The selected reference ligands are shown in chapter **2**, Figure **2.8**. The model was validated by reproducing experimental information such as mutational data and corresponding affinity data of known ligands. We examined the different number of active molecules as well as the different number of scaffolds. We started with the generation of a preliminary A_{2B} model and subsequent docking into this crude model and finally generated a refined A_{2B}-ligand complex consistent with experimental data.

Location and preparation of the target binding site are also crucial to the success of the screening process. Structural investigation of the binding pocket is important because docking/scoring methods are sensitive to the nature of the binding cavity. Therefore, based on this model, the initial docking position of A_{2B}-selective antagonists were subsequently characterized on the basis of the site-directed mutagenesis data (see chapter **2**, Table **2.2**) and

the molecular modeling results of the interaction between the antagonists and the adenosine A$_{2B}$ receptor.

4.2.2 Database preparation

The initial compound library was obtained from the ZINC database [161]. The ZINC database is a collection of 21 million chemical compounds from different vendors. We have chosen to use the ZINC library because ZINC is an open source database; the structures have already been filtered according to the Lipinski rules [162]. Thus, ZINC provides virtual compounds ready for virtual screening, and a total of 21 000 000 compounds were downloaded from the ZINC database.

In the initial stages of a virtual screening project it is necessary to prepare the compound collections i.e. reduce the number of compounds for docking. Compound libraries used in the virtual screening should be filtered first to remove unsuitable compounds due to undesired and toxic properties. Compounds are filtered based on their chemical descriptors. Therefore, in the first step, the compound library is prepared, usually by various filters that limit the number of compounds for docking. One general filter is the "rule of five". It states that a drug-like molecule should have a molecular weight less than 500, a logP value less than 5, less than 5 hydrogen bond donors and less than 10 hydrogen bond acceptors. This rule is a good predictor of the bioavailability of the compound. The reason for these criteria is to retrieve hits small enough to allow for further optimization, thus focusing on "leadlike" hits.

The design of the compound library is very important since it plays a key role for real-life screening experiments. Therefore, similarity searching methods or pharmacophore based screening methods is often used to increase the hit rate or to reduce the size of the compound database prior to molecular docking. It is generally assumed that compounds having a structural similarity to a known drug may exhibit drug-like properties themselves, such as oral bioavailability. Thus data is collected to find structural motifs and pharmacophore features of molecules that characterize drugs [163].

In addition, we have selected binding affinity data for a series of ligands with presumably similar binding modes which include xanthine and nonxanthine ligands (as described in chapter **2**) for the adenosine A$_{2B}$ receptor in order to build a pharmacophore model. Thus the final compound library is contained among the 21 000 000 candidate molecules, a reference

set of known good binders in order to determine the success rate of retrieving suitable compounds. Therefore, virtual screening was performed through a pharmacophore search of a 3D compound database to identify molecules that satisfy the chemical and the geometrical requirements using feature trees [159]. The program FTrees is a known chemoinformatic tool able to condense molecular descriptions into a graph object and to search for actives in large databases using graph similarity. Thus, FTrees calculates the descriptors for each molecule of the database and the known active compounds. Molecular similarity search between database and training set was performed using these descriptors generated for the compound database and active known compounds. The top similar compounds in the ranks having a feature trees similarity value of 0.98 or higher were selected to show up in the filtered database.

4.2.3   Docking procedure

The ideal approach for docking is to treat both protein and ligand as flexible entities. However, because of the limitations in computing power, most programs only explore the flexibility of the ligand. The automated docking software FlexX was employed to perform scoring and ranking of the hits obtained from the previous step of database searching. FlexX is an extremely fast, highly configurable computer program for predicting protein-ligand interactions and perfectly suited for virtual high throughput screening. FlexX employs an incremental construction algorithm for molecular docking: During docking, the ligand is first divided into small fragments. A base fragment is first selected and docked into the active site as a rigid body. The remaining fragments are added to the base fragment to incrementally rebuild the ligand. This approach is capable of exploring the flexibility of the ligand and has shown to reproduce about 70% of experimentally determined protein-ligand complex structures [89]. Thus, docking was executed using the standard parameters of the FlexX program.

4.2.4   Scoring Function

Assuming the receptor structure is available, a primary challenge in lead discovery is to predict both ligand orientation and binding affinity; the former is often referred to as 'molecular docking' while the latter is referred to as 'scoring' (or ranking).

4.2.4.1 FlexX score

Besides the placement, the scoring function is another important factor in the docking approach to estimate interaction energies between receptor and ligand in structure based virtual screening. The docking results are monitored by scoring functions that predict how well the ligand binds in a particular docked pose. Scoring functions can be based on physics/physical approximations (a force field), like in AMBER, which provide the advantage of accuracy but are generally slow for calculation. Other scoring functions are empirical, i.e. based on simple rules such as hydrogen-bond counts. They use an additive approximation and are faster to compute [144].

The scoring function implemented in FlexX is an empirical scoring function derived from the interaction types of the protein-ligand complex. Both the hydrophobic contacts and hydrogen bonds contribute to the final score of a particular protein-ligand interaction. However, the hydrogen bonds (hydrogen acceptor and donor) are weighted higher than interactions resulting from hydrophobic contacts. This is a reason, why ligands that are capable of making more hydrogen bonds score better than ligands making only hydrophobic interactions [89]. In detail, the total FlexX docking score contains five terms: MatchScore, LipoScore, AmbigScore, ClashScore, and RotScore, which represent the contributions of the matched interacting groups, lipophilic contact area, lipophilic-hydrophilic contact area, clash penalty, and ligand rotational entropy, respectively. At the final stage, top 5000 ranked molecules having FlexX energy scores were selected for further inspection by using interaction fingerprints.

4.2.4.2 Interaction Fingerprints

Our scoring methodology is referred to as the interaction fingerprint based similarity. The scoring scheme [57] presented in this study is based on the incorporation of receptor-ligand interaction information from antagonist ligands already known to bind to the receptor. As antagonist ligands, all compounds, that have already been employed to support the process of homology modeling, were used (Figure **2.8**, see chapter **2**). Patterns of interaction were modeled using binary ligand-receptor fingerprints. To generate these interaction fingerprints, each of the antagonist ligands was docked into the receptor binding site using the FlexX program. The best solution was determined (as described in chapter **2**), considering mutational data and the features common to all considered antagonist ligands. FlexX

recognizes the interactions between the antagonist ligand and the receptor. All information about the type and the strength of each interaction, and about the amino acid of the receptor involved, was written to a file. In total, 19 binding site residues were defined as potential interaction points for generating interaction fingerprints: Asn254, Glu174, Phe173, Val250, Trp247, Ile276, Leu86, His251, Val85, His280, Met182, Leu172, Met272, Lys267, Lys265, Lys269, and three water molecules. This file was used to generate the interaction fingerprint, where a single bit was used to account for an interaction between a ligand and a particular residue. Information about the patterns of interactions between the reference ligands and the binding site residues was used to rank the docking solutions. Therefore, predicted patterns of interactions of the docking solutions were compared with the patterns of interactions of the reference ligands. We thus used IFS in order to reciprocally compensate the drawbacks of the scoring function used in FlexX and possibly improve the chances of identifying true positive hits. Consequently, the top 1000 ranked molecules having IFS scores were selected for further study by calculating binding free energy (ΔG) using MD simulations.

4.2.4.3   Rescoring by MM-GBSA

The Molecular Mechanics Poisson-Boltzmann Surface Area (MM-PBSA)/Molecular Mechanics Generalized Born Surface Area (MM-GBSA) procedures have recently become of interest in drug discovery for calculating binding affinities of protein-ligand complexes, based on MD simulations of the given protein–ligand complex in implicit solvent. A molecular mechanics (MM) force field is used to calculate the internal energy, while a Poisson-Boltzmann (PB) calculation yields the polar component of the solvation free energy. The nonpolar contribution correlates with the surface area (SA). The method is known as MM-PBSA. Thus the binding free energies were calculated using the MM-GBSA method and can be successfully applied in improving the binding affinity prediction and ranking the actives [164].

In the MM-PBSA approach, the binding free energy is estimated as the sum of the gas-phase energies, solvation free energies and entropic contributions, averaged over a series of snapshots from MD trajectories. The electrostatic contribution to the solvation term is calculated by solving the Poisson-Boltzmann (PB) equation. If the PB model is replaced by a generalized Born (GB) model, there comes the MM-GBSA method. The binding free energy for each system was calculated using the MM-PBSA technique [165] [166] according to

$$\Delta G_{binding} = G_{complex} - G_{protein} - G_{ligand} = \Delta E_{MM} + \Delta G_{PB} + \Delta G_{SA} - T_{\Delta S}$$

Where ΔE_{MM} is the molecular mechanics interaction energy between the protein and the ligand; ΔG_{PB} and ΔG_{SA} are the electrostatic and nonpolar contributions to desolvation upon ligand binding, respectively; and $-T\Delta S$ is the conformational entropy change, which was not considered because of the high computational cost and low prediction accuracy [165]. Here, the polar part of desolvation was calculated by solving the Poisson-Boltzmann (PB) equations [167]. The calculations for binding free energies were accomplished by using the *mm_pbsa* program in AMBER9 [168].

For the 1000 best-ranked ligands (IFS-score), the best docking solutions were minimized (5000 steps) keeping the ligand and the binding-pocket flexible using the Steepest Descent algorithm and applying the Conjugate Gradient minimization method. The purpose of this procedure was (1) to optimize the local interactions and (2) to account for protein flexibility induced by ligand binding. Then MD simulations were performed using the previously optimized structures. The time step of the simulations was 2.0 fs with a cutoff of 10 Å for the non-bonded interactions. The SHAKE algorithm was employed to keep all bonds involving hydrogen atoms rigid. The MD simulations (1 ns) are traditionally performed at constant temperature and pressure, followed by using MM-GBSA binding free energy as tools to refine and rescore the complexes obtained from docking virtual screenings. The energy score is the sum of van der Waals and electrostatic components. A more negative energy score (kcal/mol) corresponds to a higher binding affinity.

4.3   Result and discussion

The previously created A$_{2B}$ receptor homology model was evaluated for its ability to select new A$_{2B}$-antagonists from random decoy compounds in a virtual ligand screening experiment. In this contribution, we present a strategy for the computer screening of a large compound library using A$_{2B}$ receptor model. The A$_{2B}$ model-complex served as a platform to generate a structural ground for the following database search. The common binding motif for the xanthine and nonxanthine derivatives involves aromatic stacking interactions between aromatic moieties of the ligands and the conserved Phe173 side-chain of the receptor and hydrophobic interactions with Leu86, His251, Val85 Val250, Met272, Ile276, Met182, and Trp247, as well as polar interactions with the conserved Asn254 side-chain. In addition to these core interactions, most high affinity A$_{2B}$ antagonists have an aromatic group extending

deeper into the binding pocket and/or flexible extensions towards the extracellular opening of the pocket. We also included the three water molecules selected for the A_{2B} model which have the lowest B-factor values and form an extended hydrogen bonding network with the binding pocket residues, suggesting their highly structured nature similar to the ones in the A_{2A} X-ray structure.

4.3.1   FlexX-program Database Virtual Screening

The FlexX program is a flexible docking algorithm that takes into account ligand flexibility while keeping the protein rigid. It allows for fast docking of small molecules into protein active sites for the performance of 3D database searches. The introduction of FTrees contributes to the efficient filtering of inactive molecules and a decrease in the number of false positives and might improve virtual screening significantly. Therefore, FTrees were used to establish our A_{2B} receptor-based virtual screening protocol.

The evaluation and ranking of predicted ligand binding conformations at a receptor is a crucial aspect of structure-based virtual screening. The scoring functions utilized in the present scoring scheme were representatives of the two main classes of FlexX scoring functions, namely the empirical-based scoring functions and IFS functions. The combination of different scoring functions, have been developed to balance errors in single scores and improve the probability of identifying 'true' ligands [169].

In the initial screening only those compounds out of 800,000 database entries were selected, that were in agreement with to simple FTrees established as minimal requirement due to the analysis of known A_{2B} antagonists. Then, all selected compounds were docked against the optimized A_{2B} receptor binding site using the FlexX program. Thereby, a large number of diverse docking solutions were generated for each compound. All docking solutions were scored with FlexX-Score. For the 5000 best-ranked ligands, the best docking solutions were picked. Therefore, the 1000 best solutions were selected considering the agreement of their interaction fingerprint-based similarity with the putative interaction features present in known active A_{2B} antagonists.

Ideally, the selection of virtual screening hits could be solely based on the ranking of the scoring function used to evaluate the interaction geometry of the docked ligands. However, it has been shown that the performance of a scoring function possibly depends on binding
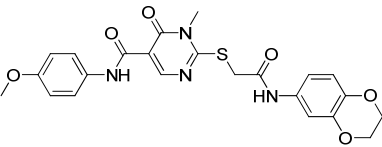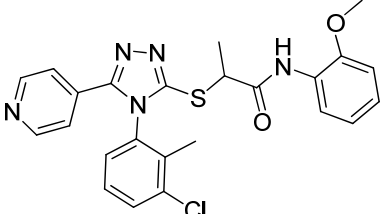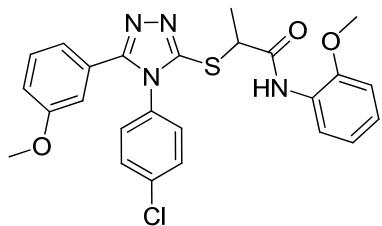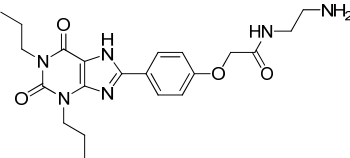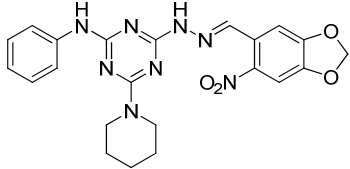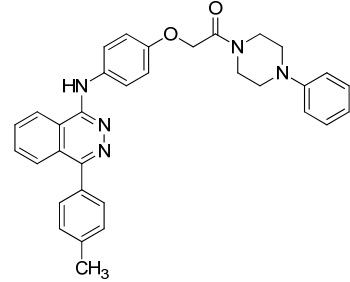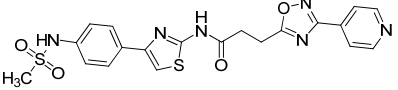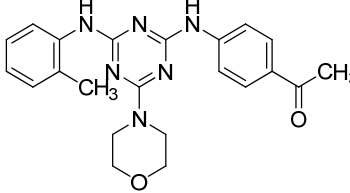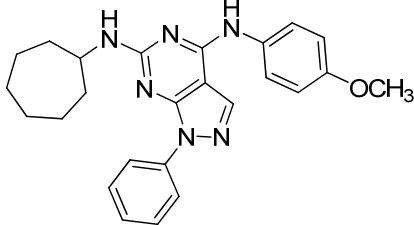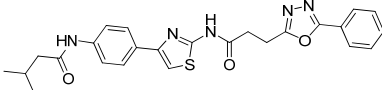
characteristics present in a particular protein-ligand interface, such as hydrophobicity, hydrophilicity, and dominance of electrostatic/H-bond properties [170]. In addition, some binding conformers of certain docked compounds interact well with the A_{2B} receptor, but their conformational energy is probably so high that the conformation or binding pose is very bad for this compound.
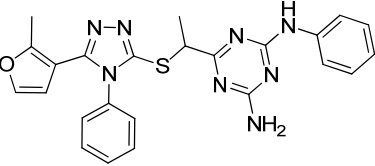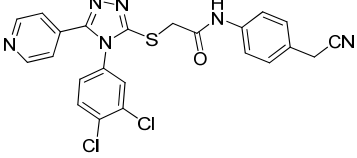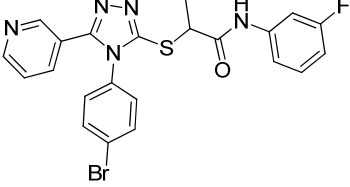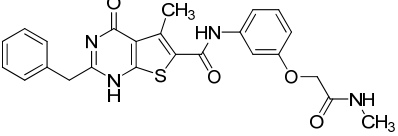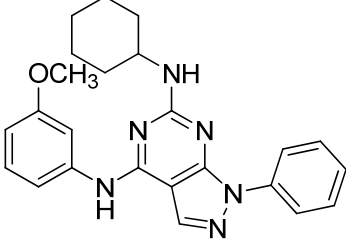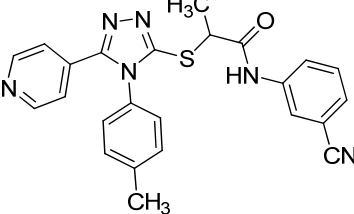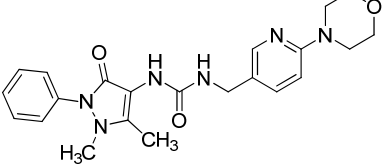
Thus, the interaction fingerprints were generated for the reference compounds and for all docking poses of the screening set compounds during the virtual screening. The maximal similarity between the fingerprint of each docking pose and the reference fingerprints was calculated; the interaction fingerprint-based similarity is directly used as an "IFS".
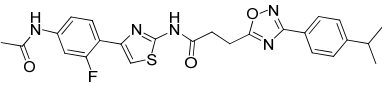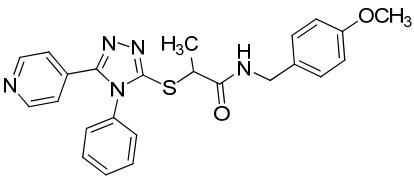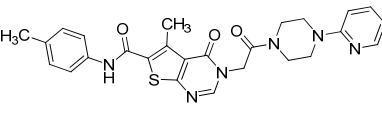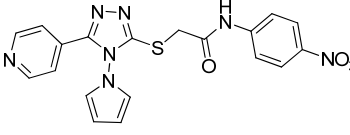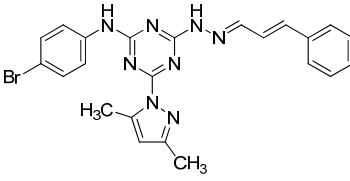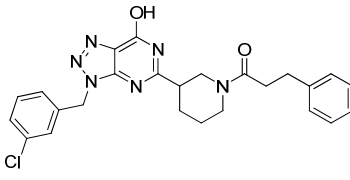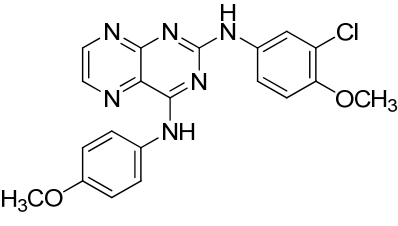
4.3.2 Rescoring by MM-GBSA
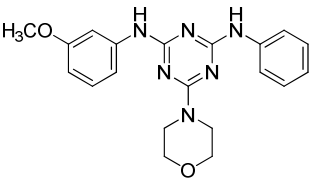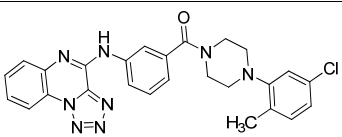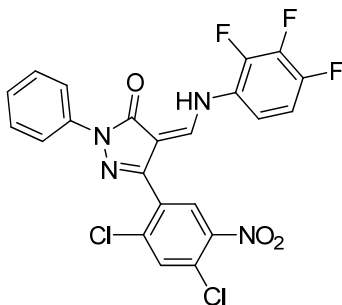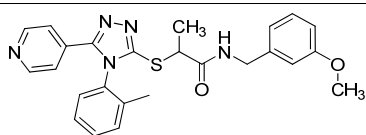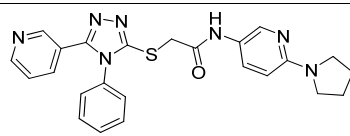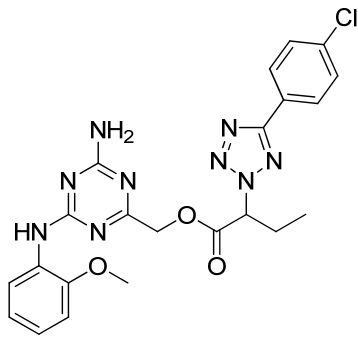
Table 4.1 Representative hits with the A_{2B} receptor model and the predicted free energy of binding (ΔG)
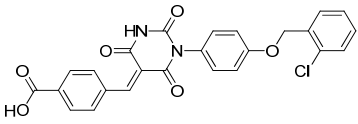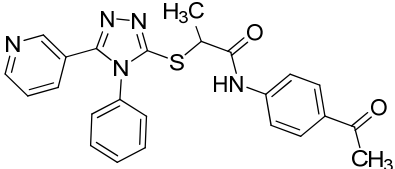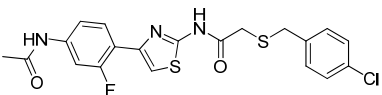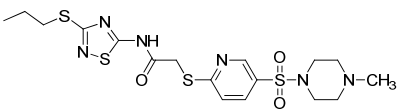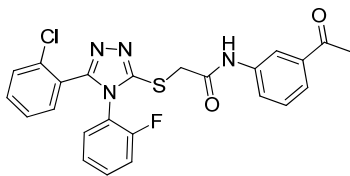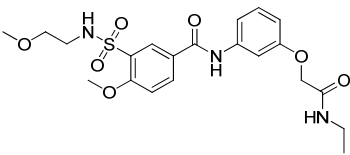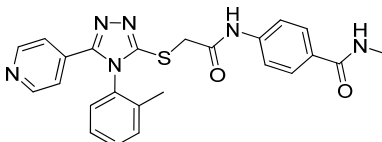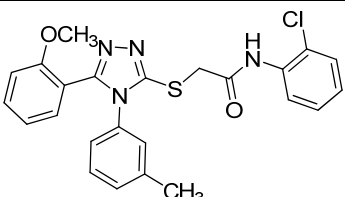
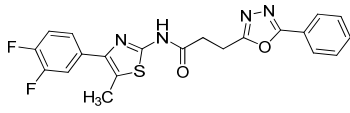| No.	Label (database)	Structure	Calculated ΔG (kcal mol^{-1})
1	ZINC22712240		-96.36
2	ZINC29826264		-49.55
3	ZINC21185835		-49
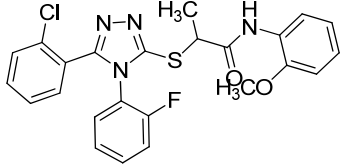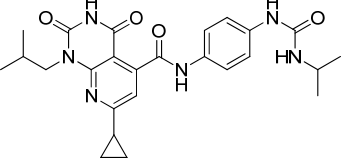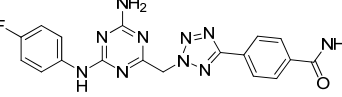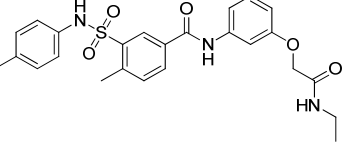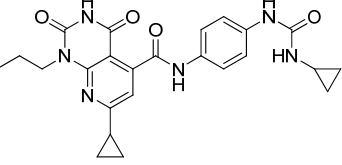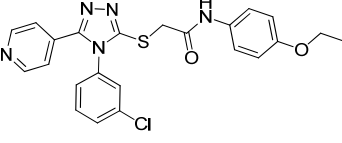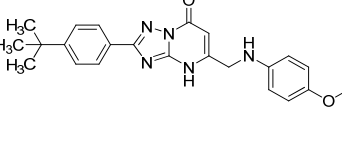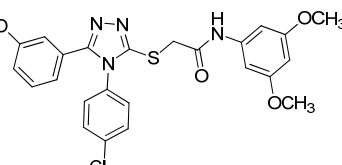
No.	Label (database)	Structure	Calculated ΔG (kcal mol^{-1})
4	ZINC09210767		-47.33
5	ZINC13133349		-47.06
6	ZINC02212325		-46.82
7	ZINC08718330		-46.61
8	ZINC27788857		-46.21
9	ZINC16954247		-46.03
10	ZINC29345837		-45.93
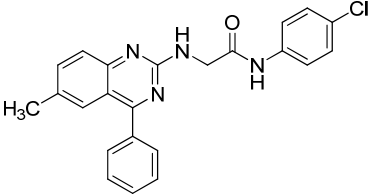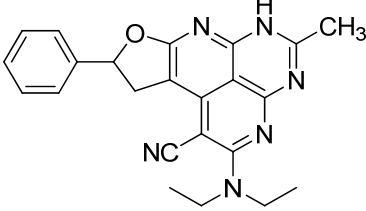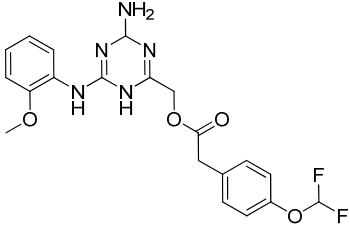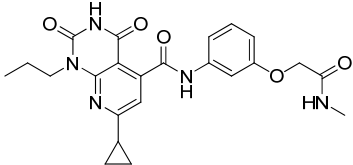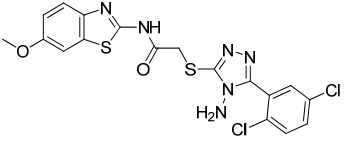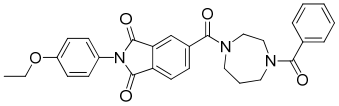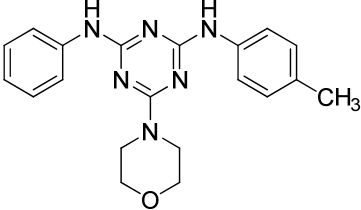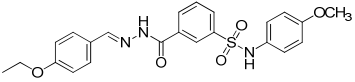
No.	Label (database)	Structure	Calculated ΔG (kcal mol^{-1})
11	ZINC25025023		-45.91
12	ZINC25931613		-45.03
13	ZINC17003771		-45.02
14	ZINC31521221		-44.8
15	ZINC28406152		-44.65
16	ZINC10730706		-44.06
17	ZINC27333228		-44.01

No.	Label (database)	Structure	Calculated ΔG (kcal mol^{-1})
18	ZINC23453848		-43.97
19	ZINC20414180		-43.75
20	ZINC02912166		-43.59
21	ZINC14434109		-43.45
22	ZINC02091761		-43.44
23	ZINC13083305		-43.33
24	ZINC09074482		-43.31
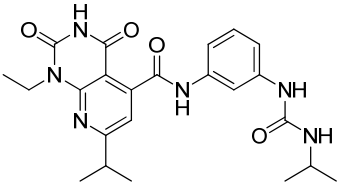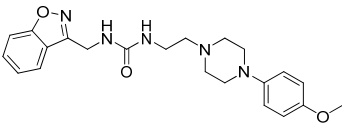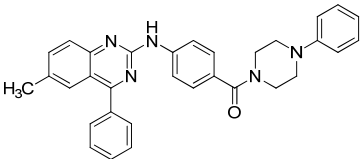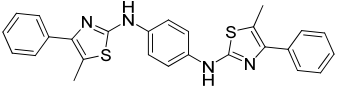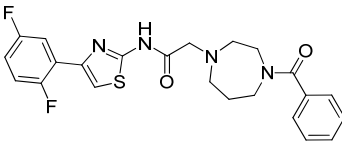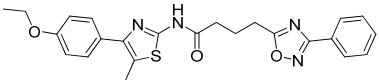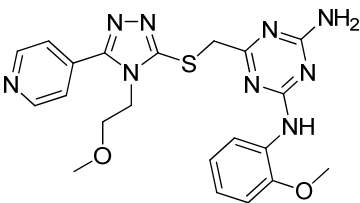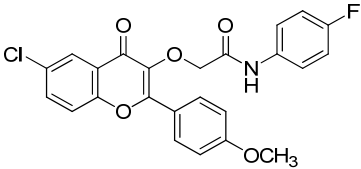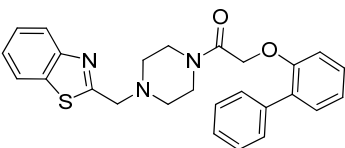
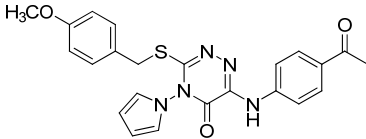| No.	Label (database)	Structure	Calculated ΔG (kcal mol^{-1})
25	ZINC09708958		-43.15
26	ZINC09561318		-42.94
27	ZINC08453947		-42.88
28	ZINC23338627		-42.59
29	ZINC22391695		-42.45
30	ZINC16679421		-42.42
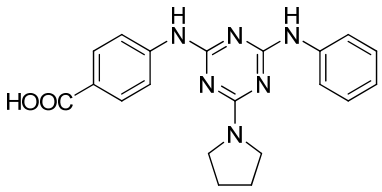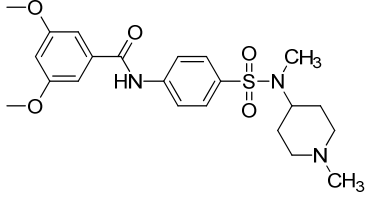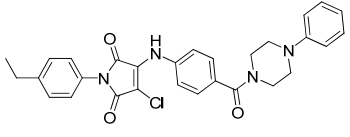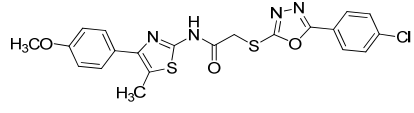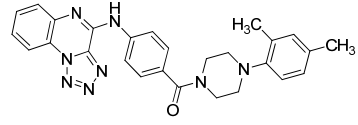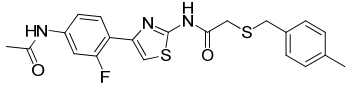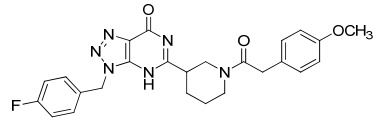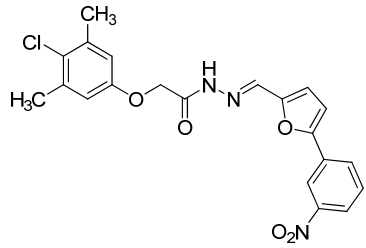
No.	Label (database)	Structure	Calculated ΔG (kcal mol^{-1})
31	ZINC02988597		-42.35
32	ZINC00976119		-42.32
33	ZINC10993446		-42.25
34	ZINC10376706		-42.12
35	ZINC08750584		-42.01
36	ZINC27504819		-41.99
37	ZINC18473258		-41.95
38	ZINC01328329		-41.9
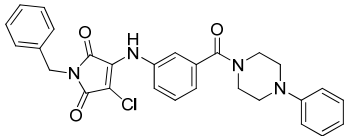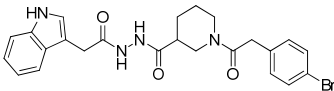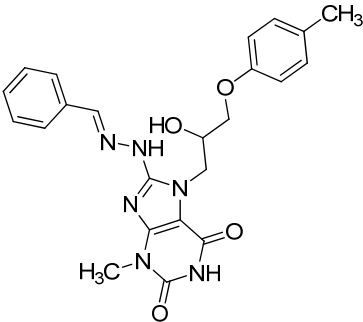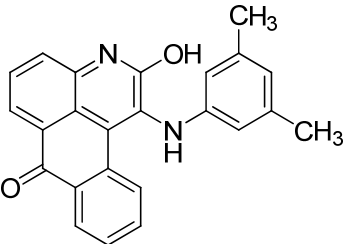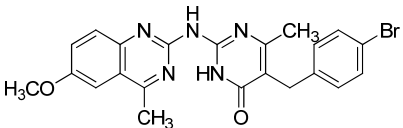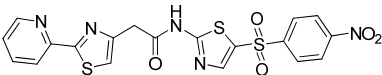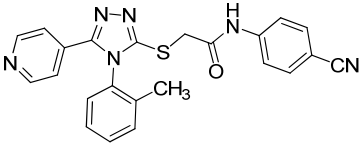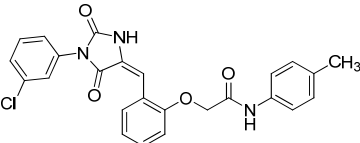
No.	Label (database)	Structure	Calculated ΔG (kcal mol^{-1})
39	ZINC20883231		-41.64
40	ZINC24466119		-41.61
41	ZINC31762791		-41.51
42	ZINC27511120		-41.49
43	ZINC24441114		-41.37
44	ZINC01223932		-41.36
45	ZINC14609110		-41.34
46	ZINC02447604		-41.33
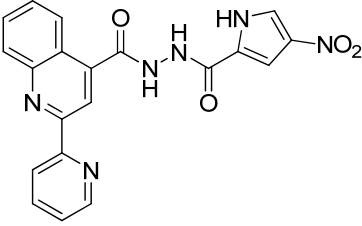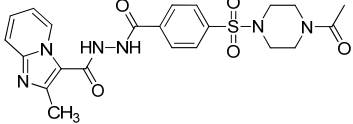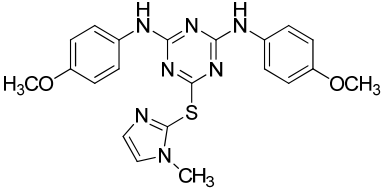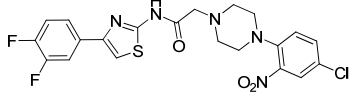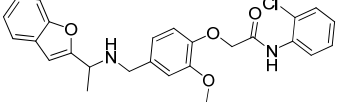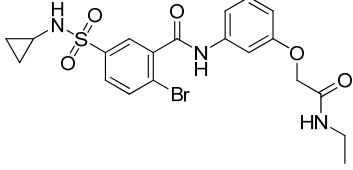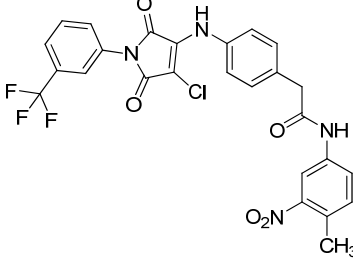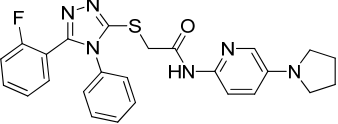
No.	Label (database)	Structure	Calculated ΔG (kcal mol^{-1})
47	ZINC06521629		-41.25
48	ZINC03358609		-41.07
49	ZINC24422457		-41.01
50	ZINC26977987		-40.95
51	ZINC21454865		-40.91
52	ZINC31250830		-40.89
53	ZINC09708965		-40.88
54	ZINC20755296		-40.87
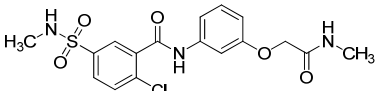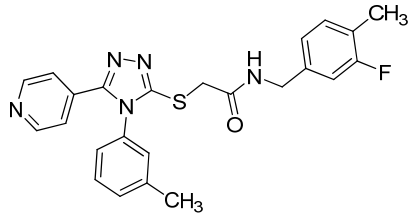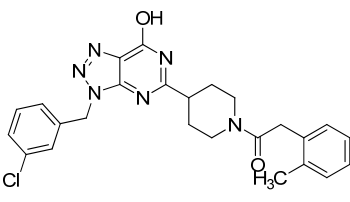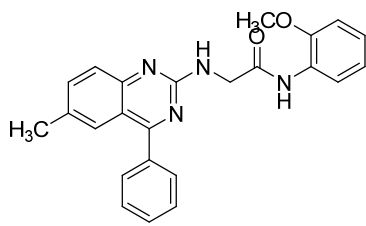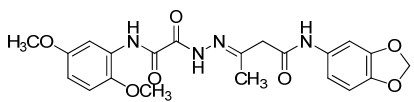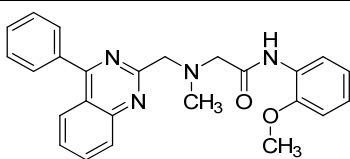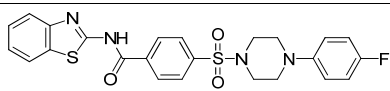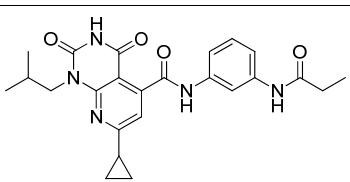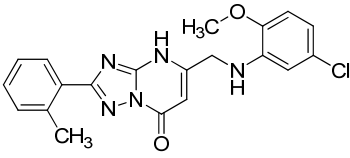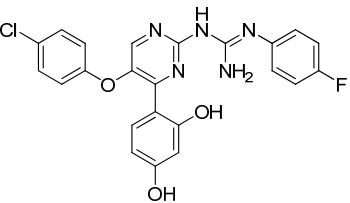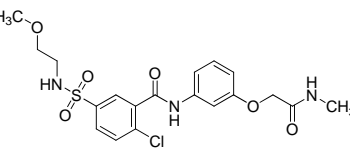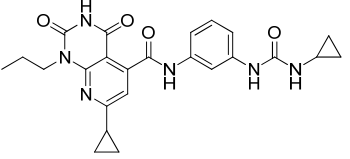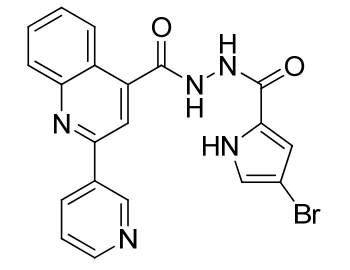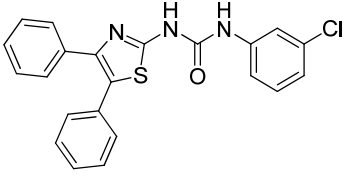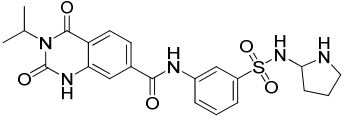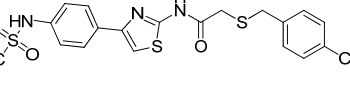
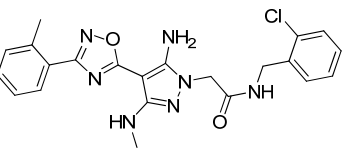| No.	Label (database)	Structure	Calculated ΔG (kcal mol^{-1})
55	ZINC24550703		-40.74
56	ZINC20516669		-40.6
57	ZINC09783203		-40.52
58	ZINC01658472		-40.42
59	ZINC29829567		-40.41
60	ZINC14678888		-40.3
61	ZINC16616335		-40.21
62	ZINC09042379		-40.09
63	ZINC09815687		-40.07
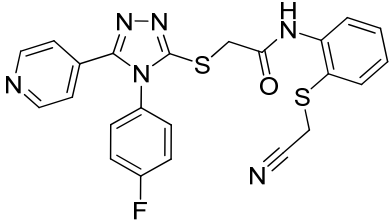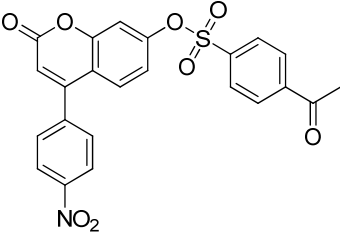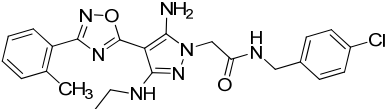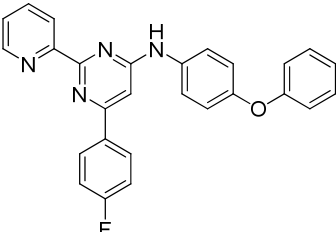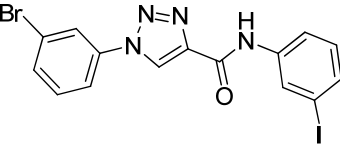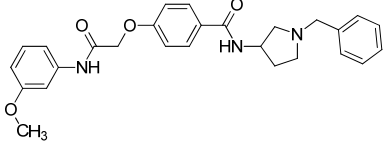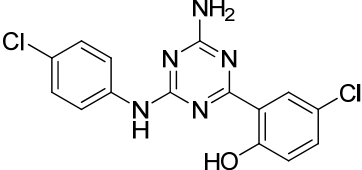
No.	Label (database)	Structure	Calculated ΔG (kcal mol⁻¹)
64	ZINC02597668		-40
65	ZINC14513790		-39.96
66	ZINC00950277		-39.92
67	ZINC14501364		-39.82
68	ZINC08594547		-39.8
69	ZINC10993449		-39.75
70	ZINC21178116		-39.73
71	ZINC30937420		-39.72
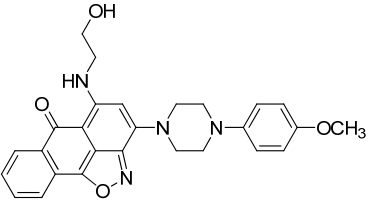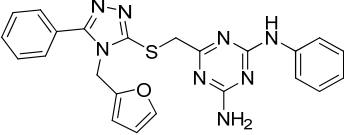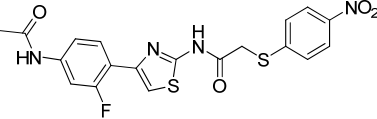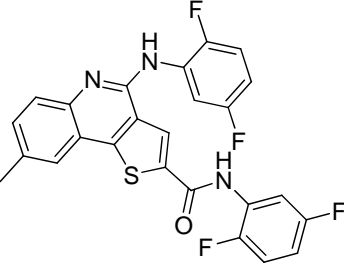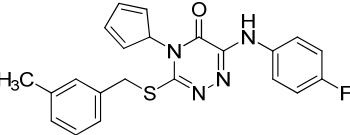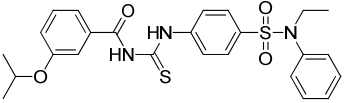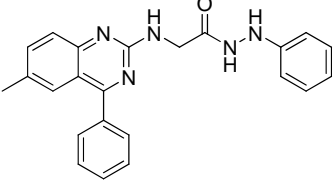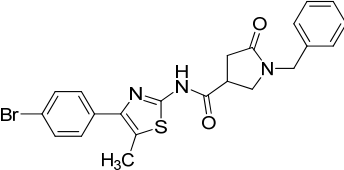
No.	Label (database)	Structure	Calculated ΔG (kcal mol⁻¹)
72	ZINC00959966		-39.69
73	ZINC32038892		-39.62
74	ZINC09015227		-39.61
75	ZINC08818322		-39.45
76	ZINC20797946		-39.44
77	ZINC17369473		-39.25
78	ZINC02637385		-39.25
79	ZINC15013181		-39.24

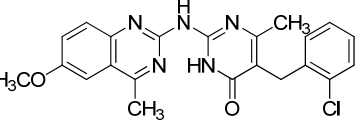| No.	Label (database)	Structure	Calculated ΔG (kcal mol^{-1})
80	ZINC23915434		-39.2
81	ZINC14841883		-39.16
82	ZINC00847492		-39.13
83	ZINC14925328		-39.1
84	ZINC26313320		-39.08
85	ZINC31814805		-39.08
86	ZINC01286096		-39.08
87	ZINC25665181		-39.05
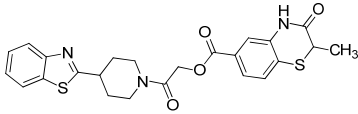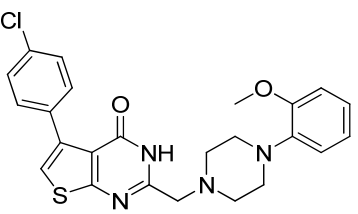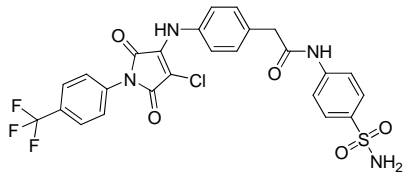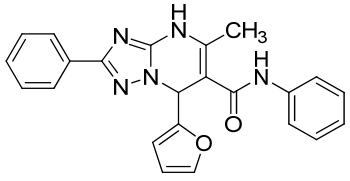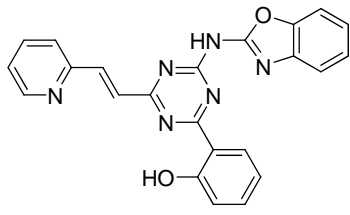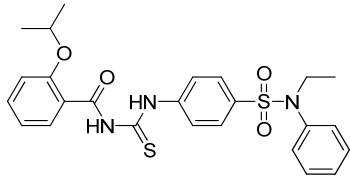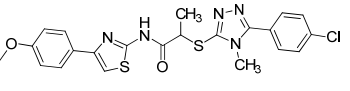
No.	Label (database)	Structure	Calculated ΔG (kcal mol^{-1})
88	ZINC26968634		-39.03
89	ZINC09803986		-38.85
90	ZINC21178177		-38.83
91	ZINC06521731		-38.81
92	ZINC08742739		-38.77
93	ZINC30961068		-38.75
94	ZINC20836919		-38.74
95	ZINC30229204		-38.74
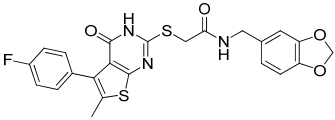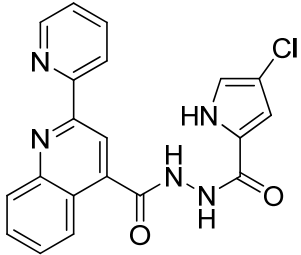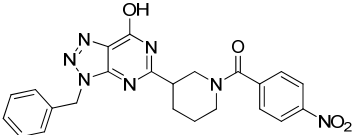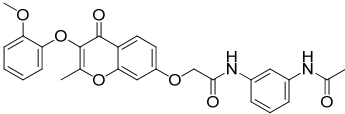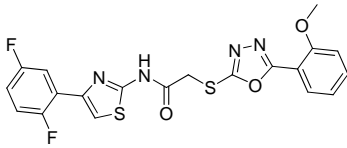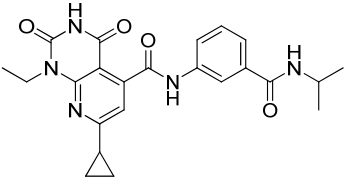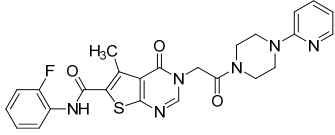
No.	Label (database)	Structure	Calculated ΔG (kcal mol^{-1})
96	ZINC14609132		-38.73
97	ZINC16050904		-38.71
98	ZINC31520683		-38.64
99	ZINC24440438		-38.6
100	ZINC23914775		-38.59
101	ZINC06530238		-38.59
102	ZINC32035556		-38.5
103	ZINC22064545		-38.45
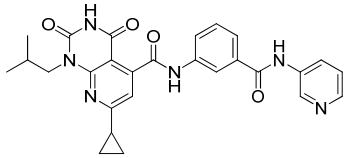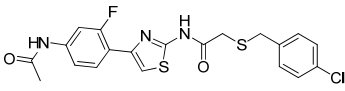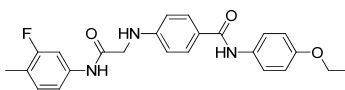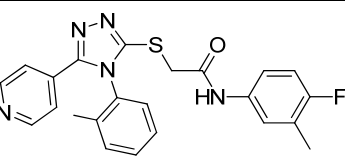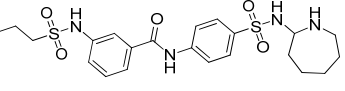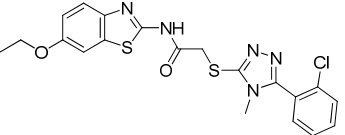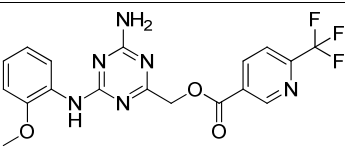
No.	Label (database)	Structure	Calculated ΔG (kcal mol^{-1})
104	ZINC23552498		-38.45
105	ZINC21820882		-38.35
106	ZINC23125426		-38.23
107	ZINC01738880		-38.22
108	ZINC31874383		-38.12
109	ZINC09315632		-38.05
110	ZINC00347213		-37.97
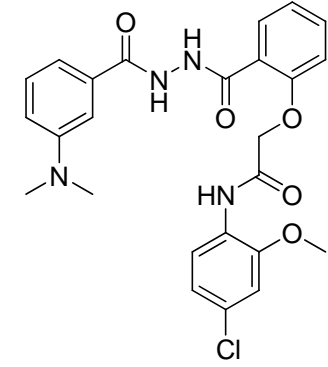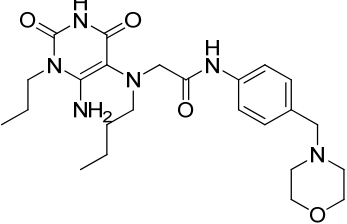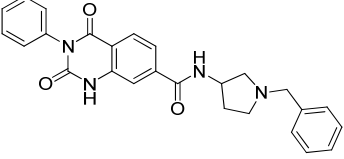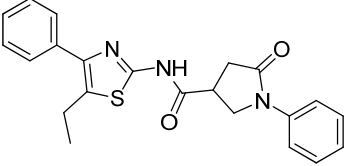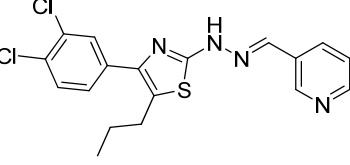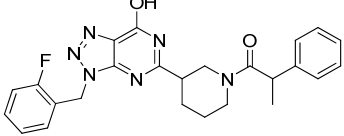
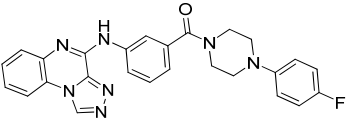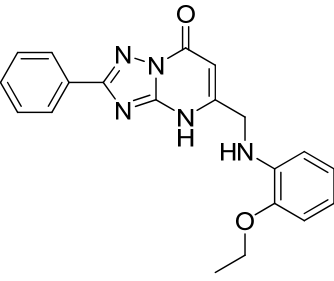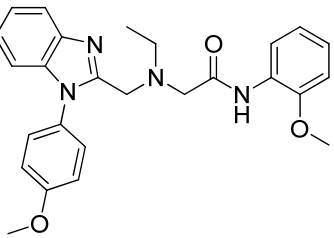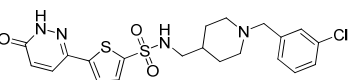| No.	Label (database)	Structure	Calculated ΔG (kcal mol^{-1})
111	ZINC09612275		-37.96
112	ZINC20056909		-37.91
113	ZINC10966899		-37.91
114	ZINC09860192		-37.85
115	ZINC28535105		-37.83
116	ZINC10122440		-37.77
117	ZINC06521579		-37.75
118	ZINC15326775		-37.69
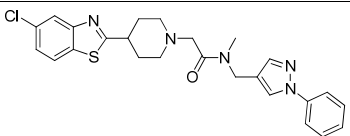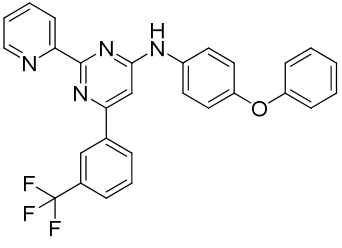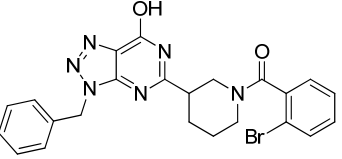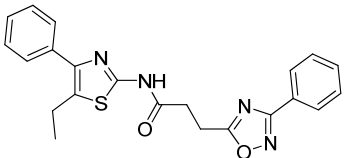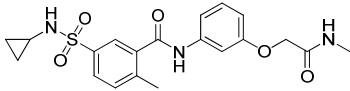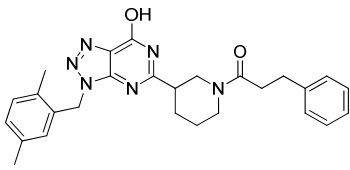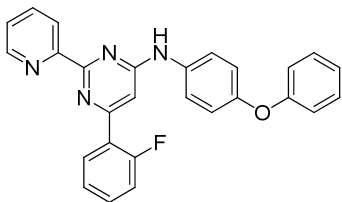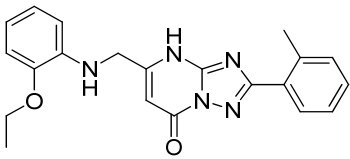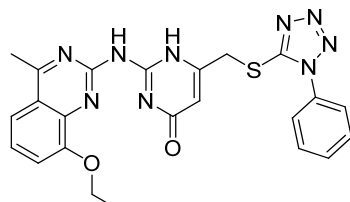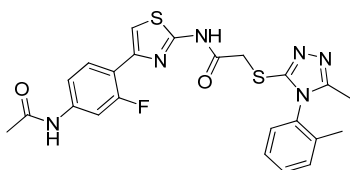
No.	Label (database)	Structure	Calculated ΔG (kcal mol^{-1})
119	ZINC27250419		-37.56
120	ZINC09245384		-37.55
121	ZINC01286080		-37.53
122	ZINC04965961		-37.52
123	ZINC22744976		-37.51
124	ZINC08036230		-37.48
125	ZINC14664367		-37.47
126	ZINC21761149		-37.45
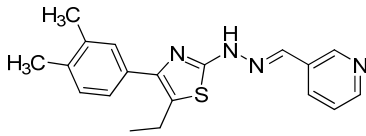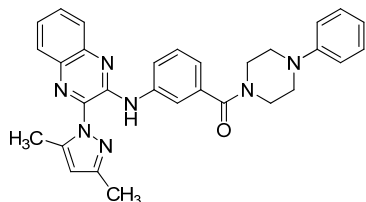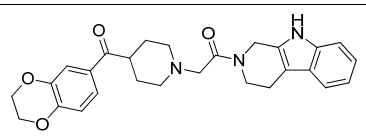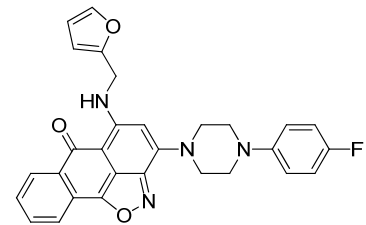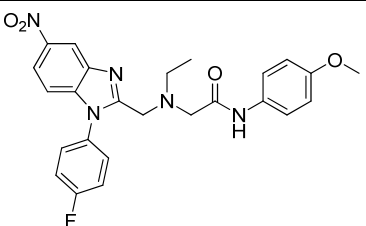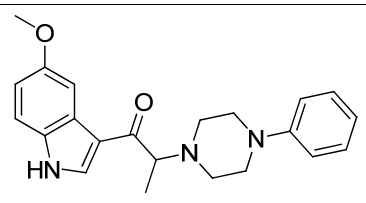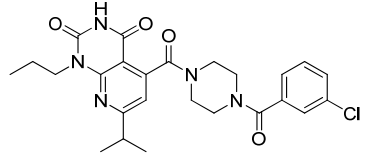
No.	Label (database)	Structure	Calculated ΔG (kcal mol^{-1})
127	ZINC17206984		-37.45
128	ZINC26644586		-37.42
129	ZINC01335030		-37.41
130	ZINC09485425		-37.38
131	ZINC28534995		-37.38
132	ZINC23648614		-37.33
133	ZINC27734839		-37.33
134	ZINC09495232		-37.23
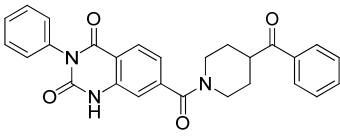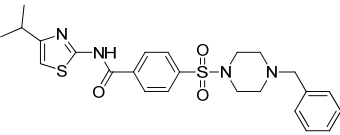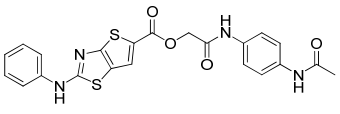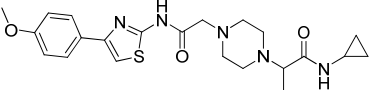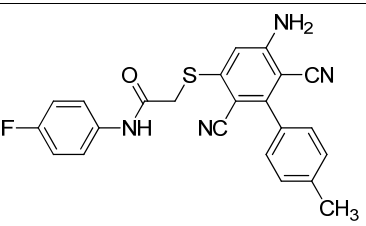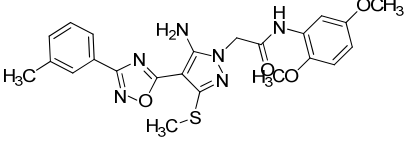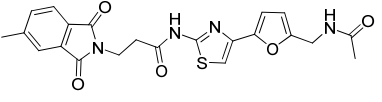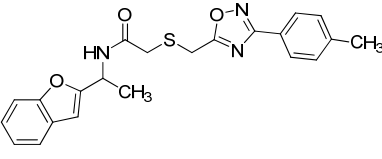
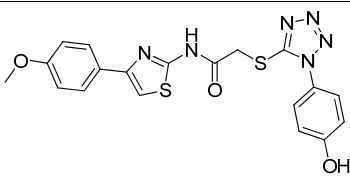| No.	Label (database)	Structure	Calculated ΔG (kcal mol^{-1})
135	ZINC24910688		-37.21
136	ZINC10993454		-37.13
137	ZINC07973781		-37.12
138	ZINC23338470		-37.12
139	ZINC23125406		-37.12
140	ZINC29816970		-37.05
141	ZINC09809482		-37.04
142	ZINC26436832		-37.04

No.	Label (database)	Structure	Calculated ΔG (kcal mol^{-1})
143	ZINC17405915		-37
144	ZINC22993850		-36.95
145	ZINC16261388		-36.85
146	ZINC08990933		-36.81
147	ZINC08216589		-36.8
148	ZINC04893261		-36.78
149	ZINC09202264		-36.75
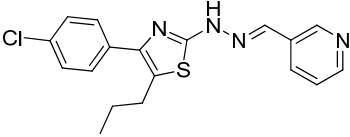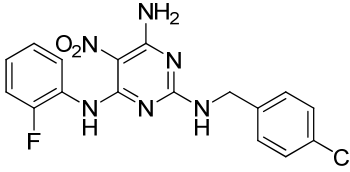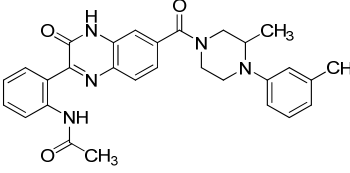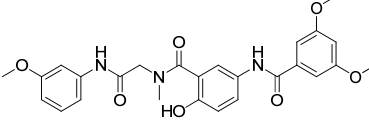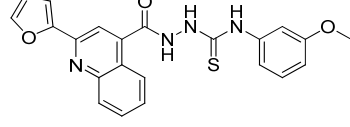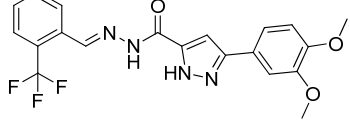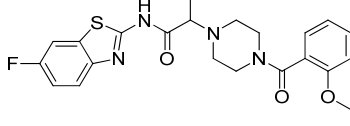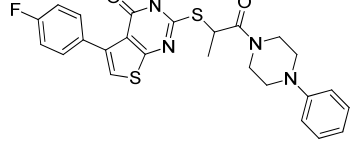
No.	Label (database)	Structure	Calculated ΔG (kcal mol^{-1})
150	ZINC09561308		-36.75
151	ZINC14608989		-36.66
152	ZINC30961071		-36.62
153	ZINC20985033		-36.55
154	ZINC25037102		-36.54
155	ZINC01739419		-36.51
156	ZINC01335000		-36.5
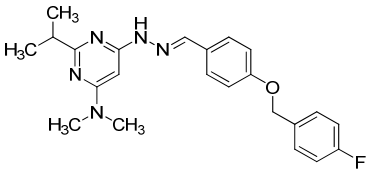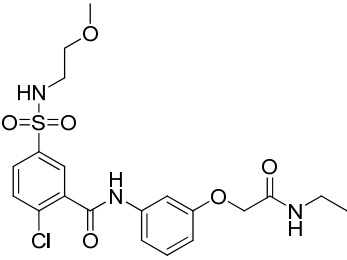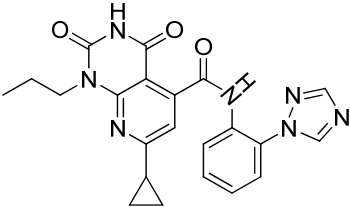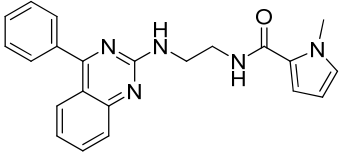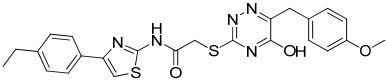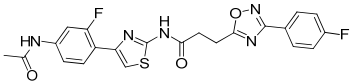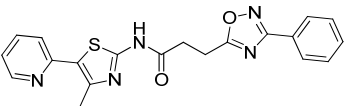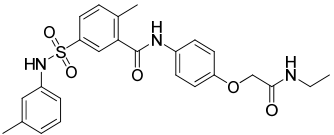
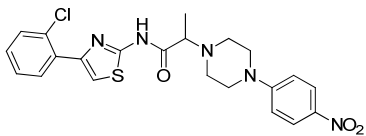| No.	Label (database)	Structure	Calculated ΔG (kcal mol^{-1})
157	ZINC21029375		-36.5
158	ZINC26974277		-36.43
159	ZINC01324552		-36.39
160	ZINC01739098		-36.39
161	ZINC28802383		-36.38
162	ZINC14609153		-36.38
163	ZINC20798076		-36.37
164	ZINC22356852		-36.37
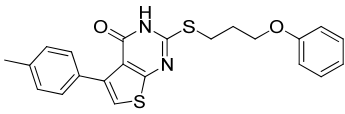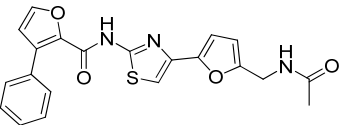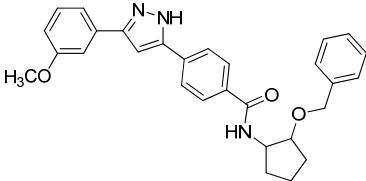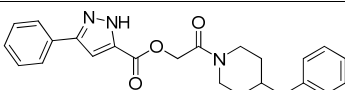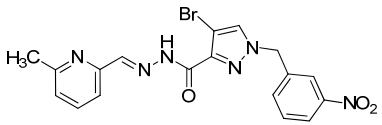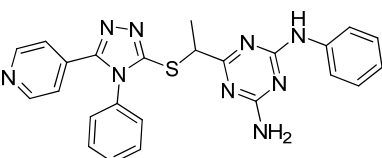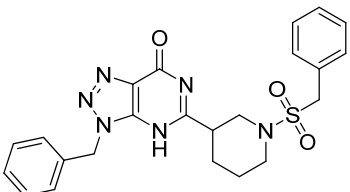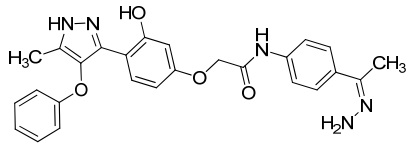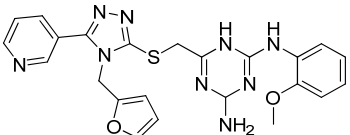
No.	Label (database)	Structure	Calculated ΔG (kcal mol^{-1})
165	ZINC05952274		-36.31
166	ZINC09561330		-36.29
167	ZINC25153213		-36.28
168	ZINC09612289		-36.24
169	ZINC25555969		-36.2
170	ZINC30221512		-36.14
171	ZINC02304062		-36.13
172	ZINC29793849		-36.12
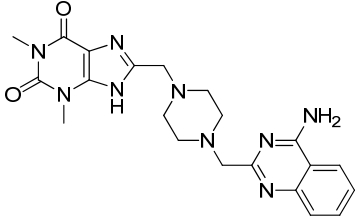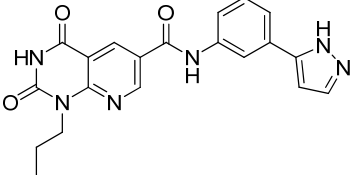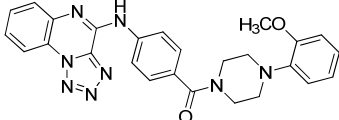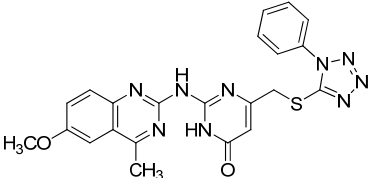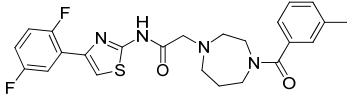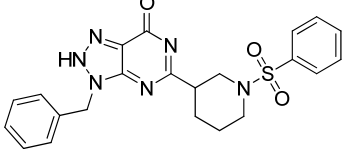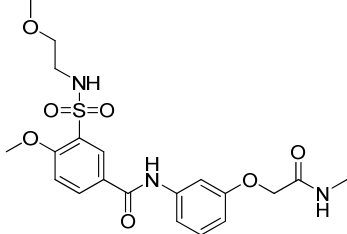
No.	Label (database)	Structure	Calculated ΔG (kcal mol^{-1})
173	ZINC10820133		-36.12
174	ZINC29776070		-36.08
175	ZINC10712138		-36.06
176	ZINC22194827		-36.05
177	ZINC20348532		-36.04
178	ZINC23816488		-36.04
179	ZINC16840416		-36.03
180	ZINC12052640		-35.96
181	ZINC28909077		-35.95
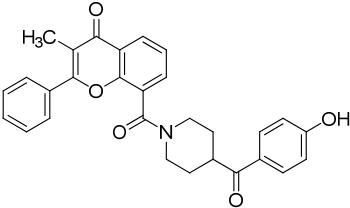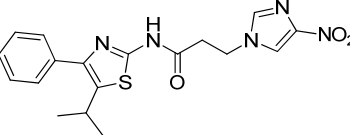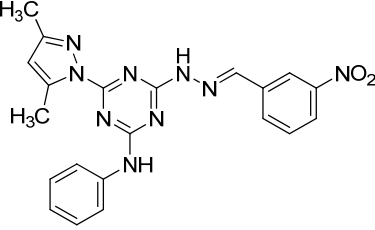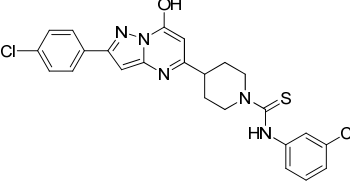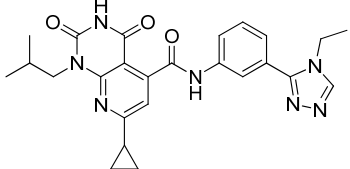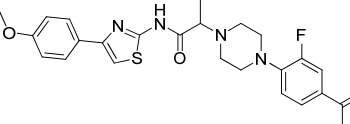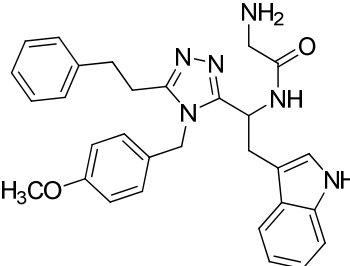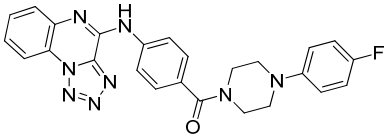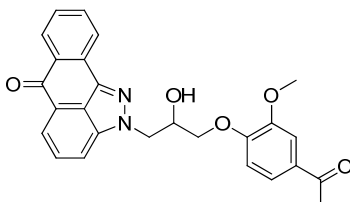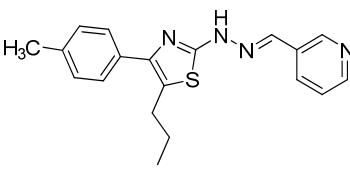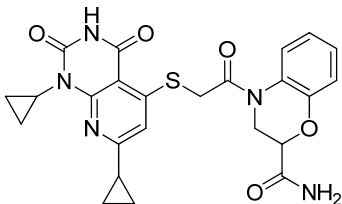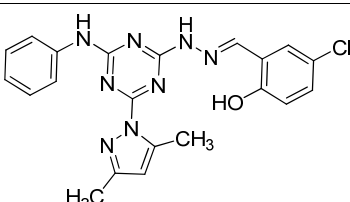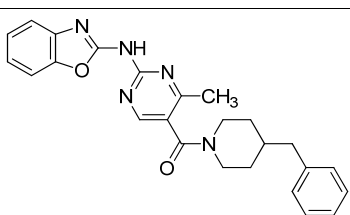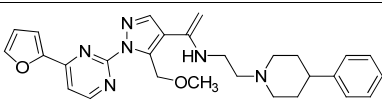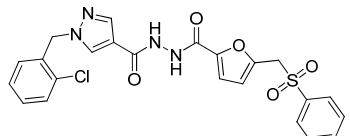
No.	Label (database)	Structure	Calculated ΔG (kcal mol^{-1})
182	ZINC19894522		-35.92
183	ZINC05164532		-35.92
184	ZINC09833481		-35.9
185	ZINC30040786		-35.9
186	ZINC16273672		-35.87
187	ZINC25154639		-35.86
188	ZINC05352217		-35.85
189	ZINC26619133		-35.84
190	ZINC20993997		-35.82
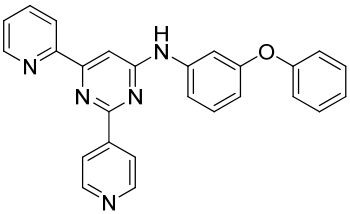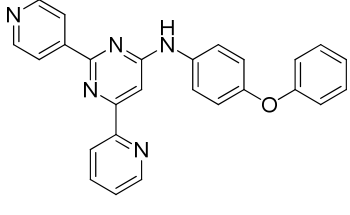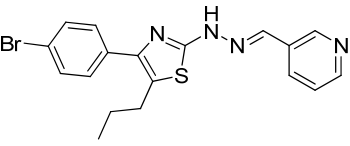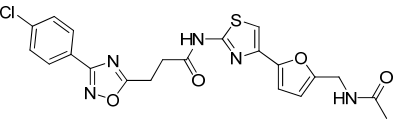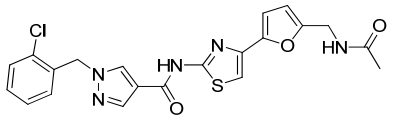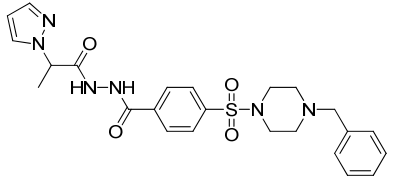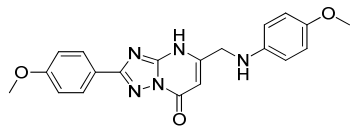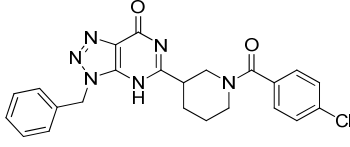
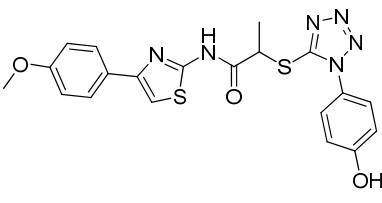| No.	Label (database)	Structure	Calculated ΔG (kcal mol^{-1})
191	ZINC04547220		-35.81
192	ZINC31814724		-35.77
193	ZINC25006029		-35.71
194	ZINC30676510		-35.68
195	ZINC22854665		-35.64
196	ZINC29941784		-35.61
197	ZINC10994911		-35.61
198	ZINC24031981		-35.6
199	ZINC27511105		-35.6

No.	Label (database)	Structure	Calculated ΔG (kcal mol^{-1})
200	ZINC02613835		-35.56
201	ZINC28729475		-35.54
202	ZINC23454553		-35.54
203	ZINC07027790		-35.53
204	ZINC01091988		-35.52
205	ZINC24968081		-35.52
206	ZINC06161937		-35.51
207	ZINC13721980		-35.5
208	ZINC16252120		-35.44

No.	Label (database)	Structure	Calculated ΔG (kcal mol^{-1})
209	ZINC25946503		-35.43
210	ZINC24891590		-35.36
211	ZINC08594299		-35.35
212	ZINC18266477		-35.35
213	ZINC29831247		-35.33
214	ZINC13116573		-35.33
215	ZINC26968816		-35.3
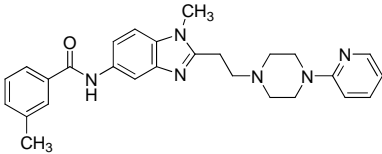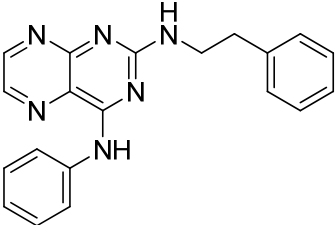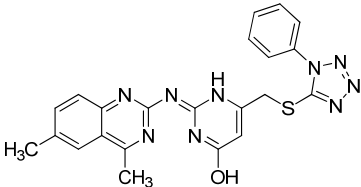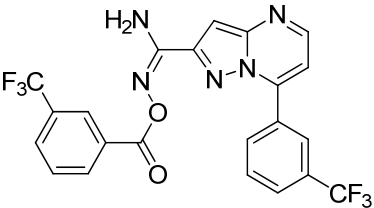
No.	Label (database)	Structure	Calculated ΔG (kcal mol^{-1})
216	ZINC25071443		-35.29
217	ZINC31777346		-35.29
218	ZINC27498172		-35.28
219	ZINC20213462		-35.26
220	ZINC25286251		-35.26
221	ZINC26909392		-35.25
222	ZINC14970387		-35.25

No.	Label (database)	Structure	Calculated ΔG (kcal mol^{-1})
223	ZINC08594336		-35.18
224	ZINC28917276		-35.18
225	ZINC18192515		-35.16
226	ZINC23564109		-35.13
227	ZINC15221705		-35.1
228	ZINC10157591		-35.09
229	ZINC15007420		-35.08
230	ZINC26907231		-35.07

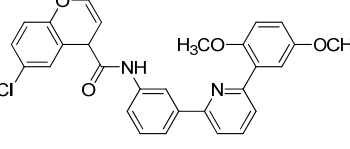| No.	Label (database)	Structure	Calculated ΔG (kcal mol^{-1})
231	ZINC29355832		-34.95
232	ZINC01497755		-34.93
233	ZINC18173244		-34.84
234	ZINC12053474		-34.82
235	ZINC22191077		-34.77
236	ZINC30562674		-34.69
237	ZINC14609075		-34.63
238	ZINC26416977		-34.62

No.	Label (database)	Structure	Calculated ΔG (kcal mol^{-1})
239	ZINC16260073		-34.52
240	ZINC09986460		-34.44
241	ZINC21178111		-34.4
242	ZINC06771826		-34.36
243	ZINC18407299		-34.35
244	ZINC24967091		-34.23
245	ZINC29596632		-34.15
246	ZINC21882860		-34.09

No.	Label (database)	Structure	Calculated ΔG (kcal mol^{-1})
247	ZINC09487020		-34.05
248	ZINC09075197		-34.05
249	ZINC18249581		-34.00
250	ZINC12369177		-34.00

The final candidate compounds were selected based on free energy of binding (ΔG). Subsequently, the top 250 solutions were inspected carefully considering the agreement of their predicted ligand-stabilized receptor conformations with the inactive state of the A$_{2B}$ receptor model (as described in chapter **3**). This resulted in a final set of 250 diverse drugs-like or lead-like compounds. As shown in Table **4.1**, the top 250 ligands which were obtained from virtual screening using FlexX program had energy scores are ranging from -96.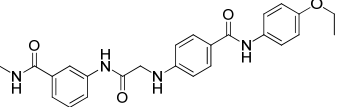36 to -34.00 kcal/mol as computed with the MMGBSA method on the basis of MD simulations. In addition, figures **4.2, 4.3, 4.4, 4.5, 4.6, 4.7 and 4.8** illustrate predicted A$_{2B}$ binding poses of selected candidate compounds representing different chemical scaffolds.
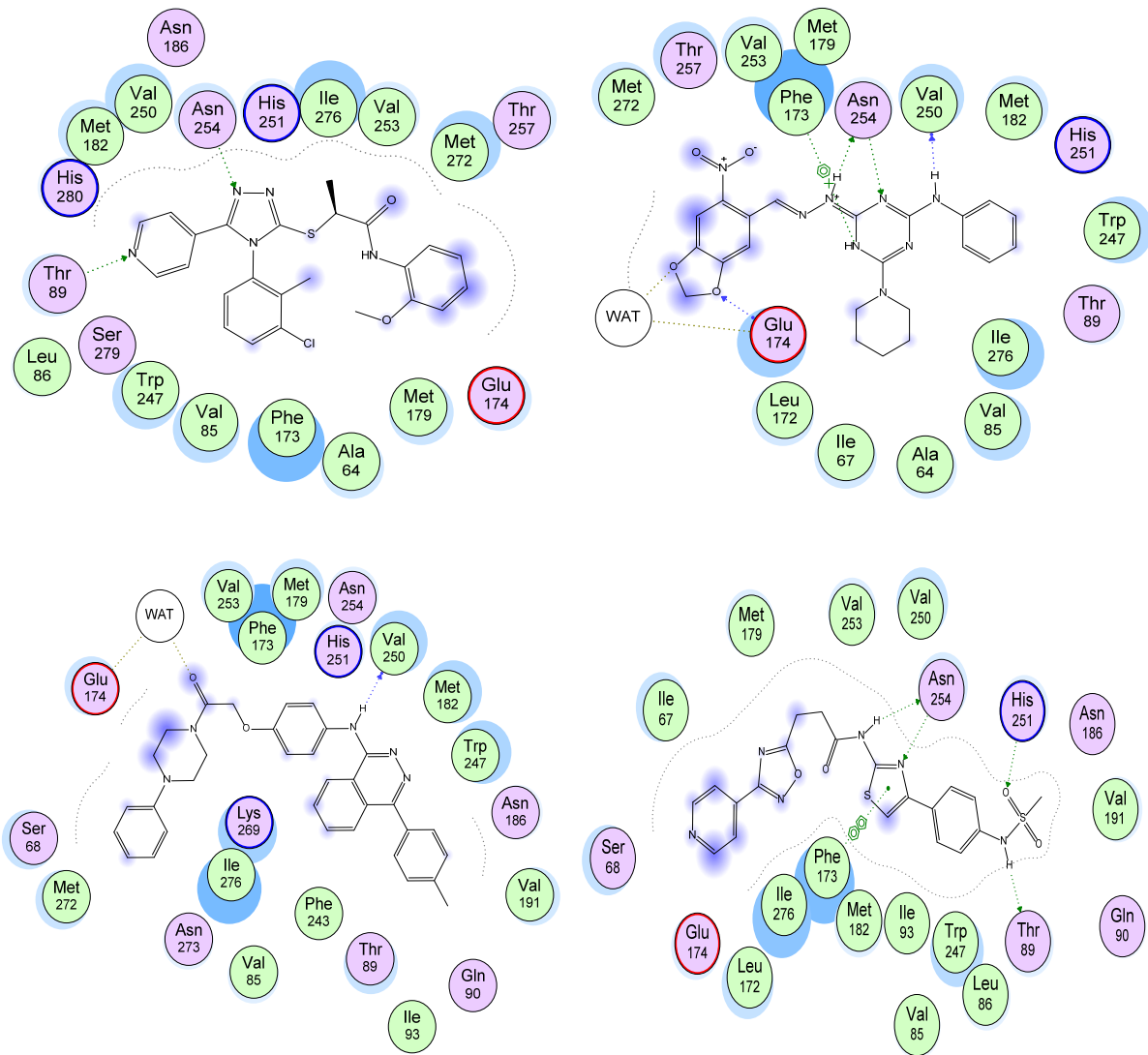
Figure 4.2 Predicted binding modes for **No. 2** (top left), **No. 5** (top right), **No. 6** (bottom left) and **No. 7** (bottom right) in the A$_{2B}$ receptor model. Shown are the hydrogen bonds and aromatic stacking interactions
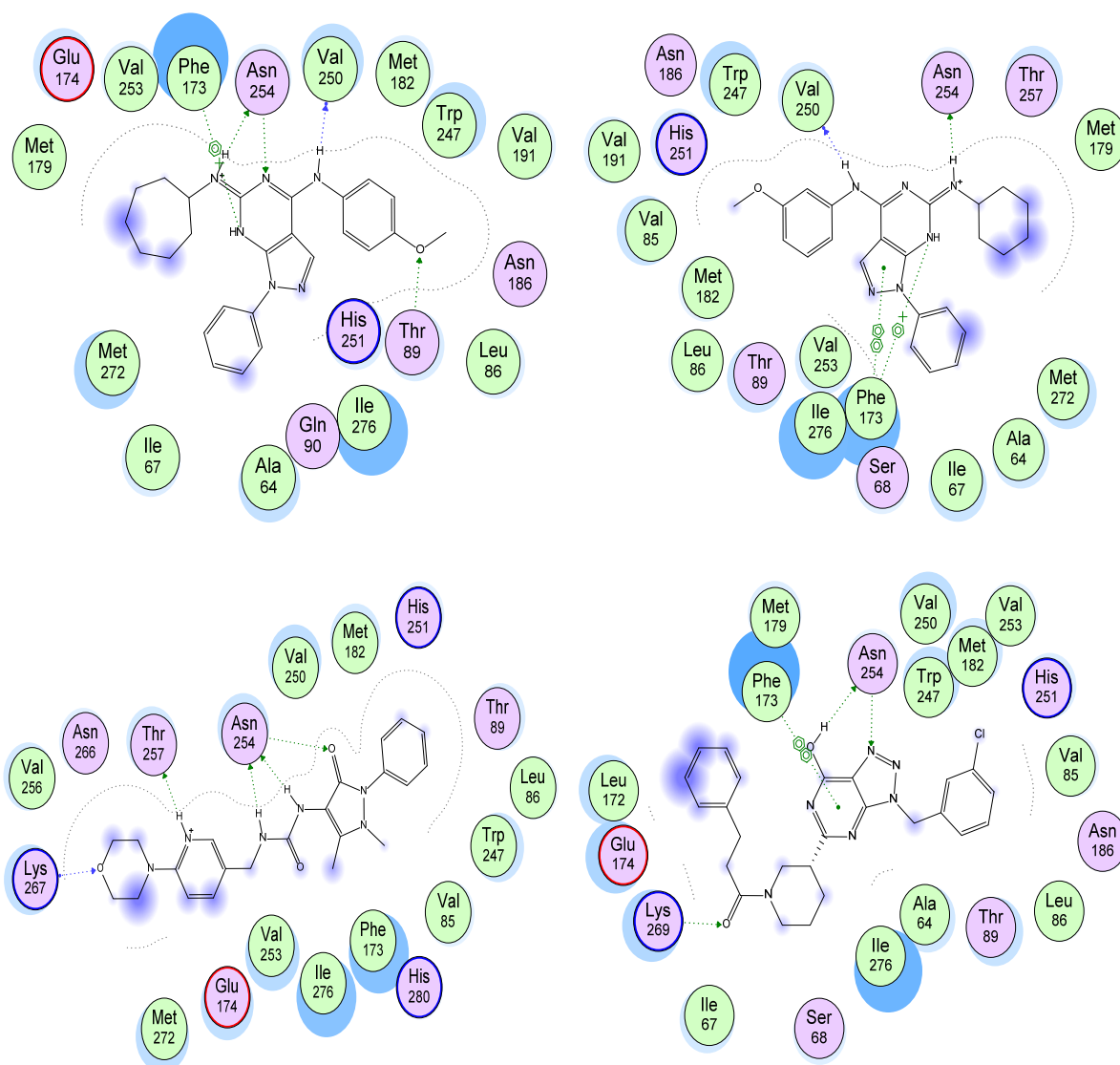
Figure 4.3 Predicted binding modes for **No. 9** (top left), **No. 15** (top right), **No. 17** (bottom left) and **No. 23** (bottom right) in the A$_{2B}$ receptor model. Shown are the hydrogen bonds and aromatic stacking interactions
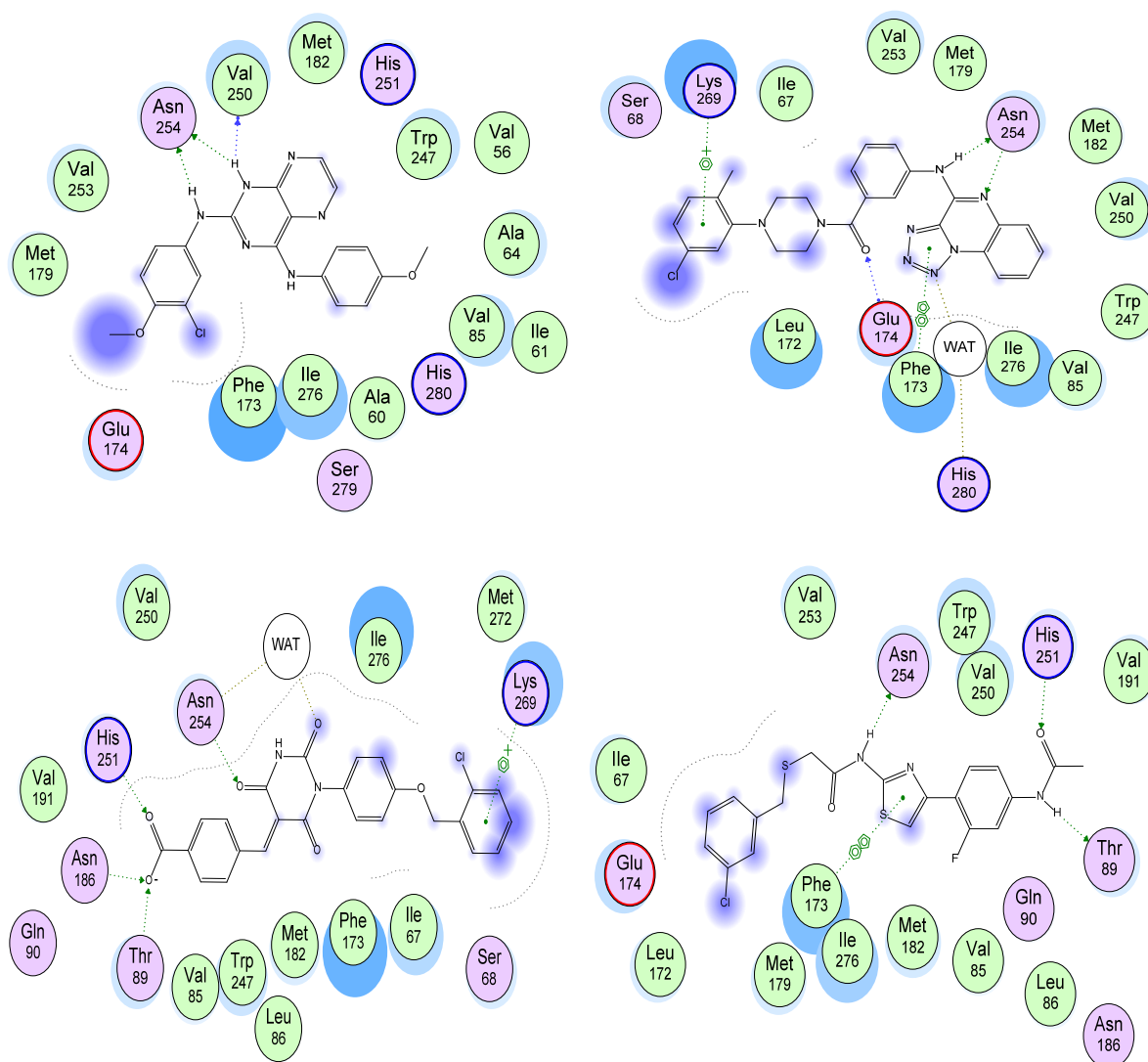
Figure 4.4 Predicted binding modes for **No. 24** (top left), **No. 26** (top right), **No. 31** (bottom left) and **No. 33** (bottom right) in the A$_{2B}$ receptor model. Shown are the hydrogen bonds, aromatic stacking and aromatic-cation interactions
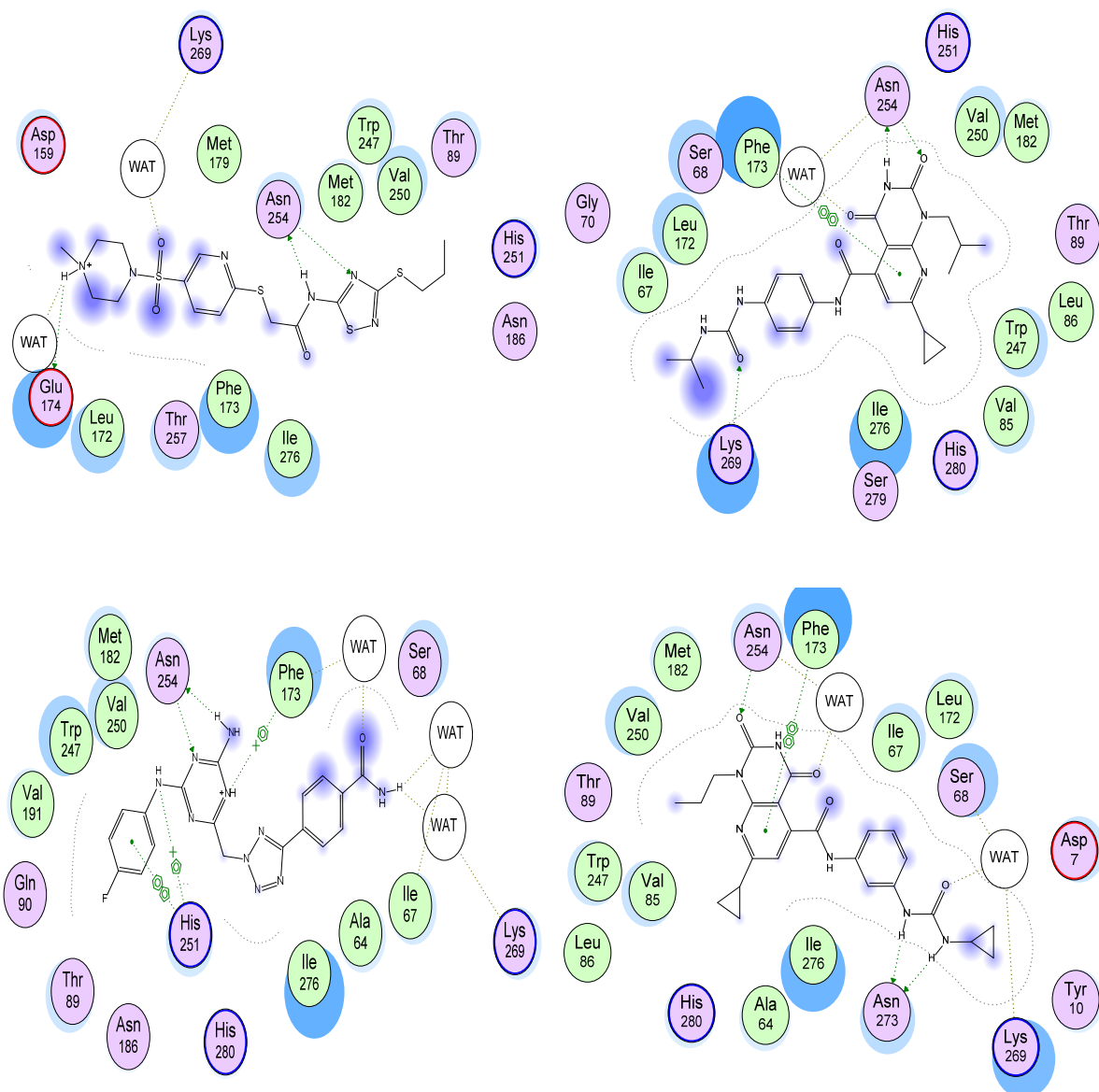
Figure 4.5 Predicted binding modes for **No. 34** (top left), **No. 40** (top right), **No. 41** (bottom left) and **No. 43** (bottom right) in the A_{2B} receptor model. Shown are the hydrogen bonds and aromatic stacking interactions
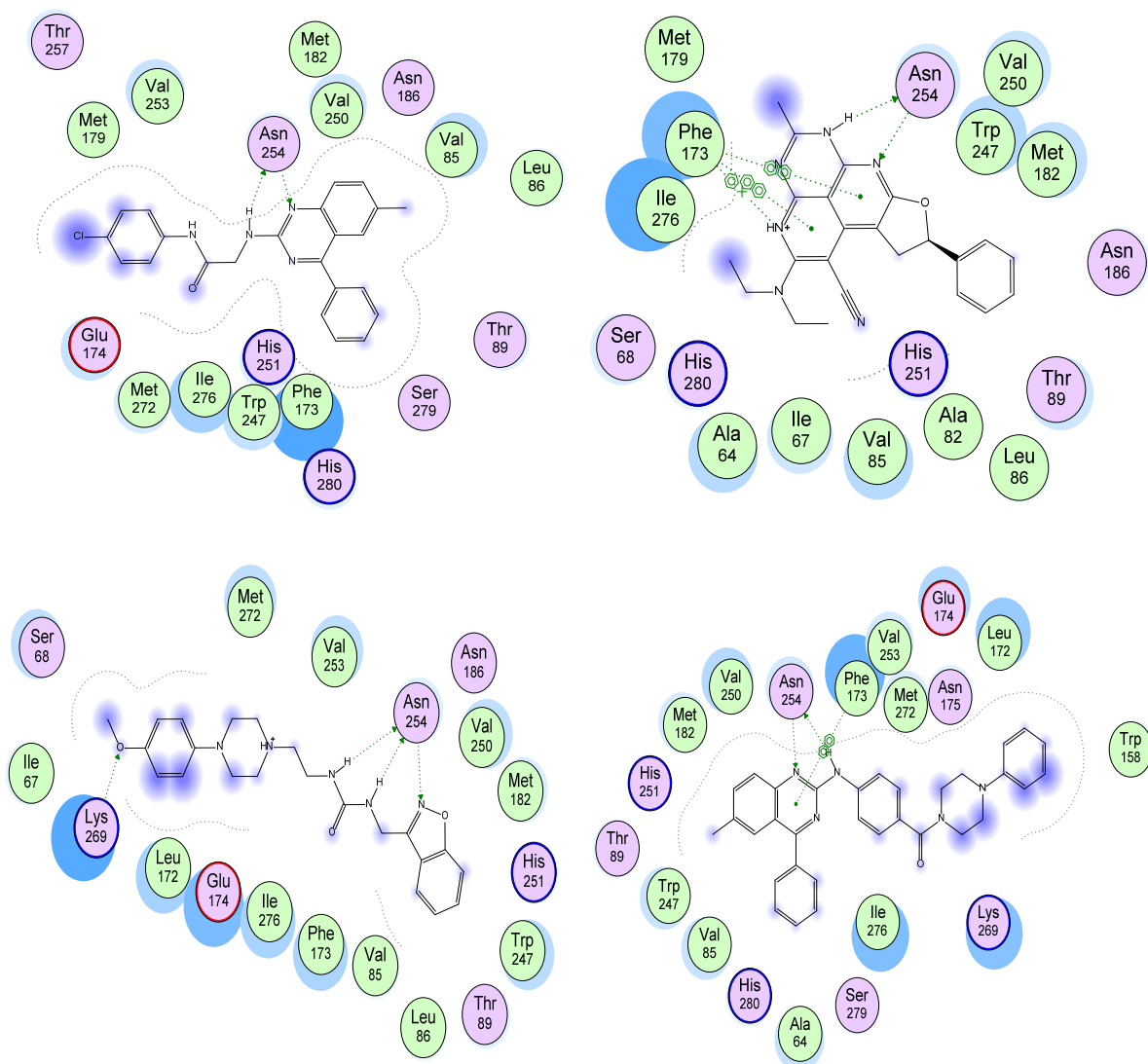
Figure 4.6 Predicted binding modes for **No. 47** (top left), **No. 48** (top right), **No. 56** (bottom left) and **No. 57** (bottom right) in the A$_{2B}$ receptor model. Shown are the hydrogen bonds and aromatic stacking interactions
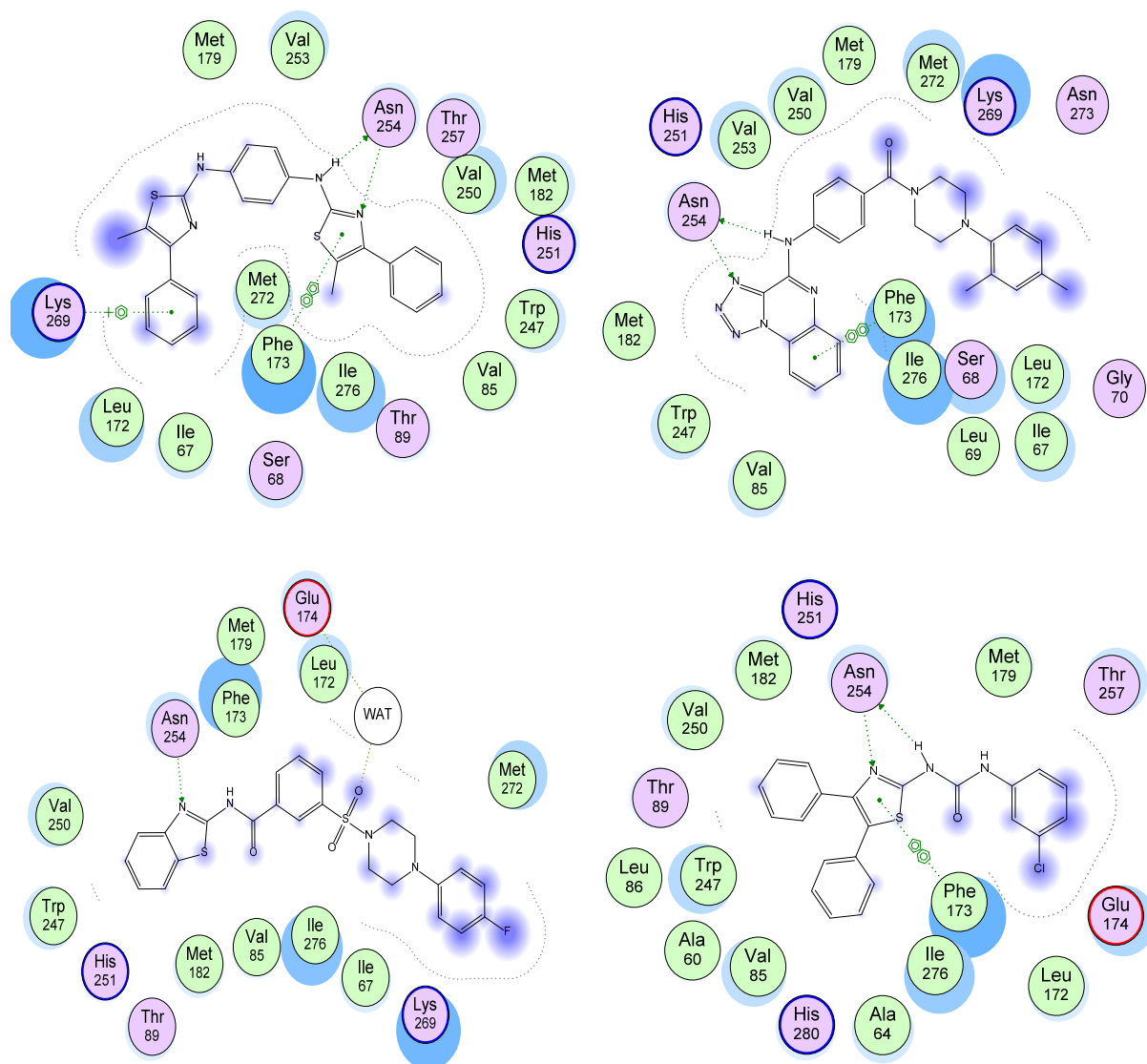
Figure 4.7 Predicted binding modes for **No. 58** (top left), **No. 68** (top right), **No. 94** (bottom left) and **No. 101** (bottom right) in the A$_{2B}$ receptor model. Shown are the hydrogen bonds, aromatic stacking and aromatic-cation interactions
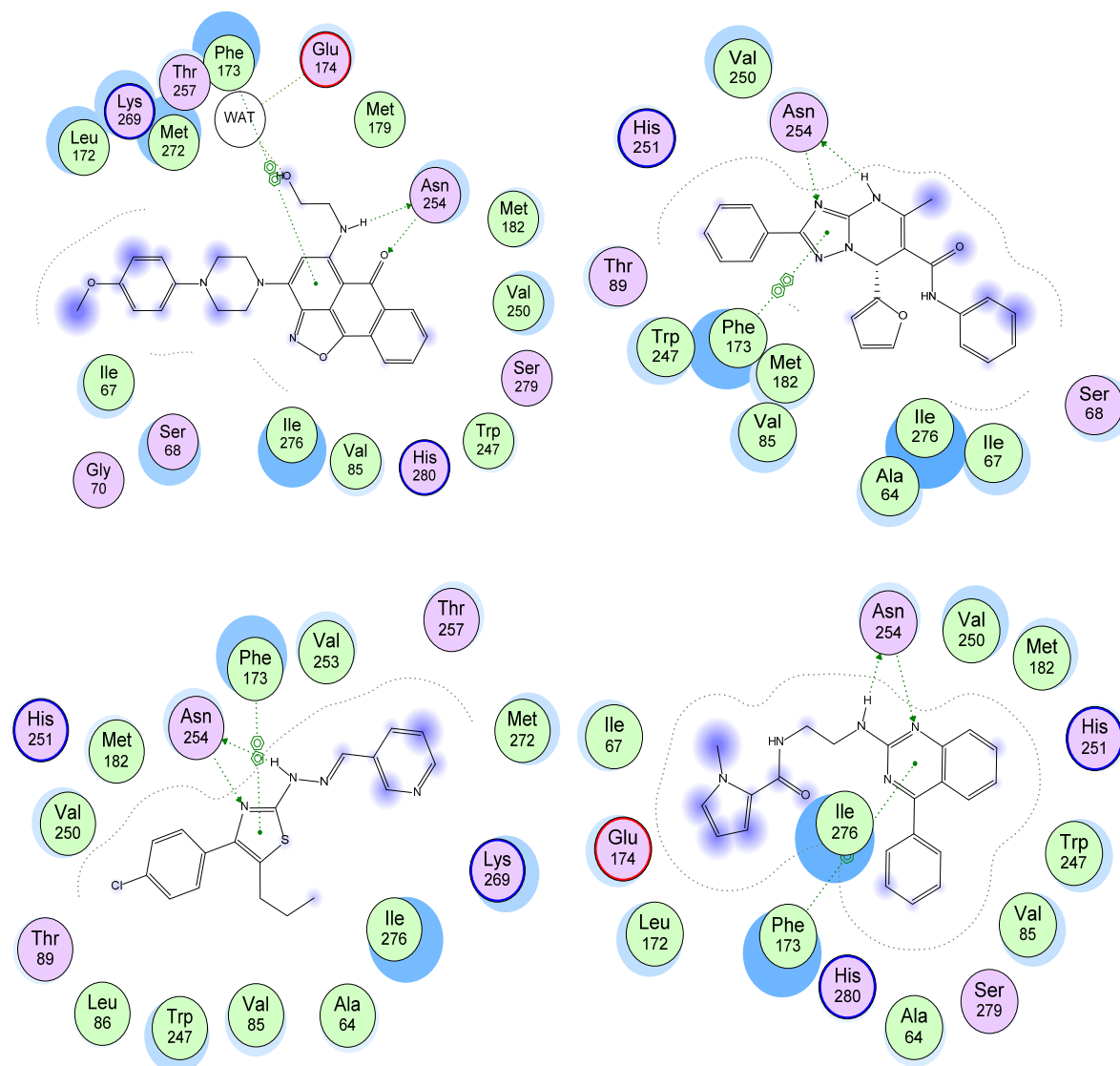
Figure 4.8 Predicted binding modes for **No. 111** (top left), **No. 122** (top right), **No. 182** (bottom left) and **No. 194** (bottom right) in the A$_{2B}$ receptor model. Shown are the hydrogen bonds and aromatic stacking interactions

All candidates were predicted to share most of the key features with the reference antagonists binding in the A$_{2B}$ structure, including an aromatic stacking interaction with the Phe173 side-chain, hydrophobic interactions with Leu86, His251, Val85, Val250, Met272, Ile276, Met182 and Trp247 and hydrogen bonding interactions with Asn254 and Glu174 side-chains. Most compounds have an additional interaction, forming a hydrogen bonding interaction to Asn254 in the A$_{2B}$ model. The docking analysis of the candidates using different scaffolds showed similar binding mode patterns.

In addition, the results of the virtual screening showed that the reference ligands were included in the top ranked database. Therefore, our in silico screening protocol not only regained the active ligands but also recovered other kinds of active antagonists for example **No. 4** XAC (xanthine amine congener) with a K_i value of 16 nM [171]. Furthermore, the screening approaches used in the current study were not screened A_{2B} agonists with our structure-based A_{2B} antagonist virtual screening protocol. This ensured the reliability of our established method. Thus, the generated A_{2B} homology model-based virtual screening protocol can be applied to efficiently retrieve different kinds of A_{2B}-antagonists, including novel scaffolds. However, such finding would require experimental analysis to confirm the results.

4.4 Conclusion

Homology modeling has significant potential as a tool in rational drug design, in particular in high throughput in silico screening. The present project was aimed at finding novel drug-like antagonists for the adenosine A_{2B} receptor. The X-ray structure of the adenosine A_{2B} receptor is still not generated, for this the X-ray crystal structure of the closely related adenosine A_{2A} receptor was considered as a template. In this study, we assessed the performance of the adenosine A_{2B} receptor homology model in a structure-based antagonist virtual screening study, which resulted in identification of several novel ligands for the adenosine A_{2B} receptors having better energy scores using combined ligand-based approach (FTrees), flexible docking, MD simulations and MM-GBSA approaches as well as a database of commercially available chemical entities. Using binary ligand-receptor fingerprints, virtual screening could significantly be improved. 3D structures of the top 250 ligand molecules were visualized and it was found that these ligands or drug-like molecules are docked in the same active site similar to the reference ligands and can be fitted into the cavity of the receptor. Therefore, these ligands may act as potent and selective antagonists for the adenosine A_{2B} receptor, although their pharmacological properties need to be studied experimentally. Furthermore, the results show that the homology model, combined with accurate docking and virtual ligand screening methods provides a highly efficient tool for the potential identification of new GPCR antagonists as lead candidates for drug discovery.

5   Summary and Outlook

The adenosine A_{2B} receptor belongs to the class A of G protein-coupled receptors. It is playing a crucial role in cell signalling and various physiological responses. The adenosine A_{2B} receptor, a promising target in the challenge of improving human health, was and will be an important subject in the pharmacological research field. However, the X-ray structure of the adenosine A_{2B} receptor has still not yet been resolved. Therefore, variants of a 3D homology model of the adenosine A_{2B} receptor were generated using the crystal structures of the three related GPCRs (bovine rhodopsin, the β_2-adrenergic receptor and the adenosine A_{2B} receptor) as templates in order to proceed with looking into binding behaviour of antagonists and agonists by computational methods.

In detail, a comparison of the three models revealed a great deal of similarities among them and yielded concordant binding modes, which overlap significantly with the location of the binding site found in the adenosine A_{2B} receptor. For further studies we chose the A_{2A}-based model which is the one with the highest sequence identity (56%), the lowest rmsd value, and the most favourable gap ratio. The obtained results for the A_{2B} receptor were in accordance with experimental data. This suggests that the 3D structure predicted by the homology method is sufficiently accurate for use in further studies.

The novel A_{2B} structural model furthers our understanding of the adenosine A_{2B} receptor by analyzing complexes with a series of adenosine A_{2B} receptor antagonists and agonists using molecular modelling techniques. The homology model of the A_{2B} receptor was used to explore the molecular basis for the affinity and selectivity of these ligands. The emerging predictions provided a basis for subsequent experimental molecular pharmacological studies.

In particular, the results provide valuable information concerning the optimal structural requirements for selective antagonist and agonist recognition by the human adenosine A_{2B} receptor. Most of the amino acid residues covering the putative binding sites are conserved among the four adenosine receptor subtypes. Asn254, His280, Trp247, Leu86, and Ile276, which are common to all subtypes, are believed to play an important role in the binding of both agonists and antagonists. In order to design new receptor subtype-selective ligands, we need to target the non-conserved amino acid residues that point to the center of the trans-

membrane part according to the present study, namely as Asn273, Leu81, Lys170, Val256, Ala271, Asn266, Lys269, Lys267 and Val250.

In this context, the protein modelling methodologies introduced and applied in this thesis provide a novel A_{2B} structural model that is capable of assisting in the development of structural hypotheses on ligand-receptor complexes. As such it provides a structural framework not only for a more detailed insight into ligand-GPCR interaction, but also for guiding the design process towards next-generation compounds, which should display enhanced affinity. Also, this work shows the power of molecular modelling in modern macromolecular, as well as small molecule, research projects.

By using the new A_{2B} structural model by the research described in this thesis, new insights were gained concerning conformational changes induced by agonists. An improved knowledge of the binding modes of A_{2B} antagonists and agonists may facilitate the development of more potent and selective derivatives. The adenosine A_{2B} receptor model was subjected to MD simulations both in complex with an antagonist and in complex with an agonist. A lipid bilayer and water molecules were added to realistically simulate the membrane environment of the receptor. The formation and deletion of intermolecular interactions were dependent on the presence of antagonist or agonist in the binding pocket which was proposed to represent perturbations that are necessary for the transition from an inactive towards an active receptor state. The results from simulations help on further refining the binding mode of the A_{2B} complex models. In particular, the analysis of the putative receptor-ligand interactions has shown that part of the highly conserved (D/E)RY motif, changes in the NPxxY(x)5,6F motif, separation of the intracellular sides of TM3 and TM6 as well as conformational changes in the extracellular loops are suggested to form the activation mechanism for the A_{2B} receptor. Our results also demonstrated a critical role for Glu14 and Asn25 in TM1, Asp53 in TM2, Arg103 in TM3, Glu229 and Trp247 in TM6, and His280, Asn282, Asn286 and Tyr290 in TM7 as anchor sites in agonist binding and receptor activation. Moreover, results from this study are not restricted to the adenosine receptors but may also apply to other members of G protein-coupled receptor family.

The goal of this work was aimed at finding novel potent antagonists for the adenosine A_{2B} receptor using structure-based drug design which may be targeted in virtual screening experiments. In this study, we assessed the performance of the adenosine A_{2B} receptor

homology model in structure-based antagonist virtual screening by using combined ligand-based approach (FTrees), flexible docking, MD simulations and MM-GBSA approaches as well as database of commercially available chemical moieties. In addition, using binary ligand-receptor fingerprints, virtual screening could significantly be improved.

Thus chapter 4 of this thesis describes the procedure used for finding novel ligands with different scaffolds having better energy scores using the FlexX program and a database of commercially available chemical entities. In fact, promising as well as known reference compounds were identified. Therefore, these ligands may act as potent and selective antagonists for the adenosine A_{2B} receptor, although their pharmacological properties need to be studied experimentally. Furthermore, the results show that the homology model, combined with accurate docking and virtual ligand screening methods provide a highly efficient tool for the identification of new GPCR antagonists as lead candidates for drug discovery. The overall study presented in this thesis is primarily aimed to deliver a feasibility study on generating model structures of GPCRs by a conceptual combination of tailor-made bioinformatics techniques with the toolbox of protein modelling.

Outlook

- Future work will focus on substructure-pharmacophore studies of the top-scored ligands which might help in building more specific and high affinity antagonists for the adenosine A_{2B} receptor

- Virtual screening of **agonists** for the adenosine A_{2B} receptor

- Studying models of homo- and heterodimers of the adenosine A_{2B} receptor model.

6   References

[1]   Lagerström, M. C.; Schiöth, H. B. Structural diversity of G protein-coupled receptor and significance for drug discovery. *Nat. Rev. Drug Discov*. **2008**, 7, 339-357.

[2]   Overington, J. P, Al-Lazikani, B, Hopkins, A. L. How many drug targets are there?. *Nature Rev. Drug Discov*. **2006**, *5*, 993-996.

[3]   Svoboda, P.; Teisinger, J.; Novotny, J.; Bourova, L.; Drmota, T.; Hejnova, L.; Moravcova, Z.; Lisy, V.; Rudajev, V.; Stöhr, J.; Vokurkova, A.; Svandova, I.; Durchankova, D. Biochemistry of transmembrane signalling mediated by trimeric G proteins. *Physiol. Res.* **2004**, *53*, S141-S152.

[4]   Lomize, A. L.; Pogozheva, I. D.; Mosberg, H. I. Structural organization of G-protein-coupled receptors. *Comput. Aided Mol. Des*. **1999**, *13*, 325-353.

[5]   Kristiansen, K. Molecular mechanisms of ligand binding, signalling, and regulation within the superfamily of G protein-coupled receptors: molecular modelling and mutagenesis approaches to receptor structure and function. *Pharm. Ther.* **2004**, *103*, 21-80.

[6]   Kolakowski, L. J. GCRDb: A G protein-coupled receptor database. *receptors & channels* **1994**, *2*, 1-7.

[7]   Milligan, G.; Kostenis, E. Heterotrimeric G-proteins: a short history. *Br. J. Phar.* **2006**, *147*, 46-55.

[8]   Fredholm, B. B.; Abbracchio, M. P.; Burnstock, G.; Dubyak, G. R.; Harden, T. K.; Jacobson, K. A.; Schwabe, U.; Williams, M. Towards a revised nomenclature for P1 and P2 receptors. *Trends in Pharmacol. Sci.* **1997**, *18*, 79-82.

[9]   Londos, C.; Cooper, D. M.; Wolff, J. Subclasses of external adenosine receptors Proceedings of *the National Academy of Sciences of USA*. **1980**, *77*, 2551-2554.

[10]   Fredholm, B. B.; IJzerman, A. P.; Jacobson, K. A.; Klotz, K-N.; Linden, J. International union of pharmacology. XXV. Nomenclature and classification of adenosine receptors. *Pharmacol. Rev*. **2001**, *53*, 527-552.

[11]   Müller, C. E.; Stein, B. Adenosine receptor antagonists: Structures and potential therapeutic applications. *Curr. Pharm. Des*. **1996**, *2*, 501-530.

[12]   Müller, C. E. Adenosine receptor ligands - recent developments part I. Agonists. *Curr. Med. Chem*. **2000**, *7*, 1269-1288.

[13] Grenz, A.; Osswald, H.; Eckle, T.; Yanq, D.; Zhang, H.; Tran, Z. V.; Klingel, K.; Ravid, K.; Eltzschig, H. K. The reno-vascular A$_{2B}$ adenosine receptor protects the kidney from ischemia. *PloS Med.* **2008**, 5, e137.

[14] Fredholm, B. B. Adenosine receptors as drug targets. *Exp. Cell Res.* **2010**, *316*, 1284-1288.

[15] Beukers, M. W.; Dulk, H. D.; Van Tilburg, E. W.; Brouwer, J.; Ijzerman, A. P. Why are A$_{2B}$ receptors low-affinity adenosine receptors? Mutation of Asn273 to Tyr increases affinity of human A$_{2B}$ receptor for 2- (1-hexynyl) adenosine. *Mol. Pharmacol.* **2000**, *58*, 1349-1356.

[16] Pierce, K. D.; Furlong, T. J.; Selbie, L. A.; Shine, J. Molecular cloning and expression of an adenosine A$_{2B}$ receptor from human brain. *Biochem. Biophys. Res. Commun.* **1992**, *187*, 86-93.

[17] Rivkees, S. A.; Reppert, S. M. RFL9 encodes an A$_{2B}$-adenosine receptor. *Mol. Endocrinol.* **1992**, *16*, 1598-1604.

[18] Feoktistov, I.; Biaggioni, I. Adenosine A$_{2B}$ receptors. *Pharmacol. Rev.* **1997**, *49*, 381-402.

[19] Feoktistov, I.; Polosa, R.; Holgate, S. T.; Biaggioni, I. Adenosine A$_{2B}$ receptors: a novel therapeutic target in asthma?. *Trends Pharmacol. Sci.* **1998**, *19*, 148-153.

[20] Marx, D.; Ezeamuzie, C. I.; Nieber, K.; Szelenyi, I. Therapy of bronchial asthma with adenosine receptor agonists or antagonists. *Drug News Perspect.* **2001**, *14*, 89-100.

[21] Sun, C. X.; Zhong, H.; Mohsenin, A.; Morschl, E.; Chunn, J. L.; Molina, J. G.; Belardinelli, L.; Zeng, D.; Blackburn, M. R. Role of A$_{2B}$ adenosine receptor signaling in adenosine-dependent pulmonary inflammation and injury *J. Clin. Invest.* **2006**, *116*, 2173-2182.

[22] Rosi, S.; McGann, K.; Hauss-Wegrzyniak, B.; Wenk, G. L. The influence of brain inflammation upon neuronal adenosine A$_{2B}$ receptors. *J. Neurochem.* **2003**, *86*, 220-227.

[23] Fiebich, B. L.; Akundi, R. S.; Biber, K.; Hamke, M.; Schmidt, C.; Butcher, R. D.; van Calker, D.; Willmroth, F. IL-6 expression induced by adenosine A$_{2B}$ receptor stimulation in U373 MG cells depends on p38 mitogen activated kinase and protein kinase C. *Neurochem Int.* **2005**, *46,* 501-12.

[24] Papassotiropoulos, A.; Hock, C.; Nitsch, R. M. Genetics of interleukin 6: implications for Alzheimer's disease. *Neurobiol. Aging*, **2001**, *22*, 863-71.

[25] Ferrara, N. Role of vascular endothelial growth factor in regulation of physiological Angiogenesis. *Am. J. Physiol. Cell Physiol*. **2001**, *280*, C1358-C1366.

[26] Volpini, R.; Costanzi, S.; Vittori, S.; Cristalli, G.; Klotz, K. N. Medicinal chemistry and pharmacology of A_{2B} adenosine receptors. *Curr. Top. Med. Chem*. **2003**, *3*, 427-443.

[27] Allaman, I.; Lengacher, S.; Magistretti, P. J.; Pellerin, L. A_{2B} receptor activation promotes glycogen synthesis in astrocytes through modulation of gene expression. *Am. J. Physiol. Cell Physiol*. **2003**, *284*, C696-C704.

[28] Panjehpour, M.; Castro, M.; Klotz, K-N. Human breast cancer cell line MDA-MB-231 expresses endogenous A_{2B} adenosine receptors mediating a Ca^{2+} signal. *Br. J. Pharmacol*. **2005**, *145*, 211-218.

[29] Gao, Z. G.; Mamedova, L. K.; Chen, P.; Jacobson, K. A. 2-Substituted adenosine derivatives: affinity and efficacy at four subtypes of human adenosine receptors. *Biochem. Pharmacol*. **2004**, *68*, 1985-1993.

[30] Baraldi, P. G.; Preti, D.; Tabrizi, M. A.; Fruttarolo, F.; Romagnoli, R.; Carrion, M. D.; Cara, L. C.; Moorman, A. R.; Varani, K.; Borea, P. A. Synthesis and biological evaluation of novel 1-deoxy-1-[6-[((hetero)arylcarbonyl)hydrazino]-9H-purin-9-yl]-N-ethyl-β-D-ribofuranuronamide derivatives as useful templates for the development of A_{2B} adenosine receptor agonists. *J. Med. Chem*. **2007**, *50*, 374-380.

[31] Rosentreter, U.; Henning, R.; Bauser, M.; Kraemer, T.; Vaupel, A.; Huebsch, W.; Dembowsky, K.; Salcher-Schraufstaetter, O.; Stasch, J-P.; Krahn, T.; Perzborn, E. Substituted 2-thio-3, 5-dicyano-4-aryl-6-aminopyridines and the use thereof. *WO patent*. **2001**, 2001025210.

[32] Rosentreter, U.; Kraemer, T.; Shimada, M.; Huebsch, W.; Diedrichs, N.; Krahn, T.; Henninger, K.; Stasch, J.-P. Substituted 2-thio-3, 5- dicyano-4-phenyl-6-aminopyridines and their use as adenosine receptor- selective ligands *WO patent*. **2003**, 03008384.

[33] Albrecht, B.; Krahn, T.; Philipp, S.; Rosentreter, U.; Cohen, M.; Downey, J. Selective A_{2B} receptor activation mimics postconditioning in a rabbit infarct model, *Circulation*. **2006**, *114*, II-14-II-15.

[34] Eckle, T.; Krahn, T.; Grenz, A.; Köhler, D.; Mittelbronn, M.; Ledent, C.; Jacobson, M. A.; Osswald, H.; Thompson, L. F.; Unertl, K.; Eltzschig, H. K. Cardioprotection by ecto-5'-nucleotidase (CD73) and A_{2B} adenosine receptors.*Circulation*. **2007**, *115*, 1581-1590.

[35] Kim, S. A.; Marshall, M. A.; Melman, N.; Kim, H. S.; Müller, C. E.; Linden, J.; Jacobson, K. A. Structure-activity relationships at human and rat A_{2B} adenosine receptors of xanthine derivatives substituted at the 1-, 3-, 7-, and 8-positions. *J. Med. Chem.* **2002**, *45*, 2131-2138.

[36] Jacobson, K. A.; Ijzerman, A. P.; Linden, J. 1, 3-Dialkylxanthine derivatives having high potency as antagonists at human A_{2B} adenosine receptors. *Drug Dev. Res.* **1999**, *47*, 45-53.

[37] Baraldi, P. G.; Tabrizi, M. A.; Preti, D.; Bovero, A.; Romagnoli, R.; Fruttarolo, F.; Zaid, N. A.; Moorman, A. R.; Varani, K.; Gessi, S.; Merighi, S.; Borea, P. A. Design, synthesis, and biological evaluation of new 8-heterocyclic xanthine derivatives as highly potent and selective human A_{2B} adenosine receptor antagonists. *J. Med. Chem.* **2004**, *47*, 1434-1447.

[38] Kim, Y. C.; Ji, X.; Melman, N.; Linden, J.; Jacobson, K. A. Anilide derivatives of an 8-phenylxanthine carboxylic congener are highly potent and selective antagonists at human A(2B) adenosine receptors. *J. Med. Chem.* **2000**, *43*, 1165-1172.

[39] Zablocki, J.; Kalla, R.; Perry, T.; Palle, V.; Varkhedkar, V.; Xiao, D.; Piscopio, A.; Maa, T.; Gimbel, A.; Hao, J.; Chu, N.; Leung, K.; Zeng, D. The discovery of a selective, high affinity A_{2B} adenosine receptor antagonist for the potential treatment of asthma. *Bioorg. Med. Chem. Lett.* **2005**, *15*, 609-612.

[40] Hayallah, A. M.; Sandoval-Ramirez, J.; Reith, U.; Schobert, U.; Preiss, B.; Schumacher, B.; Daly, J. W.; Müller, C. E. 1, 8-Disubstituted xanthine derivatives: synthesis of potent A_{2B} selective adenosine receptor antagonists. *J. Med. Chem.* **2002**, *45*, 1500-1510.

[41] Borrmann, T.; Hinz, S.; Bertarelli, D. C.; Li, W.; Florin, N. C.; Scheiff, A. B.; Müller, C. E. 1-alkyl-8-(piperazine-1-sulfonyl)phenylxanthines: development and characterization of adenosine A_{2B} receptor antagonists and a new radioligand with subnanomolar affinity and subtype specificity. *J. Med. Chem.* **2009**, *52*, 3994-4006.

[42] Grahner, B.; Winiwarter, S.; Lanyner, W.; Müller, C. E. Synthesis and structure-activity relationships of deazaxanthines: analogs of potent A1- and A2-adenosine receptor antagonists. *J. Med. Chem.* **1994**, *37*, 1526-1534.

[43] Kalla, R. V.; Zablocki, J.; Tabrizi, M. A.; Baraldi, P. G. Recent developments in A_{2B} adenosine receptor ligands. *Handb. Exp. Pharmacol.* **2009**, *193*, 99-122.

[44] Esteve, C.; Nueda, A.; Diaz, J. L.; Beleta, J.; Cardenas, A.; Lozoya, E.; Cadavid, M. I.; Loza, M. I.; Ryder, H.; Vidal, B. New pyrrolopyrimidin-6-yl benzenesulfonamides:

potent A_{2B} adenosine receptor antagonists.Bioorg. *Med. Chem. Lett.* **2006**, *16*, 3642-3645.

[45] Stefanachi, A.; Brea, J. M.; Cadavid, M. I.; Centeno, N. B.; Esteve, C.; Loza, M. I.; Martinez, A.; Nieto, R.; Raviria, E.; Sanz, F.; Segarra, V.; Sotelo, E.; Vidal, B.; Carotti, A. 1-, 3- and 8-substituted-9-deazaxanthines as potent and selective antagonists at the human A_{2B} adenosine receptor. *Bioorg. Med. Chem.* **2008**, *16*, 2852-2869.

[46] Vidal, B.; Nueda, A.; Esteve, C.; Domenech, T.; Benito, S.; Reinoso, R. F.; Pont, M.; Calbet, M.; Lopez, R.; Cadavid, M. I.; Loza, M. I.; Cardenas, A.; Godessart, N.; Beleta, J.; Warrellow, G.; Ryder, H. Discovery and characterization of 4'-(2-furyl)-N-pyridin-3-yl-4, 5'-bipyrimidin-2'-amine (LAS38096), a potent, selective, and efficacious A_{2B} adenosine receptor antagonist. *J. Med. Chem.* **2007**, *50*, 2732-2736.

[47] Thompson, R. D.; Secunda, S.; Daly, J. W.; Olsson, R. A. N6, 9-disubstituted adenines: potent, selective antagonists at the A1 adenosine receptor. *J. Med. Chem.* **1991**, *34*, 2877-2882.

[48] Stewart, M.; Steinig, A. G.; Ma, C.; Song, J. P.; McKibben, B.; Castelhano, A. L.; MacLennan, S. J. [3H]OSIP339391, a selective, novel, and high affinity antagonist radioligand for adenosine A_{2B} receptors. *Biochem. Pharmacol.* **2004**, *68*, 305-312.

[49] de Zwart, M.; Vollinga, R. C.; Beukers, M. W.; Sleegers, D. F.; von Frijtag Drabbe Künzel, J. K.; de Groote, M.; IJzerman, A. P. Potent antagonists for the human adenosine A_{2B} receptor. Derivatives of the triazolotriazine adenosine receptor antagonist ZM241385 with high affinity. *Drug Dev. Res.* **1999**, *48*, 95-103.

[50] Palczewski, K.; Kumasaka, T.; Hori, T.; Behnke, C. A.; Motoshima, H.; Fox, B. A.; LeTrong, I.; Teller, D. C.; Okada, T.; Stenkamp, R. E.; Yamamoto, M.; Miyano, M. Crystal structure of rhodopsin: A G protein-coupled receptor. *Science* **2000**, *289*, 739-745.

[51] Ivanov, A. A.; Baskin, I. I.; Palyulin, V. A.; Piccagli, L.; Baraldi, P. G.; Zefirov, N. S. Molecular modelling and molecular dynamics simulation of the human A_{2B} adenosine receptor. The study of the possible binding modes of the A_{2B} receptor antagonists. *J. Med. Chem.* **2005**, *48*, 6813-6820.

[52] Okada, T.; Sugihara, M.; Bondar, A. N.; Elstner, M.; Entel, P.; Buss, V. The retinal conformation and its environment in rhodopsin in light of a new 2.2 Å crystal structure. *J. Mol. Biol.* **2004**, *342*, 571-583.

[53] Cherezov, V.; Rosenbaum, D. M.; Hanson, M. A.; Rasmussen, S. G.; Thian, F. S.; Kobilka, T. S.; Choi, H-J.; Kuhn, P.; Weis, W. I.; Kobilka, B. K.; Stevens, R. C. High-

resolution crystal structure of an engineered human β_2-adrenergic G protein-coupled receptor. *Science* **2007**, *318*, 1258-1265.

[54] Jaakola, V-P.; Griffith, M. T.; Hanson, M. A.; Cherezov, V.; Chien, EYT.; Lane, J. R.; IJzerman, A. P.; Stevens, R. C. The 2.6 Angstrom Crystal structure of a Human A_{2A} adenosine receptor bound to an antagonist *Science* **2008**, *322*, 1211-1217.

[55] Alan, Fersht. Enyzme Structure and Mechanism, *2nd edition, Freeman & Co., New York.* **1985**, p. 6.

[56] Forrest, L. R.; Tang, C. L.; Honig, B. On the accuracy of homology modelling and sequence alignment methods applied to membrane proteins. *Biophys. J.* **2006**, *91*, 508-517.

[57] Radestock, S.; Weil, T.; Renner, S. Homology model-based virtual screening for GPCR ligands using docking and target-biased scoring. *J. Chem. Inf. Model* **2008**, *48*, 1104-1117.

[58] Ferrara, P.; Jacoby, E. Evaluation of the utility of homology models in high throughput docking. *J. Mol. Model.* **2007**, *13*, 897-905.

[59] Kairys, V.; Fernandes, M. X.; Gilson, M. K. Screening drug-like compounds by docking to homology models: a systematic study. *J. Chem. Inf. Model.* **2006**, *46*, 365-379.

[60] Okada, T.; Trong, I. Le.; Fox, B. A.; Behnke, C. A.; Stenkamp, R. E.; Palczewski, K. X-Ray Diffraction Analysis of Three-Dimensional Crystals of Bovine Rhodopsin Obtained from Mixed Micelles. *J. Struct. Biol.* **2000**, *130*, 73-80.

[61] Bernstein, F. C.; Koetzle, T. F.; Williams, G. J.; Meyer, E. F. Jr.; Brice, M. D.; Rodgers, J. R.; Kennard, O.; Shimanouchi, T.; Tasumi, M. The Protein Data Bank: a computer-based archival file for macromolecular structures. *J. Mol. Biol.* **1977**, *112*, 535-542.

[62] Caffrey, M. Membrane protein crystallization. *J. Struct. Biol.* **2003**, *142*, 108-132.

[63] Bissantz, C.; Bernard, P.; Hibert, M.; Rognan, D. Protein-based virtual screening of chemical databases. II. Are homology models of G-protein coupled receptors suitable targets?. *Proteins* **2003**, *50*, 5-25.

[64] Klabunde, T.; Hessler, G. Drug design strategies for targeting G protein-coupled receptors. *Chembiochem.* **2002**, *3*, 928-944.

[65] Bröer, B. M.; Gurrath, M.; Höltje, H-D. Molecular modelling studies on the ORL1-receptor and ORL1-agonists. *J. Comput. Aided Mol. Des.* **2003**, *17*, 739-754.

[66] Stenkamp, R. E. Alternative models for two crystal structures of bovine rhodopsin. *Acta Crystallogr. D. Biol. Crystallogr.* **2008**, *64*, 902-904.

[67] Li, J.; Edwards, P. C.; Burghammer, M.; Villa, C.; Schertler, G. F. Structure of bovine rhodopsin in a trigonal crystal form *J. Mol. Biol.* **2004**, *343*, 1409-1438.

[68] Okada, T.; Fujiyoshi, Y.; Silow, M.; Navarro, J.; Landau, E. M.; Shichida, Y. . Functional role of internal water molecules in rhodopsin revealed by X-ray crystallography. *Proc. Natl. Acad. Sci. U.S.A* **2002**, *99*, 5982-5987.

[69] Teller, D. C.; Okada, T.; Behnke, C. A.; Palczewski, K.; Stenkamp, R. E. Advances in determination of a high-resolution three-dimensional structure of rhodopsin, a model of G protein-coupled receptors (GPCRs). *Biochemistry* **2001**, *40*, 7761-7772.

[70] Standfuss, J.; Xie, G.; Edwards, P. C.; Burghammer, M.; Oprian, D. D.; Schertler, G. F. Crystal structure of a thermally stable rhodopsin mutant. *J. Mol. Biol.* **2007**, *372*, 1179-1188.

[71] Salom, D.; Lodowski, D. T.; Stenkamp, R. E.; Le Trong, I.; Golczak, M.; Jastrzebska, B.; Harris, T.; Ballesteros, J. A.; Palczewski, K. Crystal structure of a photoactivated deprotonated intermediate of rhodopsin. *Proc. Natl. Acad. Sci. U.S.A* **2006**, *103*, 16123-16128.

[72] Warne, T.; Serrano-Vega, M. J.; Baker, J. G.; Moukhametzianov, R.; Edwards, P. C.; Henderson, R.; Leslie, A. G.; Tate, C. G.; Schertler, G. F. Structure of a beta1-adrenergic G protein-coupled receptor. *Nature* **2008**, *454*, 486-491.

[73] Scheerer, P.; Park, J. H.; Hildebrand, P. W.; Kim, Y. J.; Krauss, N.; Choe, H-W.; Hofmann, K. P.; Ernst, O. P. Crystal structure of opsin in its G protein-interacting conformation. *Nature* **2008**, *455*, 497-502.

[74] Park, J. H.; Scheerer, P.; Hofmann, K. P.; Choe, H-W.; Ernst, O. P. Crystal structure of the ligand-free G protein-coupled receptor opsin. *Nature* **2008**, *454*, 183-187.

[75] Schwartz, T. W.; Hubbell, W. L. Structural biology: A moving story of receptors. *Nature* **2008**, *455*, 473-474.

[76] Mobarec, J. C.; Sanchez, R.; Filizola, M. Modern homology modelling of G protein-coupled receptors: which structural template to use?. *J. med. Chem.* **2009**, *52*, 5207-5216.

[77] Bairoch, A.; Apweiler, R. The SWISS-PROT protein sequence database and its supplement TrEMBL *Nucleic Acids Res.* **2000**, *28*, 45-48.

[78] Thompson, J. D.; Gibson, T. J.; Plewniak, F.; Jeanmougin, F.; Higgins, D. G. The CLUSTAL_X windows interface: flexible strategies for multiple sequence alignment aided by quality analysis tools. *Nucleic Acids Res.* **1997**, *25*, 4876-4882.

[79] Fredriksson, R.; Lagerström, M. C.; Lundin, L-G.; Schiöth, H. B. The G protein-coupled receptors in the human genome form five main families. Phylogenetic analysis, paralogon groups, and fingerprints. *Mol. Pharm.* **2003**, *63*, 1256-1272.

[80] Imai, T.; Fujita, N. Statistical sequence analyses of G protein-coupled receptors: Structural and functional characteristics viewed with periodicities of entropy, hydrophobicity, and volume. *proteins* **2004**, *56*, 650-660.

[81] Ballesteros, J. A.; Weinstein, H. W. Integrated methods for the construction of three-dimensional models and computational probing of structure-function relation of G protein-coupled receptors. *Methods in Neurosci.* **1995**, *25*, 366-428.

[82] GPCRDB, Information system for G protein-coupled receptors (GPCRs), www.gpcr.org. [Online]

[83] Homology Modelling with Homer. http://protein.cribi.unipd.it/homer/. [Online]

[84] Canutescu, A. A.; Shelenkov, A. A.; Dunbrack, R. L. Jr. A graph-theory algorithm for rapid protein side-chain prediction. *Protein Sci.* **2003**, *12*, 2001-2014.

[85] Schlegel, B.; Sippl, W.; Höltje, H. D. Molecular dynamics simulations of bovine rhodopsin: influence of protonation states and different membrane-mimicking environments. *J. Mol. Model.* **2005**, *12*, 49-64.

[86] Guvench, O.; Mackerell, A. D. Jr. Comparison of protein force fields for molecular dynamics simulation. *Methods Mol. Biol.* **2008**, *443*, 63-88.

[87] Pearlman, D. A.; Case, D. A.; Caldwell, J. W.; Ross, W. S.; Cheatham, T. E.; Debolt, S.; Ferguson, D.; Seibel, G.; Kollman, P. AMBER, a package of computer programs for applying molecular mechanics, normal mode analysis, molecular-dynamics and free-energy calculations to simulate the structural and energetic properties of molecules. *Comput. Phys. Commun.* **1995**, *91*, 1-41.

[88] Morris, G. M.; Lim-Wilby, M. Molecular docking Methods. *Mol. Biol.* **2008**, *443*, 365-382.

[89] Rarey, M.; Kramer, B.; Lengauer, T.; Klebe, G. A Fast flexible docking method using an Incremental Construction Algorithm. *J. Mol. Biol.* **1996**, *261*, 470-489.

[90] Rarey, M.; Kramer, B.; Lengauer, T. Multiple automatic base selection: Protein-ligand docking based on incremental construction without manual intervention. *J. Comput. Aided Mol. Des.* **1997**, *11*, 369-384.

[91] Rudnicki, W. R.; Kurzepa, M.; Szczepanik, T.; Priebe, W.; Lesyng, B. A simple model for predicting the free energy of binding between anthracycline antibiotics and DNA. *Acta Biochim Pol.* **2000**, *47*, 1-9.

[92] Åqvist, J. Calculation of absolute binding free energies for charged ligands and effects of long-range electrostatic interactions. *J. Comp. Chem.* **1996**, *17*, 1587-1597.

[93] Kuhn, B.; Kollman, P. A. Binding of a diverse set of ligands to avidin and streptavidin: an accurate quantitative prediction of their relative affinities by a combination of molecular mechanics and continuum solvent models. *J. Med. Chem.* **2000**, *43*, 3786-3791.

[94] Wang, J.; Dixon, R.; Kollmann, P. A. Ranking ligand binding affinities with avidin: A molecular dynamics-based interaction energy study. *Proteins* **1999**, *34*, 69-81.

[95] Pospisil, P.; Folkers, G. Making the best account of molecular docking in drug design. *J. Pharm. Sci.* **2004**, *29*, 81-92.

[96] Bockaert, J.; Pin, J.P. Molecular tinkering of G protein-coupled receptors: an evolutionary success. *EMBO J.* **1999**, *18*, 1723-1729.

[97] http://www.ncbi.nlm.nih.gov/blast/Blast.cgi?CMD=Web&PAGE_TYPE=BlastHom. [Online]

[98] Rosenbaum, D. M.; Cherezov, V.; Hanson, M. A.; Rasmussen, S. G.; Thian, F. S.; Kobilka, T. S.; Choi, H-J.; Yao, X-J.; Weis, WI.; Stevens, R. C.; Kobilka, B. K. GPCR Engineering yields high-resolution structural insights into β_2-adrenergic receptor function. *Science* **2007**, *318*, 1266-1273.

[99] Schlegel, B.; Laggner, C.; Meier, R.; Langer, T.; Schnell, D.; Seifert, R.; Stark, H.; Höltje, H. D.; Sippl, W. Generation of a homology model of the human histamine H(3) receptor for ligand docking and pharmacophore-based screening. *J. Comput. Aided Mol Des.* **2007**, *21*, 437-453.

[100] Rockey, W. M.; Elcock, A. H. Structure selection for protein kinase docking and virtual screening: homology models or crystal structures?. *Curr. Protein Pept. Sci.* **2006**, *7*, 437-457.

[101] Laskowski, R. A.; MacArthur, M. W.; Moss, D. S.; Thornton, J. M. PROCHECK: a program to check the stereochemical quality of protein structures. *J. Appl. Cryst.* **1993**, *26*, 283-291.

[102] Morris, A. L.; MacArthur, M. W.; Hutchinson, E. G.; Thornton, J. M. Stereochemical quality of protein structure coordinates. *Proteins* **1992**, *12*, 345-364.

[103]   Sippl, M. J. Recognition of errors in three-dimensional structures of proteins. *Proteins* **1993**, *17*, 355-362. http://www.came.sbg.ac.at/.

[104]   Ongini, E.; Dionisotti, S.; Gessi, S.; Irenius, E.; Fredholm, B. B. Comparison of CGS 15943, ZM 241385 and SCH 58261 as antagonists at human adenosine receptors. *Naunyn Schmiedebergs Arch Pharmacol*. **1999**, *359*, 7-10.

[105]   Sauer, R.; Maurinsh, J.; Reith, U.; Fülle, F.; Klotz, KN.; Müller, C. E. Water-soluble phosphate prodrugs of 1-propargyl-8-styrylxanthine derivatives, A(2A)-selective adenosine receptor antagonists. *J. Med. Chem.* **2000**, *43*, 440-448.

[106]   Knutsen, L. J.; Weiss, S. M. KW-6002 (Kyowa Hakko Kogyo). *Curr. Opin Investig Drugs*. **2001**, *2*, 668-673.

[107]   Hodgson, R. A.; Bertorelli, R.; Varty, G. B.; Lachowicz, J. E.; Forlani, A.; Fredduzzi, S.; Cohen-Williams, M. E.; Higgins, G. A.; Impagnatiello, F.; Nicolussi, E.; Parra, L. E.; Foster, C.; Zhai, Y.; Neustadt, B. R.; Stamford, A. W.; Parker, E. M.; Reggi. Characterization of the potent and highly selective A$_{2A}$ receptor antagonists preladenant and SCH 412348 [7-[2-[4-2, 4-difluorophenyl]-1-piperazinyl]ethyl]-2-(2-furanyl)-7H-pyrazolo[4,3-e][1,2,4]triazolo[1,5-c]pyrimidin-5-amine] in rodent models of movement disorders and depression. *J. Pharmacol Exp. Ther.* **2009**, *330*, 294-303.

[108]   IJzerman, A. P.; Von Frijtag Drabbe Künzel, J. K.; Kim, J.; Jiang, Q.; Jacobson, K. A. Site-directed mutagenesis of the human adenosine A$_{2A}$ receptor. Critical involvement of Glu13 in agonist recognition. *Eur. J. Pharmacol.* **1996**, *310*, 269-272.

[109]   Jiang, Q.; Lee, B. X.; Glashofer, M.; van Rhee, A. M.; Jacobson, K. A. Mutagenesis reveals structure-activity parallels between human A$_{2A}$ adenosine receptors and biogenic amine G protein-coupled receptors. *J. Med. Chem*. **1997**, *40*, 2588-2595.

[110]   Jiang, Q.; Van Rhee, A. M.; Kim, J.; Yehle, S.; Wess, J.; Jacobson, K. A. Hydrophilic side chains in the third and seventh transmembrane helical domains of human A$_{2A}$ adenosine receptors are required for ligand recognition. *Mol. Pharmacol.* **1996**, *50*, 512-521.

[111]   Beukers, M. W.; van Oppenraaij, J.; van der Hoorn, P. P.; Blad, C. C.; den Dulk, H.; Brouwer, J.; IJzerman, A. P. Random mutagenesis of the human adenosine A$_{2B}$ receptor followed by growth selection in yeast. Identification of constitutively active and gain of function mutations. *Mol. Pharmacol*. **2004**, *65*, 702-710.

[112]   Kim, J.; Jiang, Q.; Glashofer, M.; Yehle, S.; Wess, J.; Jacobson, K. A. Glutamate residues in the second extracellular loop of the human A$_{2A}$ adenosine receptor are required for ligand recognition. *Mol. Pharmacol.* **1996**, *49*, 683-691.

[113]   Kim, J.; Wess, J.; van Rhee, A. M.; Schöneberg, T.; Jacobson, K. A. Site-directed mutagenesis identifies residues involved in ligand recognition in the human A_{2A} adenosine receptor. *J. Biol. Chem.* **1995**, *270*, 13987-13997.

[114]   Gao, Z. G.; Jiang, Q.; Jacobson, K. A.; Ijzerman, A. P. Site-directed mutagenesis studies of human A(2A) adenosine receptors: involvement of glu(13) and his(278) in ligand binding and sodium modulation. *Biochem Pharmacol.* **2000**, *60*, 661-668.

[115]   Yan, L.; Bertarelli, D. C.; Hayallah, A. M.; Meyer, H.; Klotz, K. N.; Müller, C. E. A new synthesis of sulfonamides by aminolysis of p-nitrophenylsulfonates yielding potent and selective adenosine A_{2B} receptor antagonists. *J. Med. Chem.* **2006**, *49*, 4384-4391.

[116]   Jarvis, M. F.; Schulz, R.; Hutchison, A. J.; Do, U. H.; Sills, M. A.; Williams, M. [3H]CGS 21680, a selective A2 adenosine receptor agonist directly labels A2 receptors in rat brain. *J. Pharmacol Exp. Ther.* **1989**, *251*, 888-893.

[117]   Vittori, S.; Camaioni, E.; Costanzi, S.; Volpini, R.; Klotz, K. N.; Cristalli, G. Synthesis and receptor affinity of polysubstituted adenosines. *Nucleosides Nucleotides* **1999**, *18*, 739-740.

[118]   Klotz, K. N.; Hessling, J.; Hegler, J.; Owman, C.; Kull, B.; Fredholm, B. B.; Lohse, M. J. Comparative pharmacology of human adenosine receptor subtypes - characterization of stably transfected receptors in CHO cells. *Naunyn Schmiedebergs Arch Pharmacol.* **1998**, *357*, 1-9.

[119]   Ivanov, A. A.; Palyulin, V. A.; Zefirov, N. S. Computer aided comparative analysis of the binding modes of the adenosine receptor agonists for all known subtypes of adenosine receptors. *J. Mol. Graph. Model.* **2007**, *25*, 740-754.

[120]   Strader, C. D.; Fong, T. M.; Tota, M. R.; Underwood, D.; Dixon, R. A. Structure and function of G protein-coupled receptors. *Annu. Rev. Biochem.* **1994**, *63*, 101-132.

[121]   Weiss, J. M.; Morgan, P. H.; Lutz, M. W.; Kenakin, T. P. The cubic ternary complex receptor-occupancy model. III. resurrecting efficacy. *J. Theor. Biol.* **1996**, *181*, 381-397.

[122]   Kenakin, T. Ligand-selective receptor conformations revisited: the promise and the problem. *Trends Pharmacol. Sci.* **2003**, *24*, 346-354.

[123]   Rubenstein, L. A.; Lanzara, R. G. Activation of G protein-coupled receptors entails cysteine modulation of agonist binding. *J. Mol. Struct. Theochem.* **1998**, *430*, 57-71.

[124]   Mirzadegan, T.; Benko, G.; Filipek, S.; Palczewski, K. Sequence analyses of G protein-coupled receptors: similarities to rhodopsin. *Biochemistry* **2003**, *42*, 2759-2767.

[125]   Kim, S-K.; Gao, Z. G.; Van, Rompaey. P.; Gross, A. S.; Chen, A.; Van, Calenbergh. S.; Jacobson, K. A. Modeling the adenosine receptors: Comparison of the binding domains of A_{2A} agonists and antagonists. *J. Med. Chem.* **2003**, *46*, 4847-4859.

[126]   Ballesteros, J. A.; Jensen, A. D.; Liapakis, G.; Rasmussen, S. G.; Shi, L.; Gether, U.; Javitch, J. A. Activation of the β_2-adrenergic receptor involves disruption of an ionic lock between the cytoplasmic ends of transmembrane segments 3 and 6. *J. Biol. Chem.* **2001**, *276*, 29171-29177.

[127]   Dror, R.O.; Arlow, D. H.; Borhani, D. W.; Jensen, M. Ø; Piana, S.; Shaw, D. E. Identification of two distinct inactive conformations of the β_2-adrenergic receptor reconciles structural and biochemical observations. *Proc. Natl. Acad. Sci. U. S. A.* **2009**, *106*, 4689-4694.

[128]   Yao, X.; Parnot, C.; Deupi, X.; Ratnala, V. R.; Swaminath, G.; Farrens, D.; Kobilka, B. Coupling ligand structure to specific conformational switches in the β_2-adrenoceptor. *Nat. Chem. Biol.* **2006**, *2*, 417-422.

[129]   Rasmussen, S. G.; Choi, H. J.; Rosenbaum, D. M.; Kobilka, T. S.; Thian, F. S.; Edwards, P. C.; Burghammer, M.; Ratnala, V. R.; Sanishvili, R.; Fischetti, R. F.; Schertler, G. F.; Weis, W. I.; Kobilka, B. K. Crystal structure of the human β_2 adrenergic G protein-coupled receptor. *Nature* **2007**, *450*, 383-387.

[130]   Fritze, O.; Filipek, S.; Kuksa, V.; Palczewski, K.; Hofmann, K. P.; Ernst, O. P. Role of the conserved NPxxY(x)5, 6F motif in the rhodopsin ground state and during activation. *Proc. Natl. Acad. Sci. U. S. A.* **2003**, *100*, 2290-2295.

[131]   Barak, L. S.; Menard, L.; Ferguson, S. S.; Colapietro, A. M.; Caron, M. G. The conserved seven-transmembrane sequence NP(X)2, 3Y of the G protein-coupled receptor superfamily regulates multiple properties of the β_2-adrenergic receptor. *Biochemistry* **1995**, *34*, 15407-15414.

[132]   Prioleau, C.; Visiers, I.; Ebersole, B. J.; Weinstein, H.; Sealfon, S. C. Conserved helix 7 tyrosine acts as a multistate conformational switch in the 5HT2C receptor. Identification of a novel "locked-on" phenotype and double revertant mutations. *J. Biol. Chem.* **2002**, *277*, 36577-36584.

[133] Angel, T. E.; Chance, M. R.; Palczewski, K. Conserved waters mediate structural and functional activation of family A (rhodopsin-like) G protein-coupled receptors. *Proc. Natl. Acad. Sci. U. S. A.* **2009**, *106*, 8555-8560.

[134] Schwartz, T. W.; Frimurer, T. M.; Holst, B.; Rosenkilde, M. M.; Elling, C. E. Molecular mechanism of 7TM receptor activation a global toggle switch model. *Annu. Rev. Pharmacol. Toxicol.* **2006**, *46*, 481-519.

[135] Crocker, E.; Eilers, M.; Ahuja, S.; Hornak, V.; Hirshfeld, A.; Sheves, M.; Smith, S. O. Location of Trp265 in metarhodopsin II: implications for the activation mechanism of the visual receptor rhodopsin. *J. Mol. Biol.* **2006**, *357*, 163-172.

[136] Murakami, M.; Kouyama, T. Crystal structure of squid rhodopsin. *Nature* **2008**, *453*, 363-367.

[137] Ahuja, S.; Hornak, V.; Yan, E. C.; Syrett, N.; Goncalves, J. A.; Hirshfeld, A.; Ziliox, M.; Sakmar, T. P.; Sheves, M.; Reeves, P. J.; Smith, S. O.; Eilers, M. Helix movement is coupled to displacement of the second extracellular loop in rhodopsin activation *Nature. Struct. Mol. Biol.* **2009**, *16*, 168-175.

[138] Bokoch, M. P.; Zou, Y.; Rasmussen, S. G.; Liu, C. W.; Nygaard, R.; Rosenbaum, D. M.; Fung, J. J.; Choi, H. J.; Thian, F. S.; Kobilka, T. S.; Puglisi, J. D.; Weis, W. I.; Pardo, L.; Prosser, R. S.; Mueller, L.; Kobilka, B. K. Ligand-specific regulation of the extracellular surface of a G protein-coupled receptor. *Nature.* **2010**, *463*, 108-1012.

[139] Nygaard, R.; Frimurer, T. M.; Holst, B.; Rosenkilde, M. M.; Schwartz, T. W. Ligand binding and micro-switches in 7TM receptor structures. *Trends Pharmacol. Sci.* **2009,** *30*, 249-259.

[140] Heller, H.; Schaefer, M.; Schulten, K. Molecular dynamics simulation of a bilayer of 200 lipids in the gel and in the liquid crystal phase. *J. Phys. Chem.* **1993**, *97*, 8343-8360.

[141] Jojart, B.; Kiss, R.; Viskolcz, B.; Kolossvary, I.; Keseru, G. M. Molecular dynamics simulation at high sodium chloride concentration: Toward the inactive conformation of the human adenosine A_{2A} receptor. *J. Phys. Chem. Lett.* **2010**, *1*, 1008-1013.

[142] Angel, T. E.; Gupta, S.; Jastrzebska, B.; Palczewski, K.; Chance, M. R. Structural waters define a functional channel mediating activation of the GPCR, rhodopsin. *Proc. Natl. Acad. Sci. U. S. A.* **2009**, *106*, 14367-14372.

[143] Mestres, J. Virtual screening: a real screening complement to high-throughput screening. *Biochem. Soc. Trans.* **2002**, *30*, 797-799.

[144] Lyne, P. D. Structure-based virtual screening: an overview. *Drug Discov. Today* **2002**, *7*, 1047-10455.

[145] Dror, O.; Shulman-Peleg, A.; Nussinov, R.; Wolfson, H. J. Predicting molecular interactions in silico: I. A guide to pharmacophore identification and its applications to drug design. *Curr. Med. Chem.* **2004**, *11*, 71-90.

[146] Schneidman-Duhovny, D.; Nussinov, R.; Wolfson, H. J. Predicting molecular interactions in silico: II. Protein-protein and protein-drug docking. *Curr. Med. Chem.* **2004**, *11*, 91-107.

[147] Stahura, F. L.; Bajorath, J. Novel methodologies for virtual screening. *Curr. Pharm. Design.* **2005**, *11*, 1189-1202.

[148] Lengauer, T.; Lemmen, C.; Rarey, M.; Zimmermann, M. Novel technologies for virtual screening. *Drug Discov. Today* **2004**, *9*, 27-34.

[149] Evers, A.; Klebe, G. Successful virtual screening for a submicromolar antagonist of the neurokinin-1 receptor based on a ligand-supported homology model. *J. Med. Chem.* **2004**, *47*, 5381-5392.

[150] Oshiro, C.; Bradley, E. K.; Eksterowicz, J.; Evensen, E.; Lamb, M. L.; Lanctot, J. K.; Putta, S.; Stanton, R.; Grootenhuis, P. D. Performance of 3D-database molecular docking studies into homology models. *J. Med. Chem.* **2004**, *47*, 764-767.

[151] Wieman, H.; Tøndel, K.; Anderssen, E.; Drabløs, F. Homology-based modelling of targets for rational drug design. *Mini. Rev. Med. Chem.* **2004**, *4*, 793-804.

[152] Zhang, J. H.; Chung, T. D.; Oldenburg, K. R. A . Simple Statistical Parameter for Use in Evaluation and Validation of High Throughput Screening Assays. *J. Biomol. Screen.* **1999**, *4*, 67-73.

[153] Evers, A.; Klabunde, T. Structure-based drug discovery using GPCR homology modeling: successful virtual screening for antagonists of the alpha1A adrenergic recepto. *J. Med. Chem.* **2005**, *48*, 1088-1097.

[154] Bissantz, C.; Logean, A.; Rognan, D. High-throughput modeling of human G protein-coupled receptors: amino acid sequence alignment, three-dimensional model building, and receptor library screening. *J. Chem. Inf. Comput. Sci.* **2004**, *44*, 1162-1176.

[155] Varady, J.; Wu, X.; Fang, X.; Min, J.; Hu, Z.; Levant, B.; Wang, S. Molecular modeling of the three-dimensional structure of dopamine 3 (D3) subtype receptor: discovery of novel and potent D3 ligands through a hybrid pharmacophore- and structure-based database searching approach. *J. Med. Chem.* **2003**, *46*, 4377-4392.

[156] Bissantz, C.; Schalon, C.; Guba, W.; Stahl, M. Focused library design in GPCR projects on the example of 5-HT(2c) agonists: comparison of structure-based virtual screening with ligand-based search methods. *Proteins* **2005**, *61*, 938-9352.

[157] Katritch, V.; Jaakola, V. P.; Lane, J. R.; Lin, J.; Ijzerman, A. P.; Yeager, M.; Kufareva, I.; Stevens, R. C.; Abagyan, R. Structure-based discovery of novel chemotypes for adenosine A(2A) receptor antagonists. *J. Med. Chem.* **2010**, *53*, 1799-1809.

[158] ZINC. http://zinc.docking.org/. [Online]

[159] BiosolveIT GmbH. http://www.biosolveit.de/FTrees. [Online]

[160] Gerlach, C.; Broughton, H.; Zaliani, A. FTree query construction for virtual screening: a statistical analysis. *J. Comput. Aided Mol. Des*. **2008**, *22*, 111-118.

[161] Irwin, J. J.; Shoichet, B. K. ZINC A Free Database of Commercially Available Compounds for Virtual Screening. *J. Chem. Inf. Model.* **2005**, *45*, 177-182.

[162] Lipinski, C. A.; Lombardo, F.; Dominy, B. W.; Feeney, P. J. Experimental and computional approaches to estimate solubility and permeability in drug discovery and development settings. *Adv. Drug Delivery Rev*. **1997**, *23*, 3-25.

[163] Willet, P.; Bernard, J. M.; Downs, G. M. Chemical similarity searching. *J. Chem. Inf. Comput. Sci.* **1998**, *38*, 983-996.

[164] Lyne, P. D.; Lamb, M. L.; Saeh, J. C. Accurate prediction of the relative potencies of members of a series of kinase inhibitors using molecular docking and MM-GBSA scoring. *J. Med. Chem.* **2006**, *49*, 4805-4808.

[165] Wang, J. M.; Hou, T. J.; Xu, X. J. Recent advances in free energy calculations with a combination of molecular mechanics and continuum models. *Curr. Comput. Aided Drug Des*. **2006**, *2*, 287-306.

[166] Kollman, P. A.; Massova, I.; Reyes, C.; Kuhn, B.; Huo, S. H.; Chong, L.; Lee, M.; Lee, T.; Duan, Y.; Wang, W.; Donini, O.; Cieplak, P.; Srinivasan, J.; Case, D. A.; Cheatham, T. E. Calculating structures and free energies of complex molecules: Combining molecular mechanics and continuum models. *Acc. Chem. Res.* **2000**, *33*, 889-897.

[167] Gilson, M. K.; Sharp, K. A.; Honig, B. H. Calculating the Electrostatic Potential of Molecules in Solution - Method and Error Assessment. *J. Comput. Chem.* **1988**, *9*, 327-335.

[168]   Case, D. A.; Cheatham, T. E.; Darden, T.; Gohlke, H.; Luo, R.; Merz, K. M.; Onufriev, A.; Simmerling, C.; Wang, B.; Woods, R. J. The Amber biomolecular simulation programs. *J. Comput. Chem.* **2005**, *26*, 1668-1688.

[169]   Kitchen, D. B.; Decornez, H.; Furr, J. R.; Bajorath, J. Docking and scoring in virtual screening for drug discovery: methods and applications. *Nat. Rev. Drug Discov*. **2004**, *3*, 935-949.

[170]   Stahl, M.; Rarey, M. Detailed analysis of scoring functions for virtual screening. *J. Med. Chem.* **2001**, *44*, 1035-1042.

[171]   Ji, X.; Kim, Y. C.; Ahern, D. G.; Linden, J.; Jacobson, K. A. [3H]MRS 1754, a selective antagonist radioligand for A(2B) adenosine receptors. *Biochem. Pharmacol*. **2001**, *61*, 657-63.